Modélisation de la mutation humaine SCN9AR185H identifiée chez les patients souffrant de douleur chronique à l'aide de l'approche CRISPR/Cas9 chez la souris : conséquences sur la sensibilité à la douleur

Yaping Xue

Université de Strasbourg

UNIVERSITÉ DE STRASBOURG

École Doctorale des Sciences de la Vie et de la Santé STRASBOURG

ÉCOLE DOCTORALE SCIENCES DE LA VIE ET DE LA SANTE

Institut de Génétique et de Biologie Moléculaire et Cellulaire (IGBMC)

THÈSE présentée par :

[Yaping XUE]

soutenue le : **12 Octobre 2020**

pour obtenir le grade de : **Docteur de l'université de Strasbourg**

Discipline/ Spécialité : Neuroscience

Modeling the Human *SCN9A*^{R185H} Mutation Found in Patients with Chronic Pain Using CRISPR/Cas9 in the Mouse, Consequences on Pain Sensitivity

THÈSE dirigée par :

DIRECTEUR DE THESE

[M. HERAULT Yann] Directeur de Recherche, CNRS, Strasbourg

CODIRECTEUR DE THESE

[Mme. GAVERIAUX-RUFF Claire] Professeur, Université de Strasbourg

RAPPORTEURS :

[M. MONTAGUTELLI Xavier] Directeur de Recherche, Institut Pasteur, Paris

[Mme. REAUX-LE-GOAZIGO Annabelle] Chargé de Recherches, INSERM, Paris

EXAMINATEURS :

[M. BARROT Michel] Directeur de Recherche, CNRS, Strasbourg

AUTRES MEMBRES DU JURY :

[Mme. HOEIJMAKERS Jannecke] MCF-MCUPH, Maastricht University

Acknowledgements

Firstly, I would like highly to appreciate to my supervisor Dr. Yann HERAULT and my co-supervisor Professor Claire GAVERIAUX-RUFF for giving me this opportunity to work on this challenging and exciting project. Thank you so much for believing in me and coaching me through this journal. Thank you, Dr. Yann HERAULT for guiding of genetic models and give a lot of opportunity to participate in different related training courses and congresses. Thank you, Professor Claire GAVERIAUX-RUFF for experiment organization training and lots of suggestions for mice behavioral tests.

I would like to specially appreciate the two reporter of my jury Dr. Xavier MONTAGUTELLI and Dr. Annabelle REAUX-LE-GOAZIGO, my external examiner Dr. Janneke HOEIJMAKERS and my internal examiner Michel BARROT for agreeing to lend their professionally scientific expertise and their precious time to evaluate my thesis.

I would like to gratitude to Marie-Christine BIRLING for helping design strategy of establishing mouse models of my PhD project. Thank you very much, Romain LORENTZ for helping me to validate the protocol of CRISPR-Cas9a system. Also, I would like to thank you, Laurence SCHAEFFER to help me to confirm the genotype of blastocysts.

I am grateful to the animal caretakers at PHENOMIN-ICS and IGBMC animal facility for their services. I would like to appreciate the staff of IGBMC and ICS for their helpful suggestions and discussions, in particular Charley Pinault, Sophie Brignon and Dalila Ali-Hadji, Loïc Lindner and Pauline Cayrou, and Elvire Guiot.

I also extend my appreciation to our collaborators in ITN-Pain Net, a European Commission Multi Center Collaborative Project, at Center for Neuroscience and Regeneration Research in Yale University, and at Neuroscience Technologies (NT) company in Barcelona, also at Fondazione IRCCS, Istituto Neurologico “Carlo Besta” (FINCB) in Milan. I am grateful Dr. Stephen Waxman and Dr. Dib-Hajj, Sulayman in Yale, Dr. Jordi Serra in NT and Professor Lauria Pinter Giuseppe in FINCB for hosting me in their laboratories during my secondement of my PhD project. In Yale, thank you Peng Zhao and Mark Estacio to training on me for dorsal root ganglia neurons culture and virus transfection as well as clamp technique. Also thank you, Lubin Chen and Julie Labau to share their experience on rodent pain behavioral tests and rodent surgery. In NT, thank you, Romà Solà, Federico Ponente and Lenin Reyes-Haro share experience on microneurography, especially appreciate Federico Ponente for the microneurography experiment on my mutant mice and data analysis. In FINCB, I would like to thank you, Cartelli Daniele and Lombardi Raffaella for organize my samples and training on skin biopsy. Also, thank you, Mirna Andelic and Matilde Paolini for helping to set up the protocol of Immunochemistry.

I am highly appreciated to all help from team members. Thank you so much, Joelle PENSAVALLE for helping me to live in Strasbourg, she helps me to find apartment, open an bank account and resident permanent. Thank you, Celeste Chidiac and Claire GAVERIAUX-RUFF for helping me the ethic document writing in French. Thank you very much, Davide REISS for training on me to do the pain behavioral tests and pSNL surgery in mice. Thank you, Arnaud DUCHON for production order and suggestion on protocol of odor test. Thank you, Monika RATAJ BANIOWSKA, Maria Victoria HINCKELWANIN RIVAS, Claire CHEVALIER and Veronique BRAULT for laboratory organization of equipment, materials and chemicals. Thank you, Michel Roux for training on Cryostat. At end, a big package of appreciation and touched to give our PhD group, Maria del Mar MUNIZ MORENO, Helin ATAS-OZCAN, Ameer Abu Baker RASHEED, Celeste CHIDIAC and Marion PELLEN. They provide me the warmth of family, and experienced interesting, dramatic, happiness, wonderful and colorful PhD student life. Also, thank you very very much for all helps to resolve my scientific and daily life problem.

Most of all, I would like to thank you, my family members, especially my grandmother, my elder uncle and my elder aunt. I wouldn’t have made it this far without their constant support and encouragement. Thank you so much, my boyfriend for taking care of me during my thesis writing. Thank you to my other friends here in Europe who have become almost like family to me.

Abstract

The NAV1.7 channel, encoded by *Scn9a* gene, is a voltage-gated sodium channel that plays a critical role in the generation and conduction of action potentials. In peripheral sensory neurons, the expression and dynamic regulation of SCN9A is involved in pain sensitivity and chronic pain development. Several *SCN9A* gain-of-function mutations have been found in chronic pain patients with idiopathic small fiber neuropathy (SFN). Recently, loss-of-function of *SCN9A* due to bi-allelic inactivating mutations results in the striking clinical phenotype of congenital insensitivity to pain (CIP). These individuals do not perceive pain in response to noxious stimuli. However, the heterozygous carriers of one inactivating mutation have normal pain sensitivity. The generation of animal models with CRISPR/Cas9 gene editing is an important tool for investigating the role of a mutation in the pathogenesis of disease and provide an avenue for functional drug screening. We have successfully established two mouse models, one carrying the R185H patient-derived mutation and the second one, R185X carrying an early stop in the open reading frame in the *Scn9a* locus$^{R185X/+}$ using the CRISPR/Cas9 technology. We have characterized the effect of these two mutations on pain sensitivity and molecular and cellular alteration. The two mouse lines showed no alteration of growth, survival and global health state. Pain sensitivity of the new mutant mouse line was investigated on both sexes using behavioral tests of sensitivity to thermal and mechanical stimuli. Our results indicate that the *Scn9a*^{R185H} mice show an increased pain phenotype, suggesting that the *Scn9a* R185H mutation identified in the SFN patients is responsible for their pain symptoms. This exploration will benefit to drug screen. However, *Scn9a*$^{R185X/wt}$ mice did not show normal pain phenotype rather they are less sensitive to heat. In these mice, one Scn9a allele is not functional. Therefore, we provide more evidence that SCN9A plays an important role in nociception and in painful idiopathic SFN.

Résumé en Français

Introduction

La neuropathie à petites fibres (Small Fiber Neuropathy, SFN) est une pathologie des fibres nerveuses sensorielles Aδ et C. Elle est généralement caractérisée par des symptômes de douleur neuropathique et des anomalies du système nerveux autonome. Plusieurs maladies induisent la SFN telles que le diabète et le SIDA. Des mutations gain-de-fonction dans les canaux ioniques voltage-dépendants provoquent aussi une SFN. Fait intéressant, l'étude des SFN idiopathiques a montré que près de 30% de ces patients présentent des mutations de gain de fonction dans le gène *SCN9A* codant pour la sous-unité α du canal sodique. Cependant, le phénotype de SFN chez les patients est compliqué et les informations détaillées sur canal SCN9A chez les patients SFN idiopathiques ne sont pas très claires jusqu'à présent.

Le canal SCN9A est un canal sodium dépendant du voltage qui joue un rôle critique dans la génération et la conduction des potentiels d'action. Il est donc important pour la signalisation électrique par la plupart des cellules excitables. Il s'exprime préférentiellement dans le système nerveux périphérique au sein des ganglions sensoriels de la racine dorsale et des neurones ganglionnaires sympathiques et dans leurs axones périphériques de petit diamètre. En 2012, C.G. Faber et ses collègues ont découvert que deux patients non apparentés étaient hétérozygotes pour l'une de ces mutations, c.554G>A, p.R185H. Ces deux patients se plaignaient de douleurs et ont montré une sensation de douleur anormale au chaud et au froid. Le patient plus âgé a rapporté moins de douleur que la patiente plus jeune. Cette mutation entraîne une hyperexcitabilité des neurones du ganglion de la racine dorsale (DRG) chez les patients SFN et également en culture in vitro des neurones de DRG du rat, mais pas des neurones du ganglion cervical supérieur du rat. Récemment, il a été montré que la perte de fonction du gène SCN9A entraîne une insensibilité congénitale à la douleur (CIP). Ces personnes ne perçoivent pas la douleur en réponse à des stimuli nocifs. Cependant, les porteurs hétéroalléliques de cette mutation ont une sensibilité à la douleur normale. Ce phénotype de sensibilité normale à la douleur dans les porteurs hétérozygotes de la mutation CIP montre qu'une nouvelle thérapie génique des SFN idiopathiques pourrait être envisagée en inactivant l'allèle mutant gain de fonction.

L'endonucléase Cas9 guidée par l'ARN des systèmes microbiens de type II CRISPR (cluster répété régulièrement palindromique court) est un nouvel outil de recherche dans l'édition et la régulation du génome. Récemment, ce système a été exploité pour faciliter les manipulations génétiques dans une variété de types de cellules et d'organismes. Ce système polyvalent a deux composants: un ARN guide (sgRNA), qui est responsable de l'appariement avec l'ADN homologue correspondant sur le site cible et une endonucléase Cas9 qui clive l'ADN. La reconnaissance d'une cible d'ADN génomique est médiée par l'appariement de bases avec un sgRNA de 20 bases. Ce dernier recrute la protéine d'endonucléase Cas9 sur le site cible et crée des cassures double brin (DSB) dans l'ADN cible. Le DSB peut être réparé par deux systèmes principaux, la jonction d'extrémité non homologue (NHEJ), entraînant des insertions et des suppressions, ou la voie de réparation dirigée homologue (HDR), entraînant une substitution de séquence précise en présence d'un modèle de réparation.

Par conséquent, dans ce projet de doctorat, nous nous concentrons sur les objectifs suivants:

1. Etablir deux modèles de souris liés à la douleur en utilisant le même outil génétique, qui sont la mutation R185H dans le modèle de souris à canal sodique *SCN9A* par voie de réparation HDR et le modèle knock-out d'allèle à canal sodique *SCN9A* par le mécanisme NHEJ. L'effet hors cible a été testé sur deux modèles de souris liés à la douleur.

2. Caractériser les effets de ces deux mutations chez la souris au niveau biochimique, génétique et comportemental.

Ces résultats bénéficieront à la recherche sur l'association génotype-phénotype et également le rôle des mutations *SCN9A* (NAV1.7) dans les SFN idiopathiques.

Résultats

Les lignées de souris CRISPR-Cas9 *Scn9a*^{R185H} et *Scn9a*$^{R185X/wt}$ ont été générées avec succès par le système CRISPR-Cas9. Aucune délétion ou changement de paires de bases n'a été détecté dans des sites hors cible (off-target) prévus après comparaison dans la base de données du génome Ensembl. Les souris mutantes ont montré une santé générale comparable à celle des souris WT (pelage bien entretenu et posture corporelle normale, force musculaire, poids corporel de survie et fonctions locomotrices générales). La mesure de l'expression des transcrits par RT-ddPCR n'a montré aucune différence dans le niveau d'ARNm de *Scn9a* dans les DRG, la moelle épinière et le cerveau entre le mutant *Scn9a*^{R185H} et les souris témoins de deux sexes. Les souris

mutantes *Scn9a*$^{R185X/wt}$ exprime une faible quantité de *Scn9a*$^{R185X/wt}$ messager *Scn9a* par rapport aux témoins.

Pour déterminer si les souris mutantes *Scn9a*^{R185H} et *Scn9a*$^{R185X/wt}$ ont des phénotypes liés à la douleur, les souris mutantes ont été analysées dans des tests comportementaux de sensibilité aux stimuli thermiques et mécaniques à l'âge de 2 et 6 mois. À l'âge de 2 mois, la nociception thermique dans le test de Hargreaves est inchangée. Les souris femelles homozygotes *Scn9a*^{R185H} montrent une augmentation des réactions d'adaptation dans le test de la plaque chaude à 52 et 56°C, et une diminution de la latence du saut à 48, 52 et 56°C ainsi qu'une plus grande sensibilité dans le test de pression à la queue. Les souris mâles homozygotes *Scn9a*$^{R185H/R185H}$ montrent seulement des réactions d'adaptation augmentées à la plaque chaude à 56°C. Chez les souris mutantes porteuses de la mutation R185H, nous avons également détecté que les souris femelles hétérozygotes et homozygotes, ainsi que les souris mâles homozygotes, présentent une hypersensibilité significative au toucher dans le test des filaments de Von Frey. Cependant, à l'âge de 6 mois, les souris mutantes *Scn9a*^{R185H} hétérozygotes et homozygotes ont montré seulement une sensibilité à la douleur à la plaque chaude mais non pour les autres stimuli thermiques et mécaniques. Fait intéressant, nous avons trouvé un phénotype inverse chez des souris femelles mutantes *Scn9a*$^{R185X/wt}$ pour les stimuli thermiques de la plaque chaude. Les mécanismes qui sous-tendent les réponses à des stimuli douloureux distincts sont complexes et peuvent recruter plusieurs types de neurones afférents primaires.

Conclusion

Au cours de ce projet de doctorat, nous avons créé un modèle de souris pour la mutation *Scn9a*^{R185H} identifiée chez les patients douloureux souffrant de neuropathie à petite fibre grâce à l'approche CRISPR/Cas9 et nous avons étudié les conséquences sur la sensibilité à la douleur. Le modèle murin *Scn9a*^{R185H} a permis d'explorer l'association génotype-phénotype et le mécanisme de la mutation des canaux sodiques NAV1.7 et le modèle *Scn9a*$^{R185X/wt}$ d'explorer l'effet de l'inactivation d'un allèle du gène *Scn9a*. Ces deux lignées de souris n'ont montré aucune altération de la croissance, de la survie et de l'état de santé global. Nous avons montré qu'il n'y a pas de différence dans l'expression de l'ARNm de *Scn9a* dans les DRG (ganglions de la racine dorsale), la moelle épinière, le cerveau et le cervelet chez les souris *Scn9a*^{R185H}, et une diminution de l'expression chez les souris *Scn9a*$^{R185X/wt}$. La sensibilité à la douleur de ces nouvelles lignées de souris mutantes a été étudiée chez les deux sexes à l'aide de tests comportementaux de sensibilité aux stimuli thermiques et mécaniques. Nos résultats indiquent que globalement les souris *Scn9a*^{R185H} présentent un phénotype douloureux, suggérant que la mutation *Scn9a*^{R185H}

identifiée chez les patients SFN contribue à leurs symptômes douloureux. Ces résultats pourront servir à la recherche de nouveaux analgésiques. Les souris *Scn9a*$^{R185X/wt}$ sont moins sensibles à la douleur de type chaleur. Chez ces souris, un allèle Scn9a n'est pas fonctionnel. Par conséquent, nous avons montré par nos approches génétiques que le canal SCN9A joue un rôle crucial dans la nociception et dans les pathologies SFN douloureuses.

Publication and Oral Communication

Publications

1. Modeling the human *SCN9A*^{R185H} mutation found in patients with chronic pain using CRISPR/Cas9 in the mouse, consequences on pain sensitivity.

   Yaping Xue, Céleste Chidiac, Marie-Christine Birling, Claire Gavériaux-Ruff*, Yann Hérault*

   (**Under preparation**)

2. Pain Behavior in SCN9A (NAV1.7) and SCN10A (NAV1.8) mutant mice

   Yaping Xue*, Céleste Chidiac*, Claire Gavériaux-Ruff, Yann Hérault (*equal contribution)

   (**Submitted**)

Oral Presentations

Date	Place	Meeting	Author	Title
20/08/2019	Yale, USA	Secondment	Yaping Xue, Marie-Christine Birling, Claire Gavériaux-Ruff*, Yann Hérault*	Development and characterization of pain-related sodium channel CRISPR-Cas9 mouse model for *Scn9a*^{R185H} and *Scn9a*$^{R185X/wt}$
06/12/2019	FINCB, Milan, Italy	Secondment	Yaping Xue, Marie-Christine Birling, Claire Gavériaux-Ruff*, Yann Hérault*	Development and characterization of pain-related sodium channel CRISPR-Cas9 mouse model for *Scn9a*^{R185H} and *Scn9a*$^{R185X/wt}$
13/03/2020	Bordeaux, France	XVI^{ème} Symposium National du Réseau Français de Recherche sur la Douleur	Yaping Xue, Céleste Chidiac, Marie-Christine Birling, Claire Gavériaux-Ruff*, Yann Hérault*	A Pain-related Sodium Channel CRISPR/Cas9 Mouse Model for the Human *Scn9a*^{R185H} Mutation: Establishment and Behaviors

Poster Presentation

Date	Place	Meeting	Author	Title
26/09/2019	CERMB-IGBMC	33rd International Mammalian Genome Conference	Yaping Xue, Marie-Christine Birling, Claire Gavériaux-Ruff*, Yann Hérault*	Development and characterization of pain-related sodium channel CRISPR-Cas9 mouse model for *Scn9a*^{R185H} and *Scn9a*$^{R185X/wt}$
10/07/2020	Online	FENS 2020	Yaping Xue, Céleste Chidiac, Marie-Christine Birling, Claire Gavériaux-Ruff*, Yann Hérault*	Mice with the NAV1.7-*Scn9a*^{R185H} mutation show increased sensitivity to mechanical and thermal pain.

Abbreviations

Agrp: Agouti-related peptide neurons
AMs: A mechanonociceptors
ARC: arcuate nucleus
CCI: chronic constriction injury
CFA: complete Freund's adjuvant
CGRP: calcitonin gene-related peptide
CHEPs: contact heat-evoked potentials
CIP: congenital insensitivity to pain
cKO: conditional knockout
CNS: central nervous system
CRMP2: collapsing response mediator protein 2
DKO: double knockout
DPN: diabetic peripheral neuropathy
DRG: dorsal root ganglia
EMG: Electromyography
ESC: electrochemical skin conductance
fMRI: functional magnetic resonance image
GOF: gain-of-function
HDR: homology directed repair
HET: HETEROZYGOUS
HTMRs: high-threshold mechanoreceptors
IB4: isolectin B4
IEM: inherited erythromelalgia
IENFD: intraepidermal nerve fiber density
KO: knockout
LEPs: laser evoked potentials
LOF: loss-of-function
LTMRs: low-threshold mechanoreceptors
Nav: sodium channel isoforms
NCS: conduction study
NGF: nerve growth factor
NHEJ: non-homologous end joining
NPY2R: neuro peptide Y2 receptor
PAM: protospacer adjacent motif
PANs: primary afferent neuron
PBS: phosphate buffer
Penk: *Preproenkephalin*
PEPD: paroxysmal extreme pain disorder
PFA: paraformaldehyde
PNS: peripheral nervous system
pSNL: partial sciatic nerve ligation
QSART: quantitative sudomotor axon reflex test
QST: quantitative sensory testing
SFN: small fiber neuropathy
SNL: spinal cord ligation
SNT: spinal nerves transection
SUMO: small ubiquitin-like modifier
TRKA: nerve growth factor receptor
TRP: transient receptor potential channel
TTR: transthyretin
TTX: tetrodotoxin
VGSCs: voltage-gated sodium channels
WT: wild type

Table of Contents

I Introduction

1. Nociception and Pain

1.1 Nociception and Pain

Pain and nociception are different notions, and sensory neurons' activity cannot solely define pain. Pain has recently been revised by the International Association for the Study of Pain: An unpleasant sensory and emotional experience associated with, or resembling that associated with, actual or potential tissue damage, see Raja et al. 2020 [1]. Pain is known to contain sensory, emotional, and memory components. In contrast, nociception is defined as "the neural process of encoding noxious stimuli." The noxious stimuli encompass any stimuli, being thermal, mechanical, electrical, or chemical, that have the potential to damage tissue. There are four main events in the pain mechanism due to noxious stimulation, including transduction, transmission, modulation, and perception signals [2]. Transduction refers to the processes by which tissue-damaging stimuli activate nerve endings [3]. Transmission refers to the relay functions by which the message carries tissue injury to the brain regions underlying perception. Perception is the subjective awareness produced by sensory signals and integrates sensory messages into a coherent and meaningful whole. It involves attention, expectation, and interpretation.

Both the peripheral nervous system (PNS) and central nervous system (CNS) are involved in pain. PNS is composed of ganglia and nerves located outside the brain and spinal cord, and connecting our limbs and organs to the CNS. The CNS comprises the spinal cord and brain. It integrates and interprets the PNS signals, then coordinating all the activities in our body [4].

Today, most neuroscientists agree that some degree of specialization exists both peripherally and centrally, although many neurons are polymodal (that is, respond to more than one stimulus modality), and many have a broad dynamic range [5]. From the review by Prescott, Ma and De Koninck [5], two theories have been under debate, the Intensity theory and the Specificity theory. The specificity theory posited that perception depends on which single primary afferent neuron (PANs) subtype is activated and how much. The other theory is combinatorial coding posited that perception depends on what combination of PANs subtypes and activated and in what proportion [5]. Both theories required PANs specialization [5].

In the PNS, different types of primary sensory neurons commonly examined in pain pathophysiology studies are the large myelinated Aβ-fiber and the fine myelinated Aδ as well as small non-myelinated C-fiber. Their cell bodies are located in the dorsal root ganglia (DRG). Aβ-fibers typically convey innocuous tactile stimuli but have been shown to generate ectopic action potentials (APs) in some chronic pain models and are known to contribute to the development of tactile allodynia. The majority of Aδ and C-fibers are nociceptors or thermoreceptors. C-fibers typically convey noxious stimuli. Different subtypes of C-fibers exhibit different profiles of activity-dependent velocity changes. Cutaneous C-fibers classified based primarily on their activity-dependent slowing profile, including Type1A (mechano-responsive nociceptors), Type1B (mechano-insensitive nociceptors), Type2 (cold units), Type3 (unknown function), or Type 4 (presumed sympathetic) [6]. C-fibers' peripheral sensitization may generate aberrant action potentials at the site of a neuroma or tissue damage in some chronic pain conditions.

The spinal and medullary dorsal horns are the first central relay for the first neurons in DRGs inputs innervating the extracephalic and trigeminal areas. In general, myelinated low-threshold mechanoreceptive afferents, Aβ-fibers, arborize in an area extending from lamina IIi-VI (Figure 1.1) [7]. Whereas, unmyelinated C afferents and fine myelinated Aδ sensory afferents that transmit pain, itch, and temperature primarily terminate in laminae I/II, as well as lamina V and other more ventral laminae (Figure 1.1). Recently, the neuron populations in the DRGs and dorsal horn have been classified based on transcriptomic and transduction analyses [8-11].

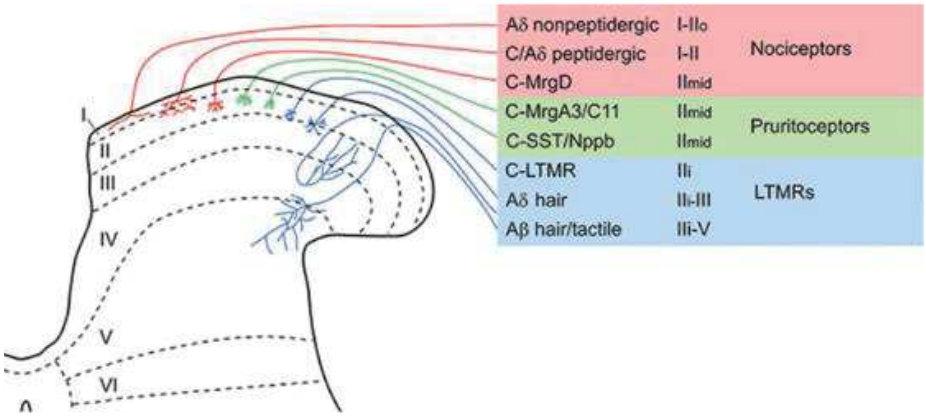

Figure 1.1 Central projections of different classes of primary afferent. The major classes of primary afferent that have been identified in recent transcriptomic studies [12, 13] are listed, together with what is currently known about their functions and their central terminations in the spinal dorsal horn. Note that pruritoceptive afferents may also function as nociceptors, and that the C-MrgD nociceptors may act as pruritoceptors. Afferents that respond to innocuous cooling or warming appear to be poorly represented in these studies and are therefore not included in this scheme. A figure taken from Wood, John N. et al., 2020 [7].

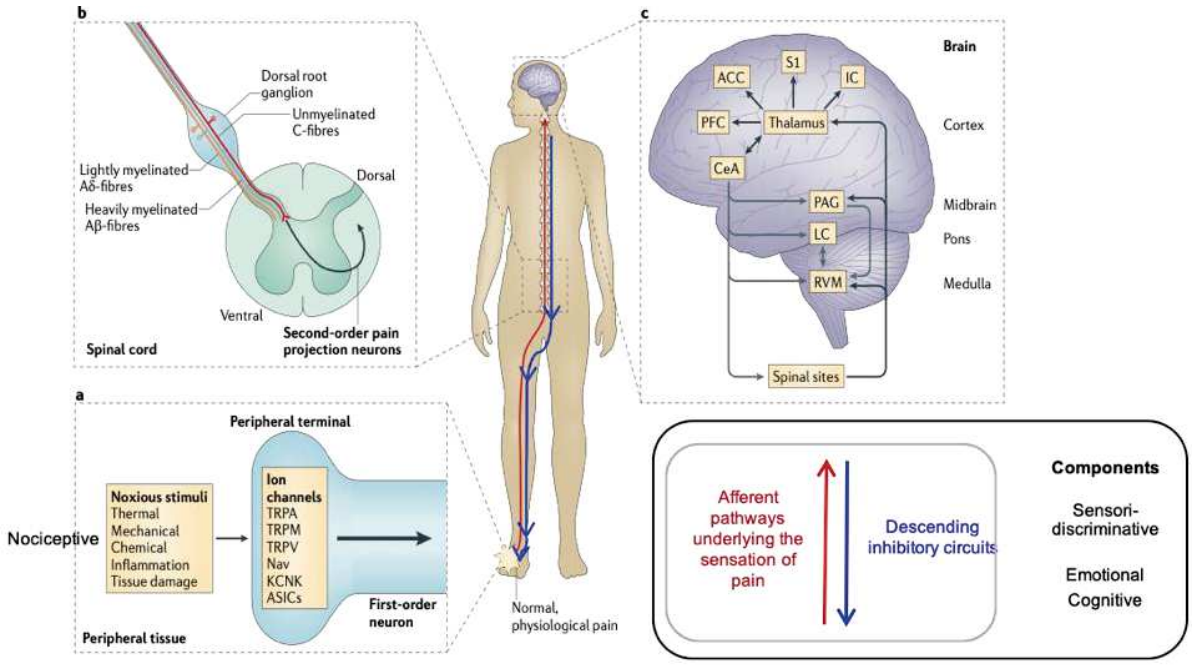

Figure 1.2 Physiological pain processing. **A)** Nociceptive signals are transmitted from the periphery by sensory neurons (first-order primary afferent neurons) the peripheral terminals of which clustered with ion channels, including transient receptor potential channel subtypes (TRPA, TRPM, and TRPV), sodium channel isoforms (Nav), potassium channel subtypes (KCNK) and acid-sensing ion channels. The transduction of external noxious stimuli is initiated by membrane depolarization due to these ion channels' activation. **B)** Action potentials are conducted along the axons of nociceptive Aβ- and C-fibers, through the cell body in the dorsal root ganglion to the axonal terminals, which form the presynaptic element of central synapses of the sensory pathway in the spinal dorsal horn or hindbrain. The central terminals of Aβ- and C- fibers synapse with interneurons and second-order nociceptive projection neurons, primarily within the spinal dorsal horn's superficial laminae. The axons of second-order nociceptive projection neurons decussate at the spinal cord level, joining the ascending fibers of the anterolateral system, and project to the brainstem and thalamic nuclei, transferring information about the intensity and duration of peripheral noxious stimuli. **C)** No single brain region is essential for pain, but pain results from the activation of a distributed group of structures. Third-order neurons from the thalamus project to several cortical and subcortical regions (black arrows) that encode sensory-discriminative (for example, the somatosensory cortex (S1)), emotional (for example, anterior cingulate cortex (ACC), amygdala (CeA) and insular cortex (IC)), and cognitive (for example, the pre-frontal cortex (PFC)) aspects of pain. Several brainstem sites are also known to contribute to the descending modulation of pain (grey arrows), including the periaqueductal grey (PAG), locus coeruleus (LC), and rostral ventromedial medulla (RVM). A figure taken from Grace, P. M. et al., 2014 [14].

Typically, noxious stimuli activate nociceptors, a subset of peripheral sensory neurons, which have a range of specialized ion channels and receptors that transduce noxious stimuli into electrical signals (action potentials), transmitting information to the dorsal horn of the spinal cord. From spinal cord, the nociceptive information is then transmitted to the brain; This is the pain ascending pathway (Figure 1.2). And the signals sent down from the brain to the reflex organs

through the spinal cord are defined as the descending pathway (Figure 1.2) [15]. In human patients, a distinction is made between stimulus-evoked pain and spontaneous pain. However, pain cannot be directly measured in animals. Instead of a direct pain measurement, pain is evaluated by using "pain-like" behaviors, such as withdrawal from a nociceptive stimulus, which is the most commonly used method to quantify nociception in animal studies [16].

1.2 Heat Stimuli

In animal studies, responses to heat stimuli typically are determined using tail flick, hot plate, and Hargreaves plantar tests. The tail-flick test and Hargreaves plantar induce a radiant heat stimulus, with a focused beam of light applied to the tail or hind paw, respectively. The tail or hind paw withdrawal responses are also used. They are pain-like behaviors involving spinal reflexes and controls by higher brain centers [16]. The hot plate test uses heat stimuli to the hind paws and is known as a more integrated test [17]. Classically, the response latency is the time taken to observe a nocifensive behavior recorded by the investigator. Additionally, diverse coping behaviors can happen, including flicking, licking, withdrawal, stamping, jumping of the hind paw. In addition, the number and time spent on coping behaviors can also be counted. Different parameters can be analyzed for the hot plate at a specific temperature within a cut-off time [18, 19]. Depending on the species and strain of rodents used in the hot plate test, some of these coping behaviors can be sensitive to analgesics, and also show differences depending on the type of behavior quantified.

It is plausible that behavior differences may relate to the type of sensory fiber activated [16]. Classical work using single-unit electrophysiological recordings has shown two major groups of thermally sensitive afferent neurons; thinly myelinated Aδ fiber and unmyelinated C-fibers [20]. In anesthetized rats, steep temperature gradients and high skin temperatures are associated with activation of Aδ fibers, while slower heating and lower temperatures will predominantly activate C fibers [16]. Histological analysis has shown that thermally sensitive afferent neurons project predominantly to laminae I and II (LI/II) of the dorsal horn of the spinal cord [21][21][21][21] (Figure 1.3).

The molecular transducers of noxious heat have been studied in mice and rats based on these behavioral tests described above. Several temperature-sensitive members of the transient receptor potential channel (TRP) family of ion channels were identified [22]. TRPV1 is expressed in a subset of nociceptive, small-diameter neurons in DRGs and trigeminal ganglia. The heterologous expression of TRPV1 not only results in capsaicin-gated currents but also revealed that TRPV1

responds to various noxious stimuli, including noxious heat, acidic, and basic solutions [20]. TRPV1 activated at noxious temperatures (>43 °C), but how its activation leads to innocuous warming responses is unclear. Other three closely related members of the TRPV subfamily, TRPV2, TRPV3, and TRPV4, were also studied as potential candidates for thermosensation [23]. TRPV2 has been a candidate for a high-threshold molecular sensor of noxious heat as the heterologous expression of rodent TRPV2 produced a cation current that activated at temperatures exceeding 52°C. However, one study reported that genetic ablation of TRPV2 in mice could not reduce the acute pain response to noxious heat or on inflammatory heat hyperalgesia, suggesting that TRPV2 is not a key thermosensor in the somatosensory system [24]. The behavior in TRPV3 or TRPV4-deficient mice showed significant abnormalities in thermal preference in the warm temperature range. Particularly, TRPV4-deficient mice preferred warmer floor temperatures on a thermal gradient, whereas TRPV3-deficient mice showed a relative indifference to temperatures ranging from 20 to 35 °C [25]. However, more recent studies indicated that the alteration in temperature preference in TRPV3-deficient mice is highly dependent on the genetic background and sex of the mice. A recent study also indicated that TRPM3 was identified as an alternative noxious-heat sensor in a large subset of sensory neurons, including nociceptors, from DRGs and trigeminal ganglia [26]. Interestingly, when heterologous expressed TRPM3 is activated by heating, the current–temperature relationship curve is shifted slightly towards higher temperatures than with TRPV1. TRPM3 knockout mice displayed deficits in avoidance responses to noxious heat and the development of heat hyperalgesia in inflamed tissue [26]. Nevertheless, pharmacological inhibition of TRPV1 in TRPM3-deficient mice did not fully abrogate avoidance responses to noxious heat, implying the existence of additional mechanisms for sensing noxious heat. Temperature-dependent excitation of a sensory neuron depends not only on the activation of a depolarizing current, which causes depolarization of the sensory nerve ending (the receptor potential), but also the combination of potassium channels and voltage-gated sodium channels that together set the threshold voltage for the generation of action potentials. More detailed information regarding molecular thermosensation can be found in the review by Vriens, J. [24]

1.3 Cold Stimuli

The sensation of cooling is essential for survival, with animals evolving multiple strategies to mitigate, avoid, and escape low temperatures. Extreme cold is experienced as pain because cold is a noxious stimulus that causes profound, irreversible tissue damage at temperatures above and below freezing. In chronic pain, cold allodynia is a maladaptive and inappropriate response of the

nociceptive sensory system to mild cooling, a common complaint of people suffering from neuropathic pain. Compared to other stimulus modalities, the cold sensation is trickier to study in mice. In animal studies, the cold plate test is one of the simplest assays to determine behavioral responses to both noxious and innocuous cold temperatures [16]. However, the literature's latencies range from 5 to 200 s for a plate held at 0 °C. Similar results were also observed in our two mutant mice. The acetone test is a technique used to measure cold allodynia. In this test, aversive behaviors are triggered by evaporative cooling to the skin with innocuous temperatures of 15-21 °C. Of note, the actual temperature varies with ambient temperature, skin temperature, and acetone amount [16].

Cool stimulus activates thinly myelinated Aδ fibers tuned to cool temperatures, and unmyelinated C fibers tuned to cold temperatures but partially activated at cool temperatures [5]. Cold-sensing afferents encompass different poly- and unimodal, small and large fiber types. Low-threshold thermoreceptors respond to mild cooling, while high-threshold cold nociceptors are activated by extreme cold. Low-threshold cold thermoreceptors are usually unimodal as the cold nociceptors also fire in response to noxious heat and mechanical stimuli [27]. The DRG neurons that detect cooling project mainly to the dorsal horn's superficial laminae, including layers I, II, and III (Figure 1.3) [11].

The non-selective cation channel TRPM8 has been studied in detail in the cold transduction, which expresses mainly in small-diameter sensory neurons, akin to the C fiber cold thermoreceptors. Deletion of *Trpm8* reduced avoidance behavior for temperatures between 30 °C and 15 °C on the thermal place preference test and a loss of firing in sensor afferents to low-threshold cooling stimuli in mice [27, 28]. However, avoidance of noxious cold is preserved in *Trpm8* KO mice, suggesting *Trmp8* is required for low-threshold cooling stimuli, but that another transducer is required to detect high-threshold cold stimuli [29]. Intracellular recordings of dorsal root ganglia revealed numerous TRPM8-negative cold afferents among all fiber classes. *Trpa1* is directly activated by cooling below 10 °C in recombinant systems and controlling the sensation of painful cold [30]. However, the channel is promiscuous and integrates numerous noxious stimuli, including force, heat, inflammatory mediators, and pungent compounds [27, 31]. However, understanding of cold transduction still needs further studies, especially a deeper exploration of noxious cold transducers.

.

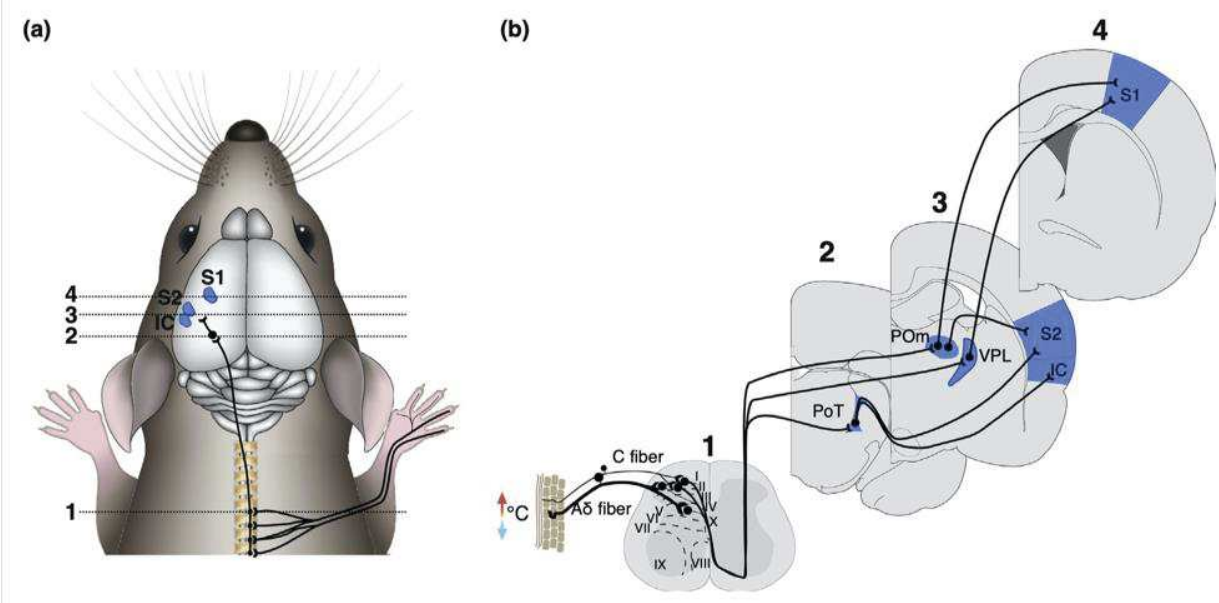

Figure 1.3 Putative thermal pathways from paw to cortex in mice. (a) Cartoon mouse showing putative thermal pathways from the skin to the cortex via spinal cord and thalamus, the primary somatosensory cortex (S1), the secondary somatosensory cortex (S2), and insular cortex (IC). The thermal pathway via the lateral parabrachial nucleus to the hypothalamus is not included. (b) Schematic cross-sections of the mouse nervous system are taken at different levels with numbers corresponding to locations (a). Thermal thalamic input to S1 is provided by ventral posterolateral (VPL) and posterior medial (POm), to S2 by POm and the posterior triangular nucleus (PoT), and IC by PoT. A figure taken from Bokiniec, P. et al., 2018 [20].

1.4 Mechanical Stimuli

Mechanical sensitivity can be divided into sensitivity to dynamic, punctate, and static stimuli [32]. Dynamical mechanical allodynia and hyperalgesia can be assessed by brushing the skin with a cotton bud, paintbrush, or cotton ball [32]. In the case of clinical allodynia, allodynia can be evoked by contact of clothing, bedsheets, or towels against the skin. Punctate mechanical allodynia and hyperalgesia can be triggered by touches, such as pinprick or monofilament, and can assess by applying von Frey filaments of varying forces. Static hyperalgesia can be superficial or deep and assessed by applying pressure to the skin or underlying tissue with a finger or using a pressure algometer [16, 32]. In rodent models, manual Von Frey is the gold standard for determining mechanical thresholds in mice, in parallel to the development of electronic Von Frey tests. One weakness of the Von Frey is that it is difficult to distinguish responses to innocuous versus noxious mechanical stimuli. The Randall-Selitto test is used for evaluation of mechanical hyperalgesia by applying a pressure on the paw or tail. This test is considered as a direct measure of mechanical nociception.

Nocicensive response to high-threshold Von Frey is predominantly mediated by A-fibers, whereas a subtype of C fiber, the MRGPRD+ unmyelinated free nerve endings (primarily nonpeptidergic nociceptors) required for normal Von Frey thresholds in mice. Thus, both C and A-fibers likely transduce the mechanical stimuli by Von Frey. C fibers are the primary mediators of nocifensive behaviors in paw pinch and tail clip assays, such as the Randall-Selitto test. Additionally, ablation of C fibers decreased both mechanical allodynia and hyperalgesia induced by injury and inflammation [33].

A-Mechano-nociceptors (AMs) are the main peripheral nerve fibers that transduce noxious mechanical stimuli. Studies have defined subsets of mechanonociceptors, including fast-conducting AMs and slow-conducting C nociceptors, as well as innocuous touch receptors that interact with the mechanical pain pathway. Depending on the difference in conduction velocity and firing patterns of fibers responding to mechanical stimulation, mechanoreceptors can distinct into two subtypes, high-threshold mechanoreceptors (HTMRs) and low-threshold mechanoreceptors (LTMRs) (Figure 1.4). AMs are the main class of HTMR and are typically lightly myelinated A-fibers thought to terminate as free nerve endings in the epidermis and dermis. A recent study by Ghitani and colleagues described an anatomically and functionally distinct subset of AMs, the lightly myelinated Aδ-high threshold mechanoreceptors (HTMRs) that express the calcitonin gene-related peptide (CGRP) transcript encoded by the *Calca* gene [34]. These fibers form circumferential endings around guard hair follicles and mediate responses to noxious hair pull, but the function in glabrous skin is unknown, as these fibers represent a specialized class of hairy skin receptors. The paper by Hill and Bautista has reviewed on the cells and molecules involved in touch and mechanical pain. They report that in glabrous skin, the Neuropeptide Y2 Receptor (NPY2R)-positive neurons constitute a subset of AMs [35]. In the paw glabrous skin, $NPY2R^+$ fibers were found to be required for proper timing of withdrawal responses to pinprick stimulation. However, a previous study indicated that NPY2R marks lanceolate guard hair nerve endings, a subset of Aβ-LTMRs innocuous touch receptors in the hairy back skin. Later, it was observed that NPY2R marks a mixed population of both AMs and Aβ-LTMR in the hairy skin, but only AMs in the glabrous skin. The $NPY2R^+$ AMs interact with a newly uncovered population of Aβ-LTMRs marked by expression of the transcription factor MAF-A to coordinate withdrawal responses to noxious mechanical stimuli. This finding suggested that Aβ-LTMRs are not only to mediate innocuously but also noxious mechanosensation.

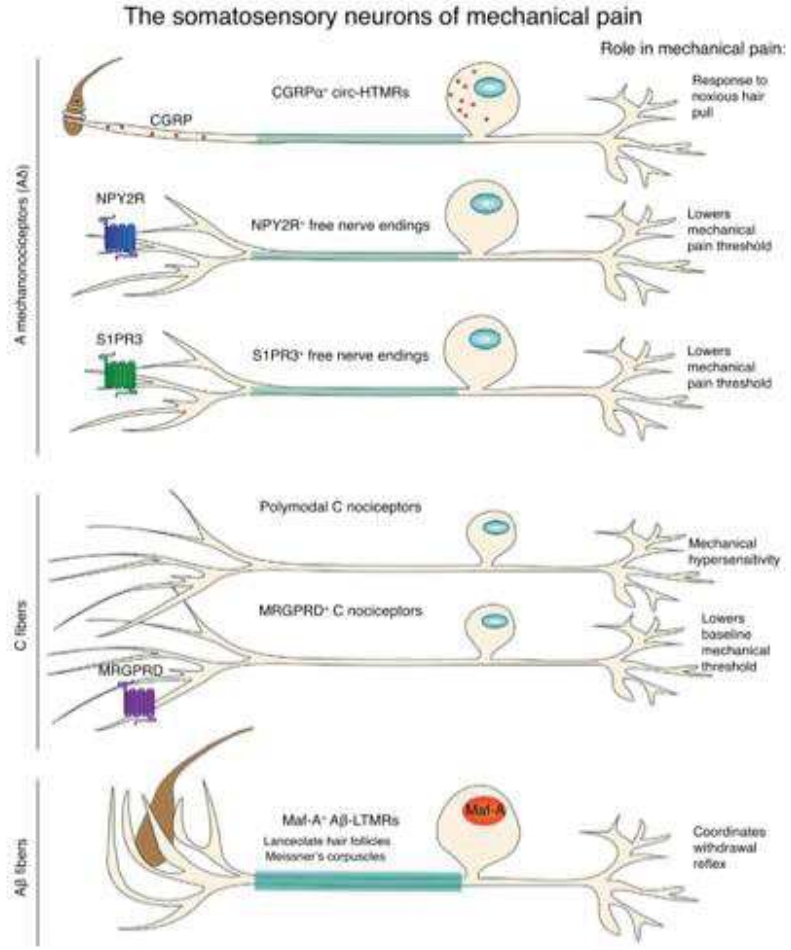

Figure 1.4 Subpopulations of Mechanical Pain-Sensing Neurons. Cartoon depicting recently described subclasses of somatosensory neurons that interact with the mechanical nociception pathway. Abbreviations: CGRP, Calcitonin gene-related peptide; HTMR, high threshold mechanoreceptor; LTMR, low threshold mechanoreceptor; NPY2R, Neuro Peptide Y 2 Receptor; S1PR3, sphingosine 1-phosphate receptor 3. A derived figure from Hill, R. Z. et al., 2020 [35].

Molecular transducers of noxious mechanical force have been definitively identified only in invertebrate model organisms, including the nematode C. elegans and the fruit fly Drosophila melanogaster. The transduction molecules identified include the degenerin/Epithelial Sodium Channel (DEG/ENaC) DEG-/MEC-4 in worms, and the TRP channel *painless* along with the mechanosensitive channel *piezo* in flies. Later, the mammalian homologs of these channels were found, that play similar roles in mammals. However, studies by multiple labs have shown that these proteins do not play wholly analogous roles in mammals.

Several studies demonstrated that PIEZO2 is a mechanotransducer. Interestingly, complete deletion of PIEZO2 from the entire caudal region of the mouse using the Hoxb8-Cre line led to

reduced the response to Von Frey filaments with minor effect on pinprick responses [35, 36]. Deleting PIEZO2 in somatosensory neurons used *Advillin*-Cre, reduced innocuous, but not noxious, mechanosensation [37]. As a novel ion channel, TACAN has been identified contributing to mechanosensitive currents in nociceptors and detecting mechanical pain stimuli [38]. This observation expands the understanding of molecular pain mechanism, and further study on conductance, ion selectivity, ion-permeation pathway, and force-activation mechanisms would explore the more detailed mechanism of TACAN-dependent mechanical pain [39].

Recent work has identified that different spinal neurons are involved in mechanonociception and persistent mechanical pain, such as dynorphin-positive (dynorphin$^+$) neurons, VGLUT3$^+$ spinal neurons, and somatostatin$^+$ neurons. Dynorphin$^+$ interneurons gate the input of Aβs onto the somatostatin +neurons to prevent innocuous stimuli from being perceived as painful. VGLUT3$^+$ spinal neurons at the lamina III can receive A β fibers input, and VGLUT3$^+$ at the lamina II/III border do not receive C fiber input. The role of somatostatin$^+$ neurons, which make up a large proportion of excitatory lamina II cells, remained mysterious until a recent study by Huang and colleagues demonstrated that they are indeed a heterogeneous population with multiple roles in itch and pain (Figure 1.5 A) [35, 40]. Spinal projection neurons marked by TAC1 are downstream in the pain circuit and drive conditioned place aversion and persistent pain behaviors following skin pinching and these 'sustained coping' TRPV1$^+$ primary afferents mediate these behaviors. By contrast, von Frey-evoked acute withdrawal reflexes ('defensive' behaviors) are mediated by TAC1 projection neurons that receive input from MRGPRD + primary sensory neurons (Figure 1.5 B). Taken together, nociceptive and non-nociceptive circuits interact extensively at the level of the spinal cord.

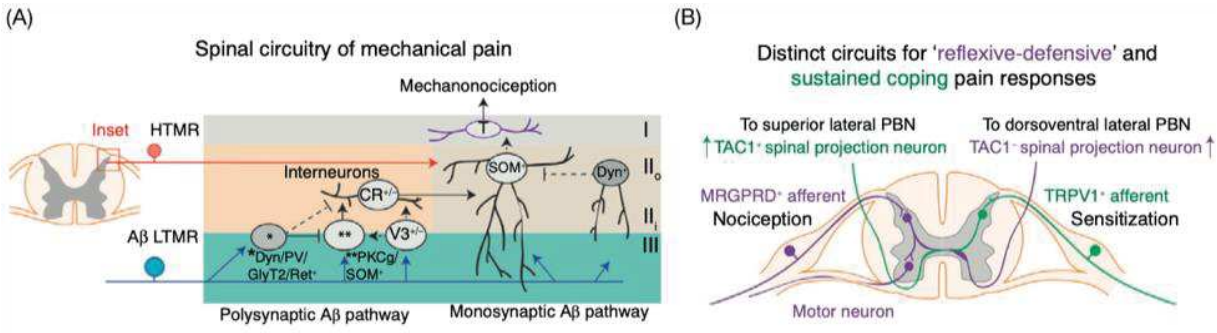

Figure 1.5 Spinal Circuitry of Mechanical Nociception. (A) Diagram of the circuitry of mechanical pain. (B) Circuit diagram of coping and nocifensive behaviors. Abbreviations: CR, Calretinin; Dyn, dynorphin; GlyT2, glycine transporter 2; HTMR, high threshold mechanoreceptor; LTMR, low threshold mechanoreceptor; PBN, parabrachial nucleus; PKCg, protein kinase C gamma; PV, parvalbumin; SOM, somatostatin; T, transmission neuron; V3, VGLUT3. A copied figure from Hill, R. Z. et al., 2020 [35].

2. Small Fiber Neuropathy (SFN)

Small fiber neuropathy (SFN) defines as a structural abnormality of small fibers (thin myelin sheath - Aδ and without myelin - C fibers) characterized pathologically by the degeneration of the distal and small endings of the fiber nerve. These fibers are responsible for mediating temperature and pain sensations and the control of autonomic functions; they build up to 80-90% of the peripheral nerves. SFN is common, and it can negatively impact the quality of life due to neuropathic pain and autonomic symptoms. It can be associated with many causes. Here, we will briefly introduce the causes, utility of diagnostic tests, and the clinical presentation of SFN.

2.1 Clinical Presentation

The clinical presentation of SFN is heterogeneous. SFN often negatively impacts the quality of life both physically and mentally due to the annoying neuropathic pain and autonomic symptoms caused by the disease. Prevalence of SFN is 52.95 cases per 100,000 people, and diabetes and idiopathy are the most common etiologies [41]. SFN is characterized by the typical symptoms mostly appearing on the extremities' distal part (burning feet and numb toes) and progressing upwards, and therefore called length-dependent (Figure 1.6 A) [42]. The non-length-dependent SFN is relatively rare, accounting for 20-25% of pure SFN (Figure 1.6 B) [43]. The sensory symptoms and signs in non-length-dependent SFN are usually patchy, asymmetric, migrating, or diffuse, and often involve the trunk and face in addition to the limbs [43]. Patients suffering from SFN usually develop somatic symptoms, which include allodynia (nonpainful stimuli perceived as painful), hyperalgesias (painful stimuli perceived as more painful than expected), reduced pinprick and thermal sensation in the affected areas, burning, tingling, and numbness [44]. They may also report a squeezing sensation, coldness, or itchy skin in the affected areas. The symptoms are usually worse at night. Autonomic symptoms at least are present in nearly half of the patients with SFN. Autonomic disturbances include dry eyes and mouth, abnormal sweating, sexual dysfunction, altered gastrointestinal motility and bladder control, abnormal heart-rate variability, and orthostatic issues such as hypotension and tachycardia [43].

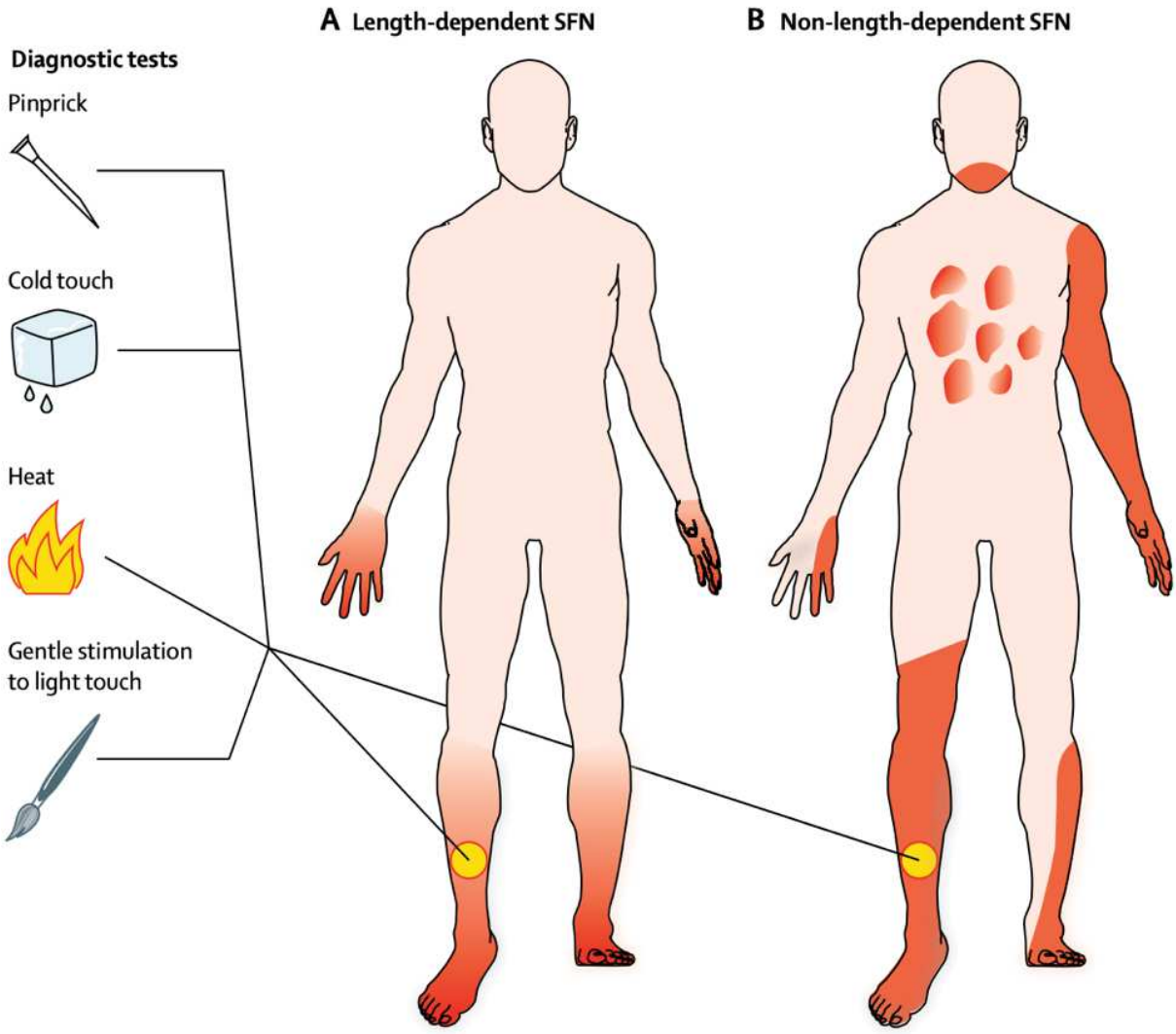

Figures 1.6 A patient with typical length-dependent polyneuropathy. might have pain, sensory loss, or hypersensitivity to cold, warm, light touch, or pinprick in a characteristic stocking-glove distribution, with intact deep tendon reflexes and preserved proprioception sensation to vibration. A patient with patchy non-length-dependent neuropathy. **B)** might have either reduced or increased small fiber function corresponding to single or multiple nerves. Derived from Terkelsen, A. J. et al., 2017 [44].

For more detailed discussion concerning these clinical aspects, please refer to the following references: Devigili, G. et al., 2020 [42]; Ghasemi, M. et al., 2020 [45]; Devigili, G. et al., 2019 [46]; Zhou L., 2019 [43]; Sene, D. 2018 [47]; Cazzato, D. et al., 2017 [48]; Terkeisen, A.J. et al., 2017 [44]; Terkeisen, A.J. et al., 2014 [49]; Hoeijmakers, J.G. et al., 2012 [50].

2.2 Diagnostic

2.2.1 Clinical Evaluation

The diagnosis of distal SFN is based on clinical symptoms, examination and specific tests. Peripheral autonomic dysfunction can be observed at bedside examination at the beginning, such as skin discoloration, dry skin, and dystrophic changes. Possible SFN is classified as the presence of length-dependent symptoms and/or signs of small fiber damage and regular sural nerve conduction study (NCS). Next, the definitive SFN is defined as low intraepidermal nerve fiber density (IENFD) (Figure 1.7) at the ankle and/or abnormal quantitative sensory testing (QST) thermal thresholds in the foot. The quantitative sudomotor axon reflex test (QSART) and cardiovascular autonomic testing may also evaluate autonomic symptoms when present [42, 47].

2.2.2 Diagnostic Tools

Routine neuroconduction study (NCS) is a valuable test for evaluating large fiber neuropathy. In contrast, the conduction velocities of small nerve fibers are too slow to be captured by routine NCS. Electromyography (EMG) is a tool to measure motor nerve fibers' function, generally large fibers. Therefore, NCS and EMG cannot detect the damage of small fiber. However, it is crucial to do NCS/EMG firstly to rule out a large fiber polyneuropathy [42].

Skin biopsy is the gold standard for diagnosing SFN. It is an office procedure, easy to perform, and minimally invasive. Skin punch biopsy of the distal leg is very well tolerated with a low complication rate. Briefly, a 3 mm diameter skin punches biopsy is collected from the distal leg and intraepidermal nerve fiber density (IENFD) is determined by staining of the protein PGP9.5. The IENFD is defined as the number of fibers that cross the dermal-epidermal junction per epidermal surface. A SFN is diagnosed when IENFD is smaller than the fifth centile relative to age and gender-matched controls [51].

Corneal confocal microscopy is a non-invasive method able to examine the microstructures of the living eye in situ, at the cellular level. Corneal confocal microscopy allows visualizing unmyelinated C fibers coming from the ophthalmic division of the trigeminal nerve [52]. A correlation between low corneal nerve fiber density has been described in SFN [42].

Abnormal mechanical and/or thermal threshold is assessed by Quantitative Sensory Testing (QST). It is an extension of the bedside clinical examination of the somatosensory system. However, the QST cannot differentiate between peripheral and central causes of a sensory deficit. Additionally, QST measurements are affected by several factors, including the training of both

examiner and patients, the methodology assessment, the location and number of stimulus sites, and baseline skin temperature. Thus, the different measures of SFN diagnostic are essential for identifying or raising suspicion for certain SFN cases [48].

Microneurography uses recording with microelectrodes placed within nerve fascicles and records simultaneously the activity of single C-nociceptors, thermoreceptors, mechanoreceptors, and sympathetic fibers from peripheral nerves in awake subjects. Microneurography can detect abnormal C-nociceptor activity in SFN patients. However, there is a limitation as the application requires both an expert investigator and a collaborative patient and takes time to perform the exam [53].

Laser evoked potentials (LEPs) and contact heat-evoked potentials (CHEPs) are recorded in the brain following the application of painful stimuli to the skin. CHEPs based on age- and gender-adjusted normative values have investigated SFN showing a good correlation with the degree of skin innervation. However, CHEPs can be absent also in healthy individuals. Recently, cool-evoked potentials have been a valuable method to study the Aδ- fiber free nerve endings and spinothalamic pathway; however, the diagnostic value in SFN has not been investigated [49].

Autonomic testing is helpful to evaluate SFN patients as dysfunction of small nerve fibers can cause sensory and autonomic symptoms. Several techniques have been standardized to quantify sweat output and the innervation of sweat. QSART is a sensitive and reproducible technique to measure sweat output in response to acetylcholine, reflecting the function of postganglionic sympathetic unmyelinated sudomotor nerve fibers [42]. Cardiovascular autonomic testing is useful to evaluate patients with cardiovascular autonomic symptoms associated with SFN, such as orthostatic intolerance, palpitations, and tachycardia [43]. Electrochemical skin conductance (ESC) is a non-invasive measurement that depends on the electrochemical reaction of the chloride component of sweat with stainless steel metal across a spectrum of transcutaneous current. The resulting measurement is proportional to the cutaneous sweat glands' density containing functional chloride channels [54]. Recently Fabry et al. [54] have evaluated a combination of six tests, including skin biopsy for IENF density, LEPs and QST for sensory fibers, and ESC, quantitative sweat measurement system (Q-sweat) and autonomic cardiovascular test for autonomic C fibers. Their study showed that the best combination of tests to diagnose SFN comprises skin biopsy, LEPs, ESC, and QST.

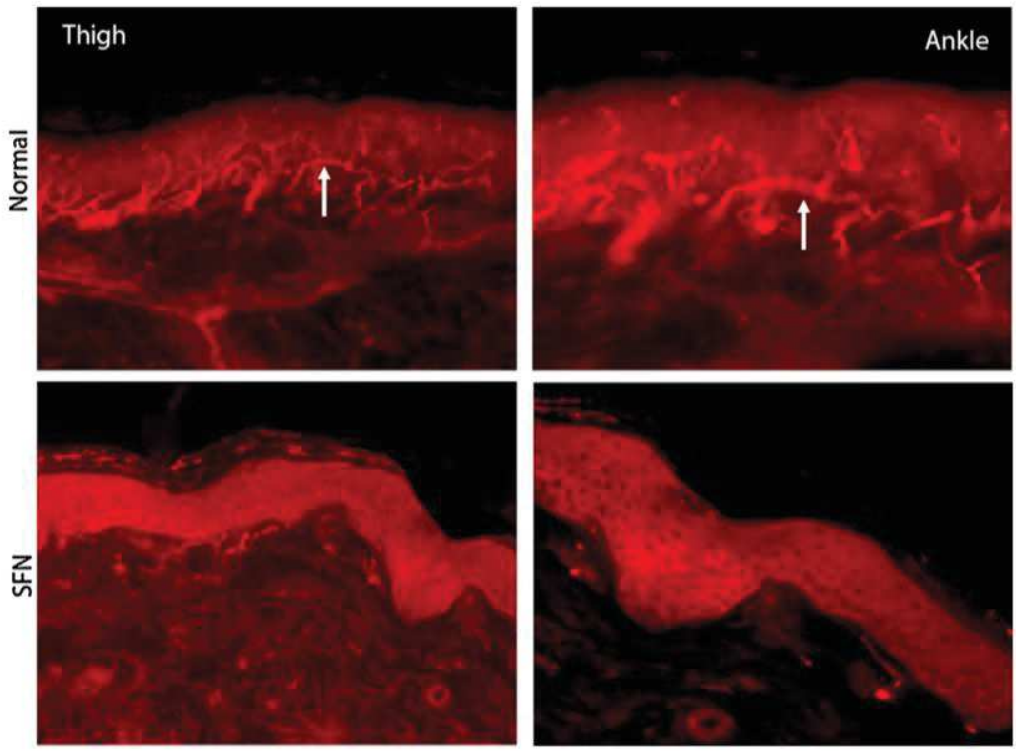

Figures 1.7 Skin biopsy labeled with anti-PGP9.5 to identify the intraepidermal nerve fibers (in red): note the difference in intraepidermal nerve fiber density at the ankle and thigh between a normal individual and in a patient with SFN. A copied figure from Sene, D. et al., 2018 [47].

There are few modern series of diabetic neuropathy confirmed by nerve tissue that were obtained by biopsy or postmortem examination available to allow clinicopathological correlation of the different neuropathic syndromes. One report presented the clinicopathological assessment of 107 patients with diabetes mellitus and peripheral neuropathy were identified from 1992 to 2002 at the New York-Presbyterian Hospital and New York University Langone Medical Center [55]. sural nerve inflammation and demyelination have been found in some patients, which may indicate an underlying autoimmune etiopathogenesis [55]. However, the spectrum of diabetic neuropathies is large, and our knowledge of these entities continues to evolve. There can be nerve damage from metabolic injury, compressive injury, ischemic injury, and altered immunity, and these varied pathologies can present in many different ways. The pain symptoms in SFN patients vary, maybe as the pathogenesis of small nerve neuropathy is variable. In order to do treatment, the physician needs to be able to make the correct diagnosis first, before starting the appropriate therapy. Unfortunately, there was no nerve biopsy study in SFN patients carrying *SCN9A* mutations. Nevertheless, in CIP patients with loss-of-function *SCN9A*, the sural nerve's nerve biopsy showed a

normal sensory nerve with all verve fiber types present, normal morphology, and normal distribution by light and electron microscopy [56]. This observations seems to distinguish CIP not due to *SCN9A* mutations, which may be due to other causes, for example, nerve growth factor (NGF) mutations [57], resulting in severe developmental degeneration of nociceptors. Further fiber neuropathy information from SFN/CIP patients will provide accuracy in pathogenic epidemiology and orient for a more precise therapy.

Diabetic neuropathy has been studied in mouse models, and some mechanisms also have been explored. There are three main approaches to establish mouse models of diabetic neuropathy: nutritional induction, genetic modification, and chemical induction [58]. In the nutritional induced type 2 diabetic neuropathic pain model, mice develop prediabetes symptoms and present signs of neuropathy, including decreased sensory nerve conduction velocity [59]. In mutation of leptin mice, widely investigated to establish type 2 diabetes animal models, also present impaired motor and sensory nerve conduction velocity and abnormal nerve morphology [58]. However, the type of mouse strain was noted to affect the development of neuropathy in this model. C57BKS strain is more stable in hyperglycemia, and neuropathy is more severe than C57BL/6 strain [60, 61]. In one study of STZ-induced type 2 diabetic mice, there were no apparent abnormalities in the morphology of the myelinated and unmyelinated axons and neuromuscular junctions [62]. However, another study showed that diabetic muscle spindle Ia fibers have high variability in their axonal width and mean interrogational distance [63]. Although the diabetic mice mainly displayed a significant decrease in large fibers, the diabetic mice also significantly increased small fibers, which could be associated with regenerating axons [64].

2.3 Causes

Many causes can induce SFN. They fall into five main groups: metabolic (metabolic syndrome, vitamin deficiency), toxic (intoxication with neurotoxics and medications), inflammatory, infections, and genetic [47]. Also, geographic location, ethnicity, and environmental factors are factors influencing the occurrence of SFN. Even after an intensive search for underlying causes of SFN, there remains some patients with no identified cause, and the SFN is this qualified as idiopathic SFN.

Metabolic syndromes consist of hypertension, glucose dysmetabolism, dyslipidemia, or central obesity [65]. Diabetes is the most common metabolic cause of SFN. In diabetes, SFN can be present and diagnosed earlier than a metabolic syndrome, or it might occur acutely, as treatment-induced neuropathy caused by fast glycemic diabetic regulation. Some SFN cases are associated with infections. The most well know is HIV and antiretroviral therapy. The alcohol toxicity, thallium

poisoning, neurotoxic agents' exposure, and chemotherapeutic agents may induce SFN. SFN may also be present in some inflammatory and immunological disorders [42].

The genetic cause of SFN emerged after discovering gain-of-function (GOF) mutations in the *SCN9A* gene encoding for the sodium channel NAV1.7 a-subunit [66]. The *SCN10A* and *SCN11A* genes also encode sodium channels (see below) and mutations of theses gene have been found in SFN patients with chronic pain [66, 67]. Also, mutations in the transthyretin (*TTR*) gene have been found in familial amyloidosis and mostly affect both large and small nerve fibers [68]. Besides, Fabry disease is an X-linked lysosome disorder that can cause SFN. However, a recent study on adult patients showed that the association of Fabry disease with SFN is extremely low [69].

2.4 Treatments

SFN patients commonly suffer from chronic pain and autonomic symptoms. There are two main directions for SFN treatment: interventions to address either the origin of the neuropathy or/and the management of symptoms. Based on the etiology of SFN, a therapy to correct metabolic or hormonal imbalance, to suppress the vitamin/mineral deficiency, to eliminate the toxic agent or to treat infectious disease can be proposed to the patients [47].

The management of symptoms mainly focuses on painful sensory symptoms and autonomic symptoms. The treatment for neuropathic pain is still a challenging task in the clinic [70]. Opioids, tricyclic antidepressants (amitriptyline, nortriptyline) and antiepileptic drugs are used as recommended drug for neuropathic pain and have been proven effective, but with side-effects [71]. Autonomic dysfunctions require a specific management depending on symptoms present [42].

Studies have indicated that a selective block of the peripheral sodium channel would improve sensory symptoms in SFN induced by sodium channel disorder, and mexiletine has successfully treated Erythromelalgia [72]. However, Pharmacological treatment remains disappointing due to the limited efficacy of available analgesics. As SFN patients' phenotypes are heterogeneous, combinational therapies and individualized patient’s management are recommended in the future.

3 The Sodium Channel SCN9A (NAV1.7)

3.1 The Sodium Channel Family

Voltage-gated sodium channels (VGSCs) are a type of microporous transmembrane protein widely expressed in the membranes of excitable cells such as neurons. VGSCs are vital for the initiation and propagation of action potentials in neurons and most electrically excitable tissues, through the transmembrane transport of Na^+. VGSCs consists of a highly glycosylated pore-forming α-subunits and independent β-subunits. Nine Mammals VGSC α-subunits have been identified in two decades, which are encoded by *SCN1A-SCN5A* and *SCNA8A-SCN11A* genes for the α-subunit. Previously they were named NAV1.1-NAV1.9. The β-subunits are considered as auxiliary subunits of the α-subunits. There are four subtypes of β-subunits, β_1- β_4 (30.4-45 kDa), encoded by SCN1B-SCN4B genes. In *vivo*, the α-subunit is generally associated with two β subunits to form a large heteromultimeric complex, of which one is linked by a non-covalent bond (β_1 or β_3), and the other subunit is linked by a covalent bond (β_2 or β_4). Although β subunits are the auxiliary subunits of the α-subunit, their co-expression with the α-subunit is considered to be very important in the regulation of the α-subunit and even the function of that Na^+ channel. The β-subunits play their specific roles, including regulating the gated kinetic of the whole Na^+ channel, the expression of the channels on the surface of the cell membrane and cell migration and aggregation [73, 74].

The molecular weight of α-subunit is large, of 240-260 kDa, consisting of 1700-2000 amino acids [75]. The three-dimensional structures of VGSCs on bacteria [76], insects, and humans have revealed the architecture of the protein (Figure 1.8 A-B) [77]. Briefly, 24 transmembrane segments are organized into four homologous domains (DI-IV). Each domain contains six hydrophobic α-helical segments (S1-S6), linked by three intracellular loops (two long loops and one short loop) [78]. Five to six positively charged arginine residues in S4 of each domain are susceptible to changes in the membrane potential. This is why these channels are called "voltage sensor sodium channels" (VGSCs). The S5 and S6 segments contain two short fragments that form the pore module (P domain), which serve as a "re-entrant" across the cell membrane [79]. In the intracellular loop between the transmembrane domains DIII and DIV, a region named IFM for isoleucine (I), phenylalanine (F), and methionine (M) is involved in the rapid inactivation of the VGSCs by facilitating intracellular signaling [80]. The N-terminus and C-terminus of the α-subunit mainly regulate the function of the VGSCs, for example, regulation of the inactivation process, interactions

between proteins, and intracellular regulators [81]. While the independent β-subunits mainly regulate channel gating and trafficking by interaction with NAV channels [82]. Three distinct locations have been identified for different small-molecule neurotoxins, such as guanidinium toxins, alkaloid toxins, and ladder polyether compounds [83].

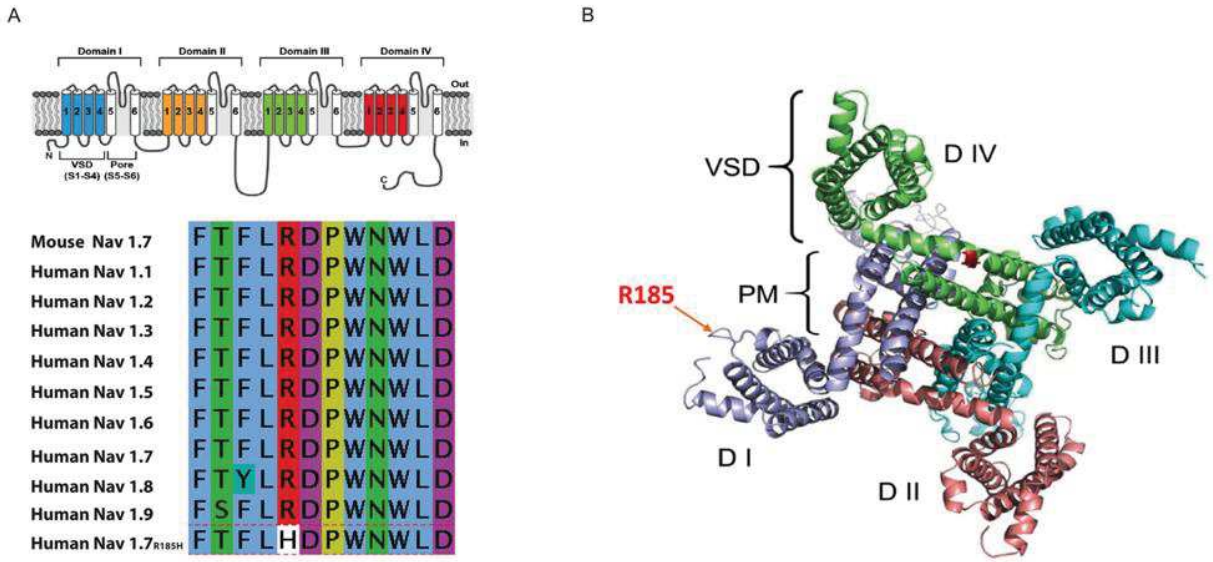

Figure 1.8 Structure of SCN9A and location of R185H mutation. **A)** Schematic of a voltage-gated sodium channels show the locations of the R185H, and R185H is both conserved in mouse SCN9A and all known human voltage-gated sodium channels. **B)** Cytosolic view of the structural model of SCN9A (SCN9A) channel transmembrane domains. R185 is located in domain I, at the hinge between S2-S3 linker. Modified figure from Yang Y. et al., 2016 [84].

The VSGCs are classified, based on their sensitivity to the specific inhibitor tetrodotoxin (TTX) as TTX-sensitive (SCN1A, SCN2A, SCN3A, SCN4A, SCN8A, and SCN9A channels) and TTX-resistant (SCN5A, SCN10A, and SCN11A channels). Currently, except for the SCN4A (NAV1.4) sodium channels expressed in muscle, the other eight subtypes can be detected in the nervous system [85], both in the central and peripheral parts. The SCN1A, SCN2A, SCN3A, SCN5A, and SCN8A sodium channels are widely distributed in the central nervous system [85]. SCN1A, SCN2A, SCN3A, SCN5A, and SCN8A sodium channels are expressed at low level in the peripheral nervous system, while SCN9A, SCN10A, and SCN11A sodium channels are mainly expressed sensory neurons in the DRG. The developmental pattern of SCN3A and SCN5A sodium channels are similar, with a high expression level during the embryonic period and a lower one in the adult brain tissue of both humans and mice [82]. SCN9A, SCN10A, SCN11A and SCN3A

sodium channels are well known to be closely related to pain. Here, we will focus on the role of SCN9A in the pain field and show more information in the next part.

For more detailed discussion on VSGCs in pain or other information on VSGCs, please refer to these references: Dokken, K. et al., 2020 [86]; Brunklaus, A. et al., 2020 [87]; Bennett, D.L et al., 2019 [88]; Lukowski, A.L. et al., 2019 [83]; Dib-Hajj, S.D. et al., 2019 [75]; Wang, J. et al., 2017 [82].

3.2 SCN9A (NAV1.7) Expression and Distribution

SCN9A is mainly expressed in sensory neurons from terminals in the skin to DRG and terminals in the dorsal horn, trigeminal ganglia, and sympathetic neurons [89]. The SCN9A is also expressed in the olfactory bulb (Figure 1.9) and in neurons of the arcuate nucleus and paraventricular nuclei of the hypothalamus where it regulates body weight [90]. Epitope-tagged SCN9A mice were generated by John Wood and his group, in which the SCN9A is tagged to the FLAG epitope that is the target of high-affinity antibodies. This allowed to purify the channel [91]. In this epitope-tagged SCN9A mouse, the SCN9A is not only present in the hypothalamic neurons but also other regions of the brain, such as the medial amygdala, medial habenula, laterodorsal thalamic nucleus, laterodorsal thalamic nucleus, and in the subfornical organ, substantia nigra reticular part and the red nucleus magnocellular part of the midbrain, and neurons of the pontine nuclei located in the hindbrain (Figure 1.9). The function of SCN9A in these specific regions remains to be understood.

The function of SCN9A has been studied more extensively in the DRG neurons. DRG neurons can be classified into several subtypes according to different classification criteria. According to immunohistochemistry, results on phosphorylated 200 kDa neurofilament subunit (pNF200) have been used to divide the DRG neurons into C-fiber neurons (pNF200-poor) and A-fiber neurons (pNF200-rich) [92]. The C-fiber neurons, likely contributing to nociception, are further subdivided into two subpopulations, peptidergic (expressing substance P and CGPR and non-peptidergic neurons (binding isolectin B4 from *Griffonia simplicifolia* (IB4) and lack neuropeptide expression). The expression of SCN9A is higher in C-fiber neurons than in A-fiber neurons [92]. In C-fiber DRG neurons, SCN9A is expressed approximately in an equal number of neurons exhibiting IB4 or CGRP labeling [89]. According to the physiological properties, the DRG neurons can be classified into eight neuron subtypes, including five low-threshold mechanoreceptors (LTMR) subtypes (C-

LTMRs, Aδ-LTMRs, Aβ RA-LTMRs, Aβ SA1-LTMRs, and Aβ Field-LTMRs), peptidergic, polymodal non-peptidergic nociceptors and proprioceptors. The SCN9A is expressed across all subtypes, with the notable exception of proprioceptors [10].

Transcripts (mRNA) of *SCN9A* are clearly detected in the DRG and spinal cord. A single-cell RNA sequencing study of isolated neurons has identified some dorsal horn neurons that express SCN9A mRNA [11]. The sensitive RNAscope technique could detect the expression of *SCN9A* mRNA in a subset of the spinal cord motor neurons, but only a few transcripts could be found in dorsal horn cells [93]. Where is the original resource of SCN9A protein in the dorsal horn neurons? Kanellopoulos and colleagues resolved this question. They demonstrated, by using a TAP-tagged nav1.7 mouse line, that sensory neurons are the source of SCN9A in dorsal horn [91].

Recently, Akin and colleagues have performed the first live visualization of SCN9A sodium channel trafficking [79] and more recently their distribution in DRG neurons[94][94], through spinning disk confocal microscopy. They showed the real-time dynamic regulation of trafficking and surface delivery of the SCN9A sodium channel in the distal axonal membrane of cultured DRG neurons. SCN9A channels are transported to distal parts of axons via microtubule-dependent trafficking in vesicles enriched in Rab6A. At the axonal terminus plasma membrane, SNC9A channels are organized into nanoclusters containing a median of 12 channels. Single-particle tracking shows low mobility of channels within these nanoclusters and greater mobility outside of them.

3.3 Loss-of-Function mutations of *SCN9A* (NAV1.7)

Congenital insensitivity to pain (CIP) is an extremely rare human condition where no pain of any type is experienced by these individuals, resulting in a shortened lifetime [95]. The mutations causing CIP also affect the development and function of nociceptors, as shown for mutations in high-affinity nerve growth factor receptor (TRKA), NGF, PR domain zinc finger protein 12 (PRDM12) [96]. Homozygote inactivating mutations in *SCN9A*, *SCN11A*, zinc finger homeobox 2 (*ZFHX2*), and fatty acid amide hydrolase (*FAAH*) result in CIP due to failure of nociceptors to respond to tissue-damage signal [96]. Most mutations are autosomal recessive, except for individuals with unique *SCN11A* mutations and a single family with a dominant mutation in *ZFHX2* [96]. Here, we mainly discuss the loss-of-function of *SCN9A* in CIPs.

Mutations in *SCN9A* cause conditions of autosomal recessive painlessness [96, 97]. The recessive nonsense, frameshift indels, and canonical splice mutations are found in CIP individuals (Table 1.2). They are usually considered as pathogenic but not all of them were studied by functional

analysis. However, the functional consequences of missense mutations cannot reliably be predicted. Except for painlessness, the CIPs patients display other phenotypes such as anosmia (Table 1.2), resulting from loss-of-function of *SCN9A* in the olfactory sensory neurons. The IENFD measurements from three CIP patients with compound heterozygous mutations in *SCN9A* showed a highly reduced number of intraepidermal nerve fiber density [98]. Using microneurography, a total of 38 C-fibers were recorded from these three SNC9A-linked CIP patients, with none displaying a specific pattern similar to C-nociceptors [98]. This showed that functional SCN9A were needed for C-nociceptors development.

3.4 Gain-of-Function of *SCN9A* (NAV1.7)

GOF mutants of *SCN9A* have been reported associated with painful disorders, inherited erythromelalgia (IEM), paroxysmal extreme pain disorder (PEPD), and some forms of SFN. In the 2012 study by Han and colleagues for diabetic peripheral neuropathy (DPN), 12 rare *SCN9A* variants were found in 10 (out of 111) participants with painful DPN, while no variant was found in 78 participants with painless DPN [99]. Five of these variants had previously been described in other neuropathic pain disorders, which are V991L/M932L (note that these variants are in complete linkage disequilibrium) [67], W1538R [72], R185H [67], and I739V [100].

IEM is characterized by a striking clinical picture of attacks of excruciating pain, usually most intense in the distal (feet, hands) and vasomotor dysfunction (skin redness) evoked by mild warmth or exercise and are relieved by cooling [101]. The electrophysiological results showed increased ramp current and slow deactivation [102]. Some mutations of *SCN9A* impair slow inactivation, leading to enhance DRG neuron hyperexcitability, whereas other IEM mutations enhance slow inactivation and therefore attenuate DRG neuron excitability [103].

PEPD typically starts in infancy, manifests in rectal pain, is accompanied by skin flushing of the lower or upper body or face and can present in a harlequin pattern. PEPD-linked SCN9A mutations produce different effects on NAV 1.7 gating compared with IEM-associated mutations [102]. Next, I will show more information on GOF mutations of *SCN9A* in SFN. A more detailed discussion about GOF mutations of *SCN9A* in IEM and PEPD can be found in the reviews published by Dib-Hajj, S.D. et al., 2013 [104]; Dib-Hajj, S.D. et al., 2019 [75]; Bennett, D.L. et al., 2019 [88]; Baker, M.D. et al., 2020 [102].

In the 2012 study by Faber and colleagues that examined the role of VGSC mutations in 28 patients with pure idiopathic SFN confirmed by skin biopsy, eight (29%) patients were found to carry new missense variants in *SCN9A* (Table 1.1) [67]. All these eight patients complained about pain.

The pain began in the distal extremities in most patients. However, patients carrying D623N and I720K mutations initially experienced pain throughout the body with muscle ache before developing distal pain [67]. Two patients carrying the R185H mutation showed different consequences. Compared to patient 2, the older male patient had less pain. Patient 2 with the R185H mutation suffered from painful neuropathy with little autonomic symptoms, whereas other mutations of *SCN9A* carriers reported more autonomic complaints [67]. The function analysis with current-clamp detection were carried out in DRG neurons. Current-clamp studies revealed that all variants are GOF mutations, rendering DRG neurons hyperexcitable (Table 1.1) [66]. Additionally, I288M mutation also lead to trigeminal ganglion neurons hyperexcitable [105]. I739V mutation [100] also induced superior cervical ganglion hyperexcitability (Table 1.1). In voltage-clamp studies, R185H and M932L/V991L mutations enhanced resurgent currents, which are known to induce repetitive firing. In comparison, other mutations impaired slow or/and fast inactivation (Table 1.1) [66].

In another study for DPN, four variants of *SCN9A*, R185H, I739V, M932L/V991L (see Table 1.1) were already found in patients with idiopathic small fiber neuropathy [99]. The five participants carrying the rare *SCN9A* variants in this study showed that the onset of neuropathic pain was associated with the diagnosis of diabetes. They reported more severe burning pain than the remaining study participants with painful DPN without rare variants of *SCN9A*. There were no differences regarding the other parameters [99]. Also, pressure pain thresholds were significantly higher for the participants carrying the rare *SCN9A* variants than the study participants with painless DPN. Here, four patients carrying R185H mutation displayed different clinical pain phenotypes, depending on the environmental context. This study proposed that these rare variants in *SCN9A* may act as risk factors promoting the development of neuropathic pain in the context of an environmental trigger (diabetes) rather than causing pain by a Mendelian inheritance [99]. The more recent work by Eijkenboom and colleagues, 1139 patients diagnosed with pure SFN were screened for SCN9A, SCN10A and SCN11A mutations and their clinical features were compared. The frequency of potentially pathogenic variants was 5% for SCN9A gene [106].

3.5 Mutation R185H of *SCN9A/Scn9a* (NAV1.7) in Human and Mouse

For many decades, researchers have used model vertebrates to study somatosensation and pain. Model organisms, particularly the mouse, have served as invaluable tools to help understand primary signaling pathways, neuronal networks, and molecular aspects involved in the transduction of sensory stimuli resulting in the perception of pain [127]. It is important to know the differences and similarities between mouse and human physiology, particularly the DRG primary sensory neurons. One study compared the combinatorial co-expression of several somatosensory molecular markers between human and mouse DRG [128]. Three neurotrophic receptors TrkA, TrkB, and TrkC, can be used to categorize sensory neurons into three main cellular populations according to the presence of TRKA, TRKB, and TRKC, which are nociceptors, mechanoreceptors, and proprioceptors, respectively. They found that the overlap of TrkB or TrkC with TrkA and distribution of somata sizes was highly similar in DRG between humans and mice. They also found no difference regarding the distribution of NAV1.7/TrkA double-positive sensory neurons obtained from both organisms, but a significantly higher fraction of NAV1.8/TRKA and NAV1.9/TRKA positive neurons were found [128].

In my Ph.D. project, we model a mutation R185H (arginine 185 substitutes to histidine) of *SCN9A* from SFN patients in mice and characterize the phenotype. This R185H mutation lacates in the linker between S2 and S3 of domain I (Figure 1.9 B). This variant R185H (rs73969684) has been reported as a single nucleotide polymorphism with an allele frequency of 0.6% (heterozygote frequency of 1.2%) in the 1000 Genomes Project and with 1.2% heterozygote frequency (55 heterozygotes among 4700 individuals) reported in the Exome Variant Database (http://evs.gs. washington.edu/EVS). Screening a panel of 1000 ethnically matched (Dutch nationals of European ancestry) control population, we report the c.554 G4A in 0.4% of 1000 control subjects (0.4% heterozygote frequency, 0.2% allele frequency) [107]. To compare the location of R185H mutation in all human VGSCs and mouse NAV1.7 sodium channel, we did sequence alignment. The location of R185 is highly conserved in all human VSGCs as well as the mouse NAV1.7 sodium channel (Figure 1.9 B).

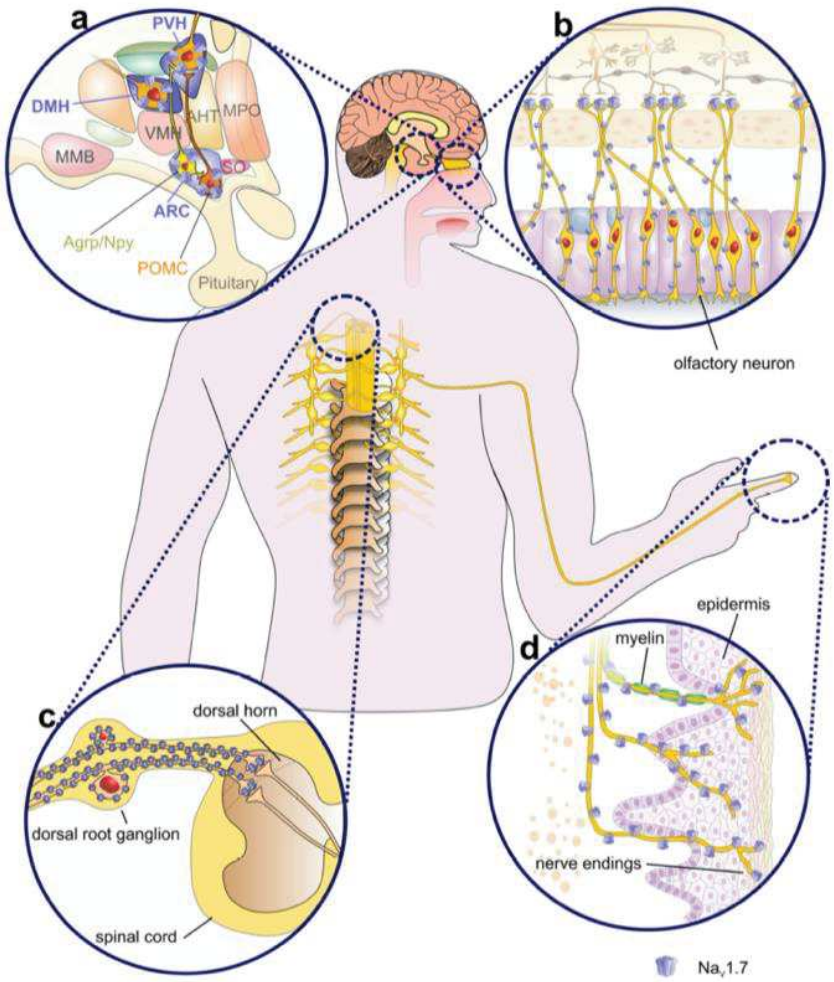

Figure 1.9 Expression profile of NAV 1.7. **a)** In the rodent central nervous system, NaV 1.7 expresses in the pituitary gland, subfornical organ, and several hypothalamic nuclei. In the arcuate nucleus (ARC), dorsomedial nucleus (DMH), and paraventricular nucleus (PVH), NaV 1.7 expresses in Agrp, Npy, and POMC-expressing neurons where it contributes a persistent current that is crucial for synaptic integration. Note that NaV 1.7 expression in these brain regions is substantially lower in primates and humans. **b)** NaV 1.7 is expressed along the olfactory sensory nerve from the olfactory epithelium to the olfactory nerve branches but absent in mitral and granule neurons receiving synaptic inputs from olfactory sensory neurons. In these neurons, NaV 1.7 is crucial for neurotransmitter release, and the absence of functional NaV 1.7 leads to anosmia. **c)** In sensory neurons, NaV 1.7 expresses in cell bodies of dorsal root ganglion, along axons, central terminals, and **d)** peripheral nerve terminals. MPO, medial preoptic nucleus; PVH, paraventricular nucleus; SO, supraoptic nucleus; AHT, anterior hypothalamic nucleus; VMH, ventromedial nucleus; MMB, the mammillary body; ARC, arcuate nucleus; DMH, dorsomedial nucleus; Agrp, Agouti-related peptide neurons; Npy, Neuropeptide Y neurons; POMC, pro-opiomelanocortin neurons. A copied figure from Vetter, I. et al., 2017 [129].

Table 1.1 Gain-of-Function mutation of *SCN9A* in SFN and Painful DPN

Mutations *SCN9A*	Gender	Onset symptoms age/referral age	Family History	Medication	Aggravated by Warmth/Relieved by Cold	Skin Biopsy (IENFD/normative value per mm)	Autonomic Dysfunction	Pain Symptoms	Voltage clamp	Current clamp	References
R185H 1	Male	24/54	Brother similar complaints; grandfather, painless burns and difficulty walking	No effect, pregabalin and amitriptyline	No/no	1.0/≥3.2	No	Skin Hyperesthesia, burning feet, sheet intolerance and restless legs	Enhanced resurgent currents	Hyperexcitability DRG neurons	[67, 107]
R185H 2	Female	23/24	father similar complaints	No relief form acetaminophen, anticonvulsants, antidepressants, mexiletine, opioids	No/no	4.9/≥6.7	Yes	Skin Hyperesthesia, burning feet, sheet intolerance and restless legs	Enhanced resurgent currents	Hyperexcitability DRG neurons Hypoexcitability SGC neurons	[67, 107]
R185H 3 painful DPN	Male	44.7/48.4	No	Pregabalin	Not completed	Not completed	No	Serve burning pain, more sensitive to deep pressure and pain at lower pressures	Not completed	Not completed	[99]
R185H 4 painful DPN	Male	62.0/64.9	No	Pregabalin, duloxetine, capsaicin ointment, and co-co-damol	Not completed	Not completed	Yes	Serve burning pain, more sensitive to deep pressure and pain at lower pressures	Not completed	Not completed	[99]
D623N	Female	22/63	sister similar complaints	Some relief from pregabalin and duloxetine	Yes/no	2.8/≥4.1	Yes	Skin Hyperesthesia, burning feet, sheet intolerance and restless legs	Depolarized slow and fast inactivation	Hyperexcitability DRG neurons	[67, 108]
I739V	Female	14/51	father, sister and 2 sons, similar complaints	Slight relief from amitriptyline	Yes/yes	3.4/≥3.3	Yes	Skin Hyperesthesia, burning feet, sheet intolerance and restless legs	Impaired slow inactivation	Hyperexcitability DRG neurons	[67, 100, 107]
I720K	Male	37/39	Unremarkable	No effect from pregabalin	No/no	4.5/≥4.7	Yes	Skin Hyperesthesia, burning feet, sheet intolerance and restless legs	Impaired slow inactivation	Hyperexcitability DRG neurons	[67, 105]
M1532I	Female	68/70	Unremarkable	No effect from pregabalin	No/no	2.3/≥2.7	Yes	Skin Hyperesthesia, burning feet, sheet intolerance and restless legs	Impaired slow inactivation	Hyperexcitability DRG neurons	[67]
M932L/V991L	Male	16/22	Unremarkable	No relief with gabapentin	Yes/no	4.0/≥5.4	Yes	Skin Hyperesthesia, burning feet	Enhanced slow inactivation	Hyperexcitability DRG neurons	[67]
I228M	Male	32/51	Sister with rheumatoid arthritis had burning hands	Pain bearable with acetaminophen; no relief antidepressants, NSAIDs	No/no	1.6/≥3.2	Yes	Skin Hyperesthesia, burning feet, sheet intolerance and restless legs	Impaired slow inactivation	Hyperexcitability trigeminal ganglion neurons	[67]
G856D	Male	10/35	father and brother similar complaints	No effect aspirin, beta-blocker and pregabalin	Yes/yes	5.0/≥5.2	Yes	Burning hand, the redness of skin and pain expanded to the feet, cheeks and ears	Hyperpolarized activation; depolarized steady-state fast-inactivation; slowed deactivation and enhanced resurgent currents	Hyperexcitability DRG neurons	[109]

DPN: diabetic peripheral neuropathy

Table 1.2 *SCN9A* mutations causing congenital indifference to pain

Mutations	Exon	Comments	Country	Anosmia	References
W897X	exon 15	family: 2 M & 1 F	North Pakistan	ND	Cox, J. J. et al., 2006 [56]
I767X	exon 13	1 M patient		ND	
S459X	exon 10	family: 1 F & 1M		ND	
Y328X	exon 8	family1: 3M family2: 1M	Canadian family	ND	Ahmad, S. et al., 2007 [110]
R277X	exon 6	family1: 1F & 1M family2: 1M	Switzerland	Y	Goldberg, Y. P. et al., 2007 [111]
Y328X	exon 8	family1: 2M family2: 1M family3: 1M	Canada	ND	
R830X	exon 15	1 M patient	France	Y	
F1200LfsX33	exon 19	1 F patient	Italy	Y	
R1488X	exon 24	1 F patient	US	UK	
W1689X	exon 26	1 F patient	Argentina	Y	
R896Q	exon 15	family: 3 F	Bedouin	ND	Cox, J. J. et al., 2010 [112]
R523X	exon 10	family: 3F & 3M	Pakistani	N	Kurban, M. et al., 2010 [113]
M899I	exon 15	1M patient	Han Chinese	N	Yuan, R. et al., 2011 [114]
M932L	exon 15	1 F patient	Han Chinese	N	
E970X		1 P patient	Canadian	ND	Bartholomew, F. et al., 2014 [115]
M1190X	exon 19	family1: 1F & 3M family2: 2F & 1M family3: 1F & 1M family4: 1F & 2M	Pakistan	only 1 M from family3 Y; others N	Sawal, H. A. et al 2016 [116]
E693X; Splice-junction mutation	exon 13 & Intron 23-24	family: 2M	US	Y	Goldberg, Y. P. et al., 2007 [111]
I1235LfsX2 & K1659X	exon 19 & 26	family: 2F	England	Y	
c.828delGT & c.2575C>T		F	Norwegian	Y; correct for smoke smell	Nilsen, K. B. et al., 2009 [117]
R1370-L1374 del & I1493fsX8	exon14 & 16	F	British	ND	Cox, J. J. et al., 2010 [112]
C1719R & IVS+3 delA		F	Caucasian	ND	Staud, R. et al., 2011 [118]
A compound heterozygous		M		ND	Ma, A. et al., 2012 [119]
3993delGinsTT	exon 22	family1: 1M & 1F family2: 1M	Japanese	all M Yes, but F no	Yuan, et al., 2013 [120]
K376Q & G375Afs		F		Y (nonalcoholic odors)	Shorer, Z. et al., 2014 [121]
K1659X & I1235LfsX2	exon 29 & exon 22	F	Caucasian	ND	Wheeler, D. W. et al., 2014 [122]
c.2488C>T & c.5318delA	exon 15 & exon 26	M	UK	Y	Ramirez, J, D., et al., 2014 [123]
c.2488C>T & c.5318delA	exon 15 & exon 26	F	UK	ND	
Y897X & G1725R	& exon 27	F	Japanese	N	Bogdanova-Mihaylova, P. et al., 2015 [124]
c.3319- 2A>G & c.5463dupT		F	Caucasian	ND	Rajasekharan, S. et al 2017 [125]
R896Q & c.1108-2A>G	exon 16 & 9	F	Italy?	Y	Marchi, M. et al., 2018 [126]

F: Female ; M: Male ; N: No; ND: Not d=Done; Y: Yes

4. Mini Review Manuscript

Pain behavior in *SCN9A* (NAV1.7) and *SCN10A* (NAV1.8) mutant rodent models

Yaping Xue*, Céleste Chidiac*, Yann Hérault[$,#] and Claire Gavériaux-Ruff[$]

Institut de Génétique et de Biologie Moléculaire et Cellulaire, Translational Medicine and Neurogenetics Department, 1 rue Laurent Fries, 67400 Illkirch, France

Université de Strasbourg, Illkirch, France

Centre National de la Recherche Scientifique, UMR7104, Illkirch, France

Institut National de la Santé et de la Recherche Médicale, U1258, Illkirch, France

* equal contribution

$ equal last authors

Support and grant information

This work has been funded by the European commission H2020 programme (grant number - 721841 – PAIN-Net)

#Corresponding author:

Name Yann Herault

Mail herault@igbmc.fr

Highlights

Rodent genetic models have highlighted the role of *SCN9A*- and *SCN10A*- encoded NAV1.7 and NAV1.8 voltage-gated sodium channels in pain control.

Global *Scn9a* knockout (KO) animals display pain insensitivity similarly to congenital insensitivity to pain patients.

The conditional KO mouse lines have allowed to assign populations of Scn9a in pain control.

The *Scn10a*-Cre mice allow to conditionally inactivate genes in the primary nociceptive neurons.

Targeting NAV1.7 and NAV1.8 constitute potential therapies for pain.

Abstract

The two voltage gated sodium channels NAV1.7 and NAV1.8 are expressed in the peripheral nervous system and some evidence showed their involvement in various pain conditions including inflammatory and neuropathic pain states. Rodent models bearing deletions or point mutations of the corresponding genes, *Scn9a* and *Scn10a*, were created in order to understand the role of these sodium channels in the pathophysiological mechanism underlying pain symptoms. Complete loss-of-function or knockout (KO) of *Scn9a* or *Scn10a*, conditional KO (cKO) of *Scn9a* in specific cell populations and double knockout (DKO) of both genes were shown to decrease sensitivity to various pain stimuli. The Possum mutant mice bearing a chemically induced dominant hypermorphic mutation in *Scn10a* revealed higher sensitivity to noxious mechanical and cold stimuli. Several gain-of-function mutations were identified in patients with painful small fiber neuropathy. Knowledge from pre-clinical models bearing these mutations will allow to understand how these mutations impact on pain. This review summarizes the pain behavior profiles reported in *Scn9a* and *Scn10a* rodent models. In addition, the review gives suggestions and perspectives for creating models mimicking patients' pain symptoms, and developing highly accurate pain behavioral assessment, in the aim of developing better analgesic strategies.

1. Introduction

Pain is “an unpleasant sensory and emotional experience associated with, or resembling that associated with, actual or potential tissue damage”, as re-defined recently by the International Association for the Study of Pain [1]. Pain is one of leading cause of disability and disease burden, and Mills and colleagues described pain as a common, complex and distressing problem that has a profound impact on individuals and society [2]. Pain is now divided into four major types: nociceptive pain, inflammatory pain, neuropathic pain and dysfunctional pain [3].

As the treatment of pain is still often unsatisfactory for some kinds of pain and for a part of the patients, it is important to identify pain mechanisms for the development of new therapeutic strategies [3, 4]. Generally, injured tissues or nerves release many pro-pain molecules including cytokines, chemokines, prostaglandins, bradykinin, histamine, serotonin and nerve growth factor, which increase sensory neurons excitability, leading to peripheral sensitization. The pain message is transmitted to spinal cord via the central terminal of primary afferents resulting in neuron-neuron and neuron-glial interactions [5]. Then the signals are sent to and integrated in the pain matrix in the brain that also exerts the descending pain control.

Small fiber neuropathies (SFNs), a disorder of Aδ-fibers and C-fibers, is usually characterized by neuropathic pain symptoms and autonomic complaints in the clinics [6]. Interestingly, in idiopathic SFNs, nearly 30% of patients have gain-of-function (GOF) mutations in the *SCN9A* gene encoding for the NAV1.7 channel protein [7]. These mutations were expressed in HEK293 cells or dorsal root ganglia (DRG) and subjected to voltage clamp analysis. They produced impaired inactivation or enhanced resurgent current of voltage-gate properties of NAV1.7 channel. They also induced Increased excitability of transfected DRG neurons [7]. NAV1.7 has been a target for analgesia for decades, but selective inhibitors could not be developed as therapeutics because they may exert effects on a broader spectrum of sodium channels [8]. Additionally, *SCN9A* loss-of-function (LOF) by bi-allelic inactivating mutations results in the striking clinical phenotype of congenital insensitivity to pain (CIP) [9]. Recently, several GOF mutations in the *SCN10A* gene encoding for the NAV1.8 α-subunit of sodium channel have also been reported in SFN patients. Similar to NAV1.7 variants, these NAV1.8 mutations provoke neuronal hyperexcitability after transfection of DRG neurons [7]. However, in contrast to *SCN9A*, there is no report for LOF mutations for *SCN10A* in humans. All of these idiopathic SFN patients display abnormal quantitative sensory testing, but with a complexed response to thermal and mechanical stimuli.

Understanding the pathophysiological mechanism underlying pain symptoms in painful SFN and other pain pathologies is important and requires relevant preclinical models. According to the different and

complex phenotypes in patients, animal models have been generated to model individual cases of idiopathic SFN.

In this review, we provide the profiles of nociceptive behaviors related to NAV1.7 and NAV1.8, by evoking the different preclinical genetic models of NAV1.7 and NAV1.8 used in research until now. It is of high benefit to discuss the advantages and disadvantages of previous studies and provide future suggestions to develop new mouse models for studying heterogeneous pain symptoms in SFN patients and other pain patients. These models may be used to develop novel analgesics targeting these channels.

2. The sodium voltage-gated channels NAV1.7 (SCN9A) and NAV1.8 (SCN10A)

NAV1.7 and NAV1.8 channels are voltage-gated sodium channels that play a critical role in the generation and conduction of action potentials and are important for electrical signaling by most excitable cells. They are composed of one α-subunit associated with one or more β-subunits. The α-subunit consists of four homologous domains (DI-DIV) and each domain consists of six transmembrane segments [10, 11]. NAV1.7 is preferentially expressed in the peripheral nervous system within sensory DRG and sympathetic ganglion neurons and their small diameter peripheral axons [12, 13]. NAV1.7 protein was also detected in lamina I, lamina IIo, and lamina IIi of superficial dorsal horn within primary afferent terminals, but very few transcripts can be detected in dorsal horn cells. Recent study demonstrated that sensory neurons are the source of NAV1.7 in dorsal horn neurons using both immunocytochemistry and immune-electron microscopy [14]. NAV1.7 is a tetrodotoxin-sensitive sodium channel, which opens in response to small depolarizations and closes to resting potential [8]. The proteins interacting with NAV1.7 were mapped using epitope-tagged gene-targeted mice, and they included membrane-trafficking proteins [13]. More detailed signal pathway of NAV1.7 involved post-synaptic density scaffolding protein Homer 2, N-acylethanolamines binding protein FABP7, Mitogen-activated protein MAP kinases and Collapsin response mediator protein 2 (CRMP2), as described in review by Chew et al [15].

NAV1.8 produces a slow inactivating, tetrodotoxin-resistant current, and is known to recover rapidly from inactivation [8, 16]. NAV1.8 is a major contributor to the uprising phase of the action potential [16]. NAV1.8 is predominately expressed in the peripheral nervous system within small-diameter neurons of trigeminal ganglion and DRG, but also in a small percentage of medium- and large-diameter neurons [8, 17, 18]. The creation of a transgenic mouse line encoding green fluorescent protein under the control of *Scn10a* promoter has allowed to reconsider NAV1.8 expression pattern. NAV1.8 protein

was detected in small and medium diameter DRG neurons as well as lamina I and II of the spinal cord dorsal horn where C-fibers predominantly terminate [19].

The pain behavior analysis of genetic animal models for *Scn9a* and *Scn10a* showed that these sodium channels play important roles for acute pain sensation (nociception) and contribute to the sensitization of pain circuits, leading to hyperalgesia [20]. The present review summarizes the findings on mutant mice and rats for these channels and their behavior in nociception and chronic pain models.

3. Role of SCN9A (NAV1.7) in pain behavior: lessons learnt from rodent models

3.1 Effect of the channel absence as assessed in homozygote global KO mice and rats

Clinical genetic studies have reported that *Scn9a* LOF results in complete inability to experience pain (CIP). Genetic animal models have proved useful tools to study the mechanism of CIP and potentially develop therapies for CIP patients. The absence of NAV1.7 protein has been assessed first by *Scn9a* gene knockout (KO) in the whole body, ie. global KO. Although the global inactivation of *Scn9a* was reported lethal in mice [21], Gingras et al. could overcome the neonatal lethality by changing the original C57BL/6J genetic background to a mixed CD1 and then to BALB/c and obtain a homozygote *Scn9a* knockout mice that were profiled in several behavioral assays as discussed below [22]. While trying to Humanize NAV1.7 in rats Grubinska et al [23] have been generated a partial KO, resulting in NAV1.7 protein loss in DRGs, sciatic nerve, brainstem and gastrointestinal tissues but not in the olfactory tract.

3.1.1 Effect on nociceptive behavior

Measurements of reflex behaviors to thermal and mechanical stimuli as well as more integrated or spontaneous pain tests were used to examine pain-like responses and pain mechanisms in rodents [24, 25]. Supraspinal responses to a noxious heat stimulus can be assessed by the hot plate test where latency to paw reaction is measured. Interestingly, withdrawal latencies of wild-type (WT) or heterozygous (HET) mice decreased as temperature increased in the hot plate from 48 to 55°C while *Scn9a* KO mice were insensitive to heat [22] (Table 1). The evaluation of sensitivity to mechanical stimuli is done with Von Frey nylon filaments of varying diameters, allowing to assess both mechanical allodynia and hyperalgesia. Other tools include tail clip, Randall-Selitto or pressure analgesimeter for pressure application to paw or tail, that produce results analogous to clinical pressure pain conditions [25, 26]. Global *Scn9a* KOs were insensitive to pressure pain in tail clip assay. However, in Von Frey test, the KOs showed similar touch sensitivity than control mice [22]. The *Scn9a* LOF rats had no or very faint responses to noxious chemical, thermal and prick stimuli [23, 27] (Table 1).

3.1.2 Effect on induced pain

The formalin test is used for testing pain to chemical irritant (phase I, 0-5 min) and subsequent acute inflammatory hyperalgesia (phase II, 10-40 min). It reflects the direct activation of primary nociceptive afferents and inflammation-induced peripheral and central sensitization. The global *Scn9a* KO mice and rat showed a strong decreased or response in phase I and II in the formalin test [23, 27]. The Complete Freund's adjuvant (CFA) model aims at studying chronic inflammatory hyperalgesia in rodents. WT and HET control mice showed expected inflammatory hypersensitivity while whole *Scn9a* KO mice did not display any pain-like behavior [22] (Table 1). The *Scn9a* LOF rats did not experience experimentally-induced neuropathic hypersensitivity [23]. In summary, *Scn9a* LOF induced CIP in rodents wholly analogous to human patients, with insensitivity or reduced sensitivity to noxious heat, cold or pressure. Also, *Scn9a* LOF rodents showed reduced hyperalgesia in inflammatory and a neuropathic model.

3.2 Effect on the *Scn9a* deletion in specific cell populations as assessed in conditional KO mice

To study the role of NAV1.7 in precise types of neurons, several mouse lines with conditional deletion of *Scn9a* have been generated. Mice with floxed *Scn9a* gene were crossed with *Scn10a*-Cre, Advillin-Cre, or Wnt-1-Cre mice to obtain *Scn9a* conditional KO (cKO) lines in, respectively, primary nociceptive neurons (small and medium size diameter [21, 28-31], all sensory neurons [28, 30] or sensory and sympathetic neurons [28, 32, 33]. Also, a new mouse line was generated ($Scn9a^{CAGERT}$) where *Scn9a* gene inactivation could be induced at the adult age. Floxed *Scn9a* mice were crossed with mice where the Cre-ERT transgene was driven by the CMV early enhancer/chicken beta-actin promoter, allowing Cre recombinase activation upon tamoxifen induction [34]. The induction of *Scn9a* deletion at adulthood may prevent compensatory mechanisms potentially occurring in the other cKO lines. Following tamoxifen induction in the $Scn9a^{CAGERT}$ mouse line, *Scn9a* expression was abolished in the DRG (mRNA, protein), trigeminal ganglia (mRNA) and sympathetic superior cervical ganglia (mRNA) [34].

3.2.1 Effect on nociceptive behavior

The sensitivity to heat noxious stimuli were determined by measuring paw withdrawal latencies in the Hargreaves and hot plate tests. Altogether the different *Scn9a* cKO lines were less sensitive in the Hargreaves test. $Scn9a^{Advillin}$, $Scn9a^{Wnt1}$ and $Scn9a^{CAGERT}$ lines showed behavioral response deficit to heat when applying either fast or slow heat ramps [28, 30, 33, 34] while $Scn9a^{Scn10a}$ lines showed an elevated threshold with the slow ramp only [21, 28, 30, 35]. These data suggest a specific role of NAV1.7 in NAV1.8-positive DRG neurons for mediating response to slowly transduced heat [30]. Furthermore, in the hot plate test that reflects supraspinal response to heat stimuli, only the $Scn9a^{Wnt1}$

and *Scn9a*^{CAGERT} mice showed a pronounced attenuation of response [28, 33, 34] (Table 1). Response to noxious cooling and extreme cold were measured by acetone and cold plate tests [25]. All cKO lines displayed normal response on the cold plate in contrast to LOF rats. Only *Scn9a*^{Advillin} and *Scn9a*^{Wnt1} lines showed deficits in the perception of cooling as assessed in the acetone test (Table 1), indicating that neuronal populations different from the NAV1.8 neurons mediate NAV1.7-dependent perception of moderate cold [28]. This mechanism is corroborated by the attenuated response of *Scn9a*^{Advillin} mice to cooling in the dynamic thermal place preference test [30] (Table 1). Randall-Selitto test and von Frey were employed to assess the responses to touch and pressure in the cKO mice. The different cKO lines displayed a pronounced analgesia to noxious mechanical stimulation in the Randall-Selitto test applied to the tail (Table 1). The cKO lines showed normal response to touch as tested with the von Frey filaments applied to hindpaw glabrous skin, in five articles from two laboratories [21, 28, 30, 32, 34] except when *Scn9a*^{Scn10a} mice were evaluated with the Electronic von Frey Anesthesiometer [14]. This difference may be due to the use of this electronic equipment which applies a maximum force continuously until withdrawal and therefore may lead to a noxious mechanical stimulus rather than a touch stimulus, consolidating the data obtained with the Randall-Selitto test. Interestingly, both *Scn9a*^{Advillin} and *Scn9a*^{Wnt1} mice, but not *Scn9a*^{Scn10a}, mice showed deficits in response when von Frey filaments were applied to the abdomen hairy skin [30] (Table 1). This demonstrated that mechanosensation by hair follicles are dependent on NAV1.7 and mainly in NAV1.8-negative neurons that innervate the hair follicles [30] and is consistent with the results that showed no change in sensitivity to the von Frey filaments in *Scn10a* KO animals (see chapter 4.2 and table 2).

Taken together, these behavioral results indicate that spinal reflex to noxious heat (Hargreaves test) is dependent on NAV1.7 expressed in NAV1.8-positive DRG neurons when using slow temperature ramp only and requires all sensory neurons (Advilin positive neurons) at fast temperature ramp. More integrated response to heat as measured by the hot plate test necessitates in addition the NAV1.7 protein expressed by sympathetic neurons as revealed in the Wnt-1-Cre and CAG-ERT mediated cKO mice. Concerning responses to noxious cold, the NAV1.7 expressed by all specific neuron populations tested in the cKO mice, either sensory or sensory plus sympathetic does not appear to be involved. However, the data on *Scn9a* LOF rats implicate the NAV1.7 channel. The results on *Scn10a* global KO and Possum mice lead to the conclusion that NAV1.8 channel is also implicated in noxious cold detection, see in chapter 4. As compared to noxious cold, the behavioral response to cooling (paw acetone test) implicates the NAV1.7 channel and would not require NAV1.7 expressed on NAV1.8 negative cells as found in the in *Scn9a*^{Scn10a}, *Scn9a*^{Advillin} and *Scn9a*^{Wnt1} mice, in agreement with the absence of phenotype in this test in *Scn10a* global KO animals. Lastly, the deletion of NAV1.7 in NAV1.8-positive neuron is sufficient to decrease the NAV1.7-mediated behavioral response to noxious

pressure (Randall-Selitto test), in addition to the role of NAV1.8 shown through the analysis of *Scn10a* KO mice (see chapter 4 and Table 2).

3.2.2 Effect on induced pain

The role of NAV1.7 expressed by NAV1.8-positive neuron in visceral pain was investigated in the *Scn9a*^{Scn10a} mice following capsaicin or mustard oil administration [29]. *Scn9a*^{Scn10a} animals were equally sensitive than controls, while *Scn9a*^{CAGERT} mice displayed a decreased response in the acetic-acid-induced model (Table 1). Together, this suggests that that NAV1.7 in other neurons than NAV1.8-positive neuron contribute to visceral pain control, although NAV1.8 was shown to be required for visceral pain control (Table 2).

The different *Scn9a* cKO lines were assessed for their response to inflammatory pain. In addition to the formalin and CFA models described above, the carrageenan model was used which elicits hyperalgesia within hours to days. Both mice with *Scn9a*^{Scn10a} or *Scn9a*^{Advillin} mutations displayed reduced response in the two formalin test phases [21, 28], while *Scn9a*^{CAGERT} mice had an attenuation of phase I response only [34]. For carrageenan-induced inflammatory pain, thermal hyperalgesia was absent in *Scn9a*^{Scn10a} mice (Table 1). In the CFA model, hypersensitivity to heat was abolished in both *Scn9a*^{Scn10a} and *Scn9a*^{CAGERT} animals while mechanical allodynia was reduced but still present in *Scn9a*^{CAGERT} mice [34]. Altogether, these results highlighted the major contribution of NAV1.7 protein in peripheral sensory neurons in inflammatory hyperalgesia.

Neuropathic pain is caused by neuron injury in the peripheral or central nervous system. It occurs in many diseases, such as spinal cord injury, peripheral nerve injury, diabetes, postherpetic neuralgia, and cancer. Several successful models have been developed to mimic neuropathic pain evoked by these etiologies [36, 37]. Chronic constriction injury (CCI), spinal nerves transection (SNT) and partial sciatic nerve ligation (pSNL) as nerve injury models were utilized in the *Scn9a* cKO mice [18, 28, 30, 34]. The *Scn9a*^{Scn10a} mice developed mechanical but no or weak cold allodynia following CCI or pSNL while they showed normal allodynia after SNT (Table 1). *Scn9a*^{Advillin} mice showed cold and mechanical allodynia during SNT but developed attenuated allodynia following CCI (Table 1). Deleting *Scn9a* in both sensory and sympathetic neurons (*Scn9a*^{Wnt1}) led to no or low allodynia upon SNT or CCI (Table 1). In *Scn9a*^{CAGERT} cKO mice, SNI induced weak cold allodynia but normal mechanical hypersensitivity [34]. In *Scn9a*^{Wnt1} and *Scn9a*^{Advillin} mice, oxaliplatin-induced neuropathic pain and cancer-induced pain developed as in their control littermates (Table 1). Furthermore, in a burn injury model, NAV1.7 in NAV1.8-positive neurons contribute to heat but not mechanical hyperalgesia [31] (Table 1).

Altogether, the behavioral analyses of KO, or cKO, animals show that NAV1.7 is a major contributor to both acute nociception and experimentally-induced chronic hyperalgesia. They suggest that NAV1.7

expressed in *SCN10A* (NAV1.8)-positive nociceptors (*Scn9a*^{Scn10a}) or all sensory neurons (*Scn9a*^{Advillin}) are required for the development of inflammatory pain and neuropathic allodynia in some of the models tested. Interestingly, constitutive ablation of *Scn9a* in both sensory and sympathetic neurons (*Scn9a*^{Wnt1}) markedly diminished neuropathic pain in both CCI and SNT models while the ablation in these same neurons at adulthood (*Scn9a*^{CAGERT}) attenuated inflammatory pain and SNI-induced neuropathic pain. This suggests that NAV1.7 channels in sympathetic neurons, in addition to sensory neurons, contribute also to neuropathic pain, at least in the SNT model. Additionally, in CIP patients the intra-epidermal nerve fibers are absent [98] whereas these fiber in *Scn9a* KO mice and LOF rats are normal [23, 27]. It means that there are still some different mechanisms between human and rodents.

3.3. Nav1.7 and the opioid receptor pathway

The global *Scn9a* KO in mice or rats and loss-of-function mutations in humans lead to insensitivity to pain. To determine whether these global gene silencing may induce compensations, gene expression was investigated in the DRG of *Scn9a*^{Advillin} mice. *Scn9a* deletion led to changes in transcripts levels in DRG. *Preproenkephalin* (*Penk*) gene encodes for the endogenous opioid peptide enkephalin, and *Penk* mRNA was elevated in *Scn9a*^{Advillin} DRGs. The opioid antagonist naloxone reversed the analgesia in a *SCN9A*-null CIP patient and in *Scn9a*^{Advillin} mice analysed in the Hargreaves and Randall-Selitto tests [38]. This suggested that the endogenous opioid system contributes to the analgesia driven by *Scn9a* gene inactivation. However, naloxone did not reverse analgesia in *Scn9a* LOF rats in the hot plate and formalin tests [27]. The reason for these contrasting findings remains unknown and may be due to the use of different pain behavioral tests. The expression of Penk was also increased in *Scn9a*^{Wnt1} [33]. In order to evaluate whether the activation of mu (MOR) or delta (DOR) opioid receptors was involved in this analgesia, *Scn9a*^{Wnt1} mice were crossed to *Mor* and *Dor* KO mice. Analgesia was abolished in triple *Scn9a*^{Wnt1}/*Mor*/*Dor* KO mice as measured with the Hargreaves test [33]. Altogether, these data showed that the combination of *Scn9a* gene inactivation and opioid system activation are required for analgesia.

4. Role of NAV1.8 in pain behavior: lessons learnt from mouse models

4.1. Pain behavior in the *Scn10a*^{T790A} possum mice.

Following N-ethyl-N-nitrosourea-induced mutation, Blasius et al. 2011 identified a mouse mutant termed Possum which carries a T790A hypermorphic mutation of the *Scn10a* gene. They reported that following scruffing at the back of the neck, the Possum mice became immobile, had apnea, and a rigid posture. When Possum mice were placed at their side or back, they were not able to right themselves, and showed a ‘waxy flexibility’ where the tail is in a raised position as applied by the

experimenter. Heterozygotes showed shorter response (1 min) compared to homozygotes (up to 5 min) [39]. The Possum mice were tested for pain sensitivity in several tests. The Possum and WT mice had similar withdrawal responses to Von Frey filaments applied to hind paw [39, 40]. But when a needle prick was applied to the plantar hind paw, Possum mice showed an increased nociceptive response to the stimulus [40]. Concerning thermal stimuli, Possum mice displayed increased sensitivity on cold plate at -1°C, but showed the same sensitivity in the hot plate at 52°C compared to WT controls [39]. Following mustard oil application to hindpaw, Possum mice entered into a Possum-like state, remaining motionless for the 5-minute experimental period while WT mice displayed expected paw lifts and licks. The Possum-like state was reversed by a NAV1.8 antagonist [40]. However, whether this is a pain behavior is not known. Following induction of inflammatory pain by CFA, Possum mice showed a mechanical allodynia similar to WT controls [39] (Table 2). In summary, the Possum mice that have hyperexcitable NAV1.8 channels showed increased sensitivity to extreme noxious mechanical and cold stimuli but no hypersensitivity to other types of pain challenges.

4.2. Effect of NAV1.8 channel absence as assessed in global KO mice

In order to investigate the role of the voltage-gated sodium channel NAV1.8 in pain control, Akopian and colleagues have first generated the *Scn10a* KO mice [41]. The *Scn10a* KO mice were evaluated for basal nociception as well as for experimentally induced chronic hyperalgesia in several studies.

4.2.1. Effect on nociceptive behavior and spontaneous pain

The studies on *Scn10a* KO mice revealed deficits in both mechano- and thermonociception. *Scn10a* KO mice showed analgesia to noxious mechanical pressure assessed in the Randall-Selitto test [18, 30, 41], but no change in mechanical threshold in the Von Frey test [18, 30, 31, 41-43]. Concerning responses to thermal stimuli, *Scn10a* KO animals showed an increased withdrawal latency in a slow but not in a fast heat ramp in the Hargreaves test [30]. The same analgesia was found by Akopian et al. 1999 [41] but not found in other studies [18, 31, 42, 43]. *Scn10a* KO mice were also less sensitive to the tail-flick test [127] but not in the hot plate test [18, 41, 43]. So globally, *Scn10a* KO mice were less or equally sensitive in conditions of spinal reflex to heat, but show no phenotype in the heat supraspinal responses. *Scn10a* deficient mice also revealed a reduced response to cold [44, 45]. *Scn10a* KO mice were less sensitive than controls to visceral pain elicited by capsaicin or mustard oil [46] (Table 2).

4.2.2. Effect on induced pain

The *Scn10a* KO animals were tested in both inflammatory and neuropathic models. The mutant mice had the same response to formalin as control mice. Following carrageenan challenge, hyperalgesia onset was slightly delayed, from 45 min in the WT to 90 min in *Scn10a* KO mice [41]. In the CFA model, the mutant mice displayed both thermal and mechanical hyperalgesia, but recovered faster from heat pain [43]. Therefore, these results suggest a role of NAV1.8 channel in the kinetics of carrageenan and CFA inflammatory pain, and not in lowering of nociceptive thresholds. The null mutants were comparable to their WT littermates for heat and mechanical hypersensitivity after burn injury [31]. The null mice developed the same allodynia as WT mice following spinal nerve transection [30]. *Scn10a* KO mice showed attenuated cold allodynia in the SNI model [43], while lowered cold allodynia to CCI injury was recorded in one out of two reports [30, 43] (Table 2). Taken globally, NAV1.8 channel plays a role in cold allodynia in some neuropathic pain conditions.

4.3. Effect on the channel as assessed in NAV1.8-Cre mice.

In order to develop conditional KO mice in nociceptive neurons, and as NAV1.8 is specifically expressed in these neurons, *Scn10a-Cre* knock-in mouse lines that express Cre-recombinase driven by the *Scn10a* locus were generated [17, 18, 21]. In these mutant lines, the Cre gene is knocked in the exon-1 of *Scn10a*, 3' UTR was inserted downstream of the Cre gene followed by a polyadenylation signal. *Scn10a -Cre* hemizygous mice were analyzed for nociception and experimentally induced pain. They had a normal phenotype towards mechanical stimulation in the Von Frey and Randall-Selitto assays as well as normal acute thermal responses in the Hargreaves and hot plate tests [17, 18, 21]. Inflammatory pain developed similarly in *Scn10a-Cre* hemizygous mice like in WT mice, in the formalin, carrageenan and CFA models [21]. *Scn10a-Cre*/0 mice were subjected to L5 spinal nerve ligation (SNL) neuropathy model and were then tested for mechanical and heat allodynia. They developed mechanical and thermal pain to the same extent as their littermate controls [18] (Table 2). Therefore, as these *Scn10a-Cre* HET mice behaved as WT mice in nociception and chronic hyperalgesia models, they have been used since then by many teams to conditionally inactivate their genes of interest in nociceptive neurons.

4.4. Role of NAV1.8 channel as assessed by optogenetics

The global knockout approach may lead to compensations at the cellular or circuit levels. As compared to global KO where gene inactivation occurs very early in embryonic stem cells, the optogenetics approach enables a precise spatiotemporal control of the activity of neurons expressing specific pain-related sodium channels [47]. The activity of NAV1.8-positive neurons could be inhibited or activated by light in the NAV1.8-Arch+ and NAV1.8-ChR2+ genetic mouse models, respectively. Transdermal

illumination of NAV1.8-Arch+ mouse hindpaw did not change baseline sensitivity to the von Frey filaments, in agreement with the lack of phenotype of NAV1.8 mice in this test [48]. However, under inflammatory or neuropathic pain conditions, light exposure decreased mechanical allodynia in NAV1.8-Arch+ mice [48]. Light-induced activation of bladder afferent terminals of NAV1.8-ChR2+ mice potentiated the bladder response [49]. These experiments showed that optical silencing or activation of NAV1.8+ afferent neurons in these new optogenetic mouse models modulate the pain behavioral responses. The selective delivery of inhibitory opsins leads to control pain circuits in vivo, with a potential development of clinical trials in patients with chronic irretractable pain

4.5 Role of NAV1.7 and NAV1.8 channels as assessed in double knockout strategies.

4.5.1 Double *Scn10a-Scn9a* knockouts (DKO)

Generating global KOs for both NAV1.7 and NAV1.8 channels and comparing them to single KOs was important to study how the absence of both channels contributes to analgesia. Since *Scn9a* global deletion is lethal at P0 [21], global KO of both *Scn9a* and *Scn10a* could not be obtained from global *Scn9a* KO. Using the *Scn10a-Cre* allele [21], Nassar et al. 2005 could generate double-KO (DKO) mice where the *Scn10a* gene is globally deleted and *Scn9a* is suppressed in NAV1.8-expressing neurons [18]. DKO mice showed similar touch withdrawal thresholds to Von Frey filaments as *Scn10a* KO and WT mice. But when tested for noxious pressure using the Randall-Selitto apparatus, the DKO mice exhibited profound analgesia compared to WT and *Scn10a* KO mice. On the hot plate, DKO mice had same reaction latencies as WT and *Scn10a* KO mice. However, when tested in the Hargreaves plantar test, withdrawal latency was doubled in DKO mice compared to *Scn10a* KO or WT mice [18] (Table 2). Therefore, deleting both *Scn9a* gene from NAV1.8+ neurons and *Scn10a* gene allowed to show that NAV1.7 and NAV1.8 provide additive controls of noxious mechanical and heat pain thresholds.

In the formalin model, DKO, KO and WT groups had similar response during phase 1. However, DKO mice showed a reduced response during phase 2, compared to *Scn10a* KO and WT mice. So, deleting both *Scn10a* and *Scn9a* in nociceptive neurons leads to a higher deficit toward formalin-induced behavior, stressing the additive role of both channels in inflammatory pain [18]. DKO mice developed mechanical allodynia after SNL to the same extent as *Scn10a* KO and WT mice [18] (Table 2). Therefore, the presence of both NAV1.7 and NAV1.8 channels is not essential for mechanical allodynia following SNL [18].

5. Perspectives

The genetic rodent models described here, together with pharmacological approaches that are beyond the scope of this short review, have shown that NAV1.7 and NAV1.8 play important roles in nociception

and chronic hyperalgesia. Adverse effects of sodium channel blocking analgesics is still a problem for both animals and humans, despite the clear utility of nerve block in pain treatment. To understand the mechanism of chronic pain in patients and explore novel analgesics require novel relevant pre-clinical models. Steve Waxman's team has developed sensory neurons differentiated from patient-derived Induced Pluripotent Stem Cells that model inherited erythromelalgia in vitro [50]. These cells can provide a platform which enables assessment of sodium channel blocker effects in vitro. It will then be necessary to analyze their effects and safety in the genetic models summarized in the review and additional preclinical animal models.

SFNs are a heterogeneous group of disorders affecting thinly myelinated Aδ-fibers and unmyelinated C-fibers with chronic pain symptom. GOF mutants of *SCN9A* and *SCN10A* have been reported in the SFN patients. Patients suffering from SFN usually develop somatic symptoms, which include hyperalgesia as well as reduced pinprick and thermal sensation in the affected areas. It commonly presents with pain, burning, tingling, and numbness. On the contrary, in the CIP patients, LOF of *SCN9A* causes these individuals to not perceive pain in response to noxious stimuli but *SCN10A* LOF mutations were not found yet in these patients. These data suggest that *SCN9A* is mandatory for nociception in human, and elucidating *SCN10A* role would require more clinical investigation. Novel rodent genetic models for these diseases can be generated by using homologous recombination as well as the more recent CRISPR-Cas9 techniques. The CRISPR-Cas9 systems is a research toolbox for genome editing and regulation [51]. Recently, this system has been harnessed to facilitate genetic manipulations in a variety of cell types and organisms [52] and to provide animal models for single base mutation disease [1]. Also, while there are several engineered Adeno-associated viruses successfully delivered to the central and peripheral nervous systems in rodents, the safety and accuracy for gene therapy in human are still challenging [53].

The evaluation of reflexive pain behavior in animal models has been applied in the pain research field since decades. Recently, more clinically relevant approaches to evaluate pain in rodents have been developed. These spontaneous pain behaviors include amongst others preference for the compartment with analgesics as measured by the conditioned place preference test, and avoidance of evoked stimuli recorded by the conditioned place avoidance test [24, 26, 54]. Also, innovative devices have been developed that provide high accuracy assessment of thermal preference through free walking in thermal gradients [55, 56]. Additionally, different parameters have been shown to influence pain sensitivity in behavioral assays including the body location investigated and time of day [25]. Thus, it is very important and necessary for characterizing the phenotype of novel genetic rodent models to use a range of pain behavioral tests. In addition, the exploration of *Scn* genes roles in pain behavior would necessitate the study of the mutations in different genetic backgrounds, in both sexes, and in different

laboratories, to take in account the fact that many laboratory environmental factors can influence pain behavioral results [57].

Although there are differences between rodents and humans, the genetic rodent models are key to understand the mechanism of sodium channels in pain relief and develop novel drugs. Further specific genetic animal models and highly accurate pain behavioral assessment will open a new vision for the role of NAV1.7 and NAV1.8 in pain therapy. Also, the combination of rodent genetic models and other approaches including genetic screening will allow to identify additional components of chronic pain and to design new therapeutic strategies [4].

6. Summary

Recent research has revealed the key role of NAV1.7 and NAV1.8 in pain. In this review, we have summarized published literature on pain behaviors related to *Scn9a* and *Scn10a* in genetics rodent models. Deleting *Scn9a* and *Scn10a* either in the whole body or/and specific neuron populations relieves or attenuates the pain response from thermal, mechanical and chemical stimuli and in inflammatory and neuropathic pain models respectively, which mirrors the clinical features of CIP patients. The genetic rodent models related to *Scn* genes are still needed. Further work could reveal how NAV1.7 and NAV1.8 mediate in the SFN-related pathology (or pain) by establishing animal models for the mutations found in SFN patients and developing novel targeted medicine.

Table 1. Pain Behaviors in *Scn9a*(Nav1.7)-related genetic models

		Rat	Mice				
		Scn9a LOF [23, 27]	*Scn9a* Global KO [22]	*Scn9a*^{Scn10a} cKO [21, 28-32, 35]	*Scn9a*^{Advill} cKO [28, 30, 32]	*Scn9a*^{Wnt1} cKO [28, 30, 32, 33]	*Scn9a*^{CAGERT} KO [34]
Basal nociception							
Mechanical	Von Frey	↘ =	=	Test-site- and condition-dependent deficits			=
	Randall-Selitto or tail clip	ND	↘	↘	↘	↘	↘
	Pin-prick	↘	ND	ND	ND	ND	ND
Heat	Hargreaves	↘	ND	↘ =	↘	↘	↘
	Hot Plate or Tail Immersion	↘	↘	=	=	↘	↘
Cold	Acetone	ND	ND	=	↘	↘	ND
	Cold Plate or Dry ice	↘	ND	=	=	=	ND
Dynamic thermal place preference, cooling		=	ND	ND	↘	ND	ND
Chemically induced visceral pain		ND	ND	=	ND	ND	↘
Inflammatory pain							
Formalin Phase I		↘	↘	=	↘	ND	↘
Formalin Phase II		↘	↘	↘	↘	ND	=
CFA		ND	↘	↘	ND	ND	↘ heat = touch
Carrageenan		ND	ND	↘	ND	ND	ND
Neuropathic pain							
SNT		ND	ND	=	=	↘	ND
CCI		ND	ND	↘ cool = touch	↘	↘	ND
pSNL, SNL or SNI		↘	ND	↘ cool = touch	ND	ND	↘ cool = touch
Oxaliplatin		ND	ND	=	=	=	ND
Other pain models							
Cancer-induced pain		ND	ND	ND	=	=	ND
Burn injury		ND	ND	↘ heat = touch	ND	ND	ND

CCI: Chronic Constriction Injury; CFA: Complete Freund's Adjuvant; KO, knockout; LOF: Loss-of-function; ND: Not Done; SNI: Spared Nerve Injury; pSNL: partial sciatic Nerve Ligation; SNL: Spinal Nerve Ligation; SNT: Spinal Nerve Transection;

=: no change; ↘ : less sensitive compared control

Table 2. Pain Behaviors in *Scn10a*(Nav1.8)-related genetic models

		Scn10a^{T790A} [39, 40]	*Scn10a* Global KO [18, 30-31,41-46]	*Scn10a*^{Cre} Heterozygotes [17-18, 21]	*Scn10a-Scn9a* Double KO [18]
			Basal nociception		
Mechanical	Von Frey	=	=	=	=
	Randall-Selitto	ND	↘	=	↘
	Needle prick	↗	ND	ND	ND
Heat	Hargreaves	ND	= ↘	=	↘
	Tail Flick or immersion	ND	= ↘	ND	ND
	Hot Plate	=	=	=	=
Cold	Acetone	ND	=	ND	ND
	Cold plantar	ND	=	ND	ND
	Cold plate	↗	↘	ND	ND
Chemically induced Visceral pain		ND	↘	ND	ND
			Inflammatory pain		
Formalin	Phase 1	ND	=	=	=
	Phase 2	ND	=	=	↘
Carrageenan	Hargreaves	ND	=, delayed	=	ND
CFA	Von Frey	=	=	=	ND
	Hargreaves	ND	=, recover faster	=	ND
			Neuropathic pain		
SNT/SNL	Acetone	ND	=	ND	ND
	Von Frey	ND	=	=	=
	Hargreaves	ND	=	=	ND
CCI	Acetone	ND	= ↘	ND	ND
	Von Frey	ND	=	ND	ND
SNI	Acetone	ND	↘	ND	ND
	Von Frey	ND	=	ND	ND
Oxaliplatin	Acetone	ND	=	ND	ND
	Von Frey	ND	=	ND	ND
			Other pain model		
Burn injury		ND	=	ND	ND

CCI: Chronic Constriction Injury; CFA: Complete Freund's Adjuvant; KO: knockout; SNI: Spared Nerve Injury; SNL: Spinal Nerve Ligation; SNT: Spinal Nerve Transection

ND: Not Done; =: no change; ↘ less sensitive compared control; ↗ : More sensitive compared control

7. References

1. Raja, S.N., et al., *The revised International Association for the Study of Pain definition of pain: concepts, challenges, and compromises.* Pain, 2020.
2. Mills, S.E.E., K.P. Nicolson, and B.H. Smith, *Chronic pain: a review of its epidemiology and associated factors in population-based studies.* Br J Anaesth, 2019. **123**(2): p. e273-e283.
3. Woolf, C.J., *Capturing Novel Non-opioid Pain Targets.* Biol Psychiatry, 2020. **87**(1): p. 74-81.
4. Calvo, M., et al., *The Genetics of Neuropathic Pain from Model Organisms to Clinical Application.* Neuron, 2019. **104**(4): p. 637-653.
5. Zhang, Z.J., B.C. Jiang, and Y.J. Gao, *Chemokines in neuron-glial cell interaction and pathogenesis of neuropathic pain.* Cell Mol Life Sci, 2017. **74**(18): p. 3275-3291.
6. Cazzato, D. and G. Lauria, *Small fibre neuropathy.* Curr Opin Neurol, 2017. **30**(5): p. 490-499.
7. Faber, C.G., et al., *Gain of function Nanu1.7 mutations in idiopathic small fiber neuropathy.* Ann Neurol, 2012. **71**(1): p. 26-39.
8. Bennett, D.L., et al., *The Role of Voltage-Gated Sodium Channels in Pain Signaling.* Physiol Rev, 2019. **99**(2): p. 1079-1151.
9. McDermott, L.A., et al., *Defining the Functional Role of NaV1.7 in Human Nociception.* Neuron, 2019. **101**(5): p. 905-919 e8.
10. Baker, M.D. and M.A. Nassar, *Painful and painless mutations of SCN9A and SCN11A voltage-gated sodium channels.* Pflugers Arch, 2020. **472**(7): p. 865-880.
11. Shen, H., et al., *Structures of human Nav1.7 channel in complex with auxiliary subunits and animal toxins.* Science, 2019. **363**(6433): p. 1303-1308.
12. Black, J.A., et al., *Expression of Nav1.7 in DRG neurons extends from peripheral terminals in the skin to central preterminal branches and terminals in the dorsal horn.* Mol Pain, 2012. **8**: p. 82.
13. Kanellopoulos, A.H., et al., *Mapping protein interactions of sodium channel NaV1.7 using epitope-tagged gene-targeted mice.* EMBO J, 2018. **37**(3): p. 427-445.
14. Alles, S.R.A., et al., *Sensory neuron-derived NaV1.7 contributes to dorsal horn neuron excitability.* Sci Adv, 2020. **6**(8): p. eaax4568.
15. Chew, L.A., et al., *Mining the Nav1.7 interactome: Opportunities for chronic pain therapeutics.* Biochem Pharmacol, 2019. **163**: p. 9-20.
16. Wood, J.N., et al., *Sodium Channels and Pain*, in *The Oxford Handbook of the Neurobiology of Pain*. 2020. p. 232-262.
17. Agarwal, N., S. Offermanns, and R. Kuner, *Conditional gene deletion in primary nociceptive neurons of trigeminal ganglia and dorsal root ganglia.* Genesis, 2004. **38**(3): p. 122-9.

18. Nassar, M.A., et al., *Neuropathic pain develops normally in mice lacking both Na(v)1.7 and Na(v)1.8.* Mol Pain, 2005. **1**: p. 24.

19. Lu, V.B., S.R. Ikeda, and H.L. Puhl, 3rd, *A 3.7 kb fragment of the mouse Scn10a gene promoter directs neural crest but not placodal lineage EGFP expression in a transgenic animal.* J Neurosci, 2015. **35**(20): p. 8021-34.

20. Hameed, S., *Nav1.7 and Nav1.8: Role in the pathophysiology of pain.* Mol Pain, 2019. **15**: p. 1744806919858801.

21. Nassar, M.A., et al., *Nociceptor-specific gene deletion reveals a major role for Nav1.7 (PN1) in acute and inflammatory pain.* Proc Natl Acad Sci U S A, 2004. **101**(34): p. 12706-11.

22. Gingras, J., et al., *Global Nav1.7 knockout mice recapitulate the phenotype of human congenital indifference to pain.* PLoS One, 2014. **9**(9): p. e105895.

23. Grubinska, B., et al., *Rat NaV1.7 loss-of-function genetic model: Deficient nociceptive and neuropathic pain behavior with retained olfactory function and intra-epidermal nerve fibers.* Mol Pain, 2019. **15**: p. 1744806919881846.

24. Tappe-Theodor, A. and R. Kuner, *A common ground for pain and depression.* Nat Neurosci, 2019. **22**(10): p. 1612-1614.

25. Minett, M.S., K. Quick, and J.N. Wood, *Behavioral Measures of Pain Thresholds.* Curr Protoc Mouse Biol, 2011. **1**(3): p. 383-412.

26. Barrot, M., *Tests and models of nociception and pain in rodents.* Neuroscience, 2012. **211**: p. 39-50.

27. Chen, L., et al., *Pharmacological characterization of a rat Nav1.7 loss-of-function model with insensitivity to pain.* Pain, 2020. **161**(6): p. 1350-1360.

28. Minett, M.S., et al., *Distinct Nav1.7-dependent pain sensations require different sets of sensory and sympathetic neurons.* Nat Commun, 2012. **3**: p. 791.

29. Hockley, J.R., et al., *Visceral and somatic pain modalities reveal NaV 1.7-independent visceral nociceptive pathways.* J Physiol, 2017. **595**(8): p. 2661-2679.

30. Minett, M.S., N. Eijkelkamp, and J.N. Wood, *Significant determinants of mouse pain behaviour.* PLoS One, 2014. **9**(8): p. e104458.

31. Shields, S.D., et al., *Sodium channel Na(v)1.7 is essential for lowering heat pain threshold after burn injury.* J Neurosci, 2012. **32**(32): p. 10819-32.

32. Minett, M.S., et al., *Pain without nociceptors? Nav1.7-independent pain mechanisms.* Cell Rep, 2014. **6**(2): p. 301-12.

33. Pereira, V., et al., *Analgesia linked to Nav1.7 loss of function requires micro- and delta-opioid receptors.* Wellcome Open Res, 2018. **3**: p. 101.

34. Shields, S.D., et al., *Insensitivity to Pain upon Adult-Onset Deletion of Nav1.7 or Its Blockade with Selective Inhibitors.* J Neurosci, 2018. **38**(47): p. 10180-10201.

35. Zhou, X., et al., *Spider venom-derived peptide induces hyperalgesia in Nav1.7 knockout mice by activating Nav1.9 channels.* Nat Commun, 2020. **11**(1): p. 2293.

36. Withey, S.L., D.R. Maguire, and B.D. Kangas, *Developing Improved Translational Models of Pain: A Role for the Behavioral Scientist.* Perspect Behav Sci, 2020. **43**(1): p. 39-55.

37. Gregory, N.S., et al., *An overview of animal models of pain: disease models and outcome measures.* J Pain, 2013. **14**(11): p. 1255-69.

38. Minett, M.S., et al., *Endogenous opioids contribute to insensitivity to pain in humans and mice lacking sodium channel Nav1.7.* Nat Commun, 2015. **6**: p. 8967.

39. Blasius, A.L., et al., *Hypermorphic mutation of the voltage-gated sodium channel encoding gene Scn10a causes a dramatic stimulus-dependent neurobehavioral phenotype.* Proc Natl Acad Sci U S A, 2011. **108**(48): p. 19413-8.

40. Garrison, S.R., et al., *A gain-of-function voltage-gated sodium channel 1.8 mutation drives intense hyperexcitability of A- and C-fiber neurons.* Pain, 2014. **155**(5): p. 896-905.

41. Akopian, A.N., et al., *The tetrodotoxin-resistant sodium channel SNS has a specialized function in pain pathways.* Nat Neurosci, 1999. **2**(6): p. 541-8.

42. Kerr, B.J., et al., *A role for the TTX-resistant sodium channel Nav 1.8 in NGF-induced hyperalgesia, but not neuropathic pain.* Neuroreport, 2001. **12**(14): p. 3077-80.

43. Leo, S., R. D'Hooge, and T. Meert, *Exploring the role of nociceptor-specific sodium channels in pain transmission using Nav1.8 and Nav1.9 knockout mice.* Behav Brain Res, 2010. **208**(1): p. 149-57.

44. Luiz, A.P., et al., *Cold sensing by NaV1.8-positive and NaV1.8-negative sensory neurons.* Proc Natl Acad Sci U S A, 2019. **116**(9): p. 3811-3816.

45. Zimmermann, K., et al., *Sensory neuron sodium channel Nav1.8 is essential for pain at low temperatures.* Nature, 2007. **447**(7146): p. 855-8.

46. Laird, J.M., et al., *Deficits in visceral pain and referred hyperalgesia in Nav1.8 (SNS/PN3)-null mice.* J Neurosci, 2002. **22**(19): p. 8352-6.

47. Mickle, A.D. and R.W.t. Gereau, *A bright future? Optogenetics in the periphery for pain research and therapy.* Pain, 2018. **159 Suppl 1**: p. S65-S73.

48. Daou, I., et al., *Optogenetic Silencing of Nav1.8-Positive Afferents Alleviates Inflammatory and Neuropathic Pain.* eNeuro, 2016. **3**(1).

49. DeBerry, J.J., et al., *Differential Regulation of Bladder Pain and Voiding Function by Sensory Afferent Populations Revealed by Selective Optogenetic Activation.* Front Integr Neurosci, 2018. **12**: p. 5.

50. Wu, W., Y. Yang, and H. Lei, *Progress in the application of CRISPR: From gene to base editing.* Med Res Rev, 2019. **39**(2): p. 665-683.

51. Shah, S.Z., et al., *Advances In Research On Genome Editing Crispr-Cas9 Technology.* J Ayub Med Coll Abbottabad, 2019. **31**(1): p. 108-122.

52. Li, Z.M., L.X. Chen, and H. Li, *Voltage-gated Sodium Channels and Blockers: An Overview and Where Will They Go?* Curr Med Sci, 2019. **39**(6): p. 863-873.

53. Hudry, E. and L.H. Vandenberghe, *Therapeutic AAV Gene Transfer to the Nervous System: A Clinical Reality.* Neuron, 2019. **101**(5): p. 839-862.

54. Turner, P.V., D.S. Pang, and J.L. Lofgren, *A Review of Pain Assessment Methods in Laboratory Rodents.* Comp Med, 2019. **69**(6): p. 451-467.

55. Bohic, M., et al., *Loss of bhlha9 Impairs Thermotaxis and Formalin-Evoked Pain in a Sexually Dimorphic Manner.* Cell Rep, 2020. **30**(3): p. 602-610 e6.

56. Touska, F., et al., *Comprehensive thermal preference phenotyping in mice using a novel automated circular gradient assay.* Temperature (Austin), 2016. **3**(1): p. 77-91.

57. Mogil, J.S., *Laboratory environmental factors and pain behavior: the relevance of unknown unknowns to reproducibility and translation.* Lab Anim (NY), 2017. **46**(4): p. 136-141.

II Thesis Project

Neuropathic pain causes by a lesion or disease of the somatosensory system, including peripheral fibers (thinly myelinated nerve fibers-Aβ, Aδ fibers, and unmyelinated nerve fibers-C fibers) and central neurons. It affects the life quality of 5% of the general population. SFN, a disorder of Aδ-fibers and C-fibers, is usually characterized by neuropathic pain symptoms and autonomic complaints in the clinic. The NAV1.7 sodium channel preferentially expresses the peripheral nervous system within sensory dorsal root ganglion and sympathetic ganglion neurons and their small diameter peripheral axons. Interestingly, in idiopathic SFN, nearly 30% of patients have been found with gain-of-function mutations in *the Scn9a* gene encoding for the NAV1.7 α-subunit of sodium channel [128]. In 2012, Faber, C.G., and her colleagues found eight gain-function mutations in NAV1.7 sodium channel in idiopathic small nerve fiber neuropathy [67]. One of these mutations, c.554G>A, p.R185H at the heterozygous state in two unrelated patients. This mutation resulted in DRG neuron hyperexcitability in SFN patients and in vitro culture of rat DRG neurons, but not in the rat's superior cervical ganglion neurons. However, the *in vivo* role of this SCN9A-R185H sodium channel mutation remained to be determined

The RNA-guided endonuclease Cas9 from microbial type II CRISPR systems is a research hotspot in genome editing and regulation. Recently, this system has been harnessed to facilitate facile genetic manipulations in various cell types and organisms.

Therefore, in this project, we focus on the following objectives:

1. To establish in parallel two pain-related mouse models, which are the R185H mutation in NAV1.7 sodium channel mouse modeled by homology-directed repair (HDR) repair pathway and the NAV1.7 sodium channel knockout modeled by non-homologous end joining (NHEJ) pathway. The off-target effect was tested on the two pain-related mouse models.
2. To characterize these two mouse models' effects using biochemical, genetic, behavioral assays, neurophysiology, and neuropathology study.

All of these explorations will benefit to research on genotype-phenotype association and the role of NAV1.7 mutations in idiopathic SFN.

III Materials and Methods

My methods section is split into two parts. The first part is described in the Method of publication manuscript, including the Animals, Behavioral test, RNA extraction, and mRNA quantification, and the Statistic Analysis. The second part is described here and contain additional techniques or experimental steps used during my project.

1. Establish Mouse Models Strategy by CRISPR-Cas9

1.1 sgRNA and donor oligonucleotides design

We used the CRISPOR online software (http://tefor.net/crispor/crispor.cgi), developed by the French TEFOR infrastructure, to select sgRNAs. Simply, we downloaded the C57BL/6CNr mouse *Scn9a* sequence from the Ensembl database (http://www.ensembl.org/index.html) and put the targeted exon (*Scn9a* exon5) sequence into CRISPOR software. Then we selected the species genome and protospacer adjacent motif (PAM) to submit. Finally, we got all of the possible sgRNA with specificity score and off-targets. We selected high specificity score sgRNA with a low number of off-targets to use (Supplementary Figure 2.1).

We designed sequences for donor templates with homology arms at least 60nt in size flanking the intended point mutation. To prevent re-cutting of the modified allele by Cas9, we design a silence mutation in PAM loci, TTC change to TTT. Furthermore, another silence mutation designed into ssODN, CTC changed to CTT for introducing restriction digest site to aid with subsequent animal genotyping. Single-stranded oligo-deoxynucleotide donor sequences were ordered using GATC-Biotech services (Figure 1).

1.2 Cas9 Synthesis and sgRNA transcription *in Vitro*

The Cas9 vector (T7-Cas9 wt cloned in pUC57) with T7 promoter was first linearized with AccI as a template, using in vitro transcription with T7 polymerase. Cas9 mRNA transcribed using mMESSAGEmMACHINE T7 Ultra Kit according to the manufacturer's manual (Life Technologies). 1 µg plasmid containing sgRNA scaffold (C5648) was linearized with BglI restriction enzyme. Purify the linearized plasmid with the Nucleospin Gel and PCR Clean-up (Macherey Nagel) following the kit instructions. gDNA was obtained by PCR amplification with primers (Supplementary Figure. 2.2A). The gDNA has to purify with the Nucleospin Gel and PCR Clean-up (Macherey Nagel). Then it was used to transcribe sgRNAs using Megashort script T7 kit (Supplementary Figure. 2.2B). Cas9 mRNA and sgRNAs were purified with the PCR Clean up (Macherey Nagel) and eluted in TE buffer (10 mM Tris-HCl, 0.1 mM EDTA, Invitrogen) for microinjections.

1.3 Genomic DNA Extraction from Tail Biopsies

Primer sequences were selected using Vector NTI 5.0 software. Optimal primers annealed at least 200nt away from the intended sgRNAs cutting sites to ensure them not to be included within large deletion events and allow for the full characterization of nucleotide changes induced by the

CRISPR/Cas9 system. Care was taken to avoid amplicons containing repeat sequence wherever possible as these would potentially affect subsequent sequence analysis.

Phusion Hot Start II High-Fidelity DNA polymerase kit (Thermo Scientific) used for experiments. PCR reaction contained 500 ng genomic DNA extracted from a wild type mouse, 4 µl 5×Phusion HF Buffer, 0.4 µl dNTP mix (dATP, dCTP, dGTP, dTTP at 10 mM, Thermo Scientific), 0.2 µl each primer at 0.5 µM, and H2O in a total volume of 20 µl. Using a T100 thermocycler (Bio-Rad), PCRs were subject to the following thermal conditions; 98°C for the 30s followed by 30 cycles of 98°C for 8s, a gradient of annealing temperatures between 55-65°C for 10s and 72°C for 1 min/kb and a final elongation step for 5min at 72°C. PCR outcome was analyzed on a 1.5 to 2% agarose gel (Supplementary Figure. 2.3A), depending on the amplicon size and the highest efficient annealing temperature identified for the primer pair. New oligonucleotides were designed and optimized on rare occasions when initial primer sequences could not be optimized to obtain specific PCR products.

1.4 Off-targets Primer Design and Optimization of the Assay Conditions

The rule of primer sequences selection for off-targets analysis using Vector NTI 5.0 software is as same as before primer design and optimized (Supplementary Figure. 2.3).

1.5 Check *in Vitro* sgRNA Validity

Before injecting sgRNAs in eggs, to validate their efficiency, sgRNA was tested on the targeted DNA PCR product in vitro. The sequence surrounded the target amplified using the optimized protocol. Then 2µL targeted DNA at 50ng/µl were mixed with 1µl Cas9 protein at 100ng/ µl, 1 µl sgRNA at 100ng/ µl, 2 µl NEB buffer 2.1, and H2O in a total volume of 20 µl. As a control, the Cas9 protein was omitted. The reactions incubate in a thermocycler 30min at 30°C, then 15min at 65°C. The reaction loaded on a 2.5% agarose gel (Supplementary Figure. 2.2C). The correct sizes after Cas9 cleavage allow for validation of the functionality of the tested guide. Only sgRNAs showing a cut (even partial) injected into eggs.

1.6 Pronuclear Microinjections of Zygotes

All mice were housed at 21 °C on a 12/12 h light-dark cycle (7:00 am–07:00 pm) in the SPF facilities. Sexually immature female C57BL/6CNr mice (4-5 weeks old) were super-ovulated by intraperitoneal injection of 5 IU eCG followed by 2.5 IU hCG interval of 48 h and mated overnight

with C57BL/6NCr male mice that were > 10 weeks old. Zygotes were collected after 20 h of hCG injection by oviductal flashing, and pronuclei-formed zygotes were put into the M2 medium (Sigma M-7167). Microinjection was performed using a microinjector (Eppendorf Femtojet 4i) equipped microscope. RNA solution injected into the cytoplasm and the pronucleus of each zygote using continuous pneumatic pressure. After injection, embryos were in vitro cultured in the M16 medium (Sigma M-7292) at 37 °C in a 5% CO2 incubator. The survivors of the injected embryos implanted into the oviducts of pseudo-pregnant CD1 mice

1.7 PCR Amplification and Sequencing

As defined above, each project's PCRs run, and an aliquot was analyzed on an agarose gel using optimized conditions. Potential PCR products were sent for Sanger sequencing by GATC-Biotech sequencing services. Sequence information was obtained from GATC-Biotech Sequencing services.

1.8 Analysis of Off Targets

The CRISPOR online software (http://tefor.net/crispor/crispor.cgi) also allowed predicting likely off-target sites within the rest of the mouse genome based on the sequence of each of the sgRNA recognition sequences chosen. We selected poteintial off-target sequences around the mouse genome that contained the minimal numbers (2 to 3) of mismatch regions and the same chromosome with the targeted region (Supplementary Table 3). PCR primers designed that flanked off-target sites at an optimal distance of 100-150 base pairs to give PCR product lengths of between 400-500 base pairs to aid in subsequent sequencing (Supplementary Table 4). Purified PCR products were sequenced by GATC-Biotech sequencing services using each of the PCR primers used for the PCR reaction. Then, sequence information obtained from GATC-Biotech Sequencing services was analyzed.

2. Histological Analysis

2.1 Tissue Preparation

Mice were anesthetized with ketamine/xylazine and perfused intracardially with 40 ml of phosphate buffer saline 0.1 M pH 7.4 (PBS) following 4% paraformaldehyde (PFA) in 0.1 M pH 7.4 PBS. Both sides of L4 to L6 lumbar DRG and sciatic nerves were dissected out and post-fixed for overnight at 4 °C in 4% PFA in PBS, cryoprotected at 4 °C in 30% sucrose in PB for 3-7 days,

embedded in Optimal Cutting Temperature medium (OCT), frozen and kept at -80 °C. DRG (8 µm thick), sciatic nerves (10 µm thick) section were cut with a cryostat and kept in -20 °C.

2.2 Immunohistochemistry

Immunohistochemistry was performed following the steps below:

1) Rinse floating sections in 0.02 M PBS, 2 x 5 minutes.
2) For light antigen retrieval, treat sections in 0.2 % hydrogen peroxide in 0.1 M phosphate buffer (PB) pH 7.3 containing 0.05% Triton X-100 for 25 minutes at room temperature.
3) Rinse sections in 0.02M PBS, 2x 5 minutes.
4) Incubate sections with the primary antibody (Rabbit anti-SCN9A-ATTO Fluor-663 antibody, 1:100, ASC-008-FR, allomone labs; Mouse anti-PGP9.5 antibody, 1:200, ab8189, abcam) diluted in a medium containing 0.05% Triton X-100, 0.05% Tween 20, 2% normal donkey serum (NDS), for 1 hour at room temperature.
5) Refrigerate overnight.
6) Rinse sections in 0.02 M PBS, containing 2% NDS, 2 x 5 minutes.
7) Incubate section with the second antibody (Alexa-488 donkey anti-mouse, 1:500, A32766, Invitrogen)
8) Rinse sections in 0.02M PBS, 3x10 minutes.
9) Mount sections on glass slides from 0.02 M PBS, pH 7.0-7.4.
10) Allow to dry in a fume hood for 1 h.
11) Stain section on slides with DAPI (Molecular Probes), by placing DAPI solution on each slide, and covering the slide with a piece of parafilm to spread the solution evenly on the slide.
12) After 2 minutes, remove the parafilm and rinse the slide with 0.5 ml distilled deionized water using a pipette (repeat twice).
13) Let slides dry in a fume hood for 0.5 h.
14) Coverslip using the Fluoromount G (FP-483331, Interchim SA).
15) Leave slides to dry overnight in the dark.
16) Store at 4 ºC until microscopy.

2.3 Image Acquisition and Analysis

Images were acquired with the Leica fluorescence microscope using a 20× (DRG) and 40× (sciatic nerves) dry objective, the 20× and 40× resolution were achieved with a digital zoom factor. Image acquisitions in the sequential mode (single excitation beams: 405, 488 and 633 nm) were used for marker co-localization to avoid potential crosstalk between the different fluorescence emissions. Images were acquired with the LCS (Leica) software using randomly selected sections.

The ImageJ software cell counter (approximately 4 non-adjacent sections per condition and per animal) was used to count on-screen neurons expressing a given fluorescent marker manually and blindly. Only neurons from L4-L6 DRGs with a visible nucleus were considered. Cells expressing a given marker fluorescence were analyzed separately. During the analysis, we recorded all cross-sectional areas of cell profiles for SCN9A. Present of positive and negative SCN9A neurons in total neurons were categorized to different size based on area. Threshold was applied to fluorescence detection in sciatic nerve. The mean of fluorescence density was measured for SCN9A fluorescence in sciatic nerve.

IV Results

In this part, firstly I will show the most important results from publication manuscript. Due to the size limitation in publication paper, I will present more detailed results that the creation of *Scn9a*^{R185H} and *Scn9a*$^{R185X/wt}$ mouse lines and other characterizations in these two mouse lines.

1. Publication Manuscript in Preparation

Modeling the human *SCN9A*^{R185H} mutation found in patients with chronic pain using CRISPR/Cas9 in the mouse, consequences on pain sensitivity

Yaping XUE, Céleste CHIDIAC, Marie-Christine BIRLING, Claire GAVERIAUX-RUFF[$], and Yann HERAULT[$,#]

Institut de Génétique et de Biologie Moléculaire et Cellulaire, Translational Medicine and Neurogenetics Department, 1 rue Laurent Fries, 67400 Illkirch, France

Université de Strasbourg, Illkirch, France

Centre National de la Recherche Scientifique, UMR7104, Illkirch, France

Institut National de la Santé et de la Recherche Médicale, U1258, Illkirch, France

$ Equal last authors

#Corresponding authors:

Yann Herault, PhD, herault@igbmc.fr

Claire Gaveriaux-Ruff, PhD, gaveriau@igbmc.fr

IGBMC, 1 rue Laurent Fries, BP10142, 67404 Illkirch Cedex, France

Abstract

The NAV1.7 channel, encoded by *Scn9a* gene, is a voltage-gated sodium channel that plays a critical role in the generation and conduction of action potentials. In peripheral sensory neurons, the expression and dynamic regulation of NAV1.7 is involved in pain sensitivity and chronic pain development. Several *SCN9A* gain-of-function (GOF) mutations have been found in small fiber neuropathy (SFN) patients with chronic pain whereas loss-of-function of *SCN9A* by bi-allelic inactivating mutations result in the striking clinical phenotype of congenital insensitivity to pain (CIP). These individuals do not perceive pain in response to noxious stimuli. However, the carriers of one allelic inactivating mutation have normal pain sensitivity. One GOF mutation was the missense R185H mutation and the patients were heterozygous for this mutation. We have successfully established two mouse models of the $Scn9a^{R185H}$ and $Scn9a^{R185X/wt}$ mutations using the CRISPR/Cas9 technology and characterized the effect of these mutations on pain sensitivity and molecular and cellular alteration in these two models. The two mouse lines showed no alteration of growth, survival and global health state. Pain sensitivity of mutant mice was investigated on both sexes using behavioral tests of sensitivity to thermal and mechanical stimuli. Our results indicate that $Scn9a^{R185H}$ mice show an increased pain phenotype, suggesting that the *SCN9A* R185H mutation identified in the SFN patients is responsible for their pain symptoms. This exploration will benefit to drug screen. The $Scn9a^{R185X/wt}$ heterozygous mice in which only one allele is functional showed a normal nociceptive behavior except a reduced sensitivity to hot plate pain test. Therefore, we provide genetic evidence that NAV1.7 encoded by *Scn9a* plays an important role in nociception and in the pain experienced by SFN patients with the *SCN9A* R185H mutation.

Introduction

Painful Small fiber neuropathy (SFN) is a disorder of Aδ-fibers and C-fibers characterized by neuropathic pain symptoms and autonomic complaints. Several common diseases, such as diabetes mellitus and HIV, have been reported to complicate SFN [1, 2]. Interestingly, gain-of-function (GOF) mutations in the *SCN9A* gene encoding for the NAV1.7 α-subunit of sodium channel have been identified in 28% of patients with painful idiopathic SFN [3]. However, the phenotype of SFN in patients is complex and the role of the mutant Nav1.7 sodium channel activity in these patients remains to be clarified.

Nav1.7 channel is a voltage-gated sodium channel that plays a critical role in the generation and conduction of action potentials and is thus important for electrical signaling by most excitable cells. It is preferentially expressed in the peripheral nervous system within sensory dorsal root ganglion and sympathetic ganglion neurons [4, 5]. In 2012, C.G. Faber and her colleagues found heterozygous c.554G>A, p.R185H mutations in *SCN9A* gene of two unrelated painful SFN patients [6]. This mutation resulted in the hyperexcitability of dorsal root ganglion (DRG) rat neurons when transfected into these neurons [7]. At the opposite, *SCN9A* loss-of-function bi-allelic mutations are known to result in congenital insensitivity to pain (CIP) while the mono-allelic carriers have normal pain sensitivity [8, 9].

In order to explore the NAV1.7-R185H genotype-phenotype association and the underlying mechanisms for NAV1.7-R185H sodium channel mutation in idiopathic SFN, we have created a *Scn9a*^{R185H} mouse model and characterized this model for nociceptive behavior. We have also generated the mutant *Scn9a*$^{R185X/wt}$ mouse model to explore potential novel therapies for CIP. These two mouse lines were generated by using the Crispr/Cas9 technology. We found that *Scn9a*^{R185H} mRNA is expressed at comparable levels in the mutant mice as wild-type (WT) mRNA in control mice. Pain sensitivity of the mutant mouse lines was investigated on both sexes using behavioral tests of sensitivity to thermal and mechanical stimuli. Our results indicate that the *Scn9a*^{R185H} mice show a pain phenotype, suggesting that the *SCN9A* R185H mutation identified in the SFN patients is responsible for their pain symptoms. Interestingly, *Scn9a*$^{R185X/wt}$ heterozygous mutant mice showed a decrease sensitivity to heat stimuli. Therefore, altogether we provide genetic evidence that the *SCN9A*-encoded NAV1.7 channel plays a crucial role in nociception behavior and painful idiopathic SFN

Methods

1. Animals

1.1. Experimental subjects and ethical approval

Animal experiments were performed with protocols approved by local ethical committee (Com'Eth, Comité) d'Ethique pour l'Expérimentation Animale IGBMC-ICS) with the agreement number 20880. C57BL/6NCr mice were used for mutant lines generation, and C57BL/6NCr was the mouse genetic background throughout the whole study. The number of mice were used following the 3R principles. Mice were bred at the ICS animal facility and the behavioral experiments were performed in the IGBMC animal facility. The mice were housed under a 12-h/12-h light/dark cycle and 21 ± 1°C, 55 ± 10% humidity condition. Food and autoclaved tap water were available ad libitum. Each cage housed 2-5 mice. All mice were habituated to the experimental environment.

1.2. Establishment of the genetic animal models

The *Scn9a*^{R185H} and *Scn9a*$^{R185X/wt}$ mouse lines were generated by using the CRISPR-Cas9 system. We used the CRISPOR online software to select high specificity-score sgRNAs with low number of predicted off-target sequences. We designed sequences for donor templates with homology arms and of at least 60nt-long flanking the intended point mutation. We designed a silence mutation into ssODN, CTCCTT for introducing restriction site to aid with subsequent animal genotyping (Fig. 1A). Before injecting sgRNAs into eggs, sgRNA efficiency was tested on the targeted DNA by PCR in vitro. After checking sgRNA validity in vitro, sgRNA, Cas9 and ssODN were microinjected into the cytoplasm and the pronucleus of zygotes. The surviving embryos were implanted into the oviducts of pseudo-pregnant C57BL/6NCr mice. Following microinjection, newborns were screened by PCR and T7 Endonuclease assay for the whole variety of potential alleles and potential founders were identified, which were confirmed by Sanger sequencing. Mutant individuals were bred with wild type C57BL/6NCr mice to generate F1 founders. F1 mice were analyzed for their genotype by Sanger Sequencing to establish the *Scn9a*^{R185H} and *Scn9a*$^{R185X/wt}$ mouse lines. These mice were also checked for off-target effects, see in the Results section. Hereafter, *Scn9a*$^{wt/wt}$ animals will be named +/+; *Scn9a*$^{R185H/wt}$ *R185H/+* ; *Scn9a*$^{R185H/R185H}$ *R185H/R185H*, and *Scn9a*$^{R185X/wt}$ *R185X/+.*

1.3. Determination of genotype

We harvested 0.5 cm tails after mouse born from two mouse lines. For *Scn9a*^{R185H} mouse line, crude genomic DNA extracted by DirectPCR Lysis Reagent-Tail (Viagen Biotech, Cat # 101-T) according to the manufacturer's instructions. Phusion Hot Start II High-Fidelity DNA polymerase kit (Thermo Scientific) was used. PCR reaction contained 500 ng genomic DNA extracted from a wild type mouse, 4 µl 5×Phusion HF Buffer, 0.4 µl dNTP mix (dATP, dCTP, dGTP, dTTP at 10 mM, Thermo Scientific), 0.2 µl each primer at 0.5 µM and H2O in a total volume of 20 ml. Using a T100 thermocycler (Bio-Rad), PCRs were subject to the following thermal conditions; 98°C for 30s followed by 30 cycles of 98°C for 8s, a gradient of annealing temperatures between 55-65°C for 10s and 72°C for 1 min/kb and a final elongation step for 5min at 72°C. PCR outcome was analyzed on a 1.5 to 2% agarose gel. Primer sequences information is showed in Supplementary Table 1.

For *Scn9a*$^{R185X/wt}$ mouse line, genomic DNA extracted by phenol-chloroform-isoamyl alcohol (PCIA) reagent. Genotyping by ddPCR was performed in 20 µL reactions containing 1× ddPCR Supermix for Probes (No dUTP), 250 nM of each probe, 900 nM specific primers, and 50 ng DNA according to manufacturer's recommendations (PCR conditions: 10 min at 95 °C, 40 cycles of 30 s at 94 °C and 30 s at 55 °C, and 10 min at 98 °C). Droplet generation and absolute droplet quantification was perfomed in a QX200 Droplet Digital PCR System (Bio-Rad) and analyzed by QuantaSoft Software (Bio-Rad). Probe and primer sequences are showed in Supplementary Table 2.

2. Determination of transcript expression by ddPCR (digital droplet PCR)

The DRGs from both sides, spinal cord and half brain were collected from mutant and +/+ mice and flash frozen in liquid nitrogen. All samples were disrupted with Precellys® CK14 Lysing Kit in TRIzol Reagent, and total RNA was purified the using the RNeasy Fibrous Tissue Mini Kit (Qiagen) according to the manufacturer's instructions. The samples quality was checked using an Agilent 2100 Bioanalyzer (Agilent Technologies). cDNA synthesis was performed using the SuperScript™ VILO™ cDNA Synthesis Kit (Invitrogen). mRNA quantification by ddPCR was performed same as *Scn9a*$^{R185X/wt}$ mouse line genotyping. Probes and primers sequence are showed in Supplementary Table 2.

3. Behavioral Tests

A series of behavioral experiments were conducted on mutants and control littermates in order to evaluate nociceptive behavior and motor conditions. For all these tests, mice were kept with free access to food and water. The light cycle was controlled as 12h light and 12h dark (lights on at 7 AM). All behavioral tests were done between 9:00 AM and 5:00 PM. Animals were transferred to the experimental room 30 min before each experimental test. The tests were administered in the following order: String test, Crenellated Bar, Von Frey, Hargreaves Plantar, Tail Flick, Tail Pressure, Hot Plate, Acetone test, Cold Plate and odor habituation and discrimination. Mice were tested at 2-month-age and then at 6-month-age with the same behavioral tests. At least 2 days were kept between two nociceptive tests. Both females and males of the different genotypes were analyzed.

3.1. String test

The grip string test (home-made) was used to measure muscle strength. The equipment was a wire stretched horizontally 40 cm above a table. The time required for a forelimb-hanging mouse to gain hindlimb traction as latency was measured, with 20 s cutoffs. Three consecutive trials were done by 5 min intervals.

3.2. Crenellated bar

The notched/crenellated bar test was used for motor coordination and balance. The method described by Carter et al. was used [10]. Briefly, mice were put on a elevated crenellated bar and had to traverse the distance from far to near to the home cage. Thereafter, the time to traverse the whole crenellated bar were recorded.

3.3. Odor habituation and discrimination

This test is adapted from the one described by Ferguson et al [11] and Duchon et al [12]. Briefly, mice are placed 5 times for 2 min in a small cage (22 cm × 15 cm). One perforated tube containing a small piece of Whatman paper soaked with orange flower water was placed in the center of cage. The time of sniffing was recorded on six trials of 2 min each with the orange flower extract. Thereafter, the extract was replaced by vanilla extract for last trail. Inter-trail time is 8 to 10 min. The time spent sniffing the odors was analyzed.

3.4. Hot Plate

Hot response refers to the method reported by Huang et al. [13]. Mice were habituated on the plate at room temperature one day before test. Mice were placed on the plate at 48 °C, 52 °C and 56 °C with respective cutoffs to avoid tissue damage: 2 min for 48 °C, 1 min for 52 °C and 30 s for 56 °C. Latency to display first reaction of hind limbs and different coping reactions before cutoff were recorded, which include flicking, licking and jumping.

3.5. Tail Flick

The mice were habituated for 30 minutes in the procedure room prior to test. During the test, mice were wrapped into 50 ml tube with the whole tail exposed. Three different distances to the tail tip were tested for reaction to the light beam. The mean of these three measurements of latency was calculated.

3.6. Hargreaves Plantar

The Hargreaves test was used to quantify responses to noxious heat at the hind paw by applying a radiant infrared heat stimulus. Before the test, the mice were habituated to the glass plate so that withdrawal latencies could be clearly determined, usually taking 30 to 45 min. A radiant heat beam was positioned underneath the mouse paws. The withdrawal latencies were recorded for both right and left hind paw. Inter time between right and left hind paw was at least 5 min. For each mouse, the response assays were tested maximum 4 times. The means of all measurements of both hind paws were calculated.

3.7. Acetone test

Mice were placed and habituated in bottom-opened plastic boxes on a mesh grid floor. One day before the test, they were habituated to the boxes for 1 hour. On the day of testing, the mice were allowed to habituate for 30 min and then 10 µL acetone was applied to the center of the plantar surface of each hind paw. The number of flicking and licking of affected paw were counted for 30s after acetone application. Acetone was applied in three successive testing sessions for each paw. The interval between each application was at least 5 min.

3.8. Cold Plate

The cold plate assay (Bioseb, France) was used to assess sensitivity to low temperatures. We used 5 °C as a test temperature. For this test, animals were habituated on the plate with room temperature in the small plastic boxes one day before test. To avoid the tissue damage, the 5 min cutoffs was used. The latency of first response and the time for hind limbs lifting were measured.

3.9. Von Frey test

Unrestrained mice were placed transparent plastic boxes and habituated in the same manner as for the acetone test. A series of eight von Frey filaments (with bending force of 0.008 to 2 g) was applied to the hind paw using the up-and-down method. Each paw was scored on two successive testing sessions. The withdrawal threshold was calculated by the Excel program generously provided by A. Basbaum (University of California San Francisco).

3.10. Tail Pressure

A gradually increasing pressure was applied to tail using the equipment Pressure AnlgesiMeter (Ugo Basile, Italy). Each mouse was measured by three successive testing sessions. The tail withdrawal threshold was recorded, with a 500 g cutoff.

4. Statistical Analysis

Results are expressed as mean ± *SEM*. Statistical analyses were performed by using GraphPad Prism 8 software. All data sets were tested for normality and t-test was used for genotype comparison when data were found normally distributed. If normality test failed, Mann-Whitney test was used. A p value < 0.05 was considered as statistically significant. Body weight per week and time spent sniffing the odor were analyzed using repeated measures ANOVA by Sidak post-hoc multiple comparation. For gene expression analysis, the genotype and sex effects were analyzed using two-way ANOVA followed by Turkey test for multiple comparisons, and genotype effect on separated males and females was analyzed with two-tailed unpaired t-test. For all the behavioral tests, genotype, sex and age effects were analyzed by three-way ANOVA and genotype and sex effects at each age were analyzed by two-way ANOVA. For Hot Plate assay, the genotype effect for both female and male group was done by one tailed t test as the limit of direction by cutoffs. The genotype effect on other parameters for different behavioral tests were analyze by two tailed t test. The Radar charts show the results as means normalized to mean of wt. The latency and threshold for Hot Plate, Tail Flick, Hargreaves Plantar, Von Frey and Tail Pressure respectively. Other parameters, including coping reactions for Hot Plate, number of flicks and licks in acetone test and paw lifts in cold plate test, firstly normalized to mean of wt, then normalized again to 1. If the value is over 1, which means the mutant mice are less sensitive compare to their wt. littermates. On contrast, if the value is less than 1, which means the mutant mice are more sensitive compare to their wt.

Results

1. Generation and characterization of CRISPR-Cas9 *Scn9a*^{R185H} and *Scn9a*$^{R185X/wt}$ mice

CRISPR-Cas9 *Scn9a*^{R185H} and *Scn9a*$^{R185X/wt}$ mouse lines were generated by CRISPR-Cas9 system. After checking sgRNA validity in vitro, different concentration of sgRNA, Cas9 and ssODN were microinjected into eggs. Four weeks after microinjection, sixty F0 founder mice were born and screened by PCR. The different product sizes found in gel analysis suggested a variety of alleles. The variety of alleles were confirmed by Sanger sequencing, see Supplementary Fig. 1 (sequencing results for founders until #58 are shown). Several F0 founders showed point mutation and high mosaicism in both alleles. Finally, five potential F0 founders were used to cross with C57BL/6NCr wild type mice to generate F1 founders. In the F1 generation, we successfully got germline transmission. We selected the 53-11 F1 animal to establish *Scn9a*^{R185H} line and the 36-5 F1 animal to establish the *Scn9a*$^{R185X/wt}$ mouse line. There has been much concern raised in the scientific community over the specificity of the CRISPR/Cas9 system. Therefore, we analyzed several predicted off-target sites that were based on the number of mismatches to the target sequences and the homologous genes by the CRISPR design tool (http://tefor.net/crispor/crispor.cgi). No evidence of Cas9 mediated deletions or base pair changes in any of the 7 mostly predicted off-target sites was found after comparing with wide-type sequence in Ensembl genome database (http://www.ensembl.org/index.html) (Supplementary Fig. 2). Thereafter, the heterozygous offspring from F1 founders (53-11 and 36-5) were crossed with each other to generate the two lines containing mutant and WT mice of both sexes for further experiments.

When evaluating *Scn9a* gene expression in the *R185H* mice, the two-way ANOVA on RT-ddPCR results showed no effect on genotype or sex on transcript expression. *Scn9a*^{wt} and *Scn9a*^{R185H} transcripts were equally expressed in the DRG, spinal cord and brain of +/+ or R185H/R185H mutant mice, respectively, and in both sexes (Figure 1B). Heterozygous *R185H/+* mice expressed about 50% of each *Scn9a*^{wt} and *Scn9a*^{R185H} transcripts. In *R185H/+* mice, the two-way ANOVA indicated an effect of genotype on +/+ transcript expression in DRG and spinal cord tissues. There was no effect of sex in any tissue of R185X/+ mutant mice. The mutants expressed low levels of *R185X* transcript as compared to +/+ transcripts (Figure 1C).

As the loss of NAV1.7 in hypothalamic neurons was reported to disrupt body weight regulation [14], we measured body weight of two mutant lines weekly. There was no difference between

mutant and wt animals for body weight (Supplementary Fig. 3A for *R185H/R185H* mice and Supplementary Fig. 4A for *R185H/+* mice). To determine whether muscle strength and motor coordination were affected in the two mutant lines, string test and crenellated bar test were performed at 2- and 6- months of age. As indicated in Supplementary Fig. 3B and Supplementary Fig. 4B, no major signs of behavioral abnormalities were found in mutant lines in these tests. The three-away ANOVA indicated an effect on sex and age for string test, but no effect on genotype and sex at each age respectively as analyzed by two-away ANOVA. For crenellated bar, there are effects on sex and age by three-way ANOVA and only sex effect was detected by two-way ANOVA at 6-month-age, but not at 2-moth age. Previous studies have showed that NAV1.7 is not only necessary for pain sensation but is also an essential requirement for odor perception in both mice and humans [15]. Here we checked the olfactory function using odor habituation and discrimination test at 2- and 6- month-age in both lines. We found that the 2-mo *R185H/R185H* females had lower sniffing time in the first trial as compared to wt controls (Supplementary Fig. 3C), and all other mutant types showed normal odor discrimination (Supplementary Fig. 3C and Supplementary Figure Fig. 4C).

2. Enhanced heat pain sensitivity in the *Scn9a*^{R185H} mice

The two SFN patients with heterozygous R185H mutation were a man and a women with abnormal warm pain sensation since they were 23-24 year old [67]. To investigate whether the R185H mutation also alters heat pain sensitivity in mutant mice, we tested mutants of both sexes and at 2-and 6-month of age on the Hot Plate in 48, 52 and 56 °C (Fig. 2, Supplementary Fig. 5 and Supplementary Fig. 6), as well as in the tail flick and Hargreaves plantar tests (Fig. 3, Supplementary Fig. 7)

Until recently, only the latency to first hindpaw response or to first jump were scored in the Hot plate test. However, in 2019, Huang et al found that their mutant mice in which spinal preprotachykinin-positive neurons have been ablated has normal first response latency on the hot plate but had reduced coping reactions [19]. Therefore, we scored the number of coping reactions (number of flicks, licks and jumps) in addition to first response and jump latencies.

First, there was no difference for first response latency between mutant and +/+ mice, for both lines, both sexes and at the three temperatures (data not shown). We compared also the jump latency and number of coping reactions of female and male +/+ mice in both mutant lines. There was no difference between +/+ females and males of the *Scn9a*^{R185H} line, at either 2- or 6-month

of age (Supplementary Fig. 5A, B). However, as compared to the *Scn9a*^{R185H} line, the +/+ 2-mo females in *Scn9a*$^{R185X/wt}$ line showed shorter jump latency and more coping reactions than males at 56 °C, while +/+ the 6-mo males had fewer coping reactions than females at 48 °C (Supplementary Fig. 5C, D).

For jump latencies in the *Scn9a*^{R185H} line, the three-way ANOVA revealed significant effects of genotype and age at 48 and 52 °C, and sex and age effects at 56 °C. Two-way ANOVA revealed a significant effect of sex at 52 and 56 °C at 2-mo and not at 6-mo of age. At 2-mo age, a sex effect was detected at 56 °C, and genotype effect was detected for the three temperatures at 6-mo age.

In the same lines, effects of genotype, sex and age were found for coping reactions by three-way ANOVA. In two-way ANOVA analysis, the genotype effect was recorded in 52 and 56 °C hot plate and sex effect in 56 °C hot plate at 2-month-age, but no effect at 6-month-age. For genotype effect at 2-mo age, we found that *R185H/+* females showed shorter jump latency at 56 °C, and R185H/R185H female mice showed also a shorter latency at all three temperatures. The male mutants showed no phenotype (Fig. 2A). The shorter jump latency occurred also at 6-mo age in the *R185H/R185H* females at 56 °C (Supplementary Fig. 6A). Similarly, the number of coping reactions was increased in female mutant mice. The 2-mo *R185H/R185H* females showed higher number of coping reactions at 52 and 56 °C (Fig. 2B), and at 6-mo *R185H/+* females showed increased coping reactions at 52 °C (Supplementary Fig. 6B). At this temperature, the increased coping reactions recorded in the 6-mo *R185H/R185H* females did not reached significance (Supplementary Fig. 6B). Increased numbers of coping reactions were also recorded in the *R185H/R185H* males at 56 °C at 2-mo age and at 48 °C at 6-month-age (Fig. 2B and Supplementary Fig. 6B).

The mutant mice were also tested for their sensitivity to radiant heat stimuli in the Tail Flick and Hargreaves Plantar tests. In the Hargreaves plantar test, no effect on genotype, sex and age were found in *Scn9a*^{R185H} mutants by three-way ANOVA. No genotype difference was detected when each sex or age of the *Scn9a*^{R185H} line was analysed individually (Fig. 3B and Supplementary Fig. 7B). In the tail flick test, three-way ANOVA showed effects of sex and age in the *Scn9a*^{R185H} mutants. The two-way ANOVA indicated a sex effect at 6-mo age but not at 2-mo age. For genotype effect, we found *R185H/R185H* females to be more sensitive at 2-mo age, with a lower reaction latency compared to +/+ (Fig. 3A) but not at 6-mo age (Supplementary Fig. 7A). The *Scn9a*^{R185H} mutant males showed no phenotype at any age.

3. Attenuated heat pain sensitivity in the *Scn9a*$^{R185/wt}$ mice

In the hotplate test, three-way ANOVA showed genotype and age effects in the *R185X/+* mice for jump latencies at the three temperatures. Interestingly, the *R185X/+* females showed conversed results as compared to *R185H/R185H* females. At both 2-mo and 6-mo ages, they had increased jump latencies at 56 °C (Fig. 2C, Supplementary Fig. 6C) and reduced coping reactions at 48, 52 and 56 °C (Fig. 2D, Supplementary Fig. 6D). Male *R185X/+* mutants had no phenotype (Fig. 2C, D; Supplementary Fig. 6C-D). The results on Hargreaves plantar and tail flick tests indicated no effect of genotype, sex or age in the *Scn9a*$^{R185X/wt}$ line (three-way and two-way ANOVAs) in these two tests (Supplementary Fig. 8A-B), contrasting with hot plate data.

In addition, we did multiple linear regression analysis of hot plate, tail flick and Hargreaves tests results of the two mutant lines to investigate whether there were intra-class correlations of genotype, sex, age and temperatures. In the *Scn9a*^{R185H} mutant mice, significant correlations between factors were found for jump latencies and coping reactions in the hot plate test, for reaction latencies in the tail flick test but not for Hargreaves test (Supplementary Table. 5a-d). In the *R185X/+* mice, significant correlations between factors were found for jump latencies and coping reactions in the hot plate test but not in the tail flick or Hargreaves plantar tests (Supplementary Table. 5e-h). In *Scn9a*^{R185H} mutants, genotype (mutants vs +/+) was negatively correlated to the jump latency (Supplementary Table. 5a) and positively correlated to the coping reactions (Supplementary Table. 5b) while we found the opposite results for the *R185X/+* mice (Supplementary Table. 5e-f). Sex significantly correlated to jump latency (Supplementary Table. 5a) and coping reactions (Supplementary Table. 5b) in the hot plate test for *Scn9a*^{R185H} mice, but not in the *R185X/+* mice (Supplementary Table. 5e-f). The age was significantly correlated to jump latency and coping reactions in the hot plate test in both mutant lines (Supplementary Table. 5a, b, e, f). Lastly, in the tail flick assay, age was correlated to latency for *Scn9a*^{R185H} mutant mice (Supplementary Table. 5c), but not for *R185X/+* mice (Supplementary Table. 5g).

Taken together, these findings show that *R185H/R185H* mutant females were more sensitive to heat stimuli than their +/+ littermates and that *R185X/+* females were less sensitive to heat, depending on the test. The *R185H/R185H* male mutants were more sensitive than their +/+ counterparts, with a smaller mutation effect than in females, and the *R185X/+* males had no pain phenotype. We also found that the age of testing had an effect on hot plate and tail flick results in our mutant mice.

4. Sensitivity to Cool and Cold Stimuli in *Scn9a*^{R185H} and *Scn9a*$^{R185X/wt}$ mice

To determine whether *Scn9a*^{R185H} mice had abnormal cold sensation like for *SCN9A* R185H patients and *Scn9a*$^{R185X/wt}$ mice normal cold sensation, we performed the acetone test for cool (12-15 °C) stimuli and 5 °C Cold Plate for cold stimulus. In the acetone test, the three-way ANOVA on *Scn9a*^{R185H} mice indicated effect on genotype and sex, but no effect on age and the two-way ANOVA at each age showed an effect of sex but not of genotype. For *Scn9a*^{R185X} mutant mice, only sex effect was found by three-way ANOVA and two-way ANOVA at 2-mo of age. In the cold plate, the ANOVA showed only an age effect in *Scn9a*^{R185H} mice for the number of paw lifts, with no genotype or sex effect at each age in either mutant. As shown in Fig. 3C and Supplementary Fig. 7C, the reaction to acetone was comparable in *R185H/R185H, R185H/+* and *+/+* mice, at both 2-mo and 6-mo of age, and similarly for the cold plate response (Fig. 3D; Supplementary Fig. 7D). The *R185X/+* mice did not show any alteration in the two cold tests (Supplementary Fig. 8D).

Interestingly, when assessing the intra-class correlation coefficients for genotype, sex and age through multiple linear regression analysis, significant correlations were found to different factors for response to acetone (Supplementary Table. 6a) and in the cold plate test (Supplementary Table. 6b) for the *Scn9a*^{R185H} mice, but not for the *Scn9a*$^{R185X/wt}$ mutants (Supplementary Table. 6d). For *Scn9a*^{R185H} mutant mice, genotype was correlated to responses to acetone (Supplementary Table. 6a) and to the cold plate (Supplementary Table. 6b). The sex factor was correlated to the acetone response (Supplementary Table. 6a), but not to cold plate reactions (Supplementary Table. 6b). The age was correlated to all parameters of cold plate in the *Scn9a*^{R185H} mutant mice (Supplementary Table. 6a-b).

According to these findings, we conclude that although there was a significant correlation between genotype and responses to cool or cold stimuli in *Scn9a*^{R185H} mutant mice, the trends observed in the mutants did not reach significance. Also, deleting of one allele of *Scn9a* did not change behavioral responses to cool or cold stimuli.

5. Enhanced Sensitivity to Mechanical Stimuli in *Scn9a*^{R185H} mice, but no effect in *Scn9a*$^{R185X/wt}$ Mice

In order to evaluate whether *Scn9a* mutant mice had normal sensitivity to mechanical stimuli, the Von Frey and tail pressure were applied to mice of the *Scn9a*^{R185H} and *Scn9a*$^{R185X/wt}$ lines. The effect of genotype, sex and age on tail pressure and Von Frey were analyzed in both mutant lines. The *Scn9a*^{R185H} and *Scn9a*$^{R185X/wt}$ mice displayed only age effects. No effect on genotype and sex was found for tail pressure in both mutant mice at 2- and 6-month-age. No change of threshold was found for tail pressure in both *Scn9a*^{R185H} and *Scn9a*$^{R185X/wt}$ lines and at both age (Fig. 3F, Supplementary Fig. 7F and Supplementary Fig. 8F). For the Von Frey test, three-way ANOVA showed significant genotype effect in *Scn9a*^{R185H} mice but not in the *Scn9a*$^{R185X/wt}$ mutants. The genotype effect was seen at 2-mo age following two-way ANOVA, but not at 6-month-age. We found that *R185H/+ and R185H/R185H* female and *R185H/R185H* male mice showed enhanced pain sensitivity at 2-mo (Fig. 3E) but not at 6-mo age (Supplementary Fig. 7E). There was no phenotype in the *R185X/+* mutants at any age (Supplementary Fig. 8E).

As thermal stimuli tests, we also did multiple linear regression analysis for both mutant lines. Significant correlations were found for both mutant lines and for both mechanical behavioral tests. In *Scn9a*^{R185H} mutant mice, genotype was significantly correlated to Von Frey thresholds (Supplementary Table. 7a) and age to tail pressure thresholds (Supplementary Table. 7b, d). In *R185X/+* mutants, sex factor was correlated to tail pressure thresholds (Supplementary Table. 7d) and the age factor showed correlation in both Von Frey and tail pressure tests (Supplementary Table. 7b, d). Altogether, the results indicate that the *Scn9a*^{R185H} mutation in mice caused enhanced mechanical sensitivity at early ages but not when the mice were older. Silencing one allele of *Scn9a* did not influence the responses to mechanical stimuli.

Discussion

In this study, we first successfully established, using the CRISPR-Cas9 technique, the *Scn9a*^{R185H} mutant mouse line as a model for the human *SCN9A*^{R185H} mutation found in SFN patients with chronic pain. We used this genetic model to analyze the p.R185H genotype-phenotype association and thus explore pain mechanisms linked to the Nav1.7 sodium channel mutation found in idiopathic SFN patients. We also generated the *Scn9a*$^{R185X/wt}$ mice to explore the behavioral effect of the loss of NAV1.7 channels induced by the heterozygous *Scn9a* gene inactivation. The two

mouse lines showed no alteration of growth, survival and global health state. Pain sensitivity of the new mutant mouse lines was investigated on both sexes using behavioral tests of sensitivity to thermal and mechanical stimuli. Our results indicate that the *Scn9a*^{R185H} mice show a pain phenotype, suggesting that the *Scn9a*^{R185H} mutation identified in the SFN patients is responsible for their pain symptoms. This exploration will benefit to drug screen. On the other side, the *Scn9a*$^{R185X/wt}$ mice show a higher resistance to heat pain in the hot plate test. In these mice, one *Scn9a* allele is not functional. Therefore, we provide genetic evidence that Nav1.7 encoded by *SCN9A* gene plays an important role in nociceptive behavior in mice, substantiating its implication in the pain found in these idiopathic SFN patients. On the molecular basis, the *Scn9a* mRNA is clearly mainly expressed in DRG and less expressed spinal cord and brain and in both wild-type controls and *Scn9a*^{R185H} mutant mice. No alteration of *Scn9a* mRNA level was detected in *Scn9a*^{R185H} mutant mice, in neither females or males, suggesting that the behavioral changes found may not attributed to decreased or increased NAV1.7 expression. In *Scn9a*$^{R185X/wt}$ mutant female and male mice, *Scn9a* transcript levels were reduced in the DRG and spinal cord, which may contribute to the behavioral changes. These findings provide a genetic evidence that NAV1.7 plays a critical role mainly for heat sensitivity in mice.

Heat pain in *Scn9a*^{R185H} mutant mice

The SFN patients harboring the *SCN9A*^{R185H} mutation complained of abnormal warm and cold pain sensation [6]. In *Scn9a*^{R185H} mutant mice, pain-like behavioral phenotype was observed in the hot plate and tail flick tests. These results also showed sex and age effect, which will be discussed later. Interestingly, in idiopathic SFN patients with *SCN9A* GOF mutations others than *R185H*, pain was aggravated by warmth in 3 of 8 patients, but not in the patients carrying *R185H* mutation [6]. However, the SFN patients with *R185H* mutation suffer to burning feet and heat pain evaluated by QST test, suggesting that we successfully transferred the heat pain symptom with *Scn9a*^{R185H} mutation in our mutant line. The heat sensitivity phenotype was found with the tail flick and hot plate tests, with a gene dosage effect in particular in females. The pain-like behavioral phenotype in *Scn9a*^{R185H} mutant mice could be evidenced with the hot plate and tail flick assays but not with the Hargreaves plantar test. It was shown previously by using different conditional knockout (cKO) mouse lines, that heat pain sensitivity implicated NAV1.7 in the NAV1.8-positive neurons when scored with a slow temperature ramp in the Hargreaves test [16, 17] (8-12 second latency) but not when fast ramp was used [16, 18, 19] (5-6 second latency), while NAV1.7 expressed in larger neuronal populations mediate heat pain sensitivity any temperature ramp [16,

18, 20, 21]. These former studies could detect an 'analgesic' phenotype of the cKO mice (longer latencies) while we tested the *Scn9a*^{R185H} mutant mice for an 'hyperalgic' phenotype. Thus, the absence of phenotype of *Scn9a*^{R185H} mutant mice in this specific Hargreaves test condition (6-7 seconds latency) while the pain phenotype could be shown with the two other pain assays may be due to the use of a quite-fast temperature ramp. Also, in these same cKO mouse lines, pain behavior on the Hot Plate was shown to involve NAV1.7 expressed by sympathetic neurons in addition to sensory neurons in a supraspinal response. In the hot plate test, the *Scn9a*^{R185H} mutant mice had normal latency to first sign of hindpaw discomfort, but showed a shorter jump latency and increased coping reactions, suggesting central supraspinal pain mechanisms.

Cold pain in *Scn9a*^{R185H} mutant mice

Cold-sensing neurons must, by definition, reliably fire action potentials at low temperatures unfavorable to spike initiation due to cooling-induced inactivation of sodium channels [22]. The sensory neuron-enriched channels NAV1.8 and NAV1.9 display unusual biophysical adaptations to operate during extreme cold while NAV1.7 sodium channels expressed on sensory or sympathetic neurons are necessary for cooling but not extreme cold sensation as well as for surgery-induced neuropathic cool allodynia [16, 18, 20, 21, 23]. Among the *Scn9a*^{R185H} mice, females and not males showed a little tendency toward more reactions to cooling in the acetone test although this did not reach statistical significance (Fig. 3C, Supplementary Fig. 7C). Sex and age effects will be discussed later. Interesting, both female and male *Scn9a*^{R185H} mutant mice displayed less paw reactions to the cold plate (Fig. 5A-B).

Although the analysis in acetone and cold plate results did not lead to significant differences for individual signs, multiple regression analysis showed significant correlations to the different infectors, genotype, sex and age. The tendency for more reactions to acetone cooling but less cold sensitivity on the cold plate suggest that the R185H mutation leads to a mild cool allodynia in female but not males. The SFN patients usually report burning but not cold sensation. The two SFN patients carrying *SCN9A R185H* heterozygous mutation had both warm and cold impaired modalities in quantitative sensory tests [6].

Out of the eight SFN patients with *SCN9A* mutations described by Faber et al., one patient with another *SCN9A* mutation, as well as an erythromelalgia patient with another *SCN9A* mutation had burning pain that was relieved by cold [6, 24]. Although previous study indicated that there are differences between familial erythromelalgia and SFN according to the clinical features and

electrophysiological mechanisms, these two disorders lead to burning pain that is relieved by cold in some patients. The relief of burning pain sensation by cold could not be evaluated in mice. Taken globally, *Scn9a*^{R185H} mutants of both sexes had attenuated paw responses on the cold plate (Fig. 5A), which suggests that the activation of sensory neurons by noxious cold is felt as less painful by these mutants.

Mechanical hypersensitivity in *Scn9a*^{R185H} mutant mice

Scn9a gene loss of function in rats causes reduced response to Von Frey and pinprick tests [25, 26] and global *Scn9a* KO mice show attenuated sensitivity in the Randall-Selitto or Tail clip tests [27]. These results suggest that *Scn9a* plays an important role in behavioral responses to innocuous and noxious mechanical stimuli. NAV1.7 is expressed in A- and C-fiber type neurons, but is more prominently expressed in small diameter neurons, with 85% of functionally identified nociceptive neurons exhibiting NAV1.7 immunolabeling [4, 28]. In *Scn9a*^{R185H} males and females, there was a mutation-dose effect with reduced mechanical thresholds in the Von Frey test, at 2-mo but not at 6-mo age. Sex and age influences on the mutation effect will discussed later. The mutant mice showed normal noxious mechanical thresholds in tail pressure, indicating R185H mutation of *Scn9a* caused mechanical allodynia but not hyperalgesia in young adult mice. These results coincide with *Scn9a*^{R185H} SFN patient's complaint of sheet intolerance caused mechanical allodynia. However, the patterns of fiber transduction as well as cross-talks with other pain-related channels needs further exploration.

Behavioral phenotype of *Scn9a*$^{R185X/wt}$ mutant mice

The loss-of-function of *SCN9A* by bi-allelic inactivating mutations results in the striking clinical phenotype of congenital insensitivity to pain (CIP) [8, 29]. The CIP individuals do not perceive pain in response to noxious stimuli. However, the carriers of one allelic inactivating mutation have normal pain sensitivity. Potential novel gene therapies may be developed for relieving pain in GOF *SCN9A* SFN patients by inactivating the gain-of-function mutant allele according normal phenotype in the CIP carriers. In order to evaluate whether one *Scn9a* allele only can provide NAV1.7 function in mice, we developed a novel heterozygous *Scn9a* KO model (*Scn9a*$^{R185X/wt}$) and studied the pain behaviors of these mutants. We did not find any abnormal pain behaviors in the *R185X/+* males (Fig. 4D), and the female mutants showed only reduced response in some

parameters of the hot plate test (Fig. 4C, Supplemantary Fig. 6C,D). This indicates that the inactivation of one *Scn9a* allele alters specifically these parameters of the hot plate assay in these mutant mice, and not all other pain behavioral responses.

Sex effect in *Scn9a*^{R185H} mutant mice

This is first study to test the effects of both sex and age in *Scn9a*^{R185H} mutant mice. The results suggest that there are selected age and sex differences in *Scn9a*^{R185H} female mutants that show more pain-like behaviors (jump latency, coping reactions of hot plate, tail flick, acetone and Von Frey tests, Fig. 4A) than males, as only more coping reactions on hot plate and hypersensitivy to Von Frey filaments were found in male mutant mice (Fig. 4B). Also, the sex differences were found in the *Scn9a*$^{R185X/wt}$ mutant mice.

The study by Faber and colleagues [6] reported on one man with similar complaints from his brother and pain abnormalities in grand-father, and one woman whose father had similar complaints. Although these ware rare patients and a quantitative conclusion cannot be drawn, it can be observed that the mutation led to pain in individual of both sexes. More generally, a clear majority of patients with chronic pain are women. A survey of the currently available epidemiological and laboratory data indicates that the evidence for clinical and experimental sex differences in pain is overwhelming, which is explanation of hormonally and genetically driven sex differences in brain neurochemistry [30]. As an example, a clinical study in Hungary has studied a cohort of patients with SFN over the years 2012 – 2018 [31]. They found significant gender differences in pain scores, with mean of DN4, PD-Q9, NPS, and VAS higher for female patients compared to males. In addition to gender differences in pain, gender differences in response to opioid analgesics have also been reported. A meta-analysis concluded that morphine is moderately more efficacious in women than in men in both clinical and experimental studies [32]. Similar sex differences were also reported in rodent studies. Examples of sex variation is common in inbred mouse models of pain and analgesia. Also, sex differences in pain and analgesia could be demonstrated in some strains but not others. For example, mechanical allodynia was significantly greater in female Sprague-Dawley rats as compared with males following a spinal nerve transection but was not found in the Holtzman strain [33]. Several anatomic/ physiologic factors come into play when interpreting sex differences in regard to pain and analgesia. For example, adult male rodents have greater percentage of body fat than females while the opposite is true for humans. Similarly, me-

tabolism, immune response, locomotor activity level, and response to analgesics may all contribute to sex difference, although a part of the studies report no sex differences, see for example [34]. In addition, recent mouse studies have revealed another surprising factor that interacts with sex to modulate pain: social interaction [35]. Importantly, this aspect of sex bias in pain clinical studies was reviewed this year by Jeff Mogil [36]. The review could show that, although there are qualitative differences in pain processing in the two sexes, there are as many clinical studies reporting sex bias than no sex bias for pain (Mogil J 2020, see supplementary Fig.1).

Recently, a real-time dynamic regulation of trafficking and surface delivery of the NAV1.7 sodium channel in cultured DRG neurons has been reported. In this study, they demonstrated substantial enhancement of channel vesicular delivery to distal axons and increased number of channels within the plasma membrane upon treatment of DRG neurons with a cocktail of inflammatory mediators [37]. It was shown that, amongst the regulators of NaV1.7, the cytosolic collapsin response mediator protein 2 (CRMP2). CRMP2, modified at Lysine 374 (K374) by addition of a small ubiquitin-like modifier (SUMO), bound to NaV1.7 to regulate its membrane localization and function [38]. Recent study generated CRMP2 K374A knock-in (CRMP2K374A/K374A) mice in which Lys374 was replaced with Ala. CRMP2 K374A/K374A mice had reduced NaV1.7 membrane localization and function in female, but not male, sensory neurons, which indicated there is sex effect on CRMP2 SUMOylation [39]. Therefore, the sex effect in R185H mutant mice may be explained by the mutation impacting NAV1.7 trafficking pattern mediated via CRMP2 SUMOylation. However, this needs confirmation by further studies.

Age effect in *Scn9a*^{R185H} mutant mice

In this study, we also found age effect on responses to different nociceptive stimuli in *Scn9a*^{R185H} and *Scn9a*$^{R185X/wt}$ mutant mice. Some pain-like behaviors were present in *Scn9a*^{R185H} mutant mice at 2-month-age, such as *R185H/R185H* females displaying increased sensitivity to Hot Plate, Tail flick, Von Frey, but the genotype effect was absent at 6-months of age. In contrast, previous studies, both clinical or on rodent models, showed that advancing age was associated with increased prevalence of several chronic pain disorders [40-42]. Additionally, aging is known as a major risk factor for the structure and function of the nervous system. The reduction of density of unmyelinated and myelinated fibers have been reported in elderly individuals, i.e. large diameter afferents and the most finely myelinated afferents that are known to correspond to the diameter of fibers subserving thermal and noxious sensation [42]. One recent study showed that peripheral

nerves of 24-month-old aged C57BL/6 mice of either sex show similar pathological alterations as nerves from aging human individuals, whereas 12-month-old adult mice lack such alterations [43]. It seems that there may be no alteration of the nervous system in 6-month-age mice used in our project, although this was not specifically investigated. Therefore, the age effect on our mutant mice may be caused by the wild-type control littermates being more sensitive at 6-month-age, so that leading to a sufficient window to detect statistically allodynia and hypoalgesia. Moreover, we found an age effect on tail pressure values from both mouse sexes and in the two mutant lines despite no effect on genotype. Related results were found in one clinic study showing young subjects with significantly greater activity in the contralateral putamen and caudate but could not be accounted for by increased age-associated shrinkage in these regions when applying noxious pressure stimulation in both adults [44]. Given the effect of sex and age in our two mutant mouse lines, we suggest that sex and age should be considered as factors to be taken in account in further experimental investigation of SFN, and also in the assessment of potential analgesic.

Perspectives for *Scn9a*^{R185H} mutant mice

The genetic rodent models together with pharmacological approaches have shown that NAV1.7 play important roles in nociception and chronic hyperalgesia. Side-effect of sodium channel blocking analgesics is still a problem for both animals and humans, despite the clear utility of nerve block in pain treatment. The understanding of chronic pain mechanisms in patients and exploration of novel analgesics require novel relevant pre-clinical models. Steve Waxman's team has developed sensory neurons differentiated from patient-derived Induced Pluripotent Stem Cells that model inherited erythromelalgia in vitro [45]. These cells can provide a platform which enables assessment of sodium channel blocker effects in vitro. It will then be necessary to analyze their effects and safety in preclinical and then clinical models.

Here, we successfully created a single *Scn9a* mutation-p. R185H mice model and consequently transfer the chronic pain phenotype from painful SFN patients by CRISPR-Cas9 technique. However, pain is a multidimensional experience of sensory-discriminative, cognitive, and affective processes. The quantification of reflexive pain behavior in animal models has been applied in the pain research field since decades, by passing the supraspinal processing that ultimately gives rise to the pain experience. More recently, preference for the compartment with analgesics as measured by the conditioned place preference test, and avoidance of evoked stimuli recorded by

the conditioned place avoidance test, were used to assess spontaneous pain behavior in inflammatory and neuropathic pain conditions [46, 47]. Also, innovative devices have been developed which provide high accuracy assessment of thermal preference through free walking in thermal gradients [48, 49]. A novel device for assessing thermal pain tolerance in mice also have been developed recently [50]. The operant plantar thermal assay utilizes operant learning and decision-making within an approach-avoidance conflict paradigm to establish the duration and intensity of a noxious stimulus an animal will withstand to obtain a reward [50]. This device can be used to complement standard threshold-level thermal noncaptive testing [50].

Chronic pain also is highly prevalent among patients with mood, anxiety, personality, and somatic symptom disorders. And patients with chronic pain often suffer from persistent interpersonal distress. However, the neural mechanisms underlying these phenomena and their possible roles in the etiology of chronic pain are not yet understood. Functional magnetic resonance imaging (fMRI) of brain can be used to study neural activity underlying pain experienced in the context of ongoing interpersonal interaction in humans. One clinical study in individual IEM subject carrying the NAV1.7-S241T mutation, showed a shift in brain activity from valuation/emotional decision-making regions such as the anterior cingulate cortex and nucleus accumbens (a pattern of brain activity associated with chronic neuropathic pain) to somatosensorimotor regions by treatment with CBZ, suggesting normalization of brain activity [51]. Recently, the establishment of multi-sensory paradigms could be provided to perform awake mouse fMRI, which can be used to further explore the pain related emotion mechanism of SFN in brain [52].

Although there are differences between rodents and humans, the genetic rodent models still help to understand the mechanism of sodium channels in pain relief and develop novel drugs. Further study on mechanism of SFN based on our mutant animal models and the development of clinically relevant pain behavioral models will open a new vision for the role of NAV1.7 in painful SFN therapy. Also, the combination of rodent genetic models and other approaches including genetic screening will allow to identify additional components of chronic pain and to design new drugs and therapeutic strategies [53].

Acknowledgments

We are grateful to the animal caretakers at PHENOMIN-ICS and IGBMC animal facility for their services. We thanks the staff of IGBMC and ICS for their helpful suggestions and discussions, in particular Charley Pinault, Sophie Brignon and Dalila Ali-Hadji, Loïc Lindner and Pauline Cayrou, and Elvire Guiot. We thank the team members including Maria del mar Muniz Moreno for their help.

Funding

This work has been funded by the Molecule-to-Man PainNetwork, a European Commission Multi-Center Collaborative Project through the European Union's Horizon 2920 research and innovation program under grant agreement No. 721841 – Pain-Net. This work has been supported by the National Centre for Scientific Research (CNRS), the French National Institute of health and medical research (INSERM) and the University of Strasbourg (Unistra). The French state funds through the "Agence nationale de la recherche" under the frame of Programme Investissements d'Avenir labelled ANR-10-IDEX-0002-02 and ANR-10-LABX-0030-INRT.

References

1. Cazzato, D. and G. Lauria, *Small fibre neuropathy.* Curr Opin Neurol, 2017. **30**(5): p. 490-499.
2. Themistocleous, A.C., et al., *The clinical approach to small fibre neuropathy and painful channelopathy.* Pract Neurol, 2014. **14**(6): p. 368-79.
3. Waxman, S.G., et al., *Sodium channel genes in pain-related disorders: phenotype-genotype associations and recommendations for clinical use.* Lancet Neurol, 2014. **13**(11): p. 1152-1160.
4. Black, J.A., et al., *Expression of Nav1.7 in DRG neurons extends from peripheral terminals in the skin to central preterminal branches and terminals in the dorsal horn.* Mol Pain, 2012. **8**: p. 82.
5. Kanellopoulos, A.H., et al., *Mapping protein interactions of sodium channel NaV1.7 using epitope-tagged gene-targeted mice.* EMBO J, 2018. **37**(3): p. 427-445.
6. Faber, C.G., et al., *Gain of function Nanu1.7 mutations in idiopathic small fiber neuropathy.* Ann Neurol, 2012. **71**(1): p. 26-39.
7. Han, C., et al., *Functional profiles of SCN9A variants in dorsal root ganglion neurons and superior cervical ganglion neurons correlate with autonomic symptoms in small fibre neuropathy.* Brain, 2012. **135**(Pt 9): p. 2613-28.
8. Bennett, D.L., et al., *The Role of Voltage-Gated Sodium Channels in Pain Signaling.* Physiol Rev, 2019. **99**(2): p. 1079-1151.
9. McDermott, L.A., et al., *Defining the Functional Role of NaV1.7 in Human Nociception.* Neuron, 2019. **101**(5): p. 905-919 e8.
10. Carter, R.J., J. Morton, and S.B. Dunnett, *Motor coordination and balance in rodents.* Curr Protoc Neurosci, 2001. **Chapter 8**: p. Unit 8 12.
11. Ferguson, J.N., et al., *Social amnesia in mice lacking the oxytocin gene.* Nat Genet, 2000. **25**(3): p. 284-8.
12. Duchon, A., et al., *The telomeric part of the human chromosome 21 from Cstb to Prmt2 is not necessary for the locomotor and short-term memory deficits observed in the Tc1 mouse model of Down syndrome.* Behav Brain Res, 2011. **217**(2): p. 271-81.
13. Huang, T., et al., *Identifying the pathways required for coping behaviours associated with sustained pain.* Nature, 2019. **565**(7737): p. 86-90.
14. Branco, T., et al., *Near-Perfect Synaptic Integration by Nav1.7 in Hypothalamic Neurons Regulates Body Weight.* Cell, 2016. **165**(7): p. 1749-1761.
15. Weiss, J., et al., *Loss-of-function mutations in sodium channel Nav1.7 cause anosmia.* Nature, 2011. **472**(7342): p. 186-90.
16. Minett, M.S., N. Eijkelkamp, and J.N. Wood, *Significant determinants of mouse pain behaviour.* PLoS One, 2014. **9**(8): p. e104458.
17. Nassar, M.A., et al., *Nociceptor-specific gene deletion reveals a major role for Nav1.7 (PN1) in acute and inflammatory pain.* Proc Natl Acad Sci U S A, 2004. **101**(34): p. 12706-11.
18. Minett, M.S., et al., *Distinct Nav1.7-dependent pain sensations require different sets of sensory and sympathetic neurons.* Nat Commun, 2012. **3**: p. 791.
19. Zhou, X., et al., *Spider venom-derived peptide induces hyperalgesia in Nav1.7 knockout mice by activating Nav1.9 channels.* Nat Commun, 2020. **11**(1): p. 2293.

20. Pereira, V., et al., *Analgesia linked to Nav1.7 loss of function requires micro- and delta-opioid receptors.* Wellcome Open Res, 2018. **3**: p. 101.
21. Shields, S.D., et al., *Insensitivity to Pain upon Adult-Onset Deletion of Nav1.7 or Its Blockade with Selective Inhibitors.* J Neurosci, 2018. **38**(47): p. 10180-10201.
22. MacDonald, D.I., J.N. Wood, and E.C. Emery, *Molecular mechanisms of cold pain.* Neurobiol Pain, 2020. **7**: p. 100044.
23. Minett, M.S., et al., *Pain without nociceptors? Nav1.7-independent pain mechanisms.* Cell Rep, 2014. **6**(2): p. 301-12.
24. Ito, M., et al., *Behavioral therapy ceased cold water immersion dependence in a patient with familial erythromelalgia caused by SCN9A mutation.* JAAD Case Rep, 2019. **5**(9): p. 806-808.
25. Chen, L., et al., *Pharmacological characterization of a rat Nav1.7 loss-of-function model with insensitivity to pain.* Pain, 2020. **161**(6): p. 1350-1360.
26. Grubinska, B., et al., *Rat NaV1.7 loss-of-function genetic model: Deficient nociceptive and neuropathic pain behavior with retained olfactory function and intra-epidermal nerve fibers.* Mol Pain, 2019. **15**: p. 1744806919881846.
27. Gingras, J., et al., *Global Nav1.7 knockout mice recapitulate the phenotype of human congenital indifference to pain.* PLoS One, 2014. **9**(9): p. e105895.
28. Djouhri, L., et al., *Sensory and electrophysiological properties of guinea-pig sensory neurones expressing Nav 1.7 (PN1) Na+ channel alpha subunit protein.* J Physiol, 2003. **546**(Pt 2): p. 565-76.
29. Drissi, I., W.A. Woods, and C.G. Woods, *Understanding the genetic basis of congenital insensitivity to pain.* Br Med Bull, 2020. **133**(1): p. 65-78.
30. Mogil, J.S., *Sex differences in pain and pain inhibition: multiple explanations of a controversial phenomenon.* Nat Rev Neurosci, 2012. **13**(12): p. 859-66.
31. Pal, E., et al., *Small Fiber Neuropathy: Clinicopathological Correlations.* Behav Neurol, 2020. **2020**: p. 8796519.
32. Niesters, M., et al., *Do sex differences exist in opioid analgesia? A systematic review and meta-analysis of human experimental and clinical studies.* Pain, 2010. **151**(1): p. 61-8.
33. DeLeo, J.A. and M.D. Rutkowski, *Gender differences in rat neuropathic pain sensitivity is dependent on strain.* Neurosci Lett, 2000. **282**(3): p. 197-9.
34. Roeckel, L.A., et al., *Morphine-induced hyperalgesia involves mu opioid receptors and the metabolite morphine-3-glucuronide.* Sci Rep, 2017. **7**(1): p. 10406.
35. Langford, D.J., et al., *Social approach to pain in laboratory mice.* Soc Neurosci, 2010. **5**(2): p. 163-70.
36. Mogil, J.S., *Qualitative sex differences in pain processing: emerging evidence of a biased literature.* Nat Rev Neurosci, 2020. **21**(7): p. 353-365.
37. Akin, E.J., et al., *Building sensory axons: Delivery and distribution of NaV1.7 channels and effects of inflammatory mediators.* Sci Adv, 2019. **5**(10): p. eaax4755.
38. Dustrude, E.T., et al., *CRMP2 protein SUMOylation modulates NaV1.7 channel trafficking.* J Biol Chem, 2013. **288**(34): p. 24316-31.
39. Moutal, A., et al., *Studies on CRMP2 SUMOylation-deficient transgenic mice identify sex-specific NaV1.7 regulation in the pathogenesis of chronic neuropathic pain.* Pain, 2020.

40. Bishay, P., et al., *Anandamide deficiency and heightened neuropathic pain in aged mice.* Neuropharmacology, 2013. **71**: p. 204-15.
41. Quiton, R.L., et al., *Age-related changes in nociceptive processing in the human brain.* Ann N Y Acad Sci, 2007. **1097**: p. 175-8.
42. Gibson, S.J. and M. Farrell, *A review of age differences in the neurophysiology of nociception and the perceptual experience of pain.* Clin J Pain, 2004. **20**(4): p. 227-39.
43. Yuan, X., et al., *Macrophage Depletion Ameliorates Peripheral Neuropathy in Aging Mice.* J Neurosci, 2018. **38**(19): p. 4610-4620.
44. Cole, L.J., et al., *Age-related differences in pain sensitivity and regional brain activity evoked by noxious pressure.* Neurobiol Aging, 2010. **31**(3): p. 494-503.
45. Yang, Y., et al., *NaV1.7 as a Pharmacogenomic Target for Pain: Moving Toward Precision Medicine.* Trends Pharmacol Sci, 2018. **39**(3): p. 258-275.
46. Gregory, N.S., et al., *An overview of animal models of pain: disease models and outcome measures.* J Pain, 2013. **14**(11): p. 1255-69.
47. Barrot, M., *Tests and models of nociception and pain in rodents.* Neuroscience, 2012. **211**: p. 39-50.
48. Bohic, M., et al., *Loss of bhlha9 Impairs Thermotaxis and Formalin-Evoked Pain in a Sexually Dimorphic Manner.* Cell Rep, 2020. **30**(3): p. 602-610 e6.
49. Touska, F., et al., *Comprehensive thermal preference phenotyping in mice using a novel automated circular gradient assay.* Temperature (Austin), 2016. **3**(1): p. 77-91.
50. Reker, A.N., et al., *The Operant Plantar Thermal Assay: A Novel Device for Assessing Thermal Pain Tolerance in Mice.* eNeuro, 2020. **7**(2).
51. Geha, P., et al., *Pharmacotherapy for Pain in a Family With Inherited Erythromelalgia Guided by Genomic Analysis and Functional Profiling.* JAMA Neurol, 2016. **73**(6): p. 659-67.
52. Chen, X., et al., *Sensory evoked fMRI paradigms in awake mice.* Neuroimage, 2020. **204**: p. 116242.
53. Calvo, M., et al., *The Genetics of Neuropathic Pain from Model Organisms to Clinical Application.* Neuron, 2019. **104**(4): p. 637-653.

Figures Legends

Fig. 1 Generation of *Scn9a*^{R185H} and *Scn9a*$^{R185X/wt}$ mutant mice and *Scn9a* transcript expression. A) Scheme for *Scn9a* targeting strategy. We choose the sgRNA86 by CRISPOR online software and design ssODN with three bases mutation, including two silence mutations and one-point mutation. The first silence mutation, C>T, which is PAM mutation to avoid Cas9 recut. And second one, C>T, which design for BspHI enzyme to genotyping. **B)** *Scn9a* mRNA expression in DRG, Spinal cord, Brain and Cerebellum of *Scn9a*^{R185H} mutant mice in both sexes. There is no significanct effect of genotype. (DRG: +/+ female n=4; *R185H/+* female n=4; *R185H/R185H* female n=3; +/+ male n=5; *R185H/+* male n=4; *R185H/R185H* male n=4; Spinal cord: +/+ female n=5; *R185H/+* female n=5; *R185H/R185H* female n=6; +/+ male n=5; *R185H/+* male n=4; *R185H/R185H* male n=5; Brain: +/+ female n=5; *R185H/+* female n=5; *R185H/R185H* female n=4; +/+ male n=6; *R185H/+* male n=5; *R185H/R185H* male n=5; Cerebellum +/+ female n=4; *R185H/+* female n=4; *R185H/R185H* female n=5; +/+ male n=5; *R185H/+* male n=5; *R185H/R185H* male n=5). **C)** *Scn9a* mRNA expression in DRG, Spinal cord, Brain and Cerebellum of *Scn9a*$^{R185X/wt}$ mutant mice in both sexes. *Scn9a*$^{R185X/wt}$ mutant mice expressed low quantity *Scn9a*^{R185X} comparing to +/+ in DRG and Spinal cord. (DRG: +/+ female n=4; *R185X/+* female n=5; +/+ male n=7; *R185X/+* male n=6; Spinal cord: +/+ female n=5; *R185X/+* female n=5; +/+ male n=5; *R185X/+* male n=6; Brain: +/+ female n=5; *R185X/+* female n=5; +/+ male n=4; *R185X/+* male n=5; Cerebellum +/+ female n=5; *R185X/+* female n=5; +/+ male n=5; *R185X/+* male n=4). mRNA expression was normalized to *Hprt* expression. Data presents as means ± *SEM*. *P < 0.05, ** P < 0.01 and ***P < 0.001, *Scn9a*^{R185H} and *Scn9a*$^{R185X/wt}$ mutants compared to their +/+ littermates by two tailed unpaired student t test or Mann-Whitney test. (More detailed statistical analysis see Supplementary Table. 8)

Fig. 2 Enhanced and decreased pain sensitivity to Hot Plate in the *Scn9a*^{R185H} and *Scn9a*$^{R185X/wt}$ mice respectively at 2-month-age. A) Jump Latency to 48, 52 and 56°C Hot plate in *Scn9a*^{R185H} mice. *R185H/R185H* female mice decreased jump latency to 48, 52 and 56°C Hot plate. *R185H/+* female mice only decreased jump latency to 56 °C Hot Plate. Mutant male mice did not show decreasing jump latency in any temperature Hot plate. (+/+ female n=16; *R185H/+* female n=16; *R185H/R185H* female n=15; +/+ male n=13; *R185H/+* male n=15; *R185H/R185H* male n=11). **B)** Coping reactions of 48, 52 and 56°C Hot Plate in *Scn9a*^{R185H} mice. *R185H/R185H* female mice showed more coping reactions to 52 and 56°C Hot Plate, while *R185H/R185H* male mice to 48 and 56°C Hot Plate. (+/+ female n=16; *R185H/+* female n=15; *R185H/R185H* female n=15; +/+ male n=13; *R185H/+* male n=15; *R185H/R185H* male n=11). **C)** Jump Latency to 48, 52 and 56°C Hot Plate in *Scn9a*$^{R185X/wt}$ mice. Female +/+ mice have lower jump latency to male +/+ mice. *Scn9a*$^{R185X/wt}$ female mice increased jump latency to 56°C Hot Plate, not showed in male mutant mice. (+/+ female n=11; *R185X/+* female n=13; +/+ male n=11; *R185X/+* male n=14). **D)** Coping reactions to 48, 52 and 56°C Hot Plate in *Scn9a*$^{R185X/wt}$ mice. Decreasing coping reactions to 48, 52 and 56°C Hot Plate showed in the *Scn9a*$^{R185X/wt}$ female mice compare to controls, but not male mice. (+/+ female n=11; *R185X/+* female n=13; +/+ male n=11; *R185X/+* male n=14). Data presents as means ± *SEM*.

*P < 0.05, ** P < 0.01 and ***P < 0.001, *Scn9a*^{R185H} and *Scn9a*$^{R185X/wt}$ mutants compared to their +/+ littermates by one (jump latency) or two (coping reaction) tailed student t test or Mann-Whitney test. (More detailed statistical analysis see Supplementary Table. 9)

Fig. 3 Enhanced pain sensitivity to heat, cool and mechanical stimuli and decreased pain sensitivity to cold stimuli in the *Scn9a*^{R185H} mice at 2-month-age. A-F) Tail Flick (+/+ female n=15; *R185H/+* female n=15; *R185H/R185H* female n=14; +/+ male n=14; *R185H/+* male n=15; *R185H/R185H* male n=11), Hargreaves test (+/+ female n=14; *R185H/+* female n=13; *R185H/R185H* female n=11; +/+ male n=14; *R185H/+* male n=15; *R185H/R185H* male n=12), Acetone test (+/+ female n=16; *R185H/+* female n=15; *R185H/R185H* female n=14; +/+ male n=15; *R185H/+* male n=15; *R185H/R185H* male n=13), Cold Plate 5 °C(+/+ female n=16; *R185H/+* female n=15; *R185H/R185H* female n=14; +/+ male n=15; *R185H/+* male n=16; *R185H/R185H* male n=13), Von Frey (+/+ female n=13; *R185H/+* female n=12; *R185H/R185H* female n=10; +/+ male n=14; *R185H/+* male n=15; *R185H/R185H* male n=12) and Tail Pressure (+/+ female n=13; *R185H/+* female n=13; *R185H/R185H* female n=11; +/+ male n=14; *R185H/+* male n=15; *R185H/R185H* male n=11) were used to evaluate basal pain sensitivity in response to thermal and mechanical stimuli in female and male *Scn9a*^{R185H} mice at 2-month-age. Significant hypersensitivity of *R185H/+* and *R185H/R185H* female mice were detected in responses to heat (Tail Flick, not Hargreaves Plantar), but not for male mutant mice. No significance detected for Acetone test and Cold Plate 5 °C male mutant mice. *R185H/R185H* mice were detected the significant mechanical hypersensitivity by Von Frey filaments stimuli in both sexes, but not for Tail Pressure in all *Scn9a*^{R185H} mutant mice. Data presents as means ± *SEM*. *P < 0.05, ** P < 0.01 and ***P < 0.001, *Scn9a*^{R185H} and *Scn9a*$^{R185X/wt}$ mutants compared to their +/+ littermates by two tailed unpaired student t test or Mann-Whitney test. (More detailed statistical analysis see Supplementary Table. 10)

Fig. 4 Radar charts showing the effects of genotype on different heat and mechanical stimuli in *Scn9a*^{R185H} and *Scn9a*$^{R185X/wt}$ mice at 2-month-age. A) Genotype effect on different heat and mechanical stimuli in female *Scn9a*^{R185H} mice. **B)** Genotype effect on different heat and mechanical stimuli in male *Scn9a*^{R185H} mice. **C)** Genotype effect on different heat and mechanical stimuli in female *Scn9a*$^{R185X/wt}$ mice. **D)** Genotype effect on different heat and mechanical stimuli in male *Scn9a*$^{R185X/wt}$ mice.

Fig. 5 Radar charts showing the effects of genotype on Cold Plate in *Scn9a*^{R185H} and *Scn9a*$^{R185X/wt}$ mice at 2-month-age. A) Genotype effect on Cold Plate with different parameters in female *Scn9a*^{R185H} mice. **B)** Genotype effect on Cold Plate with different parameters in male *Scn9a*^{R185H} mice. **C)** Genotype effect on Cold Plate with different parameters in female *Scn9a*$^{R185X/wt}$ mice. **D)** Genotype effect on Cold Plate with different parameters in male *Scn9a*$^{R185X/wt}$ mice.

Figures

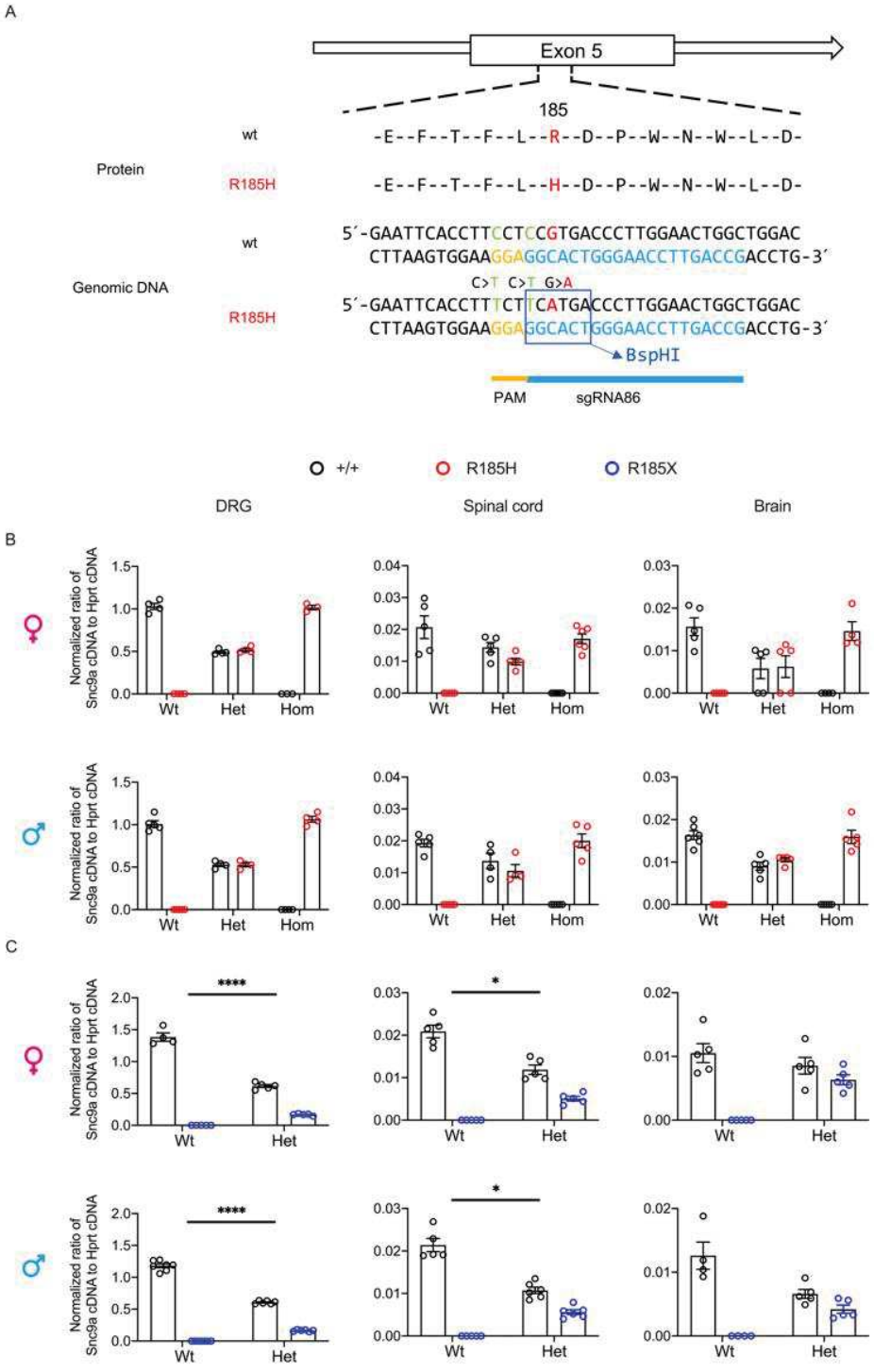

Figure 1

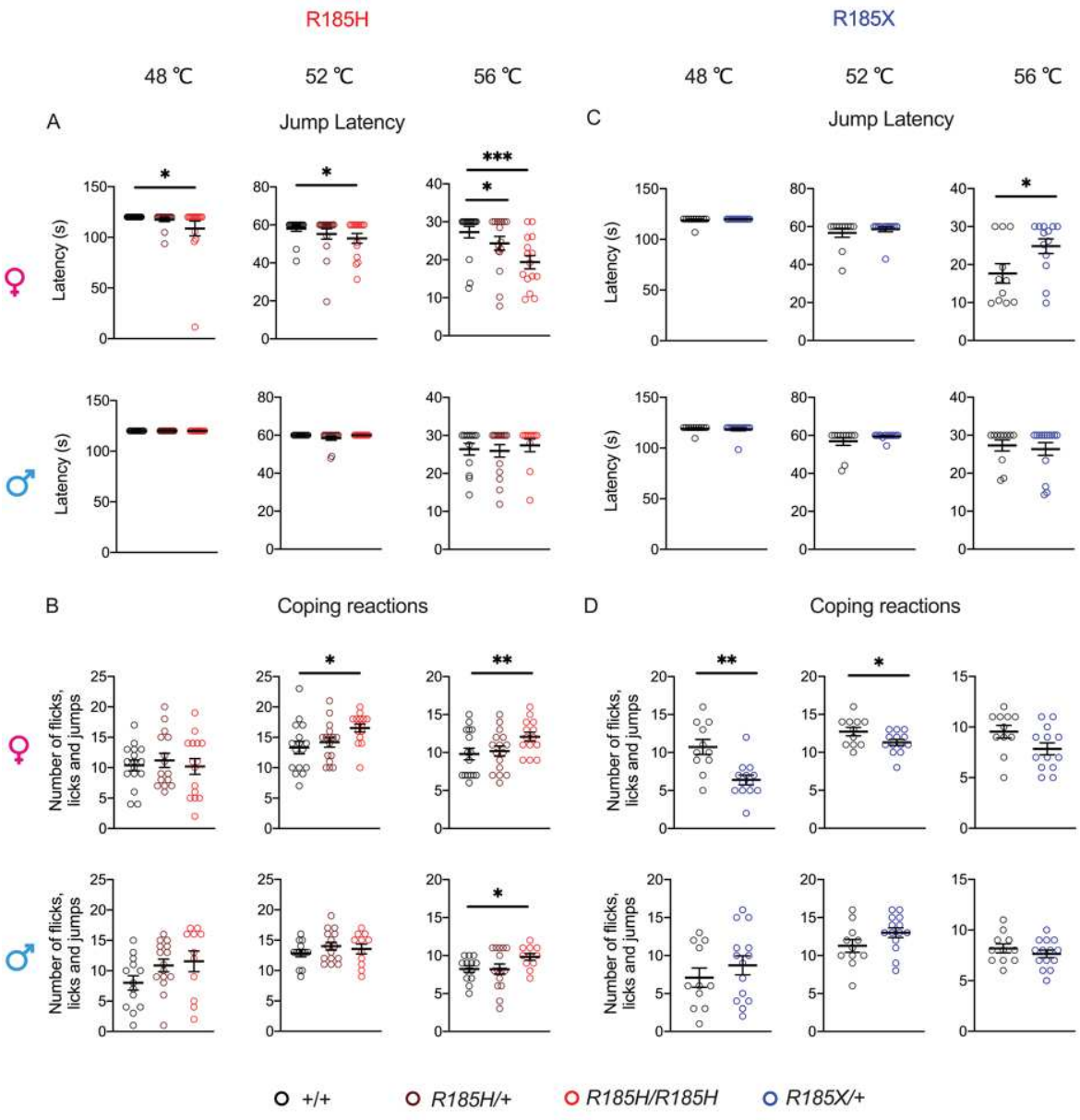
R185H
R185X
48 ℃
52 ℃
56 ℃
A
Jump Latency
C
Jump Latency
Latency (s)
B
Coping reactions
D
Coping reactions
Number of flicks, licks and jumps
+/+
R185H/+
R185H/R185H
R185X/+

Figure 2

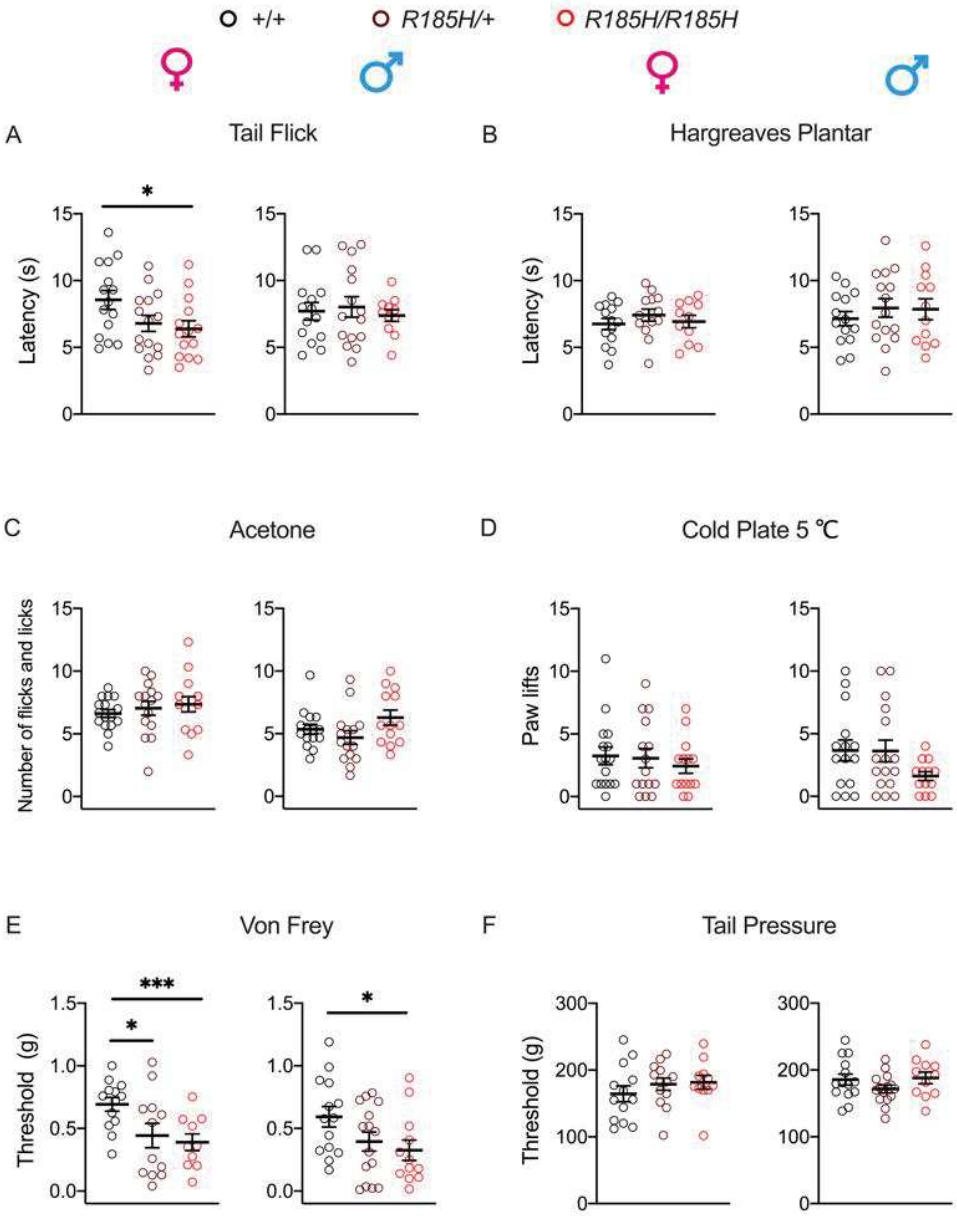
+/+
R185H/+
R185H/R185H
A
Tail Flick
B
Hargreaves Plantar
Latency (s)
C
Acetone
Number of flicks and licks
D
Cold Plate 5 ℃
Paw lifts
E
Von Frey
Threshold (g)
F
Tail Pressure
Threshold (g)

Figure 3

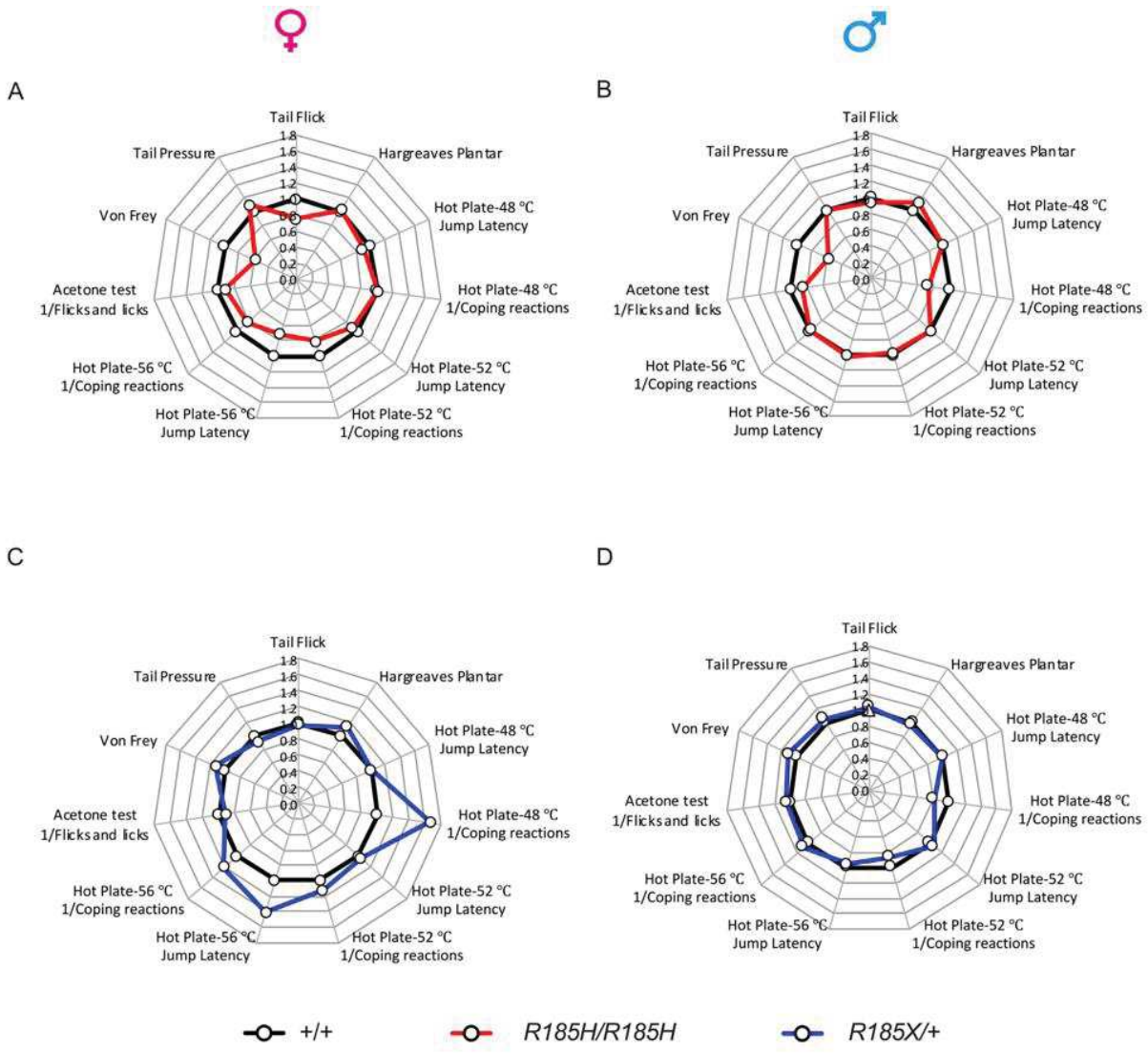
♀
♂
A
B
C
D
Tail Flick
Hargreaves Plantar
Hot Plate-48 °C Jump Latency
Hot Plate-48 °C 1/Coping reactions
Hot Plate-52 °C Jump Latency
Hot Plate-52 °C 1/Coping reactions
Hot Plate-56 °C Jump Latency
Hot Plate-56 °C 1/Coping reactions
Acetone test 1/Flicks and licks
Von Frey
Tail Pressure
1.8
1.6
1.4
1.2
1.0
0.8
0.6
0.4
0.2
0.0
+/+
R185H/R185H
R185X/+

Figure 4

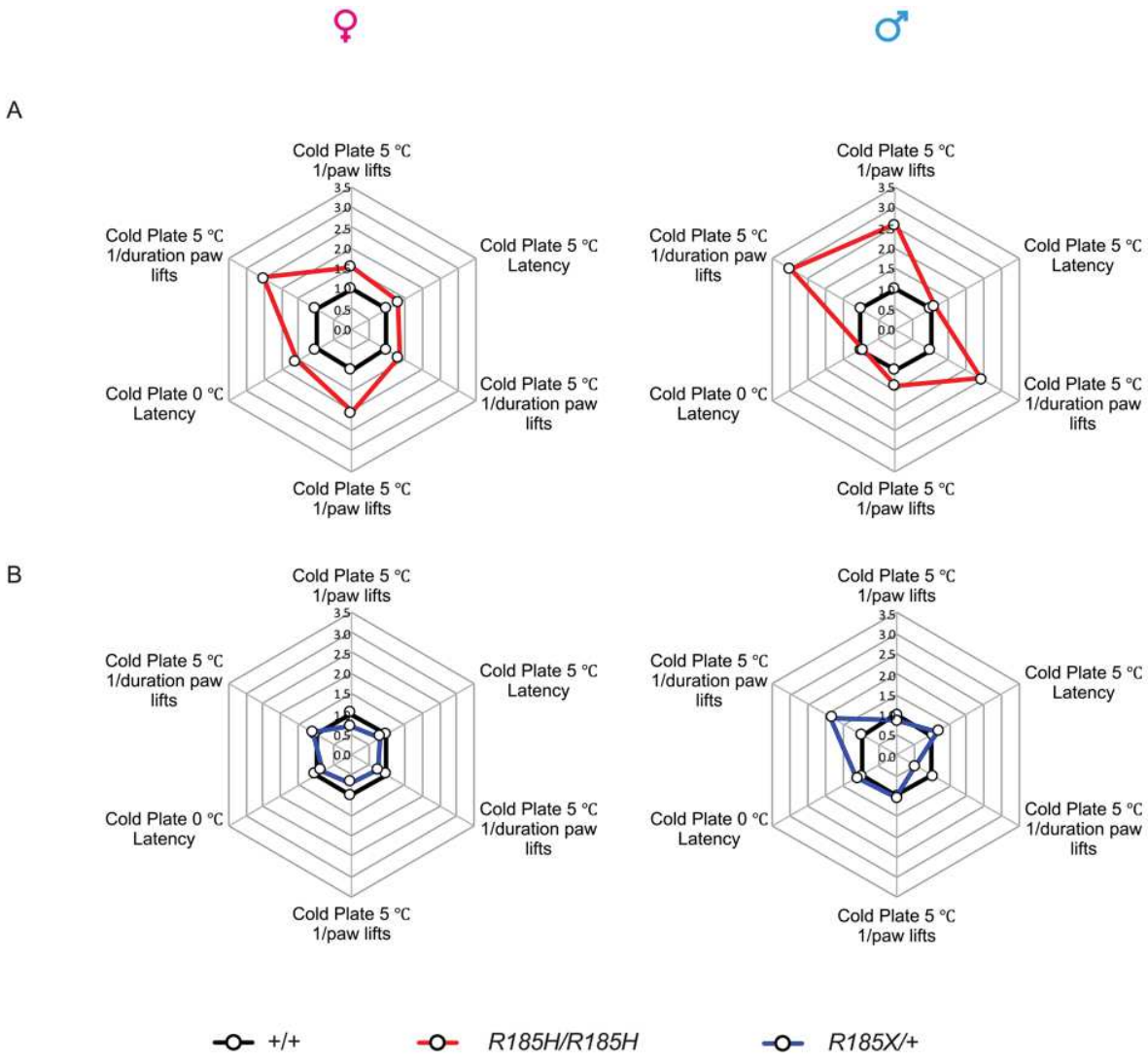
♀
♂
A
B
Cold Plate 5 ℃ 1/paw lifts
Cold Plate 5 ℃ Latency
Cold Plate 5 ℃ 1/duration paw lifts
Cold Plate 5 ℃ 1/paw lifts
Cold Plate 0 ℃ Latency
Cold Plate 5 ℃ 1/duration paw lifts
3.5
3.0
2.5
2.0
1.5
1.0
0.5
0.0
+/+
R185H/R185H
R185X/+

Figure 5

Supplementary Materials

Supplementary Fig. 1 Tail biopsy DNA analysis of *Scn9a* editing mice reveals a wide range of alleles and genotypes in F0 founders. Allele sequences characterized through Sanger sequencing, for F0 founders obtained from the micro-injection. Sequencing analysis confirms mutagenesis on-target with alleles containing HDR events with point mutation and NHEJ repair events with indel mutations including different insertions and deletions.

Supplementary Fig. 2 Off targets analysis in F1 founders. 53-11# F1 founder to establish *Scn9a*^{R185H} mice line and 36-5 founder to establish *Scn9a*$^{R185X/wt}$ mice. Seven importantly potential off targets, including gene *Scn3a*, *Scn1a*, *Scn11a*, *Scn4a*, *Scn5a* and two location between two genes (Tshz3/Zfp536 and Nipsnap3b/Abca1), have been checked in these two F1 founders. There was no off target detected in these two F1 founders.

Supplementary Fig. 3 *Scn9a*^{R185H} mice show normal healthy condition at 2- and 6-month-age. A) Weekly body weight for female and male *Scn9a*^{R185H} mice. **B)** Muscle strength and motor coordination were evaluated by String test and Crenellated bar at 2- (2-mo) and 6-month-age (6-mo). They was no detected abnormal phenotype. (String test, 2-mo: +/+ female n=14; *R185H/+* female n=13; *R185H/R185H* female n=11; +/+ male n=14; *R185H/+* male n=15; *R185H/R185H* male n=12; 6-mo +/+ female n=14; *R185H/+* female n=13; *R185H/R185H* female n=11; +/+ male n=8; *R185H/+* male n=11; *R185H/R185H* male n=9; Crenellated bar, 2-mo: +/+ female n=14; *R185H/+* female n=13; *R185H/R185H* female n=11; +/+ male n=14; *R185H/+* male n=15; *R185H/R185H* male n=12; 6-mo +/+ female n=14; *R185H/+* female n=13; *R185H/R185H* female n=11; +/+ male n=13; *R185H/+* male n=15; *R185H/R185H* male n=11). **C)** Odor discrimination test expressed in time spent sniffing odor stimuli in repeated presentations (Trail 1 to 5). All mice showed change in the amount of time spent sniffing the new olfactory stimuli in the test session. *Scn9a*^{R185H} mice have normal olfactory discrimination function at 2- and 6-month-age. (2-mo: +/+ female n=13; *R185H/+* female n=13; *R185H/R185H* female n=11; +/+ male n=13; *R185H/+* male n=15; *R185H/R185H* male n=11; 6-mo +/+ female n=10; *R185H/+* female n=11; *R185H/R185H* female n=11; +/+ male n=8; *R185H/+* male n=12; *R185H/R185H* male n=9). Data are expressed as means ± *SEM*, *P < 0.05, ** P < 0.01 and ***P < 0.001. Repeated Measures ANOVA and Sidak post-hoc multiple comparison for body weight and odor discrimination analysis. *R185H/+* and *R185H/R185H* compared to their +/+ littermates by two tailed Student t test or Mann-Whitney test for String test and Crenellated bar. (More detailed statistical analysis see Supplementary Table. 11)

Supplementary Fig. 4 *Scn9a*$^{R185X/wt}$ mice show normal healthy condition at 2- and 6-month-age. A) Weekly body weight for female and male *Scn9a*$^{R185X/wt}$ mice. **B)** Muscle strength and motor coordination were evaluated by String test and Crenellated bar at 2- (2-mo) and 6-month-age (6-mo). There was not detected abnormal phenotype. (String test, 2-mo: +/+ female n=11; *R185X/+* female n=13; +/+ male n=11; *R185X/+* male n=13; 6-mo: +/+ female n=11; *R185X/+* female n=13; +/+ male n=9; *R185X/+* male n=10;

Crenellated bar, 2-mo: +/+ female n=11; *R185X/+* female n=13; +/+ male n=11; *R185X/+* male n=14; 6-mo: +/+ female n=11; *R185X/+* female n=13; +/+ male n=11; *R185X/+* male n=14). **C)** Odor discrimination test expressed in time spent sniffing odor stimuli in repeated presentations (Trail 1 to 5). All mice showed change in the amount of time spent sniffing the new olfactory stimuli in the test session. *Scn9a*$^{R185X/wt}$ mice have normal olfactory discrimination function at 2- and 6-month-age. (2-mo: +/+ female n=11; *R185X/+* female n=13; +/+ male n=11; *R185X/+* male n=14; 6-mo: +/+ female n=11; *R185X/+* female n=13; +/+ male n=8; *R185X/+* male n=6). Data are expressed as means ± *SEM*, *P < 0.05, ** P < 0.01 and ***P < 0.001. Repeated Measures ANOVA and Sidak post-hoc multiple comparation for body weight and odor discrimination analysis. *R185X/+* compared to their +/+ littermates by two tailed Student t test or Mann--Whitney test for String test and Crenellated bar. (More detailed statistical analysis see Supplementary Table. 12)

Supplementary Fig. 5 The baseline comparison between sexes to Hot Plate in *Scn9a*^{R185H} and *Scn9a*$^{R185X/wt}$ mice at 2- and 6-month-age. A) Jump Latency of 48, 52 and 56°C Hot Plate in *Scn9a*^{R185H} +/+ mice at 2- (2-mo) and 6-month-age (6-mo). **B)** Coping reactions of 48, 52 and 56°C Hot Plate in *Scn9a*^{R185H} +/+ mice at 2- and 6- month. **C)** Jump Latency of 48, 52 and 56°C Hot Plate in *Scn9a*^{R185H} +/+ mice at 2- and 6- month-age. **D)** Coping reactions of 48, 52 and 56°C Hot Plate in *Scn9a*^{R185H} +/+ mice at 2- and 6- month-age. There is no difference between female and male in *Scn9a*^{R185H} mice at 2- and 6-month-age. However, the male +/+ of *Scn9a*$^{R185X/wt}$ mice showed higher jump latency to 56°C at 2-month-age and lower number of coping reactions to 48°C at 6-month-age. Data present as means ± *SEM* *P < 0.05, ** P < 0.01 and ***P < 0.001, *Scn9a*^{R185H} and *Scn9a*$^{R185X/wt}$ female +/+ compared to male +/+ by one (jump latency) or two (coping reaction) tailed student t test or Mann-Whitney test. (More detailed statistical analysis see Supplementary Table. 13)

Supplementary Fig. 6 Enhanced and decreased pain sensitivity to Hot Plate in the *Scn9a*^{R185H} and *Scn9a*$^{R185X/wt}$ mice respectively at 6-month-age. A) Jump Latency of 48, 52 and 56°C Hot Plate in *Scn9a*^{R185H} mice at 6-month-age. *R185H/R185H* female mice showed decreased jump latency to 52°C Hot Plate, not showed in male mice. (+/+ female n=14; *R185H/+* female n=13; *R185H/R185H* female n=11; +/+ male n=13; *R185H/+* male n=15; *R185H/R185H* male n=11). **B)** Coping reactions of 48, 52 and 56°C Hot Plate in *Scn9a*^{R185H} mice at 6-month-age. *R185H/+* and *R185H/R185H* female mice have more coping reactions to 52°C Hot Plate, while *R185H/R185H* male have more coping reactions to 48°C Hot Plate. (+/+ female n=13; *R185H/+* female n=13; *R185H/R185H* female n=11; +/+ male n=13; *R185H/+* male n=15; *R185H/R185H* male n=11). **C)** Jump Latency of 48, 52 and 56°C Hot Plate in *Scn9a*$^{R185X/wt}$ mice at 6-month-age. *R185X/+* female mice increased jump latency to 56°C Hot Plate, not showed in male mutant mice. (+/+ female n=11; *R185X/+* female n=13; +/+ male n=11; *R185X/+* male n=14). **D)** Coping reactions of 48, 52 and 56°C Hot Plate in *Scn9a*$^{R185X/wt}$ mice at 6-month-age. Decreasing coping reactions to 48 and 56°C Hot Plate showed in the *R185X/+* female mice compare to +/+, but not male mice. (+/+ female n=11; *R185X/+* female n=13; +/+ male n=11; *R185X/+* male n=14). Data present as means ± *SEM* *P < 0.05, ** P < 0.01 and ***P < 0.001, *Scn9a*^{R185H} and *Scn9a*$^{R185X/wt}$ mutants compared to their +/+ littermates by one

(jump latency) or two (coping reaction) tailed student t test or Mann-Whitney test. (More detailed statistical analysis see Supplementary Table. 14)

Supplementary Fig. 7 Sensitivity to heat, cool and mechanical stimuli and decreased pain sensitivity to cold stimuli in the *Scn9a*^{R185H} mice at 6-month-age. A-F) Tail Flick, Hargreaves test, Acetone test, Cold Plate 5 °C, Von Frey filaments and Tail Pressure were used to evaluate basal pain sensitivity in response to thermal and mechanical in female and male *Scn9a*^{R185H} mice at 6-month-age. No significant change detected in responses to heat (Tail Flick and Hargreaves Plantar), cold (Acetone test and Cold Plate 5 °C) and mechanical stimuli (Von Frey and Tail Pressure). (+/+ female n=14; *R185H/+* female n=13; *R185H/R185H* female n=11; +/+ male n=13; *R185H/+* male n=15; *R185H/R185H* male n=11). Data present as means ± *SEM*. *P < 0.05, ** P < 0.01 and ***P < 0.001, *Scn9a*^{R185H} and *Scn9a*$^{R185X/wt}$ mutants compared to their +/+ littermates by two tailed unpaired student t test or Mann-Whitney test. (More detailed statistical analysis see Supplementary Table. 15)

Supplementary Fig. 8 No pain sensitivity alteration to heat, cool and mechanical stimuli in the *Scn9a*$^{R185X/wt}$ mice at 2- and 6-month-age. A-F) Tail Flick, Hargreaves test, Acetone test, Cold Plate (5 °C), Von Frey filaments and Tail Pressure were used to evaluate basal pain sensitivity in female and male *Scn9a*$^{R185X/wt}$ mice at 2- (2-mo) and 6-month-age (6-mo). There is no statistical significance for all tests at the two different age. (+/+ female n=11; *R185X/+* female n=13; +/+ male n=11; *R185X/+* male n=14). Data present as means ± *SEM*. *P < 0.05, ** P < 0.01 and ***P < 0.001, *Scn9a*^{R185H} and *Scn9a*$^{R185X/wt}$ mutants compared to their +/+ littermates by two tailed unpaired student t test or Mann-Whitney test. (More detailed statistical analysis see Supplementary Table. 16)

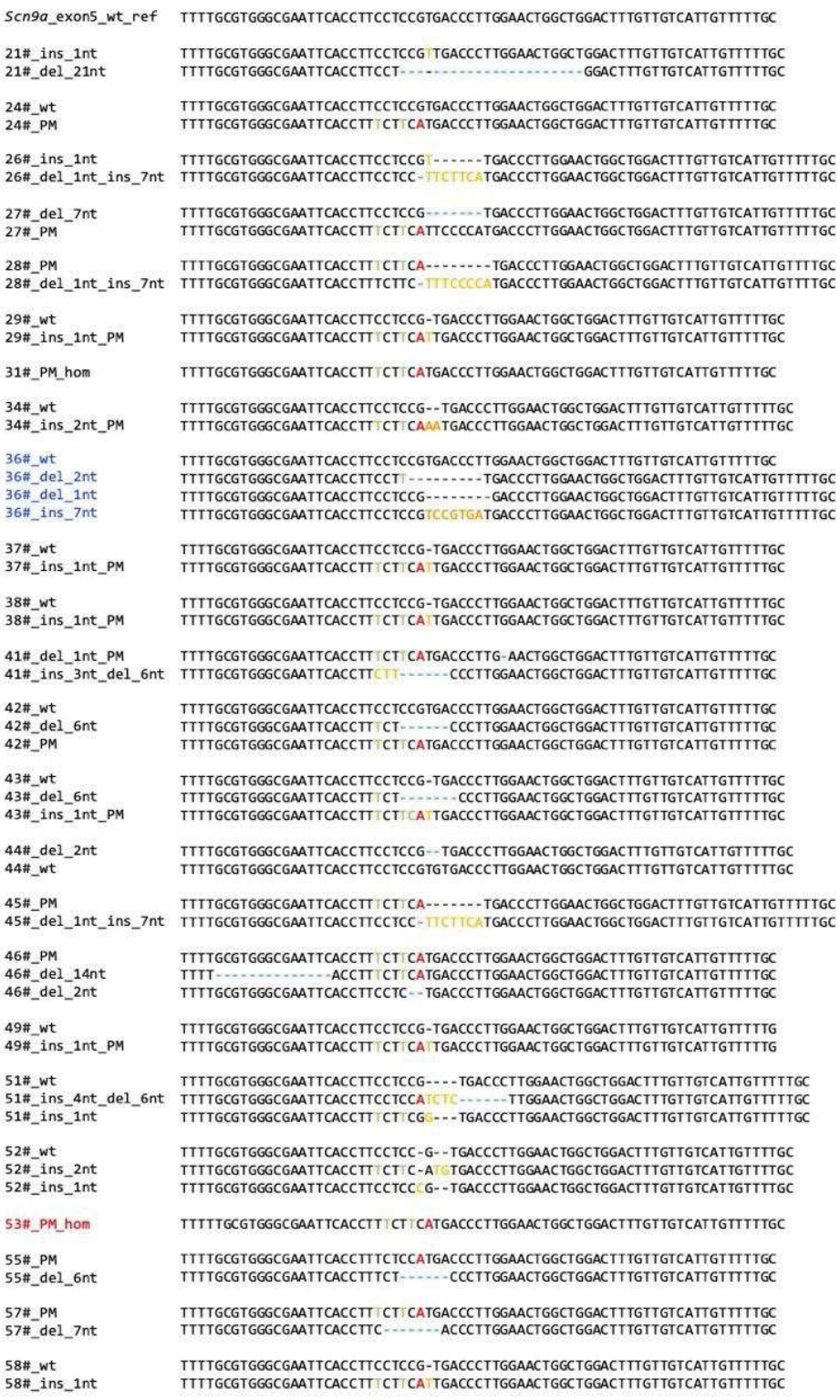

Supplementary Figure 1

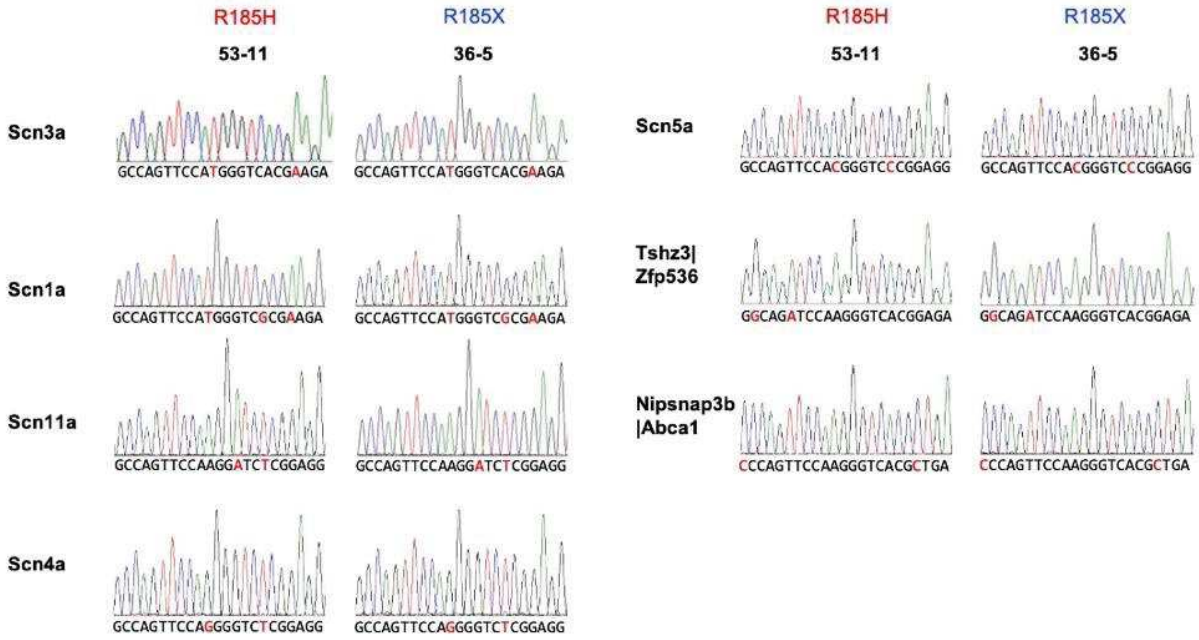

Supplementary Figure 2

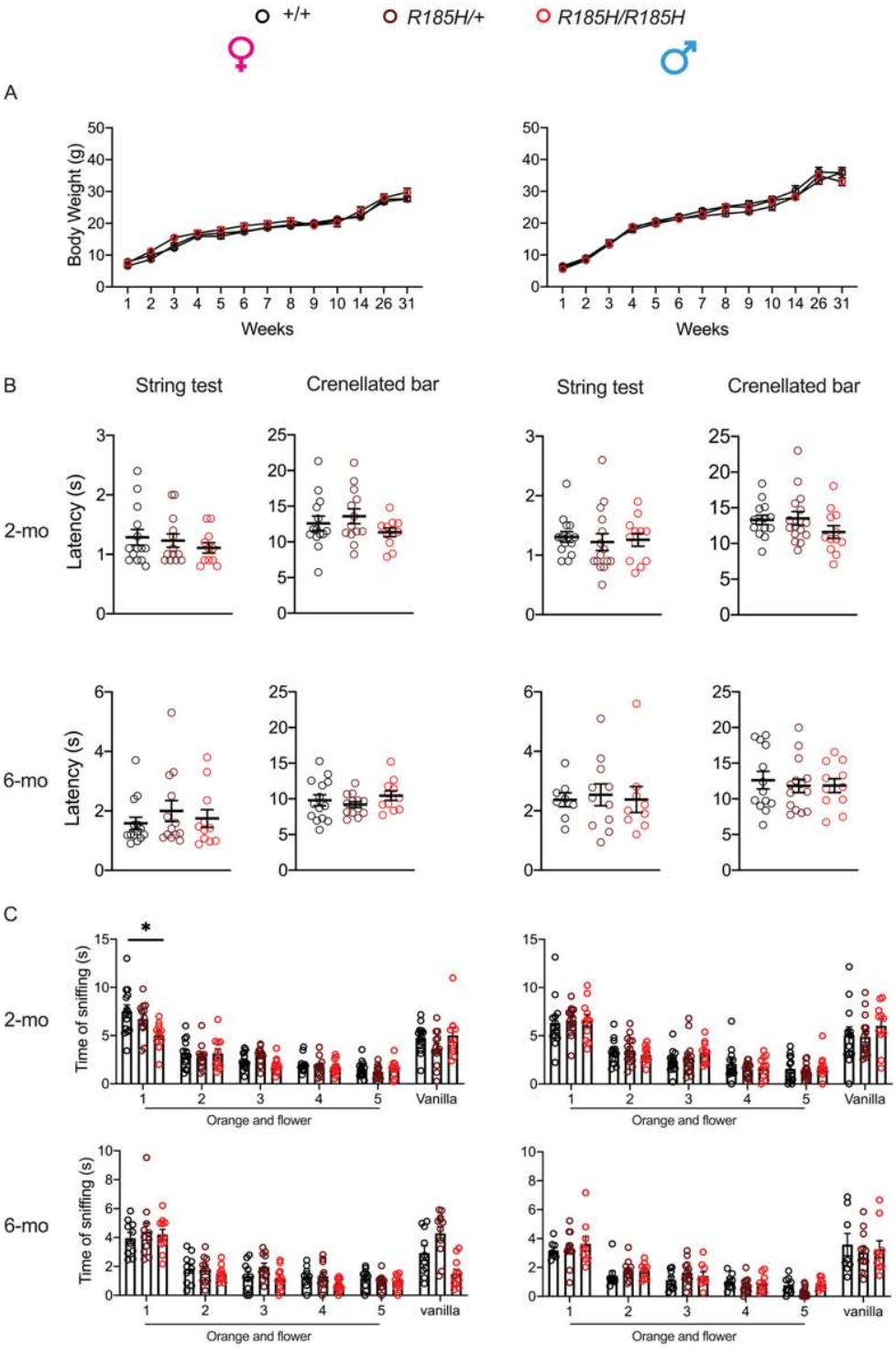

Supplementary Figure 3

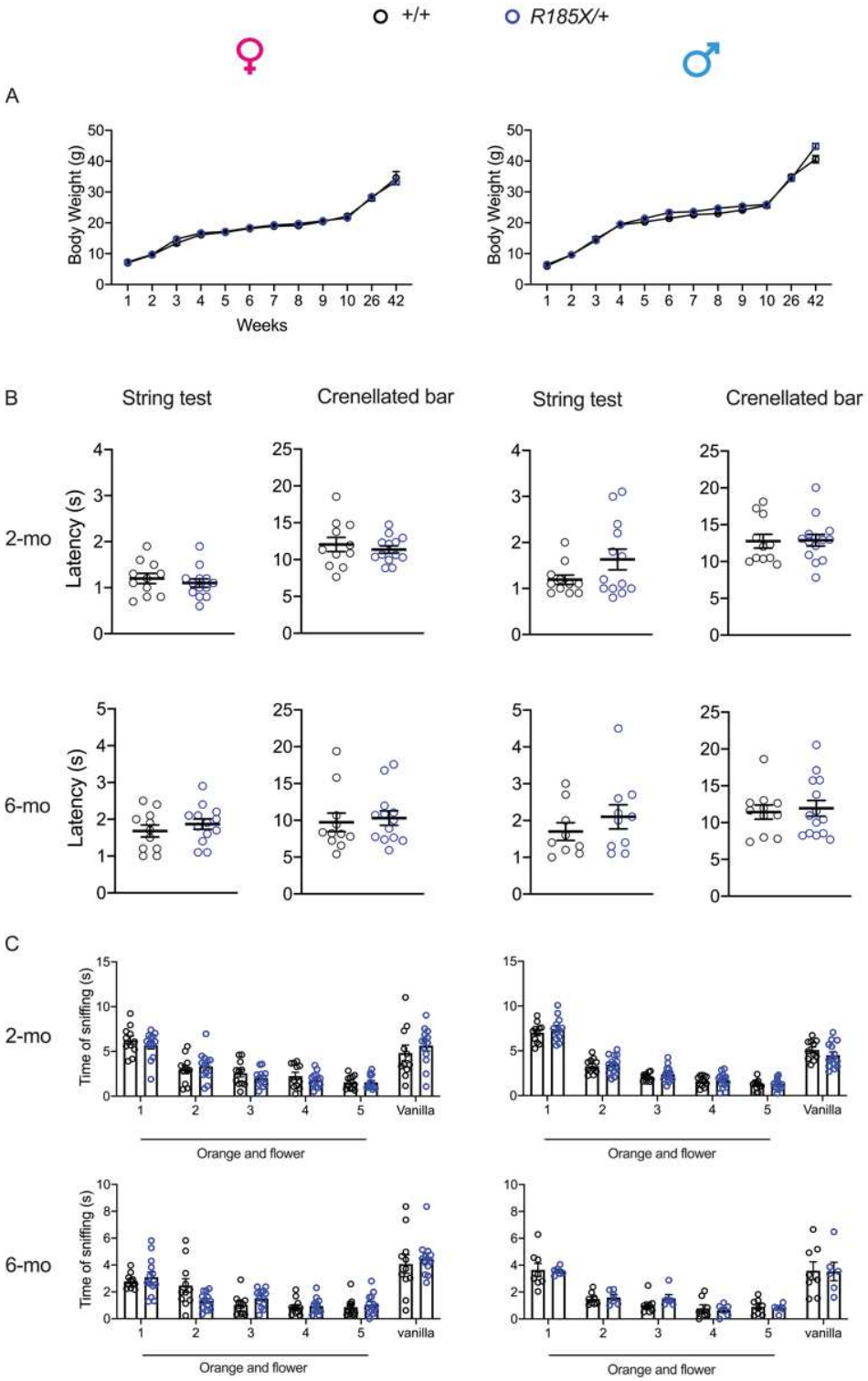

Supplementary Figure 4

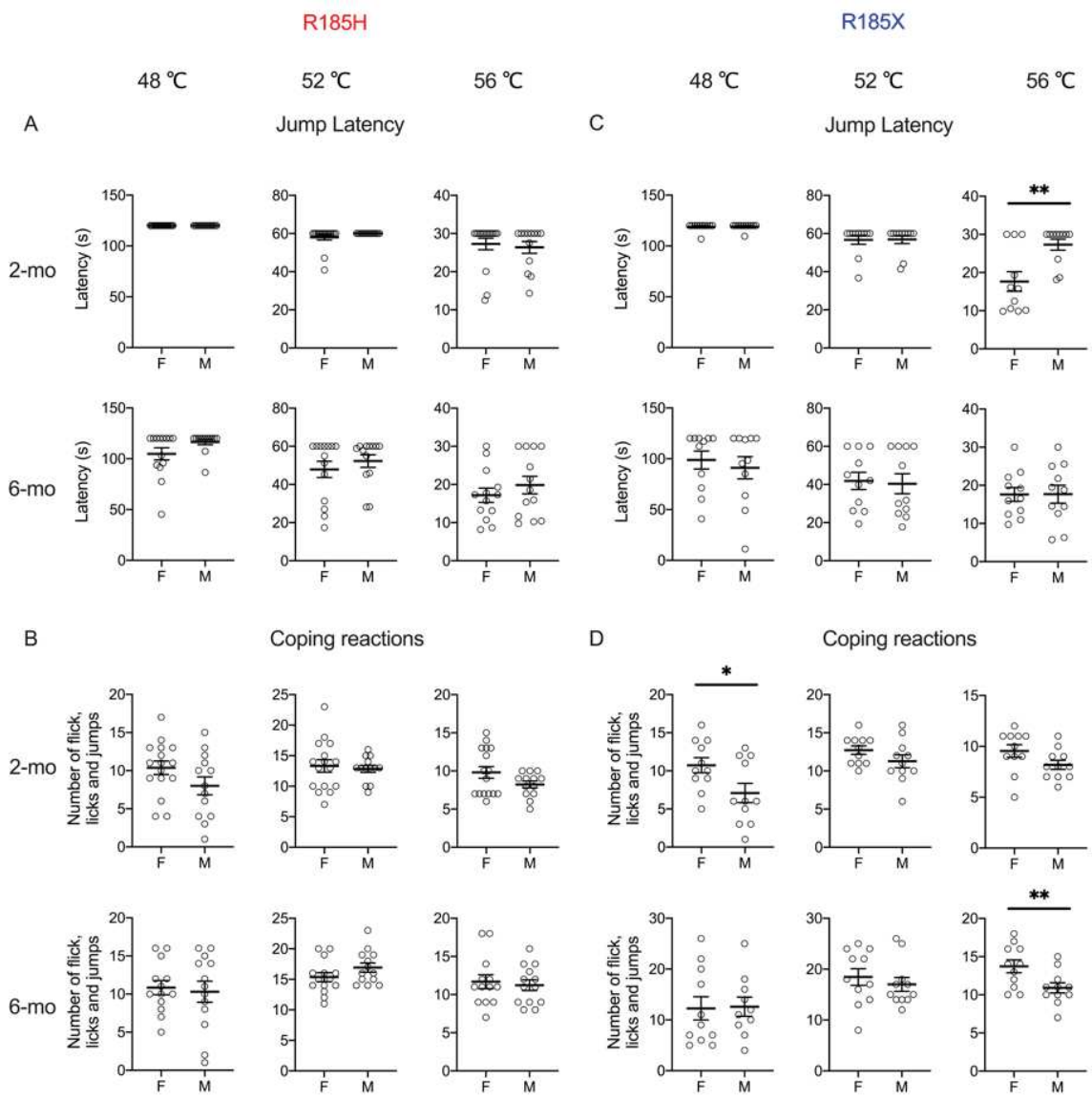

Supplementary Figure 5

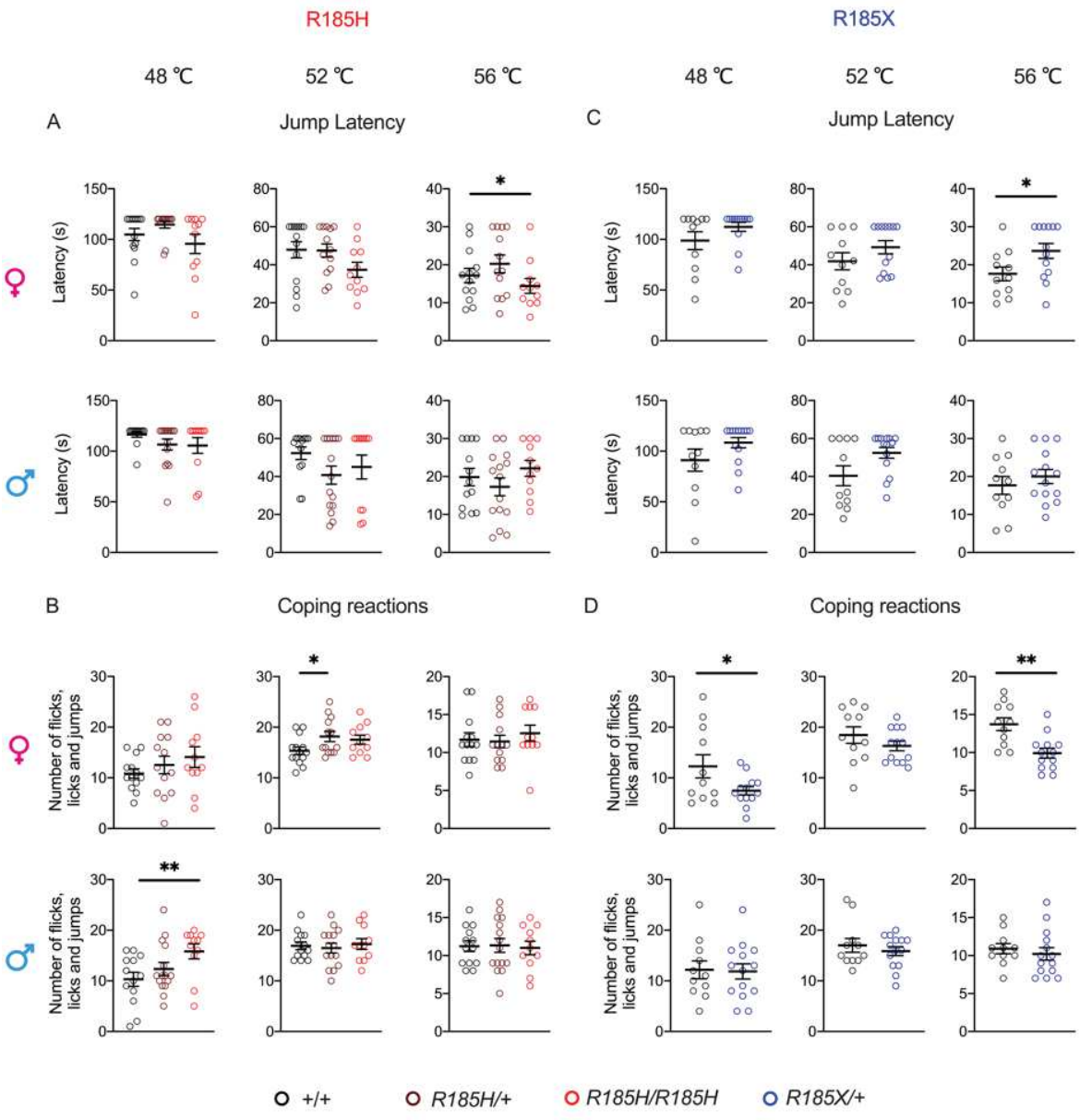

Supplementary Figure 6

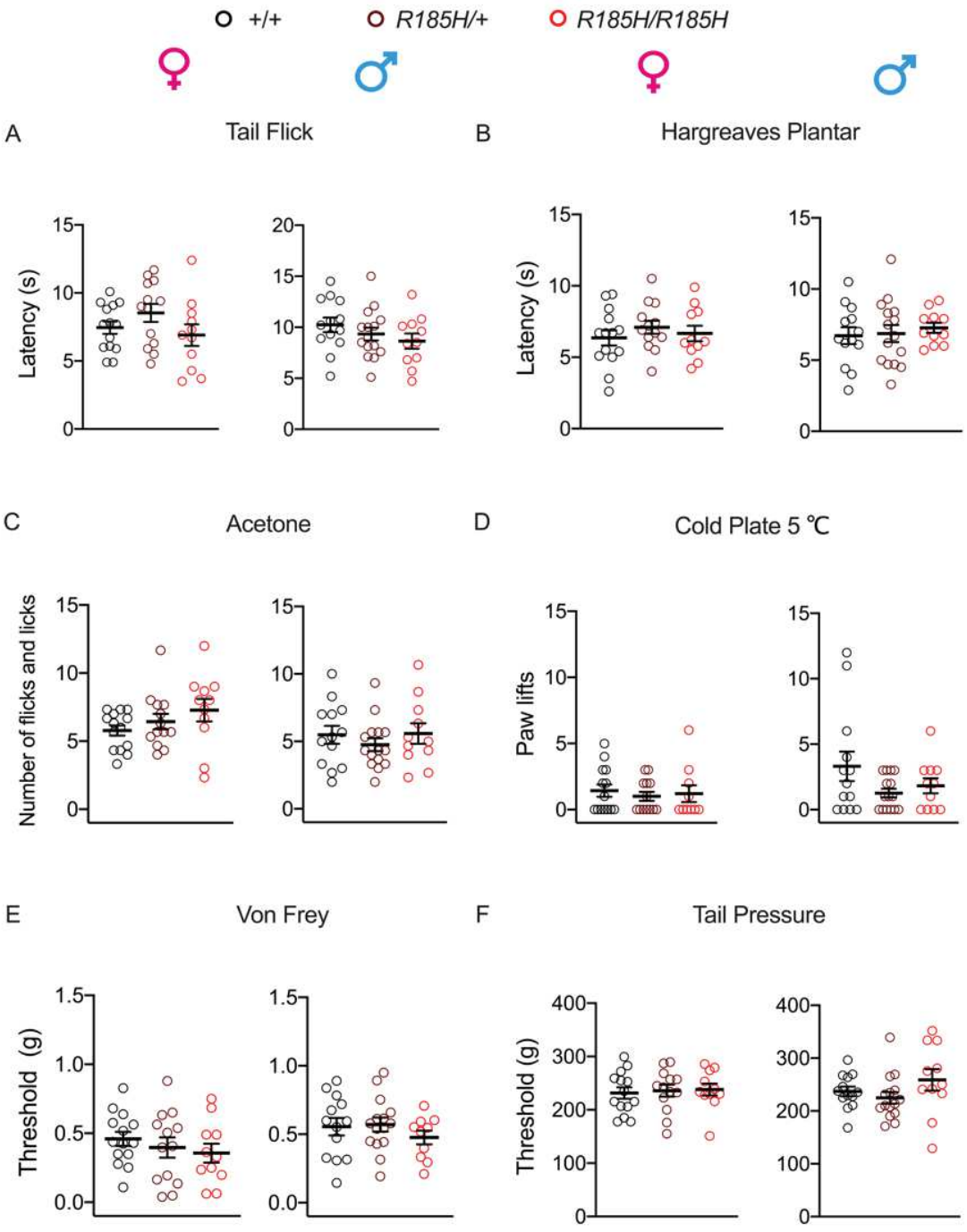

Supplementary Figure 7

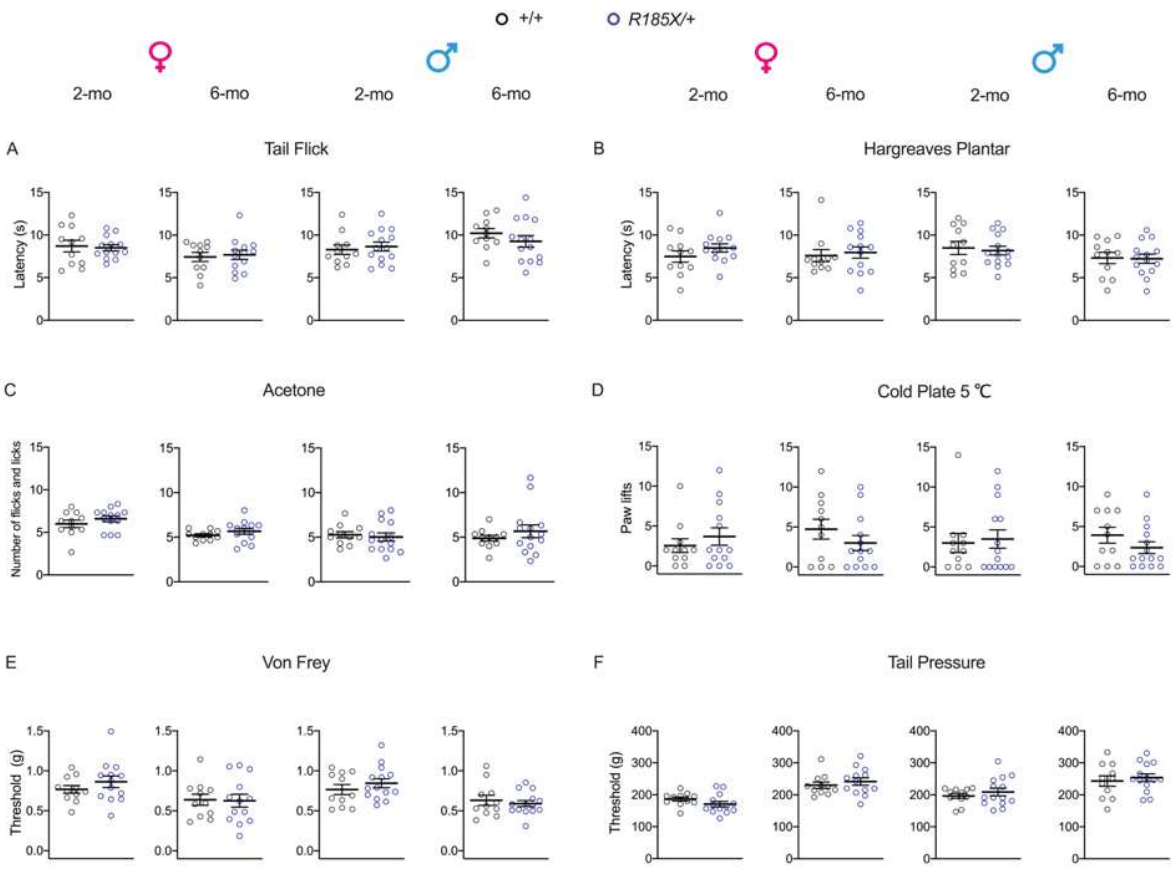

Supplementary Figure 8

Supplementary Table 1 PCR primers used for on-target genomic loci (*Scn9a*) amplification

Forward primer sequence (5´-3´)	Reverse primer sequence (5´-3´)
crF1 CTTGTGCAATGTACTTTATGAGGTG	crR1 ATCAGGAGACAAGATAATCCTTATG
crF2 ATGCTAACAGCAACCTCCAAGAGAG	crR2 ATAACACATGTCCACTCAGGTACTG
crF3 ATAAACTGTAAAGATTGTAATGAGA	crR3 AATATATGACTGGGAATAGTTAGTC

Supplementary Table 2 Primers and probe used for ddPCR

Genotyping	
Scn9a$^{R185X/wt}$-Forward primer sequence (5´-3´)	AATCCTTGCAAGAGGCTTT
Scn9a$^{R185X/wt}$-Reverse primer sequence (5´-3´)	AAACAATGACAAAGTCCAG
Scn9a^{R185X}-Probe	/56FAM/ACCTTCCTT/ZEN/TGACCCTTGGAACTGG/3IABkFQ/
Scn9a^{wt}-Probe	/56HEX/AATTCACCT/ZEN/TCCTCCGTGACCCTT/3IABkFQ/
mRNA expression	
Scn9a^{R185H}-Forward primer sequence (5´-3´)	CATGAGCAACCCTCCAGATT
Scn9a^{R185H}-Reverse primer sequence (5´-3´)	AAACAATGACAACAAAGTCCAG
Scn9a^{R185H}-Probe	/56FAM/ACCTTCCTT/ZEN/TGACCCTTGGAACTGG/3IABkFQ/
Scn9a^{wt}-Probe	/56HEX/AATTCACCT/ZEN/TCCTCCGTGACCCTT/3IABkFQ/
Scn9a$^{R185X/wt}$-Forward primer sequence (5´-3´)	CATGAGCAACCCTCCAGATT
Scn9a$^{R185X/wt}$-Reverse primer sequence (5´-3´)	AAACAATGACAACAAAGTCCAG
Scn9a$^{R185X/wt}$-Probe	56-FAM/ACCTTCCTT/ZEN/TGACCCTTGGAACTGG/3IABkFQ/
Scn9a^{wt}-Probe	/56HEX/AATTCACCT/ZEN/TCCTCCGTGACCCTT/3IABkFQ/
Hprt-Forward primer sequence (5´-3´)	CCCCAAAATGGTTAAGGTTGC
Hprt -Reverse primer sequence (5´-3´)	AACAAAGTCTGGCCTGTATCC
Hprt -Probe	5HEX/CTTGCTGGT/ZEN/GAAAAGGACCTCTCGAA/3IABkFQ/

Supplementary Table 3 Potential off-target analysis sequence

Gene ID	Potential off-target sequences	Mismatches	locus
Scn9a (on-target gene)	GCCAGTTCCAAGGGTCACGG AGG	0	chr2:66563568-66627708
Exon_Scn3a	GCCAGTTCCATGGGTCACGA AGA	2	chr2:65526522-65526544
Exon_Scn1a	GCCAGTTCCATGGGTCGCGA AGG	3	chr2:66334233-66334255
Exon_Scn11a	GCCAGTTCCAAGGATCTCGG AGG	2	chr9:119813083-119813105
Exon_Scn4a	GCCAGTTCCAGGGGTCTCGG AGG	2	chr11:106348297-106348319
Exon_Scn5a	GCCAGTTCCACGGGTCCCGG AGG	2	chr9:119550631-119550653
Intergenic_Tshz3|Zfp536	GGCAGATCCAAGGGTCACGG AGA	2	chr7:36801277-36801299
Intergenic_Nipsnap3b|Abca1	CCCAGTTCCAAGGGTCACGC TGA	2	chr4:53023676-53023698

Supplementary Table 4 Primers used for off-target genomic loci amplification

Gene ID	Forward primer sequence (5´-3´)	Reverse primer sequence (5´-3´)
Exon_Scn3a	crF1 CATTTATTGCTCAAAGACTAAGGGA crF2 CATACTGTGTATGGCATAGAGTTGA crF3 AAGTGACTAATGCTGGATTGGCATC crF4 GAGTTGACCTGATTAACAAGAAAGC	crR1 AATACTTCACTCACACTAATAAGAA crR2 GTTGTTGTTAATGCTGTTGTTCTGG crR3 CTCTAGTTGCTAACTTGGCTTGGGA crR4 TCAGCTCTTTAACCTCTTGTCTCTA
Exon_Scn1a	crF1 TGGAGCAGTGGAATGGGTTTACCCT crF2 CGGAGTTCAGGTGCCCAAATCATGC	crR1 GAAACTATGTATGTGATGGATTCTG crR2 CCGAGGACAACATGCTAAGAAGCTG
Exon_Scn11a	crF1 TACTCTCAGAGATCCACACAACTTC crF2 CAGAGCCTGGCATGTCAGAGCCACA	crR1 CTCCTTTCTTTCCCAGTCATTTATC crR2 GTTTCCTTAGCCACTTTGCCGTCTC
Exon_Scn4a	crF1 CTGCTAGAGAATGGAAGGACAAGGA crF2 TGGTCTCTGAGAATGCCCTAGATCA	crR1 CATTGTCCCTGTGACACAACACCTT crR2 GGGTAGCCTTATGCTATCTTGGTAC
Exon_Scn5a	crF1 AGTCTATCCTGTCCTCACCTTGCCA crF2 GATGAGCCAGGGTGCTCAGACACTT	crR1 CGATTGATGACTCTGGTGTGAGGAG crR2 CTTCCAGCAAGGGTGAAAGTGGAGA
Intergenic_Tshz3|Zfp536	crF1 GGCTCTGACAATCTTCCTGGTGAAA crF2 TGCGAAGTTTGGAAACCACCATCCA	crR1 AACCTAAGGAGGCCATTGCATGATG crR2 CAGTAGGCTAGACCTCCCACAACAA
Intergenic_Nipsnap3b|Abca1	crF1 CCTCTCCATATCATGTCACTCAGCT crF2 TCTCCGTGGCACATTTAATCACCGA	crR1 GTGGCAGAAGGAGAGTGAAGATCCT crR2 CAGCCATATAGGTGAGCCTGTGCAG

Supplementary Table 5 Multiple linear regression of mouse genotype, sex, age for different behavioral results-Heat

a)

Scn9a^{R185H}-Hot Plate Jump Latency				
Variable	Estimate (β)	Standard error	p-value	
Intercept	669.6	10.95	<0.0001	****
genotype	-2.629	0.8427	0.0019	**
sex	-3.12	1.346	0.0209	*
age	-2.437	0.3368	<0.0001	****
temperature	-11.37	0.2057	<0.0001	****
Model summary	R^2=0.8659, "F (4, 483) = 779.7", P<0.0001 ****			

b)

Scn9a^{R185H}-Hot Plate Coping reactions				
Variable	Estimate (β)	Standard error	p-value	
Intercept	14.85	3.227	<0.0001	****
genotype	0.8654	0.2483	0.0005	***
sex	0.8315	0.3966	0.0366	*
age	0.5827	0.09925	<0.0001	****
temperature	-0.129	0.06061	0.0339	*
Model summary	R^2=0.1002, "F (4, 483) = 13.44", P<0.0001 ****			

c)

Scn9a^{R185H} -Tail Flick				
Variable	Estimate (β)	Standard error	p-value	
Intercept	8.101	0.7578	<0.0001	****
genotype	-0.4049	0.2764	0.1449	ns
sex	-0.4154	0.4402	0.3466	ns
age	0.3171	0.1097	0.0043	**
Model summary	R2=0.06389, "F (3, 167) = 3.799", P=0.0114 *			

d)

Scn9a^{R185H}-Hargreaves Plantar				
Variable	Estimate (β)	Standard error	p-value	
Intercept	7.273	0.5434	<0.0001	****
genotype	0.2804	0.198	0.1587	ns
sex	-0.4196	0.3161	0.1864	ns
age	-0.132	0.079	0.0968	ns
Model summary	R2=0.04216, "F (3, 152) = 2.230", P=0.0870 ns			

e)

Scn9a$^{R185X/wt}$-Hot Plate Jump Latency				
Variable	Estimate (β)	Standard error	p-value	
Intercept	642.9	14.09	<0.0001	****
genotype	5.842	1.727	0.0008	***
sex	0.2501	1.718	0.8843	ns
age	-2.626	0.4293	<0.0001	****
temperature	-11.15	0.2629	<0.0001	****
Model summary	R^2=0.8647, "F (4, 289) = 461.8", P<0.0001 ****			

f)

Scn9a$^{R185X/wt}$-Hot Plate Coping reactions				
Variable	Estimate (β)	Standard error	p-value	
Intercept	9.074	4.183	0.0309	*
genotype	-1.438	0.5126	0.0054	**
sex	0.07085	0.51	0.8896	ns
age	0.852	0.1275	<0.0001	****
temperature	0.01786	0.07805	0.8192	ns
Model summary	R^2=0.1541, "F (4, 289) = 13.16", P<0.0001 ****			

g)

Scn9a$^{R185X/wt}$ -Tail Flick				
Variable	Estimate (β)	Standard error	p-value	
Intercept	9.198	0.8136	<0.0001	****
genotype	-0.1375	0.4116	0.7391	ns
sex	-1.011	0.4095	0.0153	*
age	0.02653	0.1023	0.796	ns
Model summary	R2=0.06233, "F (3, 94) = 2.083", P=0.1077 ns			

h)

Scn9a$^{R185X/wt}$-Hargreaves Plantar				
Variable	Estimate (β)	Standard error	p-value	
Intercept	8.08	0.8613	<0.0001	****
genotype	0.2314	0.4357	0.5967	ns
sex	0.1206	0.4335	0.7815	ns
age	-0.1622	0.1083	0.1376	ns
Model summary	R2=0.02688, "F (3, 94) = 0.8655", P=0.4619 ns			

Supplementary Table 6 Multiple linear regression of mouse genotype, sex, age for different behavioral results-Cold

a)

Scn9a^{R185H}-Acetone test Number of flicks and licks				
Variable	Estimate (β)	Standard error	p-value	
Intercept	5.033	0.5648	<0.0001	****
genotype	0.4581	0.2052	0.0271	*
sex	1.483	0.3264	<0.0001	****
age	-0.1375	0.08157	0.0939	ns
Model summary	R^2=0.1579, "F (3, 150) = 9.378", P<0.0001 ****			

b)

Scn9a^{R185H}-Cold Plate 5 ℃ Latency				
Variable	Estimate (β)	Standard error	p-value	
Intercept	60.73	29.38	0.0404	*
genotype	23.04	10.67	0.0325	*
sex	9.205	16.98	0.5884	ns
age	14.82	4.243	0.0006	***
Model summary	R^2=0.1024, "F (3, 150) = 5.702", P=0.0010 ***			

c)

Scn9a^{R185H}-Cold Plate 5 ℃ Number of paw lifts				
Variable	Estimate (β)	Standard error	p-value	
Intercept	4.973	0.735	<0.0001	****
genotype	-0.5898	0.2671	0.0287	*
sex	-0.3567	0.4248	0.4023	ns
age	-0.3149	0.1062	0.0035	**
Model summary	R^2=0.08714, "F (3, 150) = 4.773", P=0.0033 **			

d)

Scn9a$^{R185X/wt}$ -Acetone test Number of flicks and licks				
Variable	Estimate (β)	Standard error	p-value	
Intercept	4.938	0.6203	<0.0001	****
genotype	0.3981	0.3138	0.2077	ns
sex	0.6626	0.3122	0.0365	*
age	-0.08265	0.07803	0.2922	ns
Model summary	R^2=0.07057, "F (3, 94) = 2.379", P=0.0746 ns			

e)

Scn9a$^{R185X/wt}$ -Cold Plate 5 ℃ Latency				
Variable	Estimate (β)	Standard error	p-value	
Intercept	122.4	49.81	0.0158	*
genotype	12.72	25.2	0.6149	ns
sex	-4.07	25.07	0.8714	ns
age	-0.07352	6.266	0.9907	ns
Model summary	R^2=0.003016,"F (3, 94) = 0.09480", P=0.9627 ns			

f)

Scn9a$^{R185X/wt}$ -Cold Plate 5 ℃ Number of paw lifts				
Variable	Estimate (β)	Standard error	p-value	
Intercept	3.616	1.446	0.0142	*
genotype	-0.4101	0.7317	0.5765	ns
sex	0.3116	0.728	0.6696	ns
age	0.04592	0.1819	0.8013	ns
Model summary	R^2=0.006027, "F (3, 94) = 0.1900", P=0.9030 ns			

Supplementary Table 7 Multiple linear regression of mouse genotype, sex, age for different behavioral results-Mechanical

a)

Scn9a^{R185H}-Von Frey				
Variable	Estimate (β)	Standard error	p-value	
Intercept	0.6631	0.07174	<0.0001	****
genotype	-0.08769	0.0262	0.001	**
sex	-0.03819	0.04187	0.3633	ns
age	0.001338	0.01046	0.8983	ns
Model summary	R^2=0.07408, "F (3, 149) = 3.974", P=0.0093 **			

b)

Scn9a^{R185H}-Tail Pressure				
Variable	Estimate (β)	Standard error	p-value	
Intercept	142.3	10.66	<0.0001	****
genotype	4.458	3.899	0.2547	ns
sex	-4.974	6.203	0.4239	ns
age	14.71	1.55	<0.0001	****
Model summary	R^2=0.3796, "F (3, 150) = 30.60", P<0.0001 ****			

c)

Scn9a$^{R185X/wt}$ -Von Frey				
Variable	Estimate (β)	Standard error	p-value	
Intercept	0.8563	0.08717	<0.0001	****
genotype	0.03019	0.0441	0.4953	ns
sex	0.0173	0.04388	0.6942	ns
age	-0.04861	0.01096	<0.0001	****
Model summary	R^2=0.1774, "F (3, 94) = 6.757", P=0.0004 ***			

d)

Scn9a$^{R185X/wt}$ -Tail Pressure				
Variable	Estimate (β)	Standard error	p-value	
Intercept	167.2	15.46	<0.0001	****
genotype	4.718	7.822	0.5479	ns
sex	-19.1	7.783	0.016	*
age	12.96	1.945	<0.0001	****
Model summary	R^2=0.3509, "F (3, 94) = 16.94", P<0.0001 ****			

Supplementary Table 8 *Scn9a* transcript expression in the *Scn9a*^{R185H} and *Scn9a*$^{R185X/wt}$ mutant mice

Figure	Test: RT-ddPCR for *Scn9a*^{R185H} mice	Analysis	Groups	Statistics
Fig. 1B	DRG	Two-way ANOVA	genotype	p=0.8514 "F (2, 18) = 0.1623"
			sex	p=0.4358 "F (1, 18) = 0.6353"
Fig. 1B	Spinal Cord		genotype	p=0.7853 "F (2, 24) = 0.2441"
			sex	p=0.6151 "F (1, 24) = 0.2595"
Fig. 1B	Brain		genotype	p=0.9460 "F (2, 24) = 0.05560"
			sex	p=0.1239 "F (1, 24) = 2.542"
Fig. 1B	Cerebellum		genotype	p=0.4258 "F (2, 22) = 0.8878"
			sex	p=0.9921 "F (1, 22) = 0.0001001"
Fig. 1B	females DRG	Unpaired t-test two tailed	*+/+ vs R185H/+*	p=0.7042
			+/+ vs R185H/R185H	p=0.8017
Fig. 1B	Spinal Cord		*+/+ vs R185H/+*	p=0.6833
			+/+ vs R185H/R185H	p=0.3426
Fig. 1B	females Brain	Mann-Whitney test two tailed	*+/+ vs R185H/+*	p=0.7857
		Unpaired t-test two tailed	*+/+ vs R185H/R185H*	p=0.7439
Fig. 1B	females Cerebellum	Unpaired t-test two tailed	*+/+ vs R185H/+*	p=0.7408
			+/+ vs R185H/R185H	p=0.5843
Fig. 1B	males-DRG		*+/+ vs R185H/+*	p=0.4428
			+/+ vs R185H/R185H	p=0.3423
Fig. 1B	males Spinal Cord		*+/+ vs R185H/+*	p=0.7189
			+/+ vs R185H/R185H	p=0.7779
Fig. 1B	males Brain		*+/+ vs R185H/+*	p=0.0741
			+/+ vs R185H/R185H	p=0.7415
Fig. 1B	males Cerebellum		*+/+ vs R185H/+*	p=0.3810
			+/+ vs R185H/R185H	p=0.1151

Supplementary Table 8 *Scn9a* transcript expression in the *Scn9a*^{R185H} and *Scn9a*$^{R185X/wt}$ mutant mice

Figure	Test: RT-ddPCR for *Scn9a*$^{R185X/wt}$ mice	Analysis	Groups	Statistics
Fig. 1C	DRG	Two-way ANOVA	**genotype**	**p<0.0001 "F (1, 18) = 303.6"**
			sex	**p=0.0039 "F (1, 18) = 10.95"**
Fig. 1C	Spinal Cord		**genotype**	**p=0.0032 "F (1, 17) = 11.74"**
			sex	**p=0.9861 "F (1, 17) = 0.0003125"**
Fig. 1C	Brain		genotype	p=0.4858 "F (1, 15) = 0.5106"
			sex	p=0.5806 "F (1, 15) = 0.3189"
Fig. 1C	Cerebellum		genotype	p=0.6643 "F (1, 15) = 0.1960"
			sex	p=0.9773 "F (1, 15) = 0.0008337"
Fig. 1C	females-DRG	Unpaired t-test one tailed	***+/+ vs R185X/+***	**p<0.0001**
Fig. 1C	females Spinal Cord		***+/+ vs R185X/+***	**p=0.0282**
Fig. 1C	females Brain		*+/+ vs R185X/+*	p=0.0643
Fig. 1C	females Cerebellum		*+/+ vs R185X/+*	p=0.4048
Fig. 1C	males-DRG		***+/+ vs R185X/+***	**p<0.0001**
Fig. 1C	males Spinal Cord		***+/+ vs R185X/+***	**p=0.0136**
Fig. 1C	males Brain		*+/+ vs R185X/+*	p=0.2294
Fig. 1C	males Cerebellum		*+/+ vs R185X/+*	p=0.2297

Supplementary Table 9 Enhanced and decreased pain sensitivity to Hot Plate in the *Scn9a*^{R185H} and *Scn9a*$^{R185X/Wt}$ mice respectively at 2-month-age.

Figure	Test- Hot Plate Jump Latency for *Scn9a*^{R185H} mice		Analysis	Groups	Statistics
Fig. 2A & S36A	48 ℃		Three-way ANOVA	**Genotype**	**p=0.0436 "F (2, 151) = 3.199"**
				Sex	p=0.0935 "F (1, 151) = 2.849"
				Age	**p-0.0002 "F (1, 151) = 14.71"**
Fig. 2A & S36A	52 ℃			Genotype	p=0.0437 "F (2, 151) = 3.197"
				Sex	p=0.1233 "F (1, 151) = 2.401"
				Age	**p<0.0001 "F (1, 151) = 42.40"**
Fig. 2A & S36A	56 ℃			Genotype	p=0.4291 "F (2, 150) = 0.8508"
				Sex	**p=0.0177 "F (1, 150) = 5.754"**
				Age	**p<0.0001 "F (1, 150) = 34.39"**
Fig. 2A	48 ℃-2-mo		Two-way ANOVA	Genotype	p=0.2197 "F (2, 80) = 1.545"
				Sex	p=0.0867 "F (1, 80) = 3.009"
Fig. 2A	52 ℃-2-mo			Genotype	p=0.3406 "F (2, 80) = 1.092"
				Sex	**p=0.0082 "F (1, 80) = 7.341"**
Fig. 2A	56 ℃-2-mo			Genotype	p=0.1451 "F (1, 80) = 4.411"
				Sex	**P=0.0389 "F (2, 80) = 1.978"**
Fig. 2A	females: 2-mo	48 ℃	Mann-Whitney test one-tailed	*+/+ vs R185H/+*	p=0.2419
				+/+ vs R185H/R185H	**p=0.0434**
Fig. 2A		52 ℃	Mann-Whitney test one-tailed	*+/+ vs R185H/+*	p=0.2466
				+/+ vs R185H/R185H	**p=0.0465**
Fig. 2A		56 ℃	Mann-Whitney test one-tailed	***+/+ vs R185H/+***	**p=0.0356**
				+/+ vs R185H/R185H	**p=0.0005**
Fig. 2A	males: 2-mo	48 ℃	Mann-Whitney test one-tailed	*+/+ vs R185H/+*	p=0.5000
				+/+ vs R185H/R185H	p=0.5000
Fig. 2A		52 ℃	Mann-Whitney test one-tailed	*+/+ vs R185H/+*	p=0.2778
				+/+ vs R185H/R185H	p=0.5000
Fig. 2A		56 ℃	Mann-Whitney test one-tailed	*+/+ vs R185H/+*	p=0.5032
				+/+ vs R185H/R185H	p=0.3001

Supplementary Table 9 Enhanced and decreased pain sensitivity to Hot Plate in the *Scn9a*^{R185H} and *Scn9a*$^{R185X/Wt}$ mice respectively at 2-month-age.

Figure	Test- Hot Plate Coping reactions for *Scn9a*^{R185H} mice		Analysis	Groups	Statistics
Fig. 2B & S6B	48 ℃		Three-way ANOVA	**Genotype**	**p=0.0269 "F (2, 151) = 3.704"**
				Sex	p=0.5840 "F (1, 151) = 0.3012"
				Age	**p=0.0058 "F (1, 151) = 7.838"**
Fig. 2B & S6B	52 ℃			**Genotype**	**p=0.0283 "F (2, 151) = 3.651"**
				Sex	p=0.1748 "F (1, 151) = 1.858"
				Age	**p<0.0001 "F (1, 151) = 34.13"**
Fig. 2B & S6B	56 ℃			Genotype	p=0.1339 "F (2, 150) = 2.038"
				Sex	**p=0.0057 "F (1, 150) = 7.883"**
				Age	**p<0.0001 "F (1, 150) = 17.79"**
Fig. 2B	48 ℃-2-mo		Two-way ANOVA	Genotype	P=0.1567 "F (2, 80) = 1.897"
				Sex	P=0.4369 "F (1, 80) = 0.6105"
Fig. 2B	52 ℃-2-mo			**Genotype**	**p=0.0141 "F (2, 79) = 4.503"**
				Sex	p=0.1065 "F (1, 79) = 2.666"
Fig. 2B	56 ℃-2-mo			**Genotype**	**p=0.0260 "F (2, 80) = 3.823"**
				Sex	**p=0.0014 "F (1, 80) = 11.01"**
Fig. 2B	females: 2-mo	48 ℃	Unpaired t-test two-tailed	*+/+ vs R185H/+*	p=0.5746
				+/+ vs R185H/R185H	p=0.9105
Fig. 2B		52 ℃	Unpaired t-test two-tailed	*+/+ vs R185H/+*	p=0.5103
			Mann-Whitney test two-tailed	***+/+ vs R185H/R185H***	**p=0.0061**
Fig. 2B		56 ℃	Mann-Whitney test two-tailed	*+/+ vs R185H/+*	p=0.7012
				+/+ vs R185H/R185H	**p=0.0488**
Fig. 2B	males: 2-mo	48 ℃	Unpaired t-test two-tailed	*+/+ vs R185H/+*	p=0.0798
			Mann-Whitney test two-tailed	*+/+ vs R185H/R185H*	p=0.0788
Fig. 2B		52 ℃	Unpaired t-test two-tailed	*+/+ vs R185H/+*	p=0.2066
				+/+ vs R185H/R185H	p=0.4804
Fig. 2B		56 ℃	Mann-Whitney-test two-tailed	*+/+ vs R185H/+*	p=0.8283
			Unpaired t-test two-tailed	***+/+ vs R185H/R185H***	**p=0.0194**

Supplementary Table 9 Enhanced and decreased pain sensitivity to Hot Plate in the *Scn9a*^{R185H} and *Scn9a*$^{R185X/Wt}$ mice respectively at 2-month-age.

Figure	Test- Hot Plate Jump Latency for *Scn9a*$^{R185X/wt}$ mice		Analysis	Groups	Statistics
Fig. 2C & S6C	48 ℃		Three-way ANOVA	**Genotype**	**p=0.0373 "F (1, 90) = 4.469"**
				Sex	p=3850 "F (1, 90) = 0.7619"
				Age	**p<0.0001 "F (1, 90) = 19.46"**
Fig. 2C & S6C	52 ℃			**Genotype**	**p=0.0060 "F (1, 90) = 7.914"**
				Sex	p=0.7389 "F (1, 90) = 0.1118"
				Age	**p<0.0001 "F (1, 90) = 31.15"**
Fig. 2C & S6C	56 ℃			**Genotype**	**p=0.0103 "F (1, 90) = 6.859"**
				Sex	p=0.1776 "F (1, 90) = 1.847"
				Age	**p=0.0027 "F (1, 90) = 9.511"**
Fig. 2C	48 ℃-2-mo		Two-way ANOVA	Genotype	p=0.7951 "F (1, 45) = 0.06828"
				Sex	p=0.5642 "F (1, 45) = 0.3375"
Fig. 2C	52 ℃-2-mo			Genotype	p=0.1561 "F (1, 45) = 2.080"
				Sex	p=0.7335 "F (1, 45) = 0.1174"
Fig. 2C	56 ℃-2-mo			Genotype	p=0.1129 "F (1, 45) = 4.433"
				Sex	**p=0.0060 "F (1, 45) = 8.318"**
Fig. 2C	females: 2-mo	48 ℃	Mann-Whitney test one-tailed	*+/+ vs R185X/+*	p=0.4583
Fig. 2C		52 ℃	Mann-Whitney test one-tailed	*+/+ vs R185X/+*	p=0.4217
Fig. 2C		56 ℃	Mann-Whitney test one-tailed	***+/+ vs R185X/+***	**p=0.0393**
Fig. 2C	males: 2-mo	48 ℃	Mann-Whitney test one-tailed	*+/+ vs R185X/+*	p=0.5453
Fig. 2C		52 ℃	Mann-Whitney test one-tailed	*+/+ vs R185X/+*	p=0.3372
Fig. 2C		56 ℃	Mann-Whitney test one-tailed	*+/+ vs R185X/+*	p=0.3442

Supplementary Table 9 Enhanced and decreased pain sensitivity to Hot Plate in the *Scn9a*^{R185H} and *Scn9a*$^{R185X/Wt}$ mice respectively at 2-month-age.

Figure	Test: Hot Plate Coping reactions for *Scn9a*$^{R185X/wt}$ mice		Analysis	Groups	Statistics
Fig. 2D & S6D	48 ℃		Three-way ANOVA	**Genotype**	**p=0.0467 "F (1, 90) = 4.067"**
				Sex	p=0.4435 "F (1, 90) = 0.5924"
				Age	**p=0.0065 "F (1, 90) = 7.768"**
Fig. 2D & S6D	52 ℃			Genotype	p=0.2716 "F (1, 90) = 1.224"
				Sex	p=0.5378 "F (1, 90) = 0.3826"
				Age	**p<0.0001 "F (1, 90) = 51.33"**
Fig. 2D & S6D	56 ℃			**Genotype**	**p=0.0004 "F (1, 90) = 13.46"**
				Sex	**p=0.0283 "F (1, 90) = 4.970"**
				Age	**p<0.0001 "F (1, 90) = 39.61"**
Fig. 2D	48 ℃-2-mo		Two-way ANOVA	Genotype	p=0.2142 "F (1, 45) = 1.587"
				Sex	p=0.5480 "F (1, 45) = 0.3665"
Fig. 2D	52 ℃-2-mo			Genotype	p=0.8059 "F (1, 45) = 0.06112"
				Sex	p=0.8494 "F (1, 45) = 0.03649"
Fig. 2D	56 ℃-2-mo			**Genotype**	**p=0.0343 "F (1, 45) = 4.766"**
				Sex	p=0.1334 "F (1, 45) = 2.336"
Fig. 2D	females: 2-mo	48 ℃	Unpaired t-test two-tailed	***+/+ vs R185X/+***	**p=0.0010**
Fig. 2D		52 ℃	Unpaired t-test two-tailed	***+/+ vs R185X/+***	**p=0.0458**
Fig. 2D		56 ℃	Unpaired t-test two-tailed	*+/+ vs R185X/+*	p=0.0602
Fig. 2D	males: 2-mo	48 ℃	Unpaired t-test two-tailed	*+/+ vs R185X/+*	p=0.3779
Fig. 2D		52 ℃	Unpaired t-test two-tailed	*+/+ vs R185X/+*	p=0.1092
Fig. 2D		56 ℃	Unpaired t-test two-tailed	*+/+ vs R185X/+*	p=0.3584

Supplementary Table 10 Enhanced pain sensitivity to heat, cool and mechanical stimuli and decreased pain sensitivity to cold stimuli in the *Scn9a*^{R185H} mice at 2-month-age.

Figure	Test	Analysis	Groups	Statistics
Fig. 3A & S7A	Tail Flick	Three-way ANOVA	Genotype	p=0.0860 "F (2, 152) = 2.494"
			Sex	**p=0.0296** **"F (1, 152) = 4.826"**
			Age	**p=0.0456** **"F (1, 152) = 4.063"**
Fig. 3A	Tail Flick	Two-way ANOVA	Genotype	p=0.2869 "F (2, 81) = 1.268"
			Sex	p=0.9897 "F (1, 81) = 0.0001670"
Fig. 3A	females	Unpaired t-test two-tailed	*+/+ vs R185H/+*	p=0.0681
			+/+ vs R185H/R185H	**p=0.0286**
Fig. 3A	males	Unpaired t-test two-tailed	*+/+ vs R185H/+*	p=0.7562
			+/+ vs R185H/R185H	p=0.7087
Fig. 3B & S7B	Hargreaves Plantar	Three-way ANOVA	Genotype	p=0.2865 "F (2, 144) = 1.261"
			Sex	p=0.1848 "F (1, 144) = 1.775"
			Age	p=0.1167 "F (1, 144) = 2.491"
Fig. 3B	Hargreaves Plantar	Two-way ANOVA	Genotype	p=0.5530 "F (2, 72) = 0.5973"
			Sex	p=0.2604 "F (1, 72) = 1.287"
Fig. 3B	females	Unpaired t-test two-tailed	*+/+ vs R185H/+*	p=0.2875
			+/+ vs R185H/R185H	p=0.7673
Fig. 3B	males	Unpaired t-test two-tailed	*+/+ vs R185H/+*	p=0.3755
			+/+ vs R185H/R185H	p=0.4562

Supplementary Table 10 Enhanced pain sensitivity to heat, cool and mechanical stimuli and decreased pain sensitivity to cold stimuli in the *Scn9a*^{R185H} mice at 2-month-age.

Figure	Test	Analysis	Groups	Statistics
Fig. 3C & S7C	Acetone Flicks and Licks	Three-way ANOVA	**Genotype**	**p=0.0476 "F (2, 154) = 3.107"**
			Sex	**p<0.0001 "F (1, 154) = 19.67"**
			Age	p=0.3132 "F (1, 154) = 1.024"
Fig. 7C	Acetone Flicks and Licks	Two-way ANOVA	Genotype	p=0.0654 "F (2, 78) = 2.825"
			Sex	**p=0.0017 "F (1, 78) = 10.62"**
Fig. 7C	females	Unpaired t test two-tailed	*+/+ vs R185H/+*	p=0.2530
			+/+ vs R185H/R185H	p=0.2768
Fig. 7C	males	Unpaired t test two-tailed	*+/+ vs R185H/+*	p=0.3293
			+/+ vs R185H/R185H	p=0.2033
Fig. 3D & S7D	Cold Plate 5 ℃ Paw Lifts	Three-way ANOVA	Genotype	p=0.1137 "F (2, 142) = 2.208"
			Sex	p=0.4568 "F (1, 142) = 7.402"
			Age	**p=0.0073 "F (1, 142) = 7.402"**
Fig. 3D	Cold Plate 5 ℃ Paw Lifts	Two-way ANOVA	Genotype	p=0.0842 "F (2, 71) = 2.563"
			Sex	p=0.9447 "F (1, 71) = 0.004851"
Fig. 3D	females	Mann-Whitney test two-tailed	*+/+ vs R185H/+*	p=0.6152
			+/+ vs R185H/R185H	p=0.9851
Fig. 3D	males	Mann-Whitney test two-tailed	*+/+ vs R185H/+*	p=0.5899
		Unpaired t test two-tailed	***+/+ vs R185H/R185H***	**p=0.0455**

Supplementary Table 10 Enhanced pain sensitivity to heat, cool and mechanical stimuli and decreased pain sensitivity to cold stimuli in the *Scn9a*^{R185H} mice at 2-month-age.

Figure	Test	Analysis	Groups	Statistics
Fig. 3E & S7E	Von Frey	Three-way ANOVA	**Genotype**	**p=0.0104 "F (2, 143) = 4.714"**
			Sex	p=0.4393 "F (1, 143) = 0.6015"
			Age	p=0.9926 "F (1, 143) = 8.557e-005"
Fig. 3E	Von Frey	Two-way ANOVA	**Genotype**	**p=0.0012 "F (2, 70) = 7.368"**
			Sex	p=0.2747 "F (1, 70) = 1.212"
Fig. 3E	females	Unpaired t-test two-tailed	***+/+ vs R185H/+***	**p=0.0318**
			+/+ vs R185H/R185H	**p=0.0019**
Fig. 3E	males	Unpaired t-test two-tailed	*+/+ vs R185H/+*	p=0.0873
			+/+ vs R185H/R185H	**p=0.0309**
Fig. 3F & S7F	Tail Pressure	Three-way ANOVA	Genotype	p=0.1678 "F (2, 142) = 1.808"
			Sex	p=0.3460 "F (1, 142) = 0.8941"
			Age	**p<0.0001 "F (1, 142) = 89.64"**
Fig. 3F	Tail Pressure	Two-way ANOVA	Genotype	p=0.4944 "F (2, 71) = 0.7114"
			Sex	p=0.3677 "F (1, 71) = 0.8219"
Fig. 3F	females	Unpaired t-test two-tailed	*+/+ vs R185H/+*	p=0.3437
			+/+ vs R185H/R185H	p=0.2955
Fig. 3F	males	Unpaired t-test two-tailed	*+/+ vs R185H/+*	p=0.1667
			+/+ vs R185H/R185H	p=0.8414

Supplementary Table 11 *Scn9a*^{R185H} mice show normal healthy condition at 2- and 6-month-age

Figure	Test	Analysis	Groups	Statistics
Fig. S3A	Body Weight: females	Repeated measures ANOVA	Genotype	p=0.0.507 "F (2, 39) = 3.221"
			weeks	**p<0.0001** **"F (1.176, 27.43) = 27.70"**
Fig. S3A	Week 1: *+/+ vs R185H/+*	Sidak post-hoc multiple comparation		p=0.0531
	Week 1: *+/+ vs R185H/R185H*			p=0.7859
	Week 2: *+/+ vs R185H/+*			p=0.2039
	Week 2: *+/+ vs R185H/R185H*			p=0.1190
	Week 3: *+/+ vs R185H/+*			p=0.6162
	Week 3: *+/+ vs R185H/R185H*			p=0.0016
	Week 4: *+/+ vs R185H/+*			p=0.8123
	Week 4: *+/+ vs R185H/R185H*			p=0.6476
	Week 5: *+/+ vs R185H/+*			p=0.9954
	Week 5: *+/+ vs R185H/R185H*			p=0.6335
	Week 6: *+/+ vs R185H/+*			p=0.9896
	Week 6: *+/+ vs R185H/R185H*			p=0.1955
	Week 7: *+/+ vs R185H/+*			p=0.9994
	Week 7: *+/+ vs R185H/R185H*			p=0.4803
	Week 8: *+/+ vs R185H/+*			p=0.8333
	Week 8: *+/+ vs R185H/R185H*			p=0.2738
	Week 9: *+/+ vs R185H/+*			p=0.7944
	Week 9: *+/+ vs R185H/R185H*			p=0.9429
	Week 10: *+/+ vs R185H/+*			p=0.9204
	Week 10: *+/+ vs R185H/R185H*			p=0.9566
	Week 14: *+/+ vs R185H/+*			p=0.7863
	Week 14: *+/+ vs R185H/R185H*			p=0.7220
	Week 26: *+/+ vs R185H/+*			p=0.8671
	Week 26: *+/+ vs R185H/R185H*			p=0.7418
	Week 31: *+/+ vs R185H/+*			p>0.9999
	Week 31: *+/+ vs R185H/R185H*			p=0.3681

Supplementary Table 11 *Scn9a*^{R185H} mice show normal healthy condition at 2- and 6-month-age

Figure	Test	Analysis	Groups	Statistics
Fig. S3A	Body Weight: males	Repeated measures ANOVA	Genotype	p=0.2390 "F (2, 42) = 1.481"
			weeks	**p<0.0001** **"F (4.010, 110.6) = 509.3"**
Fig. S3A	Week 1: +/+ *vs R185H/+*	Sidak post-hoc multiple comparation		p=0.9071
	Week 1: +/+ *vs R185H/R185H*			p=0.5098
	Week 2: +/+ *vs R185H/+*			p=0.8771
	Week 2: +/+ *vs R185H/R185H*			p=0.9421
	Week 3: +/+ *vs R185H/+*			p=0.9177
	Week 3: +/+ *vs R185H/R185H*			p=0.9883
	Week 4: +/+ *vs R185H/+*			p=0.9208
	Week 4: +/+ *vs R185H/R185H*			p=0.9727
	Week 5: +/+ *vs R185H/+*			p=0.6567
	Week 5: +/+ *vs R185H/R185H*			p=0.9600
	Week 6: +/+ *vs R185H/+*			p=0.7639
	Week 6: +/+ *vs R185H/R185H*			p=0.6346
	Week 7: +/+ *vs R185H/+*			p=0.2638
	Week 7: +/+ *vs R185H/R185H*			p=0.6325
	Week 8: +/+ *vs R185H/+*			p=0.1587
	Week 8: +/+ *vs R185H/R185H*			p=0.9992
	Week 9: +/+ *vs R185H/+*			p=0.1575
	Week 9: +/+ *vs R185H/R185H*			p=0.8039
	Week 10: +/+ *vs R185H/+*			p=0.3700
	Week 10: +/+ *vs R185H/R185H*			p=0.9882
	Week 14: +/+ *vs R185H/+*			p=0.6453
	Week 14: +/+ *vs R185H/R185H*			p=0.5776
	Week 26: +/+ *vs R185H/+*			p=0.3586
	Week 26: +/+ *vs R185H/R185H*			p=0.8946
	Week 31: +/+ *vs R185H/+*			p=0.9995
	Week 31: +/+ *vs R185H/R185H*			p=0.2147

Supplementary Table 11 *Scn9a*^{R185H} mice show normal healthy condition at 2- and 6-month-age

Figure	Test		Analysis	Groups	Statistics
Fig. S3B	String test		Three-way ANOVA	Genotype	p=0.6969 "F (2, 133) = 0.3621"
				Sex	**p=0.0086** **"F (1, 133) = 42.80"**
				Age	**p<0.0001** **"F (1, 133) = 7.124"**
Fig. S3B	2-mo		Two-way ANOVA	Genotype	p=0.6290 "F (2, 73) = 0.4666"
				Sex	p=0.5801 "F (1, 73) = 0.3089"
Fig. S3B	6-mo			Genotype	p=0.4011 "F (2, 60) = 0.9275"
				Sex	p=0.1400 "F (1, 60) = 2.237"
Fig. S3B	2-mo	females	Mann-Whitney test two-tailed	*+/+ vs R185H/+*	p=0.7808
				+/+ vs R185H/R185H	p=0.4532
Fig. S3B		males	Mann-Whitney test two-tailed	*+/+ vs R185H/+*	p=0.2356
				+/+ vs R185H/R185H	p=0.9294
Fig. S3B	6-mo	females	Mann-Whitney test two-tailed	*+/+ vs R185H/+*	p=0.3679
				+/+ vs R185H/R185H	p=0.8826
Fig. S3B		males	Unpaired t test two-tailed	*+/+ vs R185H/+*	p=0.7288
			Mann-Whitney test two-tailed	*+/+ vs R185H/R185H*	p=0.4963
Fig. S3B	Crenellated bar		Three-way ANOVA	Genotype	p=0.4232 "F (2, 144) = 0.8650"
				Sex	**p=0.0134** **"F (1, 144) = 6.264"**
				Age	**p=0.0012** **"F (1, 144) = 10.96"**
Fig. S3B	2-mo		Two-way ANOVA	Genotype	p=0.0714 "F (2, 73) = 2.737"
				Sex	p=0.6935 "F (1, 73) = 0.1565"
Fig. S3B	6-mo			Genotype	p=0.6611 "F (2, 71) = 0.4163"
				Sex	**p=0.0023** **"F (1, 71) = 9.978"**
Fig. S3B	2-mo	females	Unpaired t-test two-tailed	*+/+ vs R185H/+*	p=0.4966
				+/+ vs R185H/R185H	p=0.3234
Fig. S3B		males	Mann-Whitney test two-tailed	*+/+ vs R185H/+*	p=0.7148
			Unpaired t-test two-tailed	*+/+ vs R185H/R185H*	p=0.1279
Fig. S3B	6-mo	females	Unpaired t-test two-tailed	*+/+ vs R185H/+*	p=0.5033
				+/+ vs R185H/R185H	p=0.5392
Fig. S3B		males	Unpaired t-test two-tailed	*+/+ vs R185H/+*	p=0.6041
				+/+ vs R185H/R185H	p=0.6436

Supplementary Table 11 *Scn9a*^{R185H} mice show normal healthy condition at 2- and 6-month-age

Fig. S3C	Odor Habituation and Discrimination 2-mo: females	Repeated measures ANOVA	Genotype	p=0.2070 "F (2, 35) = 1.648"
			Trails	**p<0.0001** **"F (2.976, 104.2) = 77.23"**
Fig. S3C	Trail 1: +/+ vs *R185H/+*	Sidak post-hoc multiple comparation		p=0.7154
	Trail 1: +/+ vs *R185H/R185H*			**p=0.0131**
	Trail 2: +/+ vs *R185H/+*			p=0.8850
	Trail 2: +/+ vs *R185H/R185H*			p>0.9999
	Trail 3: +/+ vs *R185H/+*			p=0.3597
	Trail 3: +/+ vs *R185H/R185H*			p=0.4730
	Trail 4: +/+ vs *R185H/+*			p=0.9259
	Trail 4: +/+ vs *R185H/R185H*			p=0.8362
	Trail 5: +/+ vs *R185H/+*			p=0.6572
	Trail 5: +/+ vs *R185H/R185H*			p=0.9953
	New odor: +/+ vs *R185H/+*			p=0.2735
	New odor: +/+ vs *R185H/R185H*			p=0.9837
	Trail 5 vs New odor: +/+			**p<0.0001**
	Trail 5 vs New odor: *R185H/+*			**p=0.0096**
	Trail 5 vs New odor: *R185H/R185H*			**p=0.0140**
Fig. S3C	Odor Habituation and Discrimination 2-mo: males	Repeated measures ANOVA	Genotype	p=0.6289 "F (2, 36) = 0.4697"
			Trails	**p<0.0001** **"F (3.240, 116.6) = 61.09"**
Fig. S3C	Trail 1: +/+ vs *R185H/+*	Sidak post-hoc multiple comparation		p=0.9873
	Trail 1: +/+ vs *R185H/R185H*			p=0.9930
	Trail 2: +/+ vs *R185H/+*			p=0.9734
	Trail 2: +/+ vs *R185H/R185H*			p=0.9051
	Trail 3: +/+ vs *R185H/+*			p=0.9464
	Trail 3: +/+ vs *R185H/R185H*			p=0.2291
	Trail 4: +/+ vs *R185H/+*			p=0.5973
	Trail 4: +/+ vs *R185H/R185H*			p=0.9198
	Trail 5: +/+ vs *R185H/+*			p=0.9182
	Trail 5: +/+ vs *R185H/R185H*			p=0.9591
	New odor: +/+ vs *R185H/+*			p=0.9973
	New odor: +/+ vs *R185H/R185H*			p=0.7768
	Trail 5 vs New odor: +/+			**p=0.0280**
	Trail 5 vs New odor: *R185H/+*			**p=0.0003**
	Trail 5 vs New odor: *R185H/R185H*			**p=0.0040**

Supplementary Table 11 *Scn9a*^{R185H} mice show normal healthy condition at 2- and 6-month-age

Fig. S3C	Odor Habituation and Discrimination 6-mo: females	Repeated measures ANOVA	**Genotype**	**p=0.0400 "F (2, 29) = 3.603"**
			Trails	**p<0.0001 "F (2.747, 79.67) = 65.96"**
Fig. S3C	Trail 1: +/+ vs *R185H/+*	Sidak post-hoc multiple comparation		p=0.8989
	Trail 1: +/+ vs *R185H/R185H*			p=0.9539
	Trail 2: +/+ vs *R185H/+*			p=0.9920
	Trail 2: +/+ vs *R185H/R185H*			p=0.6778
	Trail 3: +/+ vs *R185H/+*			p=0.3809
	Trail 3: +/+ vs *R185H/R185H*			p=0.9712
	Trail 4: +/+ vs *R185H/+*			p=0.9998
	Trail 4: +/+ vs *R185H/R185H*			p=0.0995
	Trail 5: +/+ vs *R185H/+*			p=0.7415
	Trail 5: +/+ vs *R185H/R185H*			p=0.6066
	New odor: +/+ vs *R185H/+*			p=0.1839
	New odor: +/+ vs *R185H/R185H*			p=0.0874
	Trail 5 vs New odor: +/+			p=0.1323
	Trail 5 vs New odor: *R185H/+*			**p=0.0001**
	Trail 5 vs New odor: *R185H/R185H*			p=0.8077
Fig. S3C	Odor Habituation and Discrimination 6-mo: males	Repeated measures ANOVA	Genotype	p=0.6529 "F (2, 26) = 0.4334"
			Trails	**p<0.0001 "F (2.748, 71.44) = 44.38"**
Fig. S3C	Trail 1: +/+ vs *R185H/+*	Sidak post-hoc multiple comparation		p=0.9658
	Trail 1: +/+ vs *R185H/R185H*			p=0.9580
	Trail 2: +/+ vs *R185H/+*			p=0.9972
	Trail 2: +/+ vs *R185H/R185H*			p=0.9603
	Trail 3: +/+ vs *R185H/+*			p=0.8865
	Trail 3: +/+ vs *R185H/R185H*			p=0.9833
	Trail 4: +/+ vs *R185H/+*			p=0.3628
	Trail 4: +/+ vs *R185H/R185H*			p=0.9227
	Trail 5: +/+ vs *R185H/+*			p=0.6461
	Trail 5: +/+ vs *R185H/R185H*			p=0.6179
	New odor: +/+ vs *R185H/+*			p=0.9396
	New odor: +/+ vs *R185H/R185H*			p=0.9891
	Trail 5 vs New odor: +/+			p=0.1371
	Trail 5 vs New odor: *R185H/+*			**p=0.0005**
	Trail 5 vs New odor: *R185H/R185H*			p=0.1017

Supplementary Table 12 *Scn9a*$^{R185X/wt}$ mice show normal healthy condition at 2- and 6-month-age.

Figure	Test	Analysis	Groups	Statistics
Fig. S4A	Body Weight: females	Repeated measures ANOVA	Genotype	p=0.6169 "F (1, 41) = 0.2541"
			weeks	**p<0.0001** **"F (1.950, 44.55) = 355.9"**
Fig. S4A	Week 1: +/+ vs R185X/+	Sidak post-hoc multiple comparation		p>0.9999
	Week 2: +/+ vs R185X/+			p>0.9999
	Week 3: +/+ vs R185X/+			p=0.8521
	Week 4: +/+ vs R185X/+			p=0.9732
	Week 5: +/+ vs R185X/+			p>0.9999
	Week 6: +/+ vs R185X/+			p=0.9997
	Week 7: +/+ vs R185X/+			p=0.9976
	Week 8: +/+ vs R185X/+			p=0.9531
	Week 9: +/+ vs R185X/+			p>0.9999
	Week 10: +/+ vs R185X/+			p=0.9990
	Week 11: +/+ vs R185X/+			p>0.9999
	Week 12: +/+ vs R185X/+			p=0.9977
	Week 26: +/+ vs R185X/+			p>0.9999
Fig. S4A	Body Weight: males	Repeated measures ANOVA	Genotype	p=0.5129 "F (1, 47) = 0.4348"
			weeks	**p<0.0001** **"F (4.997, 136.8) = 606.2"**
Fig. S4A	Week 1: +/+ vs R185X/+	Sidak post-hoc multiple comparation		p=0.9994
	Week 2: +/+ vs R185X/+			p>0.9999
	Week 3: +/+ vs R185X/+			p>0.9999
	Week 4: +/+ vs R185X/+			p>0.9999
	Week 5: +/+ vs R185X/+			p=0.5450
	Week 6: +/+ vs R185X/+			**p=0.0474**
	Week 7: +/+ vs R185X/+			p=0.8077
	Week 8: +/+ vs R185X/+			**p=0.0261**
	Week 9: +/+ vs R185X/+			p=0.5446
	Week 10: +/+ vs R185X/+			p>0.9999
	Week 11: +/+ vs R185X/+			p=0.9787
	Week 12: +/+ vs R185X/+			p>0.9999
	Week 26: +/+ vs R185X/+			p>0.9999

Supplementary Table 12 *Scn9a*$^{R185X/wt}$ mice show normal healthy condition at 2- and 6-month-age.

Figure	Test		Analysis	Groups	Statistics
Fig. S4B	String test		Three-way ANOVA	Genotype	p=0.0517 "F (1, 84) = 3.894"
				Sex	p=0.0934 "F (1, 84) = 2.879"
				Age	**p=0.0005** **"F (1, 84) = 12.95"**
Fig. S4B	2-mo		Two-way ANOVA	Genotype	p=0.1550 "F (1, 45) = 2.092"
				Sex	p=0.0584 "F (1, 45) = 3.772"
Fig. S4B	6-mo		Two-way ANOVA	Genotype	p=0.1870 "F (1, 39) = 1.804"
				Sex	p=0.5725 "F (1, 39) = 0.3240"
Fig. S4B	2-mo	females	Unpaired t-test two-tailed	*+/+ vs R185X/+*	p=0.4932
Fig. S4B		males	Mann-Whitney test two-tailed	*+/+ vs R185X/+*	p=0.3212
Fig. S4B	6-mo	females	Unpaired t-test two-tailed	*+/+ vs R185X/+*	p=0.3914
Fig. S4B		males	Mann-Whitney test two-tailed	*+/+ vs R185X/+*	p=0.4322
Fig. S4B	Crenellated bar		Three-way ANOVA	Genotype	p=0.8441 "F (1, 90) = 0.03889"
				Sex	**p=0.0416** **"F (1, 90) = 4.275"**
				Age	**p=0.0389** **"F (1, 90) = 4.395"**
Fig. S4B	2-mo		Two-way ANOVA	Genotype	p=0.7314 "F (1, 45) = 0.1193"
				Sex	p=0.1728 "F (1, 45) = 1.919"
Fig. S4B	6-mo		Two-way ANOVA	Genotype	p=0.6175 "F (1, 45) = 0.2529"
				Sex	p=0.1290 "F (1, 45) = 2.391"
Fig. S4B	2-mo	females	Unpaired t-test two-tailed	*+/+ vs R185X/+*	p=0.5155
Fig. S4B		males	Mann-Whitney test two-tailed	*+/+ vs R185X/+*	p=0.6374
Fig. S4B	6-mo	females	Mann-Whitney test two-tailed	*+/+ vs R185X/+*	p=0.4940
Fig. S4B		males	Unpaired t-test two-tailed	*+/+ vs R185X/+*	p=0.7293

Supplementary Table 12 *Scn9a*$^{R185X/wt}$ mice show normal healthy condition at 2- and 6-month-age.

Figure	Test	Analysis	Groups	Statistics
Fig. S2C	Odor Habituation and Discrimination 2-mo: females	Repeated measures ANOVA	Genotype	p=0.8633 "F (1, 22) = 0.02900"
			Trails	**p<0.0001** **"F (1.673, 36.48) = 34.69"**
Fig. S2C	Trail 1: +/+ vs R185X/+	Sidak post-hoc multiple comparation		p=0.9532
	Trail 2: +/+ vs R185X/+			p=0.9931
	Trail 3: +/+ vs R185X/+			p=0.8972
	Trail 4: +/+ vs R185X/+			p=0.9400
	Trail 5: +/+ vs R185X/+			p>0.9999
	New odor: +/+ vs R185X/+			p=0.9713
	Trail 5 vs New odor: +/+			**p=0.0554**
	Trail 5 vs New odor: *R185X/+*			**p=0.0003**
Fig. S2C	Odor Habituation and Discrimination 2-mo: males	Repeated measures ANOVA	Genotype	p=0.7.26 "F (1, 23) = 0.1495"
			Trails	**p<0.0001** **"F (5, 136) = 137.3"**
Fig. S2C	Trail 1: +/+ vs R185X/+	Sidak post-hoc multiple comparation		p=0.9583
	Trail 2: +/+ vs R185X/+			p=0.9974
	Trail 3: +/+ vs R185X/+			p=0.8451
	Trail 4: +/+ vs R185X/+			p>0.9999
	Trail 5: +/+ vs R185X/+			p=0.9988
	New odor: +/+ vs R185X/+			p=0.8183
	Trail 5 vs New odor: +/+			**p<0.0001**
	Trail 5 vs New odor: *R185X/+*			**p<0.0001**
Fig. S2C	Odor Habituation and Discrimination 6-mo: females	Repeated measures ANOVA	Genotype	p=0.7588 "F (1, 132) = 0.09466"
			Trails	**p<0.0001** **"F (5, 132) = 33.66"**
Fig. S2C	Trail 1: +/+ vs R185X/+	Sidak post-hoc multiple comparation		p=0.9789
	Trail 2: +/+ vs R185X/+			p=0.2733
	Trail 3: +/+ vs R185X/+			p=0.5043
	Trail 4: +/+ vs R185X/+			p>0.9999
	Trail 5: +/+ vs R185X/+			p=0.9826
	New odor: +/+ vs R185X/+			p=0.9960
	Trail 5 vs New odor: +/+			**p=0.0121**
	Trail 5 vs New odor: *R185X/+*			**p=0.0002**
Fig. S2C	Odor Habituation and Discrimination 6-mo: males	Repeated measures ANOVA	Genotype	p=0.8173 "F (1, 22) = 0.05468"
			Trails	**p<0.0001** **"F (2.828, 62.23) = 39.43"**
Fig. S2C	Trail 1: +/+ vs R185X/+	Sidak post-hoc multiple comparation		p>0.9999
	Trail 2: +/+ vs R185X/+			p=0.9992
	Trail 3: +/+ vs R185X/+			p=0.7079
	Trail 4: +/+ vs R185X/+			p=0.9987
	Trail 5: +/+ vs R185X/+			p=0.9987
	New odor: +/+ vs R185X/+			p>0.9999
	Trail 5 vs New odor: +/+			**p=0.1100**
	Trail 5 vs New odor: *R185X/+*			**p=0.0754**

Supplementary Table 13 The baseline comparation between sexes to Hot Plate in *Scn9a*^{R185H} and *Scn9a*$^{R185X/wt}$ mice at 2- and 6-month-age.

Figure	Test: Hot Plate jump latency for *Scn9a*^{R185H} +/+ mice		Analysis	Groups	Statistics
Fig. S5A	2-mo	48 ℃	Mann-Whitney test one-tailed	females vs males	equal value
Fig. S5A		52 ℃	Mann-Whitney test one-tailed		p=0.2956
Fig. S5A		56 ℃	Mann-Whitney test one-tailed		p=0.2106
Fig. S5A	6-mo	48 ℃	Mann-Whitney test one-tailed		p=0.0554
Fig. S5A		52 ℃	Mann-Whitney test one-tailed		p=0.3710
Fig. S5A		56 ℃	Unpaired t-test one-tailed		p=0.1888
Figure	Test: Hot Plate coping reaction in *Scn9a*^{R185H} +/+ mice		Analysis		Statistics
Fig. S5B	2-mo	48 ℃	Unpaired t-test two-tailed		p=0.1124
Fig. S5B		52 ℃	Unpaired t-test two-tailed		p=0.7149
Fig. S5B		56 ℃	Mann-Whitney test two-tailed		p=0.2843
Fig. S5B	6-mo	48 ℃	Unpaired t-test two-tailed		p=0.7497
Fig. S5B		52 ℃	Unpaired t-test two-tailed		p=0.1529
Fig. S5B		56 ℃	Unpaired t-test two-tailed		p=0.6937

Supplementary Table 13 The baseline comparation between sexes to Hot Plate in *Scn9a*^{R185H} and *Scn9a*$^{R185X/wt}$ mice at 2- and 6-month-age.

Figure	Test: Hot Plate jump latency in *Scn9a*$^{R185X/wt}$ +/+ mice		Analysis	females vs males	Statistics
Fig. S5C	2-mo	48 ℃	Mann-Whitney test one-tailed		p=0.5000
Fig. S5C		52 ℃	Mann-Whitney test one-tailed		p=0.5000
Fig. S5C		56 ℃	Mann-Whitney test one-tailed		**p=0.0038**
Fig. S5C	6-mo	48 ℃	Mann-Whitney test one-tailed		p=0.3691
Fig. S5C		52 ℃	Mann-Whitney test one-tailed		p=0.4221
Fig. S5C		56 ℃	Unpaired t-test one-tailed		p=0.4909
Figure	Test: Hot Plate coping reactions in *Scn9a*$^{R185X/wt}$ +/+ mice		Analysis		Statistics
Fig. S5D	2-mo	48 ℃	Unpaired t-test two-tailed		**p=0.0352**
Fig. S5D		52 ℃	Unpaired t-test two-tailed		p=0.1656
Fig. S5D		56 ℃	Unpaired t-test two-tailed		p=0.0898
Fig. S5D	6-mo	48 ℃	Unpaired t-test two-tailed		p=0.4876
Fig. S5D		52 ℃	Mann-Whitney test two-tailed		p=0.2643
Fig. S5D		56 ℃	Unpaired t-test two-tailed		**p=0.0082**

Supplementary Table 14 Enhanced and decreased pain sensitivity to Hot Plate in the *Scn9a*^{R185H} and *Scn9a*$^{R185X/wt}$ mice respectively at 6-month-age.

Figure	Test- Hot Plate Jump Latency for *Scn9a*^{R185H} mice		Analysis	Groups	Statistics
Fig. S6A	48 ℃		Two-way ANOVA	Genotype	p=0.1864 "F (2, 71) = 1.720"
				Sex	p=0.3582 "F (1, 71) = 0.8552"
Fig. S6A	52 ℃			Genotype	p=0.1344 "F (2, 71) = 2.065"
				Sex	p=0.6301 "F (1, 71) = 0.2339"
Fig. S6A	56 ℃			Genotype	p=0.9778 "F (2, 70) = 0.02242"
				Sex	p=0.1736 "F (1, 70) = 1.889"
Fig. S6A	females	48 ℃	Mann-Whitney test one-tailed	*+/+ vs R185H/+*	p=0.1488
				+/+ vs R185H/R185H	p=0.1999
Fig. S6A		52 ℃	Mann-Whitney test one-tailed	*+/+ vs R185H/+*	p=0.3187
				+/+ vs R185H/R185H	p=0.0520
Fig. S6A		56 ℃	Mann-Whitney test one-tailed	*+/+ vs R185H/+*	p=0.1708
				+/+ vs R185H/R185H	p=0.1548
Fig. S6A	males	48 ℃	Mann-Whitney test one-tailed	*+/+ vs R185H/+*	p=0.0694
				+/+ vs R185H/R185H	p=0.1724
Fig. S6A		52 ℃	Mann-Whitney test one-tailed	*+/+ vs R185H/+*	p=0.0962
				+/+ vs R185H/R185H	p=0.4665
Fig. S6A		56 ℃	Unpaired t-test one-tailed	*+/+ vs R185H/+*	p=0.2224
				+/+ vs R185H/R185H	p=0.2365

Supplementary Table 14 Enhanced and decreased pain sensitivity to Hot Plate in the *Scn9a*^{R185H} and *Scn9a*$^{R185X/wt}$ mice respectively at 6-month-age.

Figure	Test- Hot Plate Coping Reactions for *Scn9a*^{R185H} mice		Analysis	Groups	Statistics
Fig. S6B	48 ℃		Two-way ANOVA	Genotype	p=0.0681 "F (2, 71) = 2.791"
				Sex	p=0.9502 "F (1, 71) = 0.003925"
Fig. S6B	52 ℃		Two-way ANOVA	Genotype	p=0.3008 "F (2, 71) = 1.222"
				Sex	p=0.8609 "F (1, 71) = 0.03091"
Fig. S6B	56 ℃		Two-way ANOVA	Genotype	p=0.9090 "F (2, 70) = 0.09559"
				Sex	p=0.3322 "F (1, 70) = 0.9535"
Fig. S6B	females	48 ℃	Unpaired t-test two-tailed	*+/+ vs R185H/+*	p=0.3979
				+/+ vs R185H/R185H	p=0.1419
Fig. S6B		52 ℃	Unpaired t-test two-tailed	***+/+ vs R185H/+***	**p=0.0318**
				+/+ vs R185H/R185H	p=0.0687
Fig. S6B		56 ℃	Mann-Whitney test two-tailed	*+/+ vs R185H/+*	p=0.7483
				+/+ vs R185H/R185H	p=0.4061
Fig. S6B	males	48 ℃	Mann-Whitney test two-tailed	*+/+ vs R185H/+*	p=0.5460
				+/+ vs R185H/R185H	**p=0.0045**
Fig. S6B		52 ℃	Unpaired t-test two-tailed	*+/+ vs R185H/+*	p=0.7197
				+/+ vs R185H/R185H	p=0.7874
Fig. S6B		56 ℃	Unpaired t-test two-tailed	*+/+ vs R185H/+*	p=0.9316
				+/+ vs R185H/R185H	p=0.8386

Supplementary Table 14 Enhanced and decreased pain sensitivity to Hot Plate in the *Scn9a*^{R185H} and *Scn9a*$^{R185X/wt}$ mice respectively at 6-month-age.

Figure	Test- Hot Plate Jump Latency for *Scn9a*$^{R185X/wt}$ mice		Analysis	Groups	Statistics
Fig. S6C	48 ℃		Two-way ANOVA	**Genotype**	**p=0.0415 "F (1, 45) = 4.404"**
				Sex	p=0.4312 "F (1, 45) = 0.6310"
Fig. S6C	52 ℃		Two-way ANOVA	**Genotype**	**p=0.0181 "F (1, 45) = 6.015"**
				Sex	p=0.8247 "F (1, 45) = 0.04966"
Fig. S6C	56 ℃		Two-way ANOVA	**Genotype**	**p=0.0434 "F (1, 45) = 4.320"**
				Sex	p=0.3798 "F (1, 45) = 0.7866"
Fig. S6C	females	48 ℃	Mann-Whitney test one-tailed	*+/+ vs R185X/+*	p=0.0671
Fig. S6C		52 ℃	Mann-Whitney test one-tailed	*+/+ vs R185X/+*	p=0.0980
Fig. S6C		56 ℃	Mann-Whitney test one-tailed	***+/+ vs R185X/+***	**p=0.0225**
Fig. S6C	males	48 ℃	Mann-Whitney test one-tailed	*+/+ vs R185X/+*	p=0.0758
Fig. S6C		52 ℃	Mann-Whitney test one-tailed	*+/+ vs R185X/+*	p=0.0657
Fig. S6C		56 ℃	Unpaired t-test one-tailed	*+/+ vs R185X/+*	p=0.2191

Supplementary Table 14 Enhanced and decreased pain sensitivity to Hot Plate in the *Scn9a*^{R185H} and *Scn9a*$^{R185X/wt}$ mice respectively at 6-month-age.

Figure	Test- Hot Plate Coping Reactions for *Scn9a*$^{R185X/wt}$ mice		Analysis	Groups	Statistics
Fig. S6D	48 ℃		Two-way ANOVA	Genotype	p=0.1202 "F (1, 45) = 2.509"
				Sex	p=0.1910 "F (1, 45) = 1.763"
Fig. S6D	52 ℃		Two-way ANOVA	Genotype	p=0.1757 "F (1, 45) = 1.893"
				Sex	p=0.4298 "F (1, 45) = 0.6348"
Fig. S6D	56 ℃		Two-way ANOVA	**Genotype**	**p=0.0050** **"F (1, 45) = 8.720"**
				Sex	p=0.1042 "F (1, 45) = 2.751"
Fig. S6D	females	48 ℃	Unpaired t-test two-tailed	***+/+ vs R185X/+***	**p=0.0467**
Fig. S6D		52 ℃	Unpaired t-test two-tailed	*+/+ vs R185X/+*	p=0.2504
Fig. S6D		56 ℃	Unpaired t-test two-tailed	***+/+ vs R185X/+***	**p=0.0014**
Fig. S6D	males	48 ℃	Unpaired t-test two-tailed	*+/+ vs R185X/+*	p=0.8890
Fig. S6D		52 ℃	Mann-Whitney test two-tailed	*+/+ vs R185X/+*	p=0.9464
Fig. S6D		56 ℃	Unpaired t-test two-tailed	*+/+ vs R185X/+*	p=0.5360

Supplementary Table 15 Sensitivity to heat, cool and mechanical stimuli and decreased pain sensitivity to cold stimuli in the *Scn9a*^{R185H} mice at 6-month-age.

Figure	Test	Analysis	Groups	Statistics
Fig. S7A	Tail Flick	Two-way ANOVA	Genotype	p=0.1819 "F (2, 71) = 1.206"
			Sex	**p=0.0017** **"F (1, 71) = 10.67"**
Fig. S7A	females	Unpaired t-test two-tailed	*+/+ vs R185H/+*	p=0.1851
			+/+ vs R185H/R185H	p=0.5356
Fig. S7A	males	Unpaired t-test two-tailed	*+/+ vs R185H/+*	p=0.3457
			+/+ vs R185H/R185H	p=1388
Fig. S7B	Hargreaves Plantar	Two-way ANOVA	Genotype	p=0.5457 "F (2, 74) = 0.6107"
			Sex	p=0.6673 "F (1, 74) = 0.1863"
Fig. S7B	females	Unpaired t-test two-tailed	*+/+ vs R185H/+*	p=0.3017
			+/+ vs R185H/R185H	p=0.6884
Fig. S7B	males	Unpaired t-test two-tailed	*+/+ vs R185H/+*	p=0.8672
			+/+ vs R185H/R185H	p=0.4553
Fig. S7C	Acetone Flicks and Licks	Two-way ANOVA	Genotype	p=0.3364 "F (2, 71) = 1.106"
			Sex	**p=0.0156** **"F (1, 71) = 6.141"**
Fig. S7C	females	Unpaired t-test two-tailed	*+/+ vs R185H/+*	p=0.3376
			+/+ vs R185H/R185H	p=0.0917
Fig. S7C	males	Unpaired t-test two-tailed	*+/+ vs R185H/+*	p=0.3681
			+/+ vs R185H/R185H	p=0.9304
Fig. S7D	Cold Plate 5 ℃ Paw Lifts	Two-way ANOVA	Genotype	p=0.1649 "F (2, 71) = 1.849"
			Sex	p=0.2158 "F (1, 71) = 1.560"
Fig. S7D	females	Mann-Whitney test two-tailed	*+/+ vs R185H/+*	p=0.9347
			+/+ vs R185H/R185H	p=0.2984
Fig. S7D	males	Mann-Whitney test two-tailed	*+/+ vs R185H/+*	p=0.2331
			+/+ vs R185H/R185H	p=0.5328
Fig. S7E	Von Frey	Two-way ANOVA	Genotype	p=0.6257 "F (2, 71) = 0.4720"
			Sex	**p=0.0051** **"F (1, 71) = 8.339"**
Fig. S7E	females	Unpaired t-test two-tailed	*+/+ vs R185H/+*	p=0.4803
			+/+ vs R185H/R185H	p=0.2294
Fig. S7E	males	Unpaired t-test two-tailed	*+/+ vs R185H/+*	p=0.4803
			+/+ vs R185H/R185H	p=0.2294
Fig. S7F	Tail Pressure	Two-way ANOVA	Genotype	p=0.3309 "F (2, 71) = 1.123"
			Sex	p=0.6145 "F (1, 71) = 0.2560"
Fig. S7F	females	Unpaired t-test two-tailed	*+/+ vs R185H/+*	p=0.7737
			+/+ vs R185H/R185H	p=0.6721
Fig. S7F	males	Unpaired t-test two-tailed	*+/+ vs R185H/+*	p=0.4034
			+/+ vs R185H/R185H	p=0.3147

Supplementary Table 16 No pain sensitivity alteration to heat, cool and mechanical stimuli in the *Scn9a*$^{R185X/wt}$ mice at 2- and 6-month-age.

Figure	Test		Analysis	Groups	Statistics
Fig. S8A	Tail Flick		Three-way ANOVA	Genotype	p=0.7370 "F (1, 90) = 0.1135"
				Sex	**p=0.0119** **"F (1, 90) = 6.586"**
				Age	p=0.7768 "F (1, 90) = 0.08087"
Fig. S8A	Tail Flick 2-mo		Two-way ANOVA	Genotype	p=0.8771 "F (1, 45) = 0.02414"
				Sex	p=0.8149 "F (1, 45) = 0.05544"
Fig. S8A	Tail Flick 6-mo			Genotype	p=0.5566 "F (1, 45) = 0.3508"
				Sex	**p=0.0007** **"F (1, 45) = 13.40"**
Fig. S8A	2-mo	females	Unpaired t-test two-tailed	*+/+ vs R185X/+*	p=0.7903
Fig. S8A		males	Unpaired t-test two-tailed	*+/+ vs R185X/+*	p=0.6382
Fig. S8A	6-mo	females	Unpaired t-test two-tailed	*+/+ vs R185X/+*	p=0.7486
Fig. S8A		males	Unpaired t-test two-tailed	*+/+ vs R185X/+*	p=0.3043
Fig. S8B	Hargreaves Plantar		Three-way ANOVA	Genotype	P=0.5889 "F (1, 90) = 0.2941"
				Sex	P=0.8633 "F (1, 90) = 0.02983"
				Age	P=0.1533 "F (1, 90) = 2.074"
Fig. S8B	Hargreaves Plantar 2-mo		Two-way ANOVA	Genotype	p=0.5699 "F (1, 45) = 0.3276"
				Sex	p=0.5629 "F (1, 45) = 0.3397"
Fig. S8B	Hargreaves Plantar 6-mo			Genotype	p=0.8377 "F (1, 45) = 0.04247"
				Sex	p=0.4363 "F (1, 45) = 0.6170"
Fig. S8B	2-mo	females	Unpaired t-test two-tailed	*+/+ vs R185X/+*	p=0.2277
Fig. S8B		males	Unpaired t-test two-tailed	*+/+ vs R185X/+*	p=0.7294
Fig. S8B	6-mo	females	Mann-Whitney test two-tailed	*+/+ vs R185X/+*	p=0.8163
Fig. S8B		males	Unpaired t-test two-tailed	*+/+ vs R185X/+*	p=0.9164

Supplementary Table 16 No pain sensitivity alteration to heat, cool and mechanical stimuli in the *Scn9a*$^{R185X/wt}$ mice at 2- and 6-month-age.

Figure	Test		Analysis	Groups	Statistics
Fig. S8C	Acetone Flicks and Licks		Three-way ANOVA	Genotype	p=0.2092 "F (1, 90) = 1.600"
				Sex	**p=0.0391** **"F (1, 90) = 4.385"**
				Age	p=0.2459 "F (1, 90) = 1.364"
Fig. S8C	Acetone Flicks and Licks 2-mo		Two-way ANOVA	Genotype	p=0.6747 "F (1, 45) = 0.1784"
				Sex	**p=0.0070** **"F (1, 45) = 7.985"**
Fig. S8C	Acetone Flicks and Licks 6-mo		Two-way ANOVA	Genotype	p=0.2001 "F (1, 45) = 1.691"
				Sex	p=0.7288 "F (1, 45) = 0.1217"
Fig. S8C	2-mo	females	Unpaired t test two-tailed	*+/+ vs R185X/+*	p=0.2940
Fig. S8C		males	Unpaired t test two-tailed	*+/+ vs R185X/+*	p=0.6807
Fig. S8C	6-mo	females	Unpaired t test two-tailed	*+/+ vs R185X/+*	p=0.2578
Fig. S8C		males	Unpaired t test two-tailed	*+/+ vs R185X/+*	p=0.3680
Fig. S8D	Cold Plate 5 ℃ Paw Lifts		Three-way ANOVA	Genotype	p=0.5800 "F (1, 90) = 0.3085"
				Sex	p=0.6843 "F (1, 90) = 0.1664"
				Age	p=0.6702 "F (1, 90) = 0.1826"
Fig. S8D	Cold Plate 5 ℃ Paw Lifts 2-mo		Two-way ANOVA	Genotype	p=0.4591 "F (1, 45) = 0.5575"
				Sex	p=0.9059 "F (1, 45) = 0.01414"
Fig. S8D	Cold Plate 5 ℃ Paw Lifts 6-mo		Two-way ANOVA	Genotype	p=0.0983 "F (1, 45) = 2.850"
				Sex	p=0.4559 "F (1, 45) = 0.5657"
Fig. S8D	2-mo	females	Mann-Whitney test two-tailed	*+/+ vs R185X/+*	p=0.7370
Fig. S8D		males	Mann-Whitney test two-tailed	*+/+ vs R185X/+*	p=0.9007
Fig. S8D	6-mo	females	Mann-Whitney test two-tailed	*+/+ vs R185X/+*	p=0.3766
Fig. S8D		males	Mann-Whitney test two-tailed	*+/+ vs R185X/+*	p=0.2676

Supplementary Table 16 No pain sensitivity alteration to heat, cool and mechanical stimuli in the *Scn9a*$^{R185X/Wt}$ mice at 2- and 6-month-age.

Figure	Test		Analysis	Groups	Statistics
Fig. S8E	Von Frey		Three-way ANOVA	Genotype	p=0.6858 "F (1, 89) = 0.1648"
				Sex	p=0.9478 "F (1, 89) = 0.004306"
				Age	**p<0.0001** **"F (1, 89) = 16.79"**
Fig. S8E	Von Frey 2-mo		Two-way ANOVA	Genotype	p=0.2827 "F (1, 44) = 1.183"
				Sex	p=0.7772 "F (1, 44) = 0.08106"
Fig. S8E	Von Frey 6-mo		Two-way ANOVA	Genotype	p=0.6831 "F (1, 45) = 0.1688"
				Sex	p=0.7383 "F (1, 45) = 0.1130"
Fig. S8E	2-mo	females	Unpaired t-test two-tailed	*+/+ vs R185X/+*	p=0.3042
Fig. S8E		males	Unpaired t-test two-tailed	*+/+ vs R185X/+*	p=0.3557
Fig. S8E	6-mo	females	Unpaired t-test two-tailed	*+/+ vs R185X/+*	p=0.9123
Fig. S8E		males	Unpaired t-test two-tailed	*+/+ vs R185X/+*	p=0.5721
Fig. S8F	Tail Pressure		Three-way ANOVA	Genotype	p=0.5600 "F (1, 90) = 0.3422"
				Sex	**p=0.0216** **"F (1, 90) = 5.470"**
				Age	**p<0.0001** **"F (1, 90) = 42.71"**
Fig. 8F	Tail Pressure 2-mo		Two-way ANOVA	Genotype	p=0.8568 "F (1, 45) = 0.03294"
				Sex	**p=0.0138** **"F (1, 45) = 6.562"**
Fig. 8F	Tail Pressure 6-mo		Two-way ANOVA	Genotype	p=0.3914 "F (1, 45) = 0.7491"
				Sex	p=0.3196 "F (1, 45) = 1.013"
Fig. 8F	2-mo	females	Unpaired t-test two-tailed	*+/+ vs R185X/+*	p=0.1645
Fig. 8F		males	Mann-Whitney test two-tailed	*+/+ vs R185X/+*	p=0.6475
Fig. 8F	6-mo	females	Mann-Whitney test two-tailed	*+/+ vs R185X/+*	p=0.4331
Fig. 8F		males	Unpaired t-test two-tailed	*+/+ vs R185X/+*	p=0.5973

2. Generation of CRISPR-Cas9 *Scn9a*^{R185H} and *Scn9a*$^{R185X/wt}$ Mice

2.1 Successful Segmental Inversion, Deletion and Point Mutation of Mouse *Scn9a* by CRISPR-Cas9 in F0 Founders

In order to generate the p.Arg185His Scn9a mutation in mice with the CRISPR/Cas9 technology, we designed single guide RNA (sgRNA) and single stranded oligonucleotides (ssODN) as shown in Figure 1.

After checking sgRNA validity in vitro, different concentrations of sgRNA, Cas9 and ssODN were microinjected into fertilized eggs. 3 weeks after microinjection, sixty F0 founders were born and screened by PCR and gel analysis for the whole variety of potential alleles, which were confirmed by Sanger sequencing (Figure 2.1A-B and Supplementary Figure 1, only before 58# founders show sequencing results). Interestingly, we detected that higher concentrations generated more point mutation pups but do not affect indel (Table 2.1). Three F0 founders showed point mutation on two alleles, including 24#, 31#, and 53# (Figure 2.1A-B). However, one wide type gel band but not sequencing, was found in F0-31# founder. Thus, we selected F0-24# and F0-53# founders as potential *Scn9a*^{R185H} lines. Other F0 founders were one allele with a point mutation, like 27#, 28#, 41#, 45#, 55#, and 57#, but they had insertion or/and deletion in another allele. Thus, these founders were not an excellent choice to establish *Scn9a*^{R185H} lines. Several F0 founders had a high mosaic in two alleles. For example, F0-36# (Figure 2.1C) has three different gene editing evens, including 2nt deletion, 1nt deletion, and 7nt insertion. Furthermore, the 2nt deletion could result in frameshifting and change NAV1.7 protein transcription. Nevertheless, for other high mosaic F0 founders (42#, 43#, 46#, 51#, 52#), we did not find some interesting insertion or deletion. However, we found that 1nt insertion of F0-27# and 2nt insertion of F0-44# also could result in frameshifting and get a small NAV1.7 protein. Thus, F0-36#, F0-27#, and F0-44# were potential *Scn9a*$^{R185X/wt}$ lines. In summary, five potential F0 founders were used to cross with C57bl/6NCr wild type mouse and generate F1 founders to establish *Scn9a*^{R185H} and *Scn9a*$^{R185X/wt}$ lines

2.2 Screening for Establishing *Scn9a*^{R185H} and *Scn9a*$^{R185X/wt}$ Lines from F1 Founders

Five potential F0 founders (24#, 27#, 36#, 44#, and 53#) were selected and bred with wt C57BL/6NCr mice. After 3-4 weeks, we obtained F1 founders (24# did not generate offspring after two months). To analyze the F1 founders' genotype, we harvested the tail biopsy and collected crude genomic DNA by lysate. BspHI was used to digest for point mutation genotype, and T7

endonuclease to test indel events, including insertion or/and deletion. In Figure 2.2A, for BspHI digestion, the F0-44# (44#-19 to 44#-28 do not show) and F0-53# (53#-6 to 53#19 do not show) produced 19 animals respectively, which are heterozygous point mutation as the *Scn9a* DNA sequence can be digested to three bands (562 bases for wt, the other two bands 268bp and 294bpfor point mutations) by BspHI. Although the TG insertion in F0-44# founder did not accomplish germline transmission (Figure 2.2B and Table 2.2), fortunately, we got the 100% heterozygous point mutation from F0-53# founders. From offspring of F0-27# including point mutation and insertion, we got two genotypes-heterozygous point mutation (genotype F) and 1nt (G) deletion, and 8nt (TTTCTTA, genotype E). Genotype E could result in frameshifting, leading to *Scn9a* translational stop and NAV1.7 protein expression quantity reduced (Figure 2.2B and Table 2.2). Moreover, as F0-36# founder is high mosaic, it generated four different genotypes. Genotype A and D could influence frameshifting and result in *Scn9a* translational stop from exon5, but genotype A without point mutation and silence mutation (Figure 2.2B and Table 2.2). Genotypes B and C (3nt GTG insertion) had point mutation, which will generate frameshifting but not leading to translational stop (Figure 2.2B and Table 2.2). In summary, we obtained five genotypes from 4 F0 founders. We select genotype A offspring of F0-36# founder and genotype E of F0-27# founder to create *the* $Scn9a^{R185X/wt}$ line and genotype F from F0-44# and F0-53# founders used to create the $Scn9a^{R185H}$ line.

2.3 Germline Transmission: Establishing $Scn9a^{R185H}$ and $Scn9a^{R185X/wt}$ Lines

In this project, all F0 founders with all mutation types (indels, point mutations, or deletions) should consider mosaic because we only analyze on-target loci of founder tail biopsy, and the possibility of additional undetected alleles in these animals can dismiss. These alleles may be present in another part of the body, such as the germline, but poorly represented in the tail clip and potentially resulting in the transmission of novel alleles not previously characterized at the screening step. We found that two base TG insertion is in the F0-44# founder, but not in its F1 pups. Therefore, allele characterization analyzing in the tail biopsies might be absent or poorly represented in these F0 animals' germline, potentially leading to the non-transmission of alleles characterized at the screening step. Thus, in our project, we selected two animals with a homozygous point mutation, two animals with point mutation and insertion and/or deletion, and one animal with high mosaic. From F1 offspring generating of five potential F0 founders, according to Sanger sequence results, we selected ideal animals to breed with a wild type mouse. After, the heterozygous offspring of F1 founders had crossed each other to generate different genotypes for further experiments. 36-11# from F0-36# founder and 53-11# from F0-53# founder had generated different

genotypes for further experiments, respectively. F1 founders from 27# and 44# as stock for *Scn9a*^{R185H} and *Scn9a*$^{R185X/wt}$ mouse lines have been done by sperm frozen.

2.4 Genotype ratio

We analyzed the genotype ratio in our two mutant mouse lines after several generations. We found that these two mouse lines have typical genotype ratios (Table 2.3 and Table 2.4). A global Nav 1.7-null mutant was reported to die shortly after birth [129]. Similarly, for *the Scn9a*$^{R185X/wt}$ line, we did not obtain homozygous survival mice.

Figures

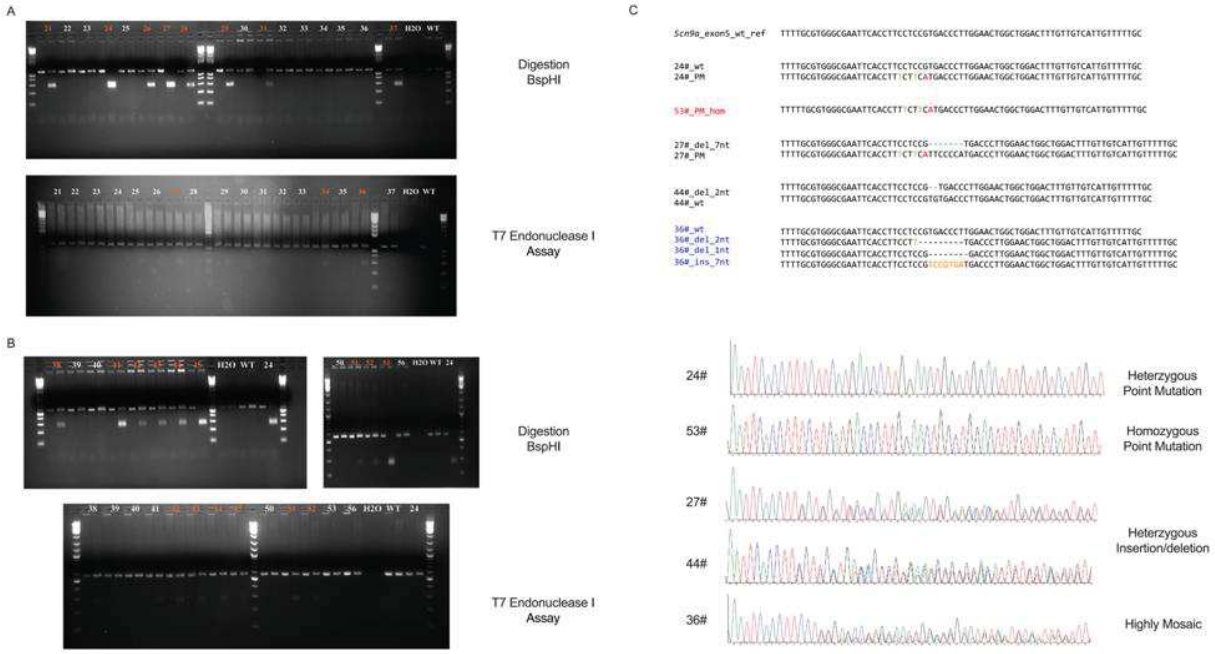

Figure 2.1 Analysis of F0 founders' genotype. A) and **B)** Gel electrophoresis analysis of PCR amplification of Scn9a target using Digestion and T7EI endonuclease assay in F0 founders. **C)** Five potential allele sequences characterized through Sanger sequencing. 24# is heterozygous with ideal point mutation and 53# is homozygous with ideal point mutation. 27# and 44# are heterozygous with several bases insertion or deletion, which resulting in reading frame shift and leading to translational stop of NAV1.7 protein and ideal point mutation.

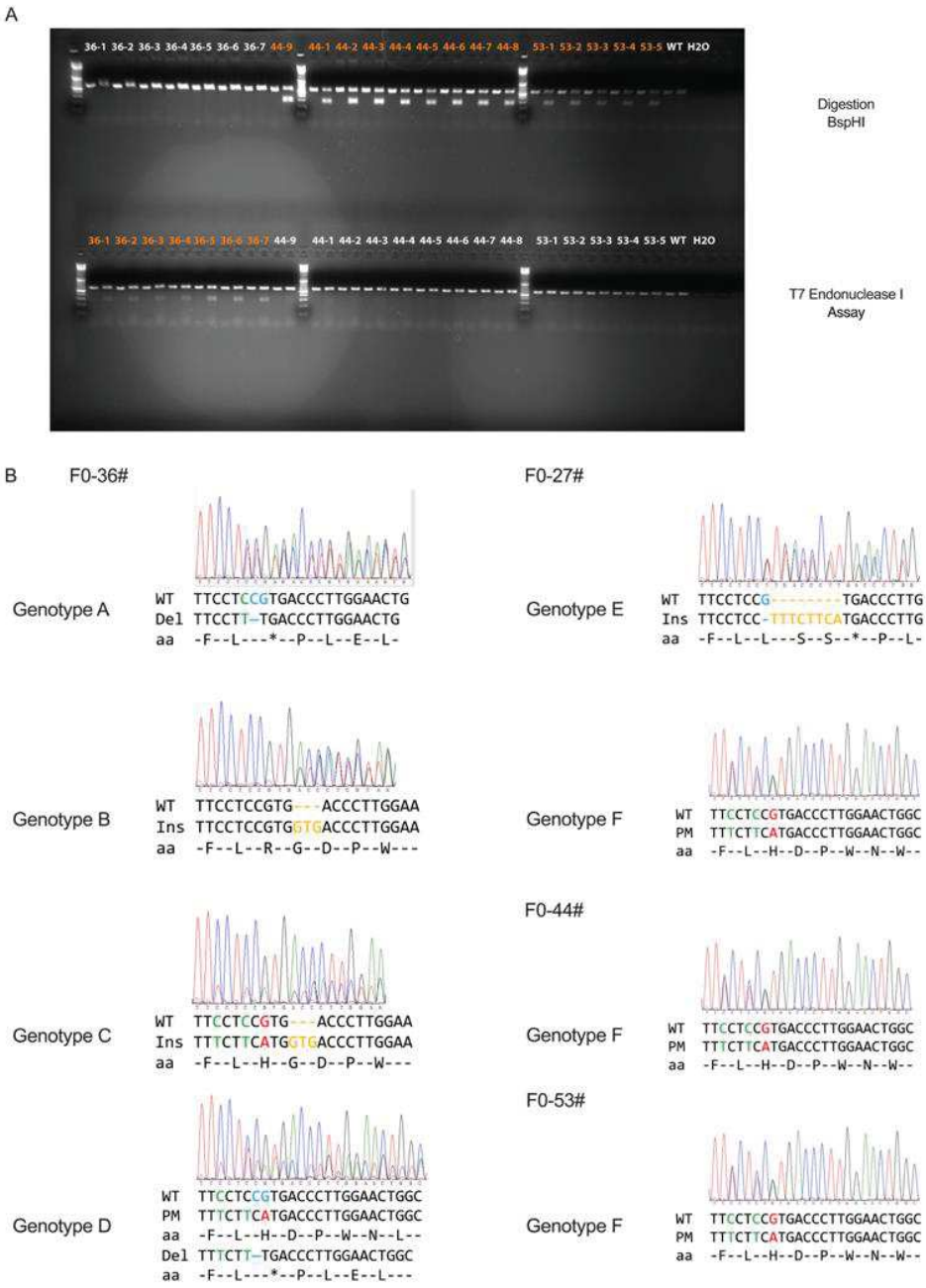

Figure 2.2 Analysis of F1 founders' genotype. A) Gel electrophoresis analysis of PCR amplification of Scn9a target using Digestion and T7EI endonuclease assay. **B)** Allele sequences from different F1 founders characterized through Sanger sequencing. F0-36# founder generated four genotypes, including insertion and deletion; Reading frame shift of Genotype A and D will result in transcription stopping; F0-27 founder generated two genotypes, which are point mutation and 1 base deletion and 8 bases insertion leading to transcription stop; F0-44# and F0-53# produced heterozygous point mutation genotype.

Table 2.1 Summary of effect on CRISPR-Cas9 editing within different concentration of sgRNA, Cas9 protein and ssODN

Concentration DNA/RNA ng/µl	Nb of oocysts implanted	Nb Pups born	PM detected	Indel detected
Cas9 50ng/µl + 25ng/µl sgRNA86 +10 ng/µl ssODN	332	36	20 (55.6%)	3 (8.3%)
Cas9 25ng/µl + 15ng/µl sgRNA86 +10 ng/µl ssODN	198	24	9 (37.5%)	2 (8.3%)

Table 2.2 Summary of F1 founder genotypes.

F0 Founder	Nb Pups born	PM detected	PM Pups ID	Indel detected	Indel Pups No.	Genotype
27#	23	13 (57%)	1 to 5; 7 to 9; 12; 13; 17; 21; 23	10 (43%)	6; 10; 11; 14 to 16; 18 to 20; 22	E, F
36#	19	0	None	38 (100%)	2; 5; 9; 10; 14; 22; 26; 28; 32; 34; 35; 38	A
					1; 3; 4; 6; 7; 12; 13; 15; 17 to 19; 20; 21; 23 to 25; 27; 29 to 31; 33; 36; 37	B
					11; 16	C
					8	D
44#	19	19 (100%)	1 to 9; 19 to 28	0	None	F
53#	19	19 (100%)	1 to 19	0	None	F
Total	80	51 (64%)		29 (46%)	Germ Line Transmission Achieved	

Table 2.3 Genotype Ratio of *Scn9a*^{R185H} mouse line

Type of bred	R185H/wt X wt			R185H/wt X R185H/wt		
Genotype	wt	R185H/wt	R185H/R185H	wt	R185H/wt	R185H/R185H
Females (51.0%)	101	96	0	46	106	46
Males (49.0%)	105	85	0	48	90	52
% in total	53.2%	46.8%	0%	24.2%	50.5%	25.3%

Table 2.4 Genotype Ratio of *Scn9a*$^{R185X/wt}$ mouse line

Type of bred	R185X/wt X wt			R185X/wt X R185X/wt		
Genotype	wt	R185X/wt	R185X/R185X	wt	R185X/wt	R185X/R185X
Females (47.9%)	41	55	0	56	101	0
Males (52.1%)	65	46	0	41	123	0
% in total	51.2%	48.8%	0	30.2%	69.8%	0

Supplementary Figures

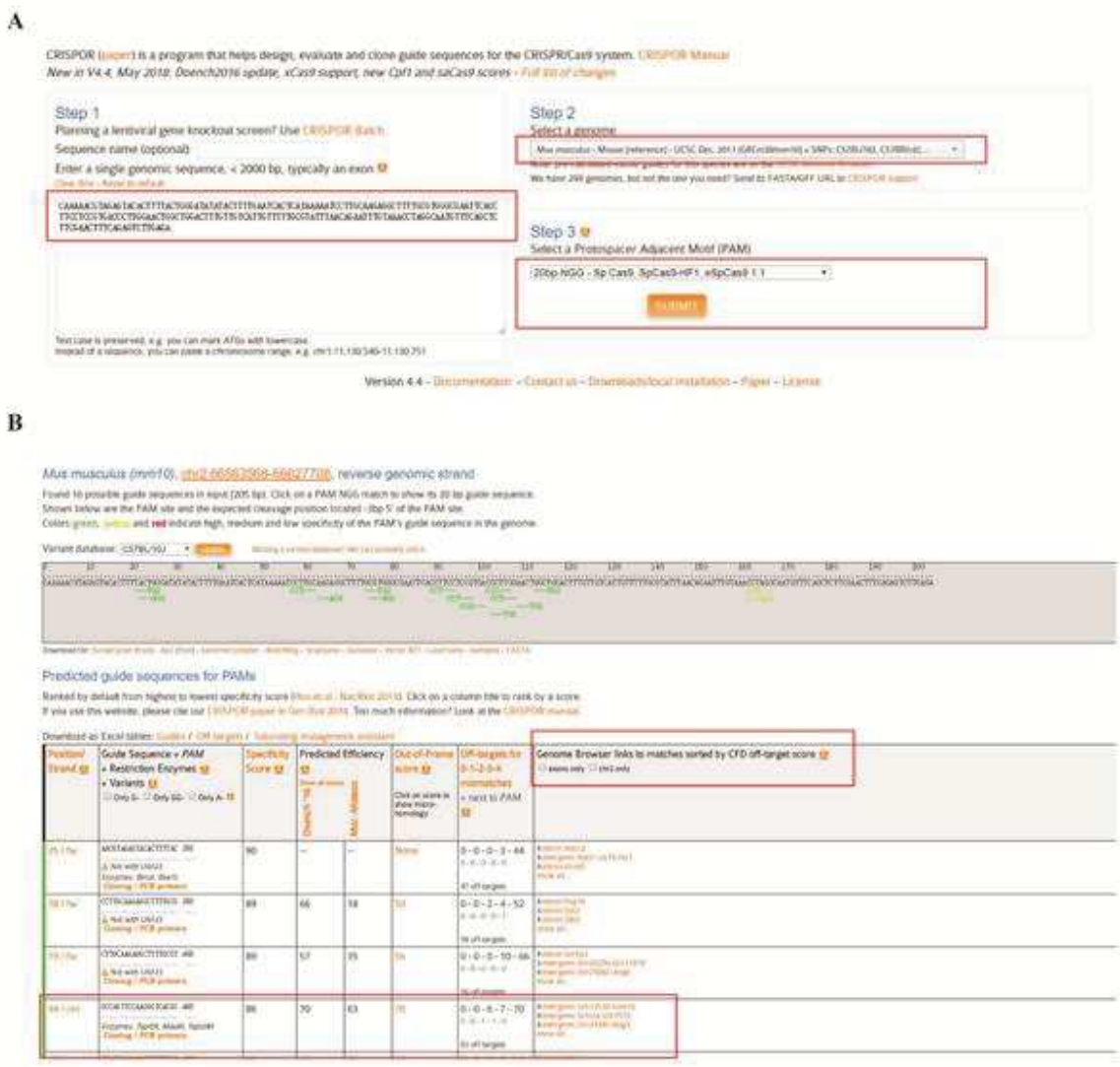

Supplementary Figure 2.1 sgRNA design protocol. A) Targeted exon (*Scn9a* sequence from Ensembl database) and the species genome and PAM were submitted into the CRISPOR software. **B)** We selected high specificity score sgRNA with low number of off targets to use.

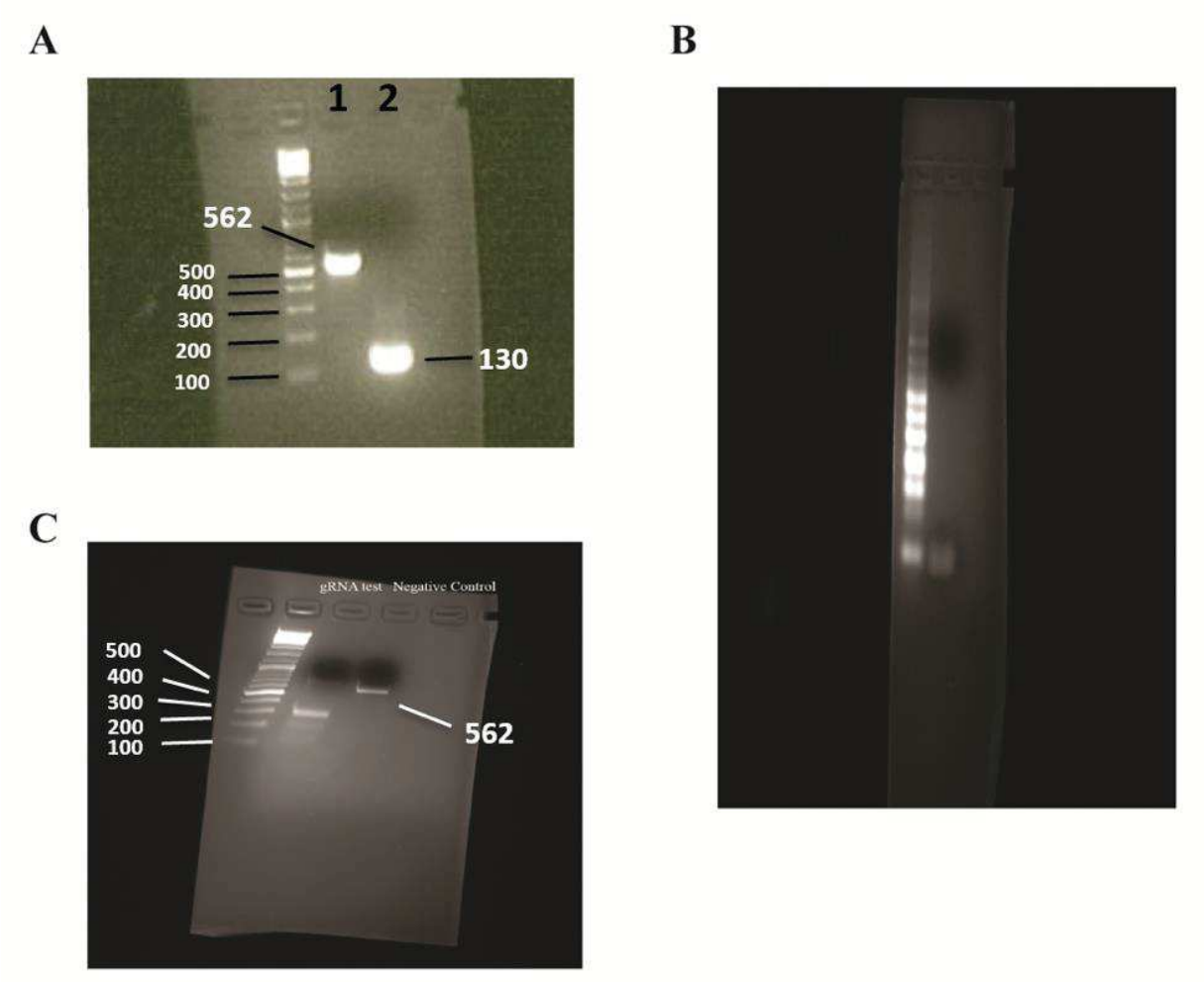

Supplementary Figure 2.2 sgRNA transcription and validity in vitro. A) No.1 band in gel is targeting DNA loci amplification production and No.2 band in gel is the synthesis sgDNA by PCR amplification. **B)** The production of sgRNA is synthesized from sgDNA.

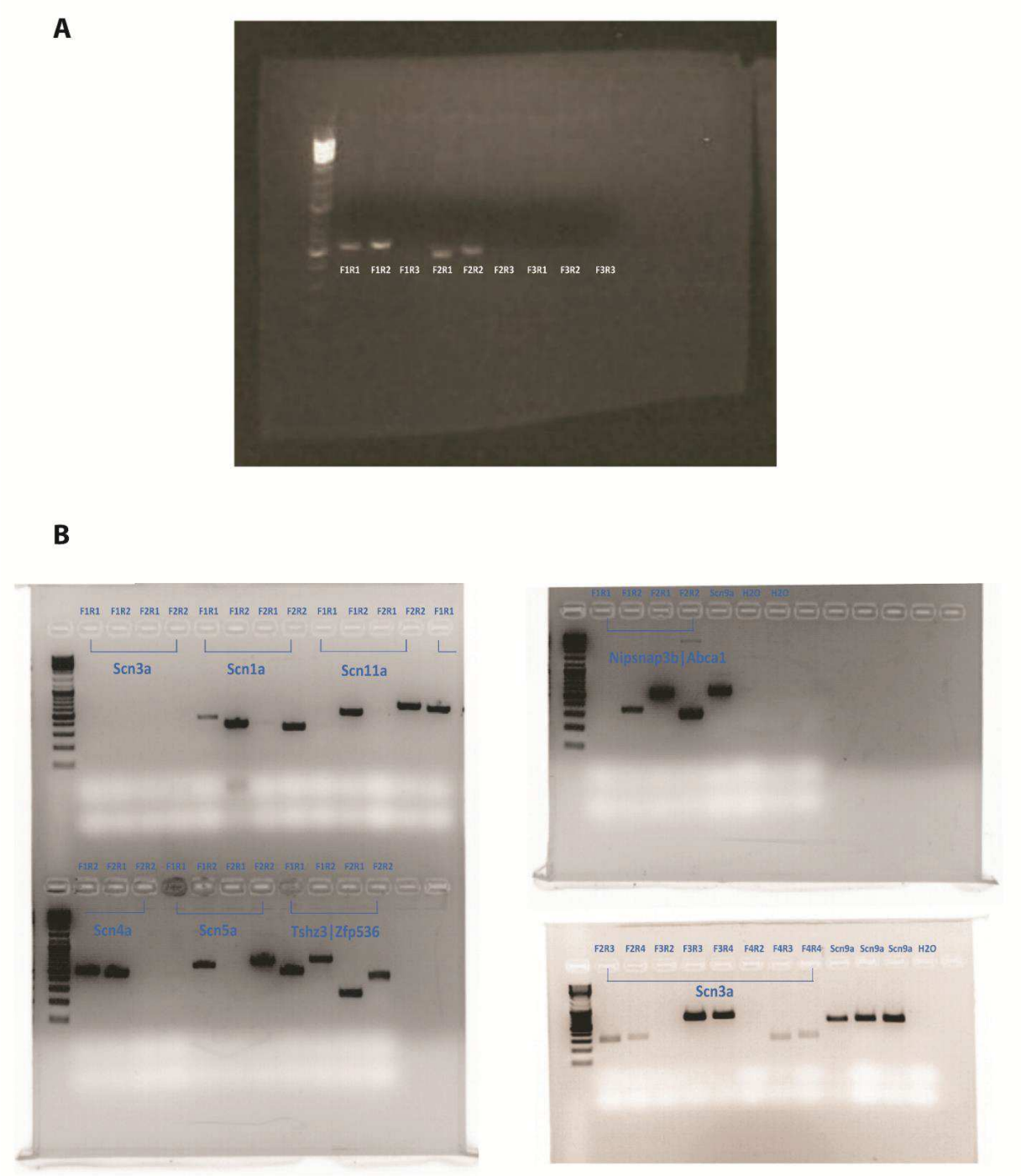

Supplementary Figure 2.3 On and off target primers optimization. **A)** PCR amplification results on *Scn9a* using different primer pairs. **B)** PCR amplification results on off targets using different primer pairs.

3. Characterization of *Scn9a*^{R185H} Mice

3.1 SCN9A protein expression in DRG and sciatic nerves of *Scn9a*^{R185H} Mice

Specific staining of the SCN9A antibody in DRG and sciatic nerves was used to analyze the impact of Scn9a-R185H mutation on SCN9A protein expression in peripheral DRG and sciatic nerves via immunofluorescence. PGP9.5 was used for staining all sensory neurons in DRG and nerve fibers in sciatic nerves. The mice with mutations had normal SCN9A protein expression levels in DRG with different size distribution (Figure 3.1 A). The cellular profile of SCN9A protein expression in controls and mutant DRGs and found it to be present 75-85% of sensory neurons across the full range of soma diameters and mostly expressed in small and medium neurons. Surprisingly, we found no difference in the SCN9A antibody staining of DRG cells between +/+ and mutant mice (Figure 3.1 B). The mean of fluorescence density (total fluorescence density/area) was analyzed for sciatic nerve staining. In statistic results by two-way ANOVA, there is no difference in genotype effect, but we found a significant difference in sex effect. Multiplied Turkey's test showed no difference between controls and mutant mice. These results indicated that SCN9A protein is typically expressed in mutant DRGs and sciatic nerves and not impacted by Scn9a-R185H mutation.

3.2 Response to Hot Plate in *Scn9a*^{R185H} mice at 2- and 6-month-age

For the Hot Plate assay, except jump latency and coping reactions, first nociceptive response latency and duration of coping reactions were analyzed for *Scn9a*^{R185H} mice. In the three-way ANOVA analysis, no statistically significant effect was found in genotype, sex, and age for the first nociceptive response latency and duration of coping reactions. However, at 6-month age, a significant sex effect was found in 52°C Hot Plate following the two-way ANOVA analysis. As described previously, for first response latency of all temperatures, there was no significant difference detected in female and male mutant mice at 2- and 6-month-age (Figure 3.2 A-B). In female mutant mice, no significant difference was found for the duration of coping reactions at both ages (Figure 3.2 C-D). However, at 6-month-age, the male *R185H/R185H* took more time for coping reaction at 48°C, which is a similar effect on the number of coping reactions. Females showed a similar coping reaction duration because female *R185H/R185H* mice performed more jumps, leading to mice not having enough time to display flick and lick. (More detailed statistical analysis in Table 3.3)

3.3 Response to Acetone and Cold plate in *Scn9a*^{R185H} mice at 2- and 6-month-age

To assess abnormal cold sensation in mutant mice, the acetone test - a behavioral test of cold allodynia - was evaluated. Duration of flick and lick was analyzed when applied acetone to the hind paw of mice. Three-way ANOVA did not detect a significant effect on genotype, sex, and age for this parameter. Also, genotype and age effect on different age did not show significance by two-way ANOVA. At 2- and 6- month-age, although there was a trend toward a higher response to acetone application in the female mutant mice compared to wt, this was not significant (Figure 3.3A). The male *R185H/R185H* mice showed more flick and lick duration at 2-month-age, but not found at 6-month-age (Figure 3.3A).

Cold Plate applied the cold noxious stimuli with two temperatures, 0 and 5°C. The latency, number, and duration of paw lift as different parameters evaluated in *Scn9a*^{R185H} mice. Three-way ANOVA showed age effect on paw lifts' duration in 5°C Cold Plate and genotype effect on the number of paw lifts and paw lift duration. However, the genotype effect disappeared at 2- and -6-month-age by two-way ANOVA. The number of paw lifts on 0°C Cold Plate at two age of both female and male mutant mice (Figure 3.3D) showed similar results with 5°C Cold Plate (Figure 3D and Supplementary Figure 7D). Although they showed decreasing tendency for male mutant mice at 6-month-age on 0 and 5 °C Cold Plate (Figure 3.3D and Supplementary Figure 7D), no significant difference was detected. For the latency, in female mutant mice at 2-month-age, an increasing trend was observed at two temperatures (Figure 3.3B and E), but only statistically significant at 0°C Cold Plate (Figure 3.3E). A similar tendency showed in female mutant mice at 6-month-age at 0°C Cold Plate, but there was no significant difference (Figure 3.3E). Male mutant mice only detected an increasing latency tendency at 6-month-age, but there was no significance (Figure 3.3B). Less duration was observed for paw lift in the female mice at both ages at 0 °C Cold Plate without statistical significance, but a similar value showing at 5 °C Cold Plate (Figure 3.3C). In contrast, male mutant mice showed paw lift time at 5 °C Cold Plate with no statistical significance, but less time at 0 °C Cold Plate (Figure 3.3F). (More detailed statistical analysis in Table 3.2)

Taken together, although some mutant mice showed abnormal sensitivity to noxious cold stimuli, but do not display cold allodynia.

3.4 Correlation analyses of mouse age and behavioral phenotypes of hot plate, tail flick, von Frey, tail pressure in female *Scn9a*^{R185H} mice

As shown in the paper manuscript, the 6-mon mutant mice exhibited lower pain phenotype, especially in females; we investigated whether this pheromone was affected by age in different genotypes. There was no significant correlation between mouse age and jump latency at 48 °C hot plate for all genotypes (Figure 3.4A and Table 3.5). A significant correlation on jump latency at 52 °C was found in +/+ mice (Figure 3.4A and Table 3.5). It might be explaining the loss phenotype at 6-month age in this parameter. Although other significant correlation on other parameters, including jump latency at 56 °C (Figure 3.4A and Table 3.5) and coping reactions 48 °C (Figure 3.4B and Table 3.5) in R185H/+ mice and tail pressure threshold in +/+ mice (Figure 3.5C and Table 3.5), it cannot explain the loss phenotype in 6-mon mice observed in this study. There was no significant correlation between age and behavioral phenotypes in other parameters of different genotype mice (Figure 3.5A-B, 3.5A-B, and Table 3.3).

Figures Legends

Figure 3.1 SCN9A protein expression in DRG and sciatic nerves of *Scn9a*^{R185H} Mice. A) Representative image of fluorescent PGP9.5 (green) and SCN9A (red) expressing neurons in lumbar DRG of +/+ animals. Scale bar 50 µm. **B)** Categorical data plot of the size distribution for SCN9A positive (red) and negative (white) neuron cross-sectional areas in +/+, R185H/+ and R185H/R185H of both female and male mice. (female: n=5/group; male: n=3/group). **C)** Representative image of fluorescent PGP9.5 (green) and SCN9A (red) expressing neurons in sciatic nerve of +/+ animals. Scale bar 25 µm. **D)** Mean of fluorescence density in +/+, R185H/+ and R185H/R185H of both female and male mice. (female: n=4-5/group; male: n=3/group). Data presents as means ± *SEM*. *P < 0.05, ** P < 0.01 and ***P < 0.001, two-way ANOVA and Turkey post-hoc multiple comparation was used to do statistical analysis. (More detailed statistical analysis see Table 3.1 and 3.2)

Figure 3.2 Response to Hot Plate in *Scn9a*^{R185H} mice at 2- and 6-month-age. A) First response latency of 48, 52 and 56°C Hot Plate in female *Scn9a*^{R185H} mice at 2- and 6-month-age. No significant difference was showed in *Scn9a*^{R185H} female mutant mice compared to +/+ mice. (2-mo: +/+ n=16; *R185H/+* n=16; *R185H/R185H* n=15; 6-mo: +/+ n=14; *R185H/+* n=13; *R185H/R185H* n=11). **B)** First response latency to 48, 52 and 56°C Hot Plate in male *Scn9a*^{R185H} mice at 2- and 6-month-age. No significant difference showed in *Scn9a*^{R185H} male mutant mice compared to +/+ mice. (2-mo: +/+ n=13; *R185H/+* n=15; *R185H/R185H* n=11; 6-mo: +/+ n=13; *R185H/+* n=15; *R185H/R185H* n=11). **C)** Duration to coping reaction of 48, 52 and 56°C Hot Plate in *Scn9a*^{R185H} female mice at 2- and 6-month-age. No significant difference showed *Scn9a*^{R185H} female mutant mice compared to +/+ mice. (2-mo: +/+ n=16; *R185H/+* n=16; *R185H/R185H* n=15; 6-mo: +/+ n=14; *R185H/+* n=13; *R185H/R185H* n=11). **D)** Duration to coping reaction of 48, 52 and 56°C Hot Plate in *Scn9a*^{R185H} male mice at 2- and 6-month-age. *R185H/R185H* male mice performed more time on coping reaction at 6-month-age. (2-mo: +/+ n=13; *R185H/+* n=15; *R185H/R185H* n=11; 6-mo: +/+ n=13; *R185H/+* n=15; *R185H/R185H* n=11). Data present as means ± *SEM*. *P < 0.05, ** P < 0.01 and ***P < 0.001, *Scn9a*^{R185H} and *Scn9a*$^{R185X/wt}$ mutants compared to their +/+ littermates by two tailed student t test or Mann-Whitney test. (More detailed statistical analysis see Table 3.3)

Figure 3.3 Response to Acetone and Cold plate in *Scn9a*^{R185H} mice at 2- and 6-month-age. **A)** Duration of flicking and licking after applying acetone in *Scn9a*^{R185H} mice at 2- and 6-month-age. *R185H/R185H* male mice performed more time on flick and lick at 2-month-age. (Female-2-mo: +/+ n=16; *R185H/+* n=15; *R185H/R185H* n=14; Female-6-mo: +/+ n=14; *R185H/+* n=13; *R185H/R185H* n=11; Male-2-mo: +/+ n=15; *R185H/+* n=16; *R185H/R185H* n=13; Male-6-mo: +/+ n=13; *R185H/+* n=15; *R185H/R185H* n=11). **B)** First response latency of 5°C Cold Plate in *Scn9a*^{R185H} mice at 2- and 6-month-age. No significant difference showed in *Scn9a*^{R185H} male mutant mice compared to +/+ mice. (Female-2-mo: +/+ n=16; *R185H/+* n=15; *R185H/R185H* n=14; Female-6-mo: +/+ n=14; *R185H/+* n=13; *R185H/R185H* n=11; Male-2-mo: +/+ n=15; *R185H/+* n=16; *R185H/R185H* n=13; Male-6-mo: +/+ n=13; *R185H/+* n=15; *R185H/R185H* n=11). **C)** Paw lifts duration to 5°C Cold Plate in *Scn9a*^{R185H} mice at 2- and 6-month-age. No significant difference was showed in *Scn9a*^{R185H} male mutant mice compared to +/+ mice. **(**Female-2-mo: +/+ n=16; *R185H/+* n=15; *R185H/R185H* n=14; Female-6-mo: +/+ n=14; *R185H/+* n=13; *R185H/R185H* n=11; Male-2-mo: +/+ n=15; *R185H/+* n=16; *R185H/R185H* n=13; Male-6-mo: +/+ n=13; *R185H/+* n=15; *R185H/R185H* n=11). **D)** Number of paw lift response to 5°C Cold Plate in *Scn9a*^{R185H} mice at 2- and 6-month-age. No significant difference was showed in *Scn9a*^{R185H} male mutant mice compared to +/+ mice (Female-2-mo: +/+ n=16; *R185H/+* n=15; *R185H/R185H* n=14; Female-6-mo: +/+ n=14; *R185H/+* n=13; *R185H/R185H* n=11; Male-2-mo: +/+ n=15; *R185H/+* n=16; *R185H/R185H* n=13; Male-6-mo: +/+ n=13; *R185H/+* n=15; *R185H/R185H* n=11). **E)** First response latency of 0°C Cold Plate in *Scn9a*^{R185H} mice at 2- and 6-month-age. *R185H/R185H* female mice showed increasing latency at 2-month-age. (Female-2-mo: +/+ n=16; *R185H/+* n=15; *R185H/R185H* n=14; Female-6-mo: +/+ n=14; *R185H/+* n=13; *R185H/R185H* n=11; Male-2-mo: +/+ n=15; *R185H/+* n=16; *R185H/R185H* n=13; Male-6-mo: +/+ n=13; *R185H/+* n=15; *R185H/R185H* n=11). **F)** Paw lifts duration of 0°C Cold Plate in *Scn9a*^{R185H} mice at 2- and 6-month-age. No significant difference was showed in *Scn9a*^{R185H} male mutant mice compared to +/+ mice. (Female-2-mo: +/+ n=16; *R185H/+* n=15; *R185H/R185H* n=14; Female-6-mo: +/+ n=14; *R185H/+* n=13; *R185H/R185H* n=11; Male-2-mo: +/+ n=15; *R185H/+* n=16; *R185H/R185H* n=13; Male-6-mo: +/+ n=13; *R185H/+* n=15; *R185H/R185H* n=11). Data present as means ± *SEM*. *P < 0.05, ** P < 0.01 and ***P < 0.001, *Scn9a*^{R185H} and *Scn9a*$^{R185X/wt}$ mutants compared to their +/+ littermates by two tailed student t test or Mann-Whitney test. (More detailed statistical analysis see Table 3.4)

Figure 3.4 Correlation analysis of age (2- and 6- mon) and hot plate behavioral phenotypes in *Scn9a*^{R185H} Mice. **A)** Correlation analyses of age and jump latency on hot plate. **B)** Correlation analyses of age and jump latency on hot plate. Data presents as means ± *SEM*. Spearman correlation analysis was used. (More detailed statistical analysis sees Table 3.5)

Figure 3.5 Correlation analysis of age (2- and 6- mon) and tail flick, von Frey and tail pressure behavioral phenotypes in *Scn9a*^{R185H} Mice. **A)** Correlation analyses of age and withdrawal latency on tail flick. **B)** Correlation analyses of age and threshold on Von Frey. **C)** Correlation analyses of age and threshold on tail pressure. Data presents as means ± *SEM*. Spearman correlation analysis was used. (More detailed statistical analysis sees Table 3.5)

Figures

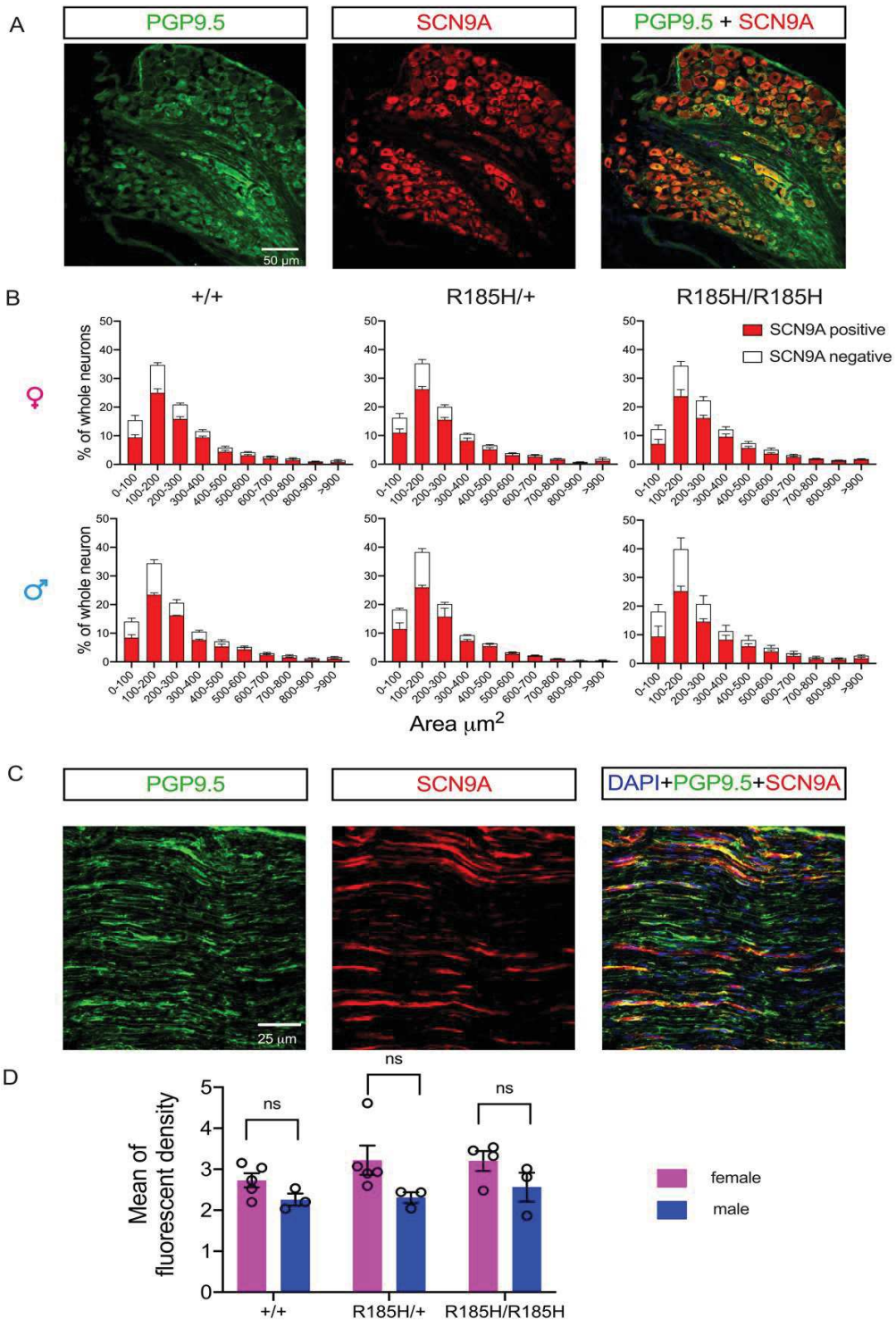

Figure 3.1 SCN9A protein expression in DRG and sciatic nerve of *Scn9a*^{R185H} mice

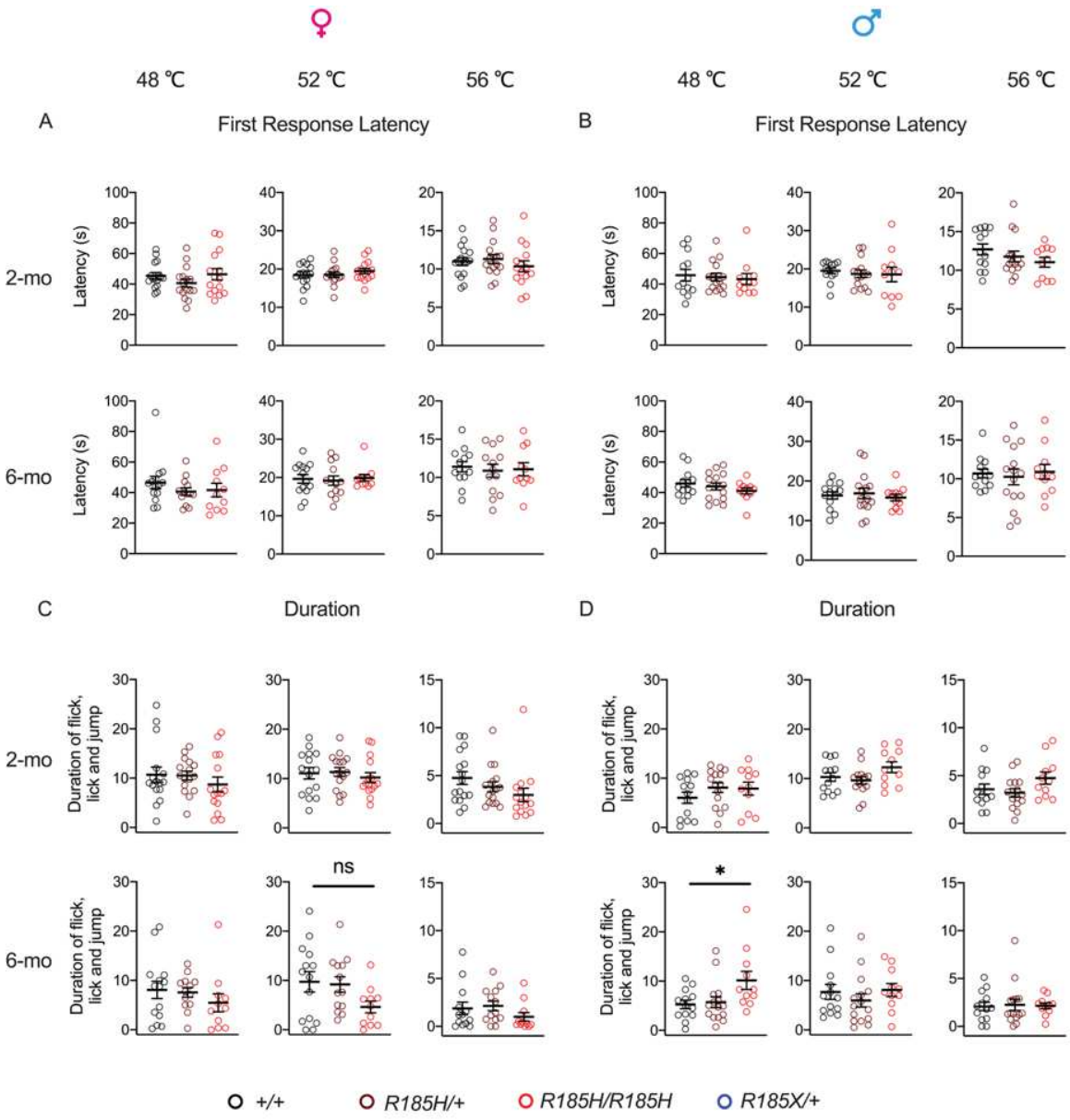

Figure 3.2 Response to Hot Plate in *Scn9a*^{R185H} mice at 2- and 6-month-age

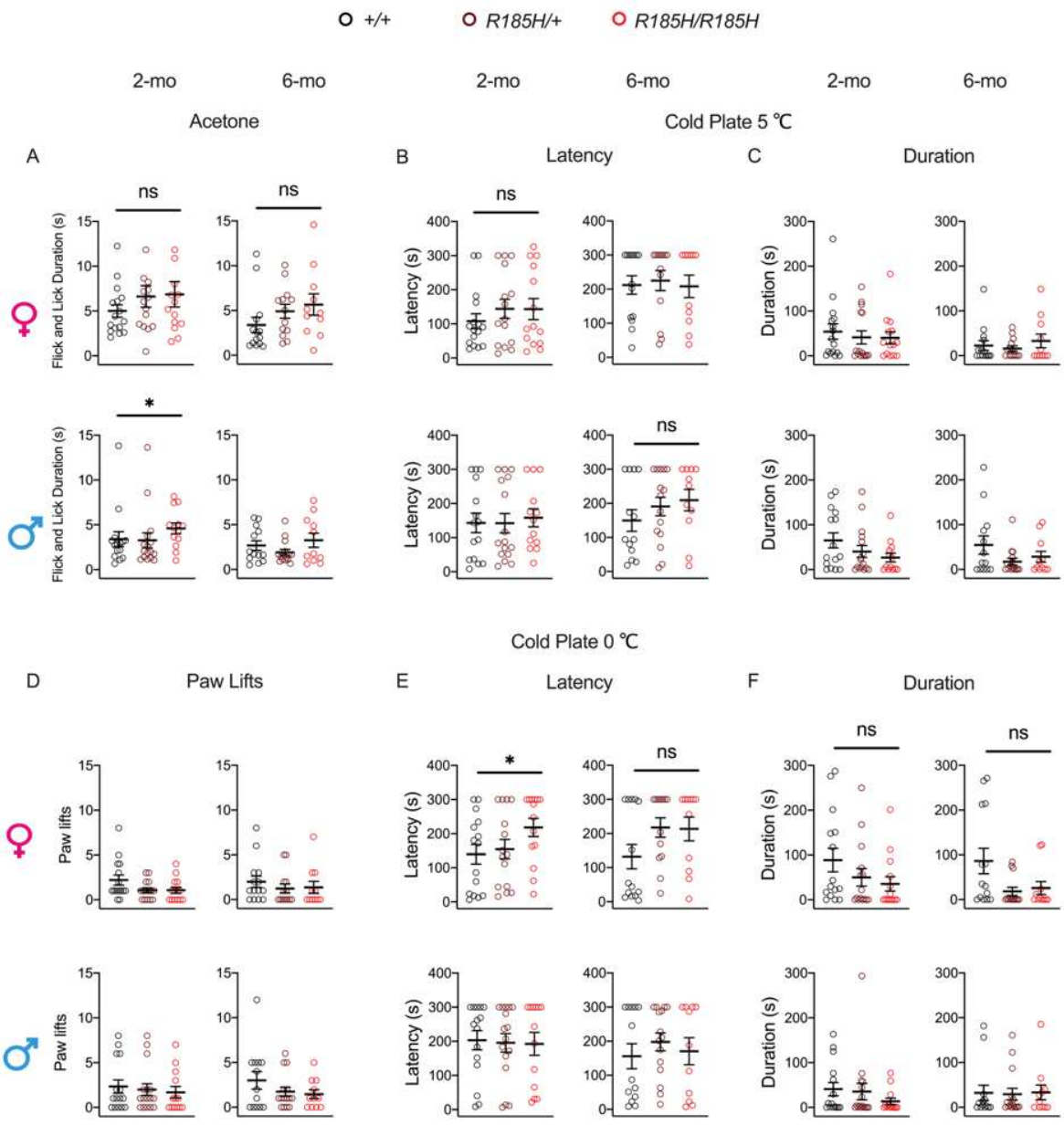

Figure 3.3 Pain response to Acetone and Cold plate in *Scn9a*^{R185H} mice at 2- and 6-month-age

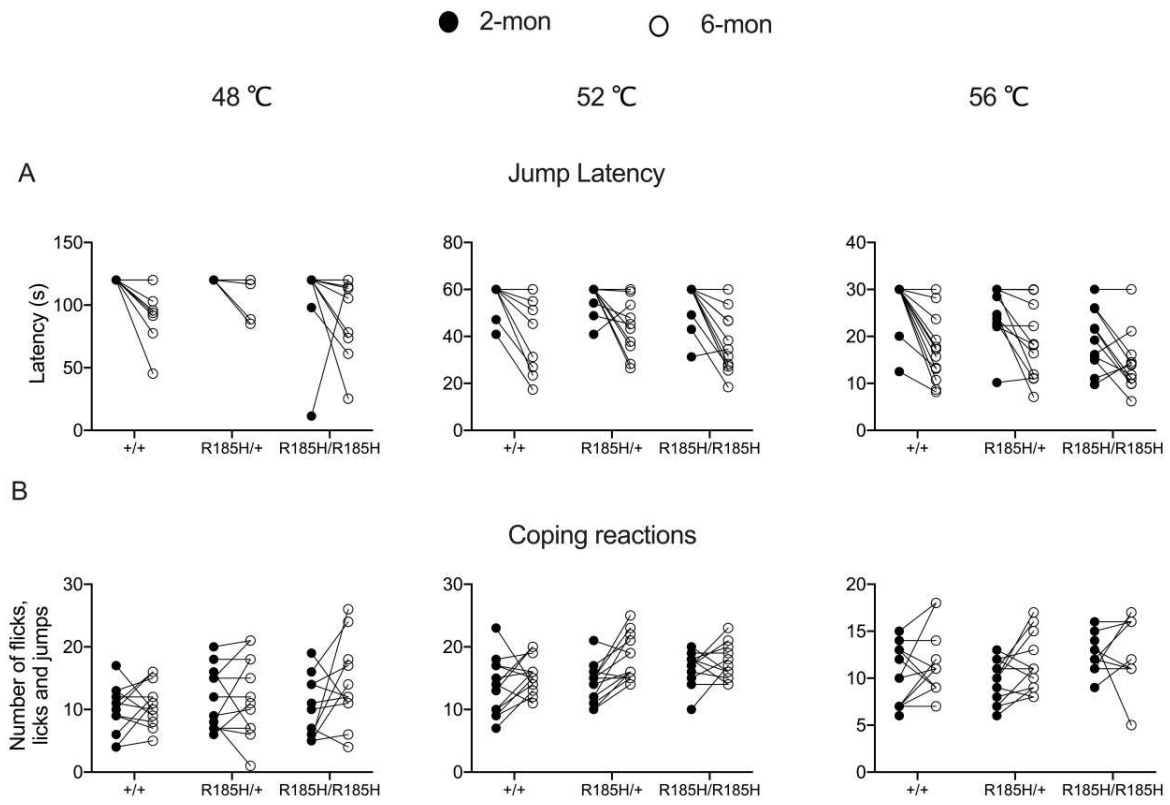

Figure 3.4 Correlation analyses of age (2- and 6-mon) and hot plate jump latency and coping reactions in *Scn9a*^{R185H} mice

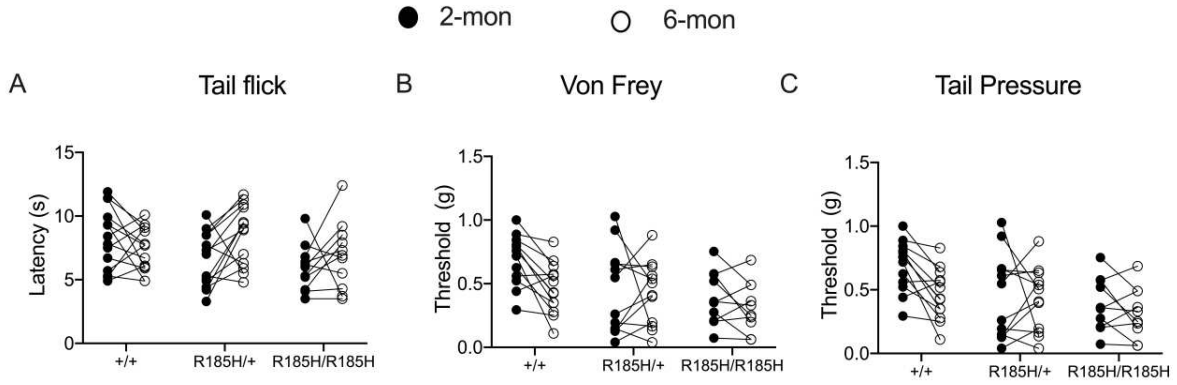

Figure 3.5 Correlation analyses of age (2- and 6-mon) and tail flick, von Frey and tail pressure in *Scn9a*^{R185H} mice

Table 3.1 SCN9A expression in DRG of *Scn9a*^{R185H} mice

Figure	Mice	Test	Analysis		Statistics
Fig. 3.1B	*Scn9a*^{R185H}	SCN9A expression in DRG: females	Two-way ANOVA	Genotype	p=0.7155 "F (2, 120) = 0.3358"
				Size	**p<0.0001** **"F (9, 120) = 267.9"**
Fig. 3.1B	*Scn9a*^{R185H}	0-100 µm^2: +/+ vs R185H/+	Turkey post-hoc multiple comparation		p>0.9999
		0-100 µm^2: +/+ vs R185H/R185H			p>0.9999
		0-100 µm^2: +/+ vs R185H/+			p>0.9999
		0-100 µm^2: +/+ vs R185H/R185H			p>0.9999
		100-200 µm^2: +/+ vs R185H/+			p>0.9999
		100-200 µm^2: +/+ vs R185H/R185H			p>0.9999
		200-300 µm^2: +/+ vs R185H/+			p>0.9999
		200-300 µm^2: +/+ vs R185H/R185H			p>0.9999
		300-400 µm^2: +/+ vs R185H/+			p>0.9999
		300-400 µm^2: +/+ vs R185H/R185H			p>0.9999
		400-500 µm^2: +/+ vs R185H/+			p>0.9999
		400-500 µm^2: +/+ vs R185H/R185H			p>0.9999
		500-600 µm^2: +/+ vs R185H/+			p>0.9999
		600-700 µm^2: +/+ vs R185H/R185H			p>0.9999
		700-800 µm^2: +/+ vs R185H/+			p>0.9999
		700-800 µm^2: +/+ vs R185H/R185H			p>0.9999
		800-900 µm^2: +/+ vs R185H/+			p>0.9999
		800-900 µm^2: +/+ vs R185H/R185H			p>0.9999
		>900 µm^2: +/+ vs R185H/+			p>0.9999
		>900 µm^2: +/+ vs R185H/R185H			p>0.9999
Fig. 3.1B	*Scn9a*^{R185H}	SCN9A expression in DRG: males	Two-way ANOVA	Genotype	p=0.7872 "F (2, 60) = 0.2402"
				Size	**p<0.0001** **"F (9, 60) = 135.4"**
Fig. 3.1B	*Scn9a*^{R185H}	0-100 µm^2: +/+ vs R185H/+	Turkey post-hoc multiple comparation		p>0.9999
		0-100 µm^2: +/+ vs R185H/R185H			p>0.9999
		0-100 µm^2: +/+ vs R185H/+			p>0.9999
		0-100 µm^2: +/+ vs R185H/R185H			p>0.9999
		100-200 µm^2: +/+ vs R185H/+			p>0.9999
		100-200 µm^2: +/+ vs R185H/R185H			p>0.9999
		200-300 µm^2: +/+ vs R185H/+			p>0.9999
		200-300 µm^2: +/+ vs R185H/R185H			p>0.9999
		300-400 µm^2: +/+ vs R185H/+			p>0.9999
		300-400 µm^2: +/+ vs R185H/R185H			p>0.9999
		400-500 µm^2: +/+ vs R185H/+			p>0.9999
		400-500 µm^2: +/+ vs R185H/R185H			p>0.9999
		500-600 µm^2: +/+ vs R185H/+			p>0.9999
		600-700 µm^2: +/+ vs R185H/R185H			p>0.9999
		700-800 µm^2: +/+ vs R185H/+			p>0.9999
		700-800 µm^2: +/+ vs R185H/R185H			p>0.9999
		800-900 µm^2: +/+ vs R185H/+			p>0.9999
		800-900 µm^2: +/+ vs R185H/R185H			p>0.9999
		>900 µm^2: +/+ vs R185H/+			p>0.9999
		>900 µm^2: +/+ vs R185H/R185H			p>0.9999

Table 3.2 SCN9A expresses in Sciatic nerve of *Scn9a*^{R185H} mice

Figure	Mice	Test	Analysis		Statistics
Fig. 3.1D	*Scn9a*^{R185H}	SCN9A express in siatic: females	Two-way ANOVA	Genotype	p=0.3836 "F (2, 17) = 1.014"
				Sex	**p=0.0090** **"F (1, 17) = 8.692"**
Fig. 3.1D	*Scn9a*^{R185H}	+/+ vs R185H/+	Turkey post-hoc multiple comparation		p=0.6920
		+/+ vs R185H/R185H			p=0.7706
Fig. 3.1D	*Scn9a*^{R185H}	SCN9A express in DRG: males	Two-way ANOVA	Genotype	p=0.7872 "F (2, 60) = 0.2402"
				Sex	**p<0.0001** **"F (9, 60) = 135.4"**
Fig. 3.1D	*Scn9a*^{R185H}	+/+ vs R185H/+	Turkey post-hoc multiple comparation		p>0.9999
		+/+ vs R185H/R185H			p=0.9794

Table 3.3 Response to Hot Plate in *Scn9a*^{R185H} mice at 2- and 6-month-age

Figure	Test: Hot Plate First Response Latency		Analysis	Groups	Statistics
Figure 3.2 A&B	48 ℃		Three-way ANOVA	Genotype	p=0.2309 "F (2, 151) = 1.480"
				Sex	p=0.7549 "F (1, 151) = 0.09781"
				Age	p=0.5696 "F (1, 151) = 0.3247"
Figure 3.2 A&B	52 ℃			Genotype	p=0.9706 "F (2, 150) = 0.02980"
				Sex	**p=0.0098** **"F (1, 150) = 6.843"**
				Age	p=0.1363 "F (1, 150) = 2.243"
Figure 3.2 A&B B	56 ℃			Genotype	p=0.5245 "F (2, 150) = 0.6482"
				Sex	p=0.6014 "F (1, 150) = 0.2741"
				Age	p=0.2561 "F (1, 150) = 1.299"
Figure 3.2 A&B	2-mo	48 ℃	Two-way ANOVA	Genotype	p=0.7169 "F (2, 80) = 0.3343"
				Sex	p=0.8924 "F (1, 80) = 0.01843"
Figure 3.2 A&B		52 ℃		Genotype	p=0.9601 "F (2, 79) = 0.04074"
				Sex	p=0.9008 "F (1, 79) = 0.01565"
Figure 3.2 A&B		56 ℃		Genotype	p=0.5484 "F (2, 76) = 0.6055"
				Sex	p=0.2570 "F (1, 76) = 1.304"
Figure 3.2 A&B	6-mo	48 ℃		Genotype	p=2277 "F (2, 71) = 1.511"
				Sex	p=0.7670 "F (1, 71) = 0.08845"
Figure 3.2 A&B		52 ℃		Genotype	p=0.8035 "F (2, 71) = 0.2389"
				Sex	**p=0.0007** **"F (1, 71) = 12.45"**
Figure 3.2 A&B		56 ℃		Genotype	p=0.6420 "F (2, 70) = 0.4460"
				Sex	p=0.4756 "F (1, 70) = 0.5144"

Table 3.3 Response to Hot Plate in *Scn9a*^{R185H} mice at 2- and 6-month-age

Figure	Test: Hot Plate First Response Latency		Analysis	Groups	Statistics
Figure 3.2 A	2-mo females	48 ℃	Unpaired t-test two-tailed	*+/+ vs R185H/+*	p=0.0800
				+/+ vs R185H/R185H	p=0.4064
Figure 3.2 A		52 ℃	Unpaired t-test two-tailed	*+/+ vs R185H/+*	p=0.4657
				+/+ vs R185H/R185H	p=0.1597
Figure 3.2 A		56 ℃	Unpaired t-test two-tailed	*+/+ vs R185H/+*	p=0.3417
				+/+ vs R185H/R185H	p=0.2410
Figure 3.2 B	2-mo males	48 ℃	Unpaired t-test two-tailed	*+/+ vs R185H/+*	p=0.3913
			Mann-Whitney test two-tailed	*+/+ vs R185H/R185H*	p=0.4101
Figure 3.2 B		52 ℃	Mann-Whitney test one-tailed	*+/+ vs R185H/+*	p=0.1176
				+/+ vs R185H/R185H	p=0.1804
Figure 3.2 B		56 ℃	Mann-Whitney test two-tailed	*+/+ vs R185H/+*	p=0.1611
			Unpaired t-test two-tailed	*+/+ vs R185H/R185H*	p=0.0505
Figure 3.2 A	6-mo females	48 ℃	Mann-Whitney test two-tailed	*+/+ vs R185H/+*	p=0.0926
				+/+ vs R185H/R185H	p=0.1865
Figure 3.2 A		52 ℃	Unpaired t-test two-tailed	*+/+ vs R185H/+*	p=0.3882
			Mann-Whitney test two-tailed	*+/+ vs R185H/R185H*	p=0.4891
Figure 3.2 A		56 ℃	Unpaired t-test two-tailed	*+/+ vs R185H/+*	p=0.3197
				+/+ vs R185H/R185H	p=0.3835
Figure 3.2 B	6-mo males	48 ℃	Unpaired t-test two-tailed	*+/+ vs R185H/+*	p=0.2851
			Mann-Whitney test two-tailed	*+/+ vs R185H/R185H*	p=0.1656
Figure 3.2 B		52 ℃	Unpaired t-test two-tailed	*+/+ vs R185H/+*	p=0.3767
				+/+ vs R185H/R185H	p=0.3338
Figure 3.2 B		56 ℃	Mann-Whitney test two-tailed	*+/+ vs R185H/+*	p=0.3755
				+/+ vs R185H/R185H	p=0.4832

Table 3.3 Response to Hot Plate in *Scn9a*^{R185H} mice at 2- and 6-month-age

Figure	Test: Hot Plate Duration		Analysis	Groups	Statistics
Figure 3.2 C&D	48 ℃		Three-way ANOVA	Genotype	p=0.8252 "F (2, 151) = 0.1924"
				Sex	p=0.0943 "F (1, 151) = 2.835"
				Age	**p=0.0383** **"F (1, 151) = 4.369"**
Figure 3.2 C&D	52 ℃			Genotype	p=0.5945 "F (2, 150) = 0.5219"
				Sex	p=0.6250 "F (1, 150) = 0.2399"
				Age	**p<0.0001** **"F (1, 150) = 19.21"**
Figure 3.2 C&D	56 ℃			Genotype	p=0.6851 "F (2, 150) = 0.3791"
				Sex	p=0.4707 "F (1, 150) = 0.5230"
				Age	**p<0.0001** **"F (1, 150) = 34.58"**
Figure 3.2 C&D	2-mo	48 ℃	Two-way ANOVA	Genotype	p=0.6608 "F (2, 80) = 0.4165"
				Sex	**p=0.0138** **"F (1, 80) = 6.336"**
Figure 3.2 C&D		52 ℃		Genotype	p=0.7236 "F (2, 79) = 0.3248"
				Sex	p=0.8690 "F (1, 79) = 0.02736"
Figure 3.2 C&D		56 ℃		Genotype	p=0.5413 "F (2, 80) = 0.6186"
				Sex	p=0.9791 "F (1, 80) = 0.0006921"
Figure 3.2 C&D	6-mo	48 ℃		Genotype	p=0.6683 "F (2, 71) = 0.4053"
				Sex	p=0.9925 "F (1, 71) = 8.841e-005"
Figure 3.2 C&D		52 ℃		Genotype	p=0.3483 "F (2, 71) = 1.071"
				Sex	p=0.6453 "F (1, 71) = 0.2137"
Figure 3.2 C&D		56 ℃		Genotype	p=0.4978 "F (2, 70) = 0.7045"
				Sex	p=0.2550 "F (1, 70) = 1.317"

Table 3.3 Response to Hot Plate in *Scn9a*^{R185H} mice at 2- and 6-month-age

Figure	Test: Hot Plate Duration		Analysis	Groups	Statistics
Figure 3.2C	2-mo females	48 ℃	Mann-Whitney test two-tailed	*+/+ vs R185H/+*	p=0.4617
				+/+ vs R185H/R185H	p=0.2054
Figure 3.2C		52 ℃	Unpaired t-test two-tailed	*+/+ vs R185H/+*	p=0.8588
				+/+ vs R185H/R185H	p=0.5765
Figure 3.2C		56 ℃	Mann-Whitney test two-tailed	*+/+ vs R185H/+*	p=0.4174
				+/+ vs R185H/R185H	**p=0.0240**
Figure 3.2D	2-mo males	48 ℃	Unpaired t-test two-tailed	*+/+ vs R185H/+*	p=0.1756
				+/+ vs R185H/R185H	p=0.2961
Figure 3.2D		52 ℃	Unpaired t-test two-tailed	*+/+ vs R185H/+*	p=0.5521
				+/+ vs R185H/R185H	p=0.1644
Figure 3.2D		56 ℃	Unpaired t-test two-tailed	*+/+ vs R185H/+*	p=0.5837
				+/+ vs R185H/R185H	p=0.1773
Figure 3.2C	6-mo females	48 ℃	Unpaired t-test two-tailed	*+/+ vs R185H/+*	p=0.8086
			Mann-Whitney test two-tailed	*+/+ vs R185H/R185H*	p=0.2385
Figure 3.2C		52 ℃	Unpaired t-test two-tailed	*+/+ vs R185H/+*	p=0.8397
				+/+ vs R185H/R185H	p=0.0588
Figure 3.2C		56 ℃	Mann-Whitney test two-tailed	*+/+ vs R185H/+*	p=0.4707
				+/+ vs R185H/R185H	p=0.2687
Figure 3.2D	6-mo males	48 ℃	Mann-Whitney test two-tailed	*+/+ vs R185H/+*	p=0.9008
				+/+ vs R185H/R185H	**p=0.0161**
Figure 3.2D		52 ℃	Mann-Whitney test two-tailed	*+/+ vs R185H/+*	p=0.2945
				+/+ vs R185H/R185H	p=0.4675
Figure 3.2D		56 ℃	Mann-Whitney-test two-tailed	*+/+ vs R185H/+*	p=0.7945
			Unpaired t-test two-tailed	*+/+ vs R185H/R185H*	p=0.8927

Table 3.4 Response to Acetone and Cold plate in *Scn9a*^{R185H} mice at 2- and 6-month-age

Figure	Test		Analysis	Groups	Statistics
Figure 3.3A	Acetone test Duration of lick and flick		Three-way ANOVA	Genotype	p=0.0724 "F (2, 154) = 2.671"
				Sex	**p<0.0001** **"F (1, 154) = 18.62"**
				Age	p=0.0110 "F (1, 154) = 6.622"
Figure 3.3A	2-mo		Two-way ANOVA	Genotype	p=0.3057 "F (2, 83) = 1.202"
				Sex	**p=0.0032** **"F (1, 83) = 9.215"**
Figure 3.3A	6-mo		Two-way ANOVA	Genotype	p=0.1753 "F (2, 71) = 1.785"
				Sex	**p=0.0016** **"F (1, 71) = 10.83"**
Figure 3.3A	2-mo	females	Mann-Whitney test two-tailed	*+/+ vs R185H/+*	p=0.2316
				+/+ vs R185H/R185H	p=0.3549
Figure 3.3A		males	Mann-Whitney test two-tailed	*+/+ vs R185H/+*	p=0.5196
				+/+ vs R185H/R185H	**p=0.0367**
Figure 3.3A	6-mo	females	Mann-Whitney test two-tailed	*+/+ vs R185H/+*	p=0.0609
				+/+ vs R185H/R185H	p=0.0507
Figure 3.3A		males	Mann-Whitney test two-tailed	*+/+ vs R185H/+*	p=0.3874
				+/+ vs R185H/R185H	p=0.6895
Figure 3.3B	Cold Plate 5 ℃ Latency		Three-way ANOVA	Genotype	p=0.3689 "F (2, 154) = 1.004"
				Sex	p=0.6312 "F (1, 154) = 0.2314"
				Age	**p=0.0004** **"F (1, 154) = 12.89"**
Figure 3.3B	2-mo		Two-way ANOVA	Genotype	p=0.6403 "F (2, 83) = 0.4482"
				Sex	p=0.4764 "F (1, 83) = 0.5118"
Figure 3.3B	6-mo		Two-way ANOVA	Genotype	p=0.5645 "F (2, 71) = 0.5764"
				Sex	p=0.1946 "F (1, 71) = 1.714"
Figure 3.3B	2-mo	females	Mann-Whitney test two-tailed	*+/+ vs R185H/+*	p=0.3997
				+/+ vs R185H/R185H	p=0.6741
Figure 3.3B		males	Mann-Whitney test two-tailed	*+/+ vs R185H/+*	p=0.9144
				+/+ vs R185H/R185H	p=0.5301
Figure 3.3B	6-mo	females	Mann-Whitney test two-tailed	*+/+ vs R185H/+*	p=0.8294
				+/+ vs R185H/R185H	p>0.9999
Figure 3.3B		males	Mann-Whitney test two-tailed	*+/+ vs R185H/+*	p=0.3787
				+/+ vs R185H/R185H	p=0.2858

Table 3.4 Response to Acetone and Cold plate in *Scn9a*^{R185H} mice at 2- and 6-month-age

Figure	Test		Analysis	Groups	Statistics
Figure 3.3C	Cold Plate 5 ℃ Duration of paw lift		Three-way ANOVA	Genotype	p=0.0794 "F (2, 154) = 2.576"
				Sex	p=0.5940 "F (1, 154) = 0.2853"
				Age	**p=0.0476** **"F (1, 154) = 3.986"**
Figure 3.3C	2-mo		Two-way ANOVA	Genotype	p=0.1910 "F (2, 83) = 1.689"
				Sex	p=0.9363 "F (1, 83) = 0.006421"
Figure 3.3C	6-mo		Two-way ANOVA	Genotype	p=0.1961 "F (2, 71) = 1.667"
				Sex	p=0.3586 "F (1, 71) = 0.8539"
Figure 3.3C	2-mo	females	Mann-Whitney test two-tailed	*+/+ vs R185H/+*	p=0.4516
				+/+ vs R185H/R185H	p=0.4473
Figure 3.3C		males	Mann-Whitney test two-tailed	*+/+ vs R185H/+*	p=0.3932
				+/+ vs R185H/R185H	p=0.1940
Figure 3.3C	6-mo	females	Mann-Whitney test two-tailed	*+/+ vs R185H/+*	p=0.9940
				+/+ vs R185H/R185H	p=0.7935
Figure 3.3C		males	Mann-Whitney test two-tailed	*+/+ vs R185H/+*	p=0.3302
				+/+ vs R185H/R185H	p=0.5510
Figure 3.3D	Cold Plate 0 ℃ Number of paw lifts		Three-way ANOVA	**Genotype**	**p=0.0451** **"F (2, 153) = 3.162"**
				Sex	p=0.1241 "F (1, 153) = 2.390"
				Age	p=0.8439 "F (1, 153) = 0.03890"
Figure 3.3D	2-mo		Two-way ANOVA	Genotype	p=0.2548 "F (2, 82) = 1.390"
				Sex	p=0.2287 "F (1, 82) = 1.471"
Figure 3.3D	6-mo		Two-way ANOVA	Genotype	p=0.1810 "F (2, 71) = 1.751"
				Sex	p=0.3282 "F (1, 71) = 0.9695"
Figure 3.3D	2-mo	females	Mann-Whitney test two-tailed	*+/+ vs R185H/+*	p=0.1393
				+/+ vs R185H/R185H	p=0.1135
Figure 3.3D		males	Mann-Whitney test two-tailed	*+/+ vs R185H/+*	p=0.9304
				+/+ vs R185H/R185H	p=0.4870
Figure 3.3D	6-mo	females	Mann-Whitney test two-tailed	*+/+ vs R185H/+*	p=0.2525
				+/+ vs R185H/R185H	p=0.3136
Figure 3.3D		males	Mann-Whitney test two-tailed	*+/+ vs R185H/+*	p=0.6647
				+/+ vs R185H/R185H	p=0.3983

Table 3.4 Response to Acetone and Cold plate in *Scn9a*^{R185H} mice at 2- and 6-month-age

Figure	Test		Analysis	Groups	Statistics
Figure 3.3E	Cold Plate 0 ℃ Latency		Three-way ANOVA	Genotype	p=0.1405 "F (2, 153) = 1.988"
				Sex	p=0.7104 "F (1, 153) = 0.1384"
				Age	p=0.8790 "F (1, 153) = 0.02325"
Figure 3.3E	2-mo		Two-way ANOVA	Genotype	p=0.4517 "F (2, 82) = 0.8025"
				Sex	p=0.2647 "F (1, 82) = 1.261"
Figure 3.3E	6-mo		Two-way ANOVA	Genotype	p=0.1335 "F (2, 71) = 2.072"
				Sex	p=0.6368 "F (1, 71) = 0.2248"
Figure 3.3E	2-mo	females	Mann-Whitney test two-tailed	*+/+ vs R185H/+*	p=0.5581
				+/+ vs R185H/R185H	**p=0.0475**
Figure 3.3E		males	Mann-Whitney test two-tailed	*+/+ vs R185H/+*	p=0.7436
				+/+ vs R185H/R185H	p=0.9253
Figure 3.3E	6-mo	females	Mann-Whitney test two-tailed	*+/+ vs R185H/+*	p=0.0522
				+/+ vs R185H/R185H	p=0.1048
Figure 3.3E		males	Mann-Whitney test two-tailed	*+/+ vs R185H/+*	p=0.5173
				+/+ vs R185H/R185H	p>0.9999
Figure 3.3F	Cold Plate 0 ℃ Duration of paw lift		Three-way ANOVA	**Genotype**	**p=0.0179** **"F (2, 153) = 4.131"**
				Sex	p=0.0620 "F (1, 153) = 3.534"
				Age	p=0.5355 "F (1, 153) = 0.3857"
Figure 3.3F	2-mo		Two-way ANOVA	Genotype	p=0.1044 "F (2, 82) = 2.323"
				Sex	p=0.0661 "F (1, 82) = 3.470"
Figure 3.3F	6-mo		Two-way ANOVA	Genotype	p=0.1048 "F (2, 71) = 2.329"
				Sex	p=0.4242 "F (1, 71) = 0.6462"
Figure 3.3F	2-mo	females	Mann-Whitney test two-tailed	*+/+ vs R185H/+*	p=0.2271
				+/+ vs R185H/R185H	p=0.0590
Figure 3.3F		males	Mann-Whitney test two-tailed	*+/+ vs R185H/+*	p=0.6551
				+/+ vs R185H/R185H	p=0.2199
Figure 3.3F	6-mo	females	Mann-Whitney test two-tailed	*+/+ vs R185H/+*	p=0.0522
				+/+ vs R185H/R185H	p=0.0929
Figure 3.3F		males	Mann-Whitney test two-tailed	*+/+ vs R185H/+*	p=0.9632
				+/+ vs R185H/R185H	p=0.6819

Table 3.5 Correlation analyses of age (2- and 6-mon) and hot plate, tail flick, von Frey and tail pressure in *Scn9a*^{R185H} mice

Test	genotype	r	95% CI	p-value		n
Hot plate-jump latency 48 ºC	+/+	Vertical line				14
	R185H/+	Vertical line				13
	R185H/R185H	-0.1820	-0.7049 to 0.4691	0.5922	ns	11
Hot plate-jump latency 52ºC	+/+	0.6899	0.2513 to 0.8934	0.0063	Yes	14
	R185H/+	-0.1028	-0.6187 to 0.4751	0.7382	ns	13
	R185H/R185H	0.4070	-0.2552 to 0.8093	0.2141	ns	11
Hot plate-jump latency 56 ºC	+/+	0.4437	-0.1420 to 0.7993	0.1289	ns	13
	R185H/+	0.5873	0.05362 to 0.8600	0.0348	Yes	13
	R185H/R185H	0.4447	-0.2116 to 0.8246	0.1706	ns	11
Hot plate-coping reactions 48 ºC	+/+	0.2882	-0.3123 to 0.7242	0.3395	ns	13
	R185H/+	0.6159	0.06489 to 0.8791	0.0330	Yes	12
	R185H/R185H	0.0851	-0.5424 to 0.6517	0.8034	ns	11
Hot plate-coping reactions 52 ºC	+/+	0.2667	-0.3074 to 0.6984	0.3567	ns	14
	R185H/+	0.2199	-0.2326 to 0.7627	0.2199	ns	13
	R185H/R185H	0.1438	-0.4992 to 0.6846	0.6732	ns	11
Hot plate-coping reactions 56 ºC	+/+	0.4019	-0.1915 to 0.7801	0.1735	ns	13
	R185H/+	0.4196	-0.1708 to 0.7883	0.1534	ns	13
	R185H/R185H	0.0985	-0.5663 to 0.6856	0.7867	ns	10
Tail flick	+/+	0.2290	-0.3433 to 0.6773	0.4310	ns	14
	R185H/+	0.2155	-0.3806 to 0.6852	0.4794	ns	13
	R185H/R185H	0.0484	-0.5680 to 0.6300	0.8876	ns	11
Von Frey	+/+	0.4612	-0.1204 to 0.8071	0.1127	ns	13
	R185H/+	0.2825	-0.3478 to 0.7369	0.3737	ns	12
	R185H/R185H	0.5555	-0.1140 to 0.8780	0.0955	ns	10
Tail pressure	+/+	0.0990	0.08873 to 0.8689	0.0269	Yes	13
	R185H/+	0.2064	-0.3888 to 0.6800	0.4988	ns	13
	R185H/R185H	0.4603	-0.1928 to 0.8308	0.1542	ns	11

4. Characterization of *Scn9a*$^{R185X/wt}$ Mice

4.1 Response to Hot Plate in *Scn9a*$^{R185X/wt}$ mice at 2- and 6-month-age

The first response latency and duration of coping reactions were analyzed in *Scn9a*$^{R185X/wt}$ mice. Following the three-way and two-way ANOVA analysis, only the age effect on the duration of coping reactions in 56 °C Hot Plate was detected. For genotype effect, only female *R185X/+* mice detected significantly less time spent at 2-month age on 48°C Hot Plate (Figure 4.1C), whereas showed similar value for latency at three temperature (Figure 4.1A). In male mutant mice, there is no difference was detected for both the latency and duration of coping reactions for three temperature Hot Plate at both two ages (Figure 4.1B and D). (More detailed statistical analysis in Table 4.1)

4.2 Response to Acetone and Cold plate in *Scn9a*$^{R185X/wt}$ mice at 2- and 6-month-age

To check other cold response parameters to acetone and cold plate in the *Scn9a*$^{R185X/wt}$ mice, the duration of flick and lick response to acetone and latency, and the duration of paw lift for cold plate observed. The sex effect showed lick and flick duration in the three-way ANOVA, but no effect on 5 and 0°C Cold Plate with different parameters. However, in two-way ANOVA analysis, there is a genotype effect on the number of paw lifts in 0°C Cold Plate at 6-month-age. No alteration of response to the acetone application was found in *Scn9a*$^{R185X/wt}$ mice (Figure 4.2A). The female *R185H/+* mutant mice displayed a decreasing number and time spent of paw lifts to 0°C Cold Plate at 6-month-age (Figure 4.2 D and F). No change was found for other mutant mice in different Cold Plate parameters (Figure 4.2 B, C, and E). (More detailed statistical analysis in Table 4.2)

Figures Legends

Figure 4.1 Response latency and coping reaction duration to Hot Plate in *Scn9a*$^{R185X/wt}$ mice at 2- and 6-month-age. **A)** First response latency of 48, 52 and 56°C Hot Plate in female *Scn9a*$^{R185X/wt}$ mice at 2- and 6-month-age. No significant difference was showed in *Scn9a*$^{R185X/wt}$ female mutant mice compared to +/+ mice. (2-mo: +/+ n=11; *R185X/*+ n=13; 6-mo +/+ n=11; *R185X/*+ n=13). **B)** First response latency of 48, 52 and 56°C Hot Plate in male *Scn9a*$^{R185X/wt}$ mice at 2- and 6-month-age. No significant difference was showed in *Scn9a*^{R185H} male mutant mice compared to +/+ mice. (2-mo: +/+ n=11; *R185X/*+ n=14; 6-mo +/+ n=11; *R185X/*+ n=14).**C)** Duration of coping reaction of 48, 52 and 56°C Hot Plate *Scn9a*$^{R185X/wt}$ female mice at 2- and 6-month-age. No significant difference was showed *Scn9a*^{R185H} female mutant mice compared to +/+ mice. (2-mo: +/+ n=11; *R185X/*+ n=13; 6-mo +/+ n=11; *R185X/*+ n=13). **D)** Duration of coping reaction of 48, 52 and 56°C Hot Plate in *Scn9a*$^{R185X/wt}$ mice at 2- and 6-month-age. R185H/R185H male mice performed more duration of coping reaction at 6-month-age. (2-mo: +/+ n=11; *R185X/*+ n=14; 6-mo +/+ n=11; *R185X/*+ n=14). Data present as means ± *SEM*. *P < 0.05, ** P < 0.01 and ***P < 0.001, *Scn9a*$^{R185X/wt}$ mutants compared to their +/+ littermates by two tailed student t test or Mann-Whitney test. (More detailed statistical analysis see Table 4.1)

Figure 4.2 Response to Acetone and Cold plate in *Scn9a*$^{R185X/wt}$ mice at 2- and 6-month-age. **A)** Duration of flicking and licking after applying acetone in *Scn9a*$^{R185X/wt}$ mice at 2- and 6-month-age. R185H/R185H male mice performed more duration of flick and lick at 2-month-age. **B)** First response latency of 5°C Cold Plate in *Scn9a*$^{R185X/wt}$ mice at 2- and 6-month-age. No significant difference was showed in *Scn9a*$^{R185X/wt}$ male mutant mice compared to +/+ mice. (**C)** Paw lifts duration of 5°C Cold Plate in *Scn9a*$^{R185X/wt}$ mice at 2- and 6-month-age. No significant difference was showed in *Scn9a*$^{R185X/wt}$ male mutant mice compared to +/+ mice. **D)** Number of paw lift response to 5°C Cold Plate in *Scn9a*$^{R185X/wt}$ mice at 2- and 6-month-age. No significant difference was showed in *Scn9a*$^{R185X/wt}$ male mutant mice compared to +/+ mice **E)** First response latency of 0°C Cold Plate in *Scn9a*$^{R185X/wt}$ mice at 2- and 6-month-age. R185H/R185H female mice was showed increasing latency at 2-month-age. **F)** Paw lifts duration of 0°C Cold Plate in *Scn9a*$^{R185X/wt}$ mice at 2- and 6-month-age. No significant difference was showed in *Scn9a*$^{R185X/wt}$ male mutant mice compared to +/+ mice. (Female-2-mo: +/+ n=16; *R185X/*+ n=16; Female-6-mo +/+ n=14; *R185X/*+ n=13; Male-2-mo: +/+ n=16; *R185X/*+ n=16; Male-6-mo +/+ n=14; *R185X/*+ n=13). Data present as means ± *SEM*. *P < 0.05, ** P < 0.01 and ***P < 0.001, *Scn9a*$^{R185X/wt}$ mutants compared to their +/+ littermates by two tailed student t test or Mann-Whitney test. (More detailed statistical analysis see Table 4.2)

Figures

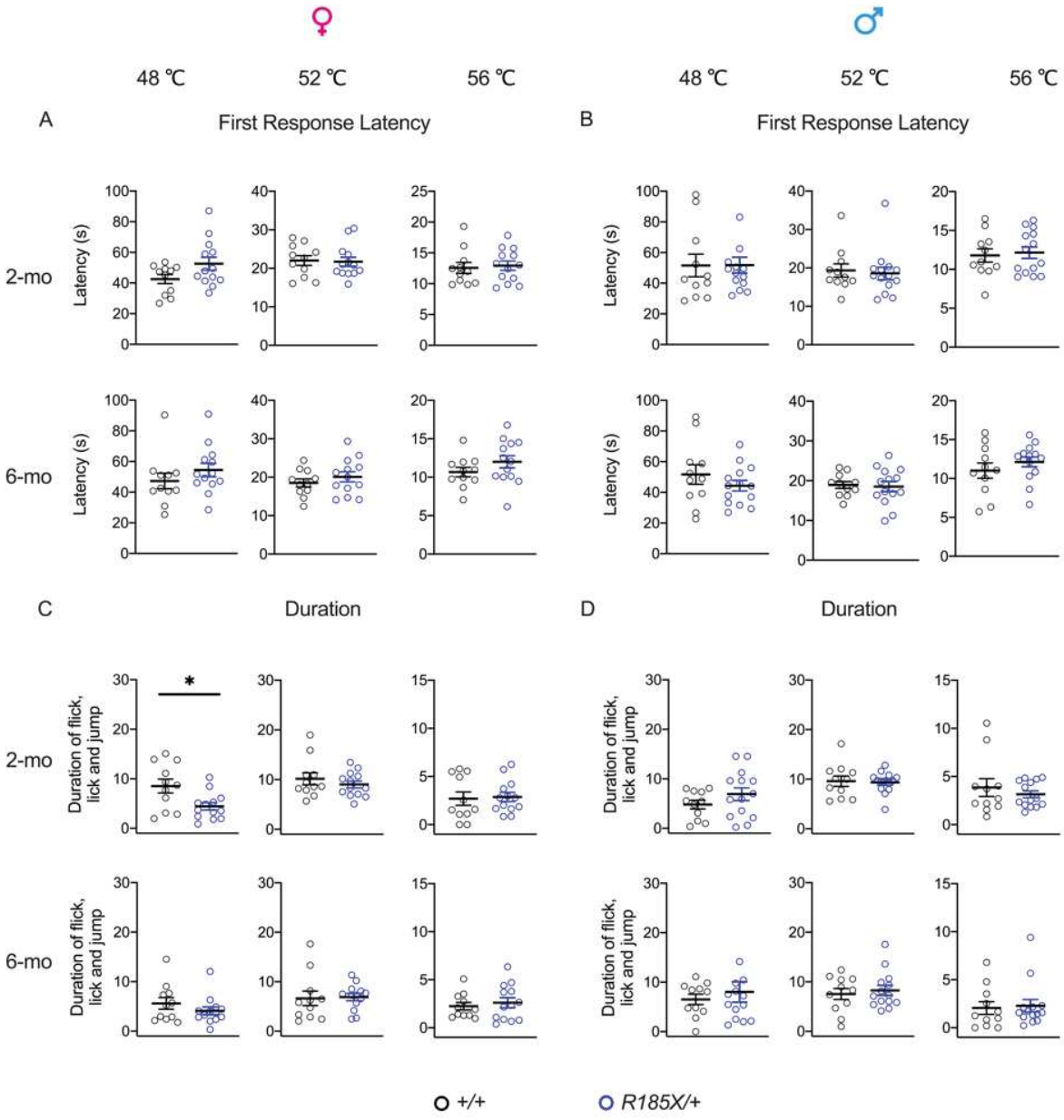

Figure 4.1 Response to Hot Plate in *Scn9a*$^{R185X/wt}$ mice at 2- and 6-month-age.

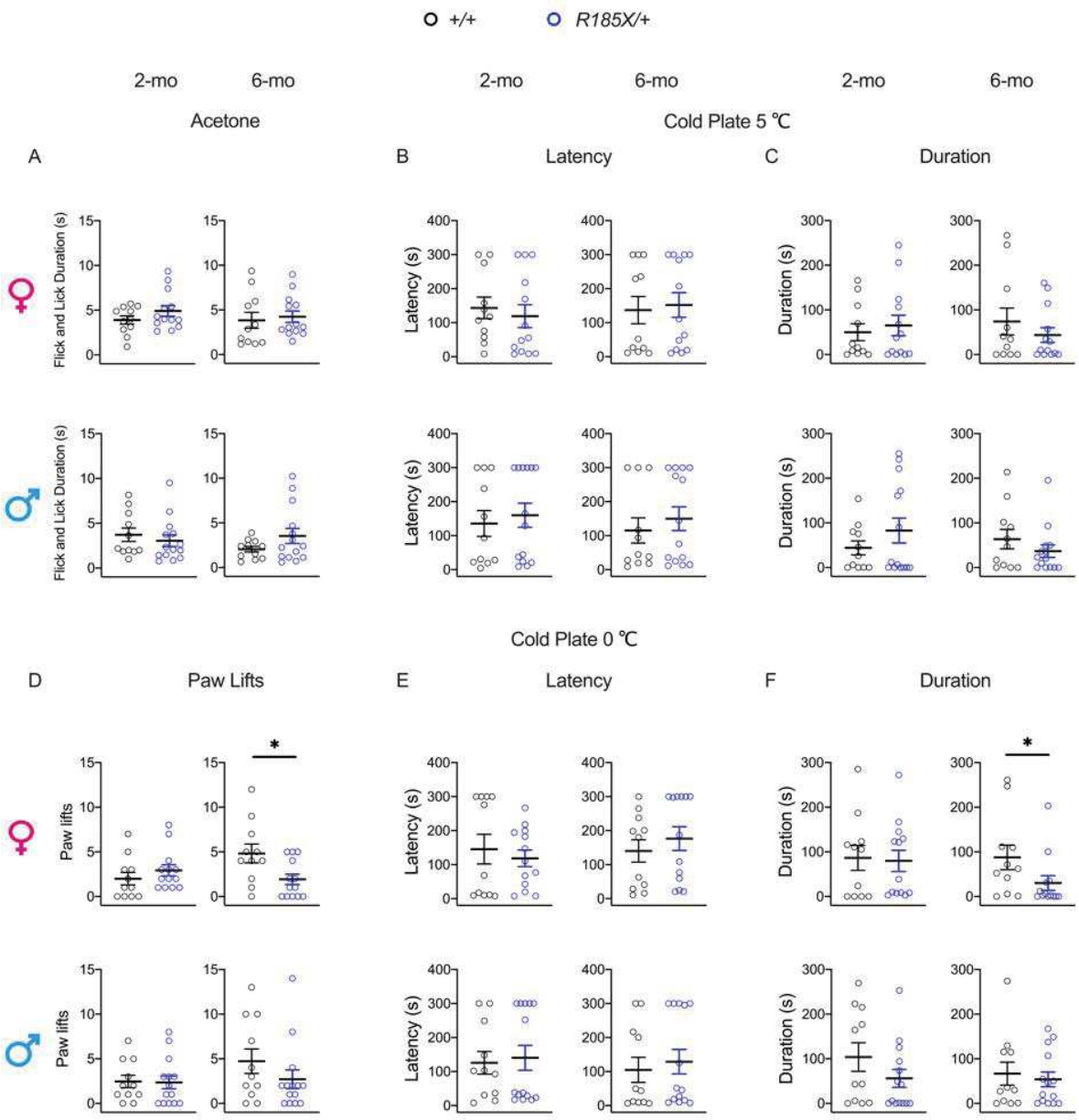

Figure 4.2 Response to Acetone and Cold plate in *Scn9a*$^{R185X/wt}$ mice at 2- and 6-month-age.

Table 4.1 Response to Hot Plate in *Scn9a*$^{R185X/wt}$ mice at 2- and 6-month-age.

Figure	Test: Hot Plate First response latency		Analysis	Groups	Statistics
Figure 4.1A&B	48 ℃		Three-way ANOVA	Genotype	p=0.4782 "F (1, 90) = 0.5072"
				Sex	p=0.8689 "F (1, 90) = 0.02740"
				Age	p=0.9528 "F (1, 90) = 0.003526"
Figure 4.1A&B	52 ℃		Three-way ANOVA	Genotype	p=0.9738 "F (1, 90) = 0.001087"
				Sex	p=0.0713 "F (1, 90) = 3.330"
				Age	p=0.1453 "F (1, 90) = 2.158"
Figure 4.1A&B	56 ℃		Three-way ANOVA	Genotype	p=0.1556 "F (1, 90) = 2.051"
				Sex	p=0.6238 "F (1, 90) = 0.2422"
				Age	p=0.1063 "F (1, 90) = 2.661"
Figure 4.1A&B	2-mo	48 ℃	Two-way ANOVA	Genotype	p=0.3263 "F (1, 45) = 0.9850"
				Sex	p=0.4380 "F (1, 45) = 0.6177"
Figure 4.1A&B		52 ℃	Two-way ANOVA	Genotype	p=0.7234 "F (1, 45) = 0.1268"
				Sex	p=0.0583 "F (1, 45) = 3.775"
Figure 4.1A&B		56 ℃	Two-way ANOVA	Genotype	p=0.6488 "F (1, 45) = 0.2102"
				Sex	p=0.3363 "F (1, 45) = 0.9446"
Figure 4.1A&B	6-mo	48 ℃	Two-way ANOVA	Genotype	p=0.9791 "F (1, 45) = 0.0006921"
				Sex	p=0.5456 "F (1, 45) = 0.3708"
Figure 4.1A&B		52 ℃	Two-way ANOVA	Genotype	p=0.6162 "F (1, 45) = 0.2548"
				Sex	p=0.6312 "F (1, 45) = 0.2337"
Figure 4.1A&B		56 ℃	Two-way ANOVA	Genotype	p=0.1177 "F (1, 45) = 2.545"
				Sex	p=0.7604 "F (1, 45) = 0.09416"

Table 4.1 Response to Hot Plate in *Scn9a*$^{R185X/wt}$ mice at 2- and 6-month-age.

Figure	Test-Hot Plate First Response Latency		Analysis	Groups	Statistics
Figure 4.1A	2-mo females	48 ℃	Unpaired t-test two-tailed	+/+ *vs R185X/+*	p=0.0739
Figure 4.1A		52 ℃	Unpaired t-test two-tailed	+/+ *vs R185X/+*	p=0.8627
Figure 4.1A		56 ℃	Mann-Whitney test two-tailed	+/+ *vs R185X/+*	p=0.7330
Figure 4.1B	2-mo males	48 ℃	Mann-Whitney test two-tailed	+/+ *vs R185X/+*	p=0.5719
Figure 4.1B		52 ℃	Mann-Whitney test one-tailed	+/+ *vs R185X/+*	p=0.8931
Figure 4.1B		56 ℃	Unpaired t-test two-tailed	+/+ *vs R185X/+*	p=0.7487
Figure 4.1A	6-mo females	48 ℃	Mann-Whitney test two-tailed	+/+ *vs R185X/+*	p=0.2066
Figure 4.1A		52 ℃	Unpaired t-test two-tailed	+/+ *vs R185X/+*	p=0.3638
Figure 4.1A		56 ℃	Unpaired t-test two-tailed	+/+ *vs R185X/+*	p=0.2131
Figure 4.1B	6-mo males	48 ℃	Unpaired t-test two-tailed	+/+ *vs R185X/+*	p=0.2891
Figure 4.1B		52 ℃	Unpaired t-test two-tailed	+/+ *vs R185X/+*	p=0.8014
Figure 4.1B		56 ℃	Unpaired t-test two-tailed	+/+ *vs R185X/+*	p=0.3318

Table 4.1 Response to Hot Plate in *Scn9a*$^{R185X/wt}$ mice at 2- and 6-month-age.

Figure	Test: Hot Plate Duration of coping reactions		Analysis	Groups	Statistics
Figure 4.1C & D	48 ℃		Three-way ANOVA	Genotype	p=0.4516 "F (1, 90) = 0.9578"
				Sex	p=0.3304 "F (1, 90) = 0.5715"
				Age	p=0.9187 "F (1, 90) = 0.01048"
Figure 4.1C & D	52 ℃		Three-way ANOVA	Genotype	p=0.8821 "F (1, 90) = 0.02211"
				Sex	p=0.4670 "F (1, 90) = 0.5335"
				Age	**p=0.0021** **"F (1, 90) = 10.07"**
Figure 4.1C & D	56 ℃		Three-way ANOVA	Genotype	p=0.9679 "F (1, 90) = 0.001629"
				Sex	p=0.5834 "F (1, 90) = 0.3029"
				Age	**p=0.0477** **"F (1, 90) = 4.031"**
Figure 4.1C & D	2-mo	48 ℃	Two-way ANOVA	Genotype	p=0.2142 "F (1, 45) = 1.587"
				Sex	p=0.5480 "F (1, 45) = 0.3665"
Figure 4.1C & D		52 ℃	Two-way ANOVA	Genotype	p=0.8059 "F (1, 45) = 0.06112"
				Sex	p=0.8494 "F (1, 45) = 0.03649"
Figure 4.1C & D		56 ℃	Two-way ANOVA	**Genotype**	**p=0.0343** **"F (1, 45) = 4.766"**
				Sex	p=0.1334 "F (1, 45) = 2.336"
Figure 4.1C & D	6-mo	48 ℃	Two-way ANOVA	Genotype	p=0.1202 "F (1, 45) = 2.509"
				Sex	p=0.1910 "F (1, 45) = 1.763"
Figure 4.1C & D		52 ℃	Two-way ANOVA	Genotype	p=0.1757 "F (1, 45) = 1.893"
				Sex	p=0.4298 "F (1, 45) = 0.6348"
Figure 4.1C & D		56 ℃	Two-way ANOVA	**Genotype**	**p=0.0050** **"F (1, 45) = 8.720"**
				Sex	p=0.1042 "F (1, 45) = 2.751"

Table 4.1 Response to Hot Plate in *Scn9a*$^{R185X/wt}$ mice at 2- and 6-month-age.

Figure	Test: Hot Plate Duration of coping reactions		Analysis	Groups	Statistics
Figure 4.1C	2-mo females	48 ℃	Unpaired t-test two-tailed	***+/+ vs R185X/+***	**p=0.0136**
Figure 4.1C		52 ℃	Mann-Whitney test two-tailed	*+/+ vs R185X/+*	p=0.6490
Figure 4.1C		56 ℃	Mann-Whitney test two-tailed	*+/+ vs R185X/+*	p=0.4849
Figure 4.1D	2-mo males	48 ℃	Unpaired t-test two-tailed	*+/+ vs R185X/+*	p=0.2107
Figure 4.1D		52 ℃	Mann-Whitney test two-tailed	*+/+ vs R185X/+*	p=0.9674
Figure 4.1D		56 ℃	Mann-Whitney-test two-tailed	*+/+ vs R185X/+*	p=0.9358
Figure 4.1C	6-mo females	48 ℃	Mann-Whitney test two-tailed	*+/+ vs R185X/+*	p=0.4244
Figure 4.1C		52 ℃	Mann-Whitney test two-tailed	*+/+ vs R185X/+*	p=0.3607
Figure 4.1C		56 ℃	Unpaired t-test two-tailed	*+/+ vs R185X/+*	p=0.5909
Figure 4.1D	6-mo males	48 ℃	Mann-Whitney test two-tailed	*+/+ vs R185X/+*	p=0.8931
Figure 4.1D		52 ℃	Mann-Whitney test two-tailed	*+/+ vs R185X/+*	p>0.9999
Figure 4.1D		56 ℃	Mann-Whitney-test two-tailed	*+/+ vs R185X/+*	p=0.5997

Table 4.2 Response to Acetone and Cold plate in *Scn9a*$^{R185X/wt}$ mice at 2- and 6-month-age.

Figure	Test		Analysis	Groups	Statistics
Figure 4.2A	Acetone test Duration of lick and flick		Three-way ANOVA	Genotype	p=0.3238 "F (1, 90) = 0.9844"
				Sex	**p=0.0216** **"F (1, 90) = 5.468"**
				Age	p=0.2535 "F (1, 90) = 1.321"
Figure 4.2A	2-mo		Two-way ANOVA	Genotype	p=0.7881 "F (1, 45) = 0.07310"
				Sex	p=0.1120 "F (1, 45) = 2.628"
Figure 4.2A	6-mo		Two-way ANOVA	Genotype	p=0.2051 "F (1, 45) = 1.653"
				Sex	p=0.0981 "F (1, 45) = 2.854"
Figure 4.2A	2-mo	females	Mann-Whitney test two-tailed	*+/+ vs R185X/+*	p=0.4846
Figure 4.2A		males	Mann-Whitney test two-tailed	*+/+ vs R185X/+*	p=0.5007
Figure 4.2A	6-mo	females	Mann-Whitney test two-tailed	*+/+ vs R185X/+*	p=0.4244
Figure 4.2A		males	Mann-Whitney test two-tailed	*+/+ vs R185X/+*	p=0.4918
Figure 4.2B	Cold Plate 5 ℃ Latency		Three-way ANOVA	Genotype	p=0.6284 "F (1, 90) = 0.2359"
				Sex	p=0.9271 "F (1, 90) = 0.008418"
				Age	p=0.9651 "F (1, 90) = 0.001923"
Figure 4.2B	2-mo		Two-way ANOVA	Genotype	p=0.9981 "F (1, 45) = 5.500e-006"
				Sex	p=0.6399 "F (1, 45) = 0.2219"
Figure 4.2B	6-mo		Two-way ANOVA	Genotype	p=0.5083 "F (1, 45) = 0.4446"
				Sex	p=0.7506 "F (1, 45) = 0.1023"
Figure 4.2B	2-mo	females	Mann-Whitney test two-tailed	*+/+ vs R185X/+*	p=0.4562
Figure 4.2B		males	Mann-Whitney test two-tailed	*+/+ vs R185X/+*	p=0.5999
Figure 4.2B	6-mo	females	Mann-Whitney test two-tailed	*+/+ vs R185X/+*	p=0.8176
Figure 4.2B		males	Mann-Whitney test two-tailed	*+/+ vs R185X/+*	p=0.8066

Table 4.2 Response to Acetone and Cold plate in *Scn9a*$^{R185X/wt}$ mice at 2- and 6-month-age.

Figure	Test		Analysis	Groups	Statistics
Figure 4.2C	Cold Plate 5 ℃ Duration of paw lift		Three-way ANOVA	Genotype	p=0.9599 "F (1, 90) = 0.002547"
				Sex	p=0.9273 "F (1, 90) = 0.008370"
				Age	p=0.6982 "F (1, 90) = 0.1514"
Figure 4.2C	2-mo		Two-way ANOVA	Genotype	p=0.2452 "F (1, 45) = 1.386"
				Sex	p=0.7997 "F (1, 45) = 0.06512"
Figure 4.2C	6-mo		Two-way ANOVA	Genotype	p=0.1705 "F (1, 45) = 1.940"
				Sex	p=0.6745 "F (1, 45) = 0.1787"
Figure 4.2C	2-mo	females	Mann-Whitney test two-tailed	*+/+ vs R185X/+*	p>0.9999
Figure 4.2C		males	Mann-Whitney test two-tailed	*+/+ vs R185X/+*	p=0.4613
Figure 4.2C	6-mo	females	Mann-Whitney test two-tailed	*+/+ vs R185X/+*	p=0.6034
Figure 4.2C		males	Mann-Whitney test two-tailed	*+/+ vs R185X/+*	p=0.7616
Figure 4.2D	Cold Plate 0 ℃ Number of paw lifts		Three-way ANOVA	Genotype	p=0.1029 "F (1, 90) = 2.716"
				Sex	p=0.8126 "F (1, 90) = 0.05651"
				Age	p=0.0759 "F (1, 90) = 3.224"
Figure 4.2D	2-mo		Two-way ANOVA	Genotype	p=0.5536 "F (1, 45) = 0.3562"
				Sex	p=0.9362 "F (1, 45) = 0.006482"
Figure 4.2D	6-mo		Two-way ANOVA	**Genotype**	**p=0.0212** **"F (1, 45) = 5.704"**
				Sex	p=0.7349 "F (1, 45) = 0.1161"
Figure 4.2D	2-mo	females	Mann-Whitney test two-tailed	*+/+ vs R185X/+*	p=0.1925
Figure 4.2D			Mann-Whitney test two-tailed	*+/+ vs R185X/+*	p=0.7647
Figure 4.2D	6-mo	males	Mann-Whitney test two-tailed	***+/+ vs R185X/+***	**p=0.0374**
Figure 4.2D			Mann-Whitney test two-tailed	*+/+ vs R185X/+*	p=0.2178

Table 4.2 Response to Acetone and Cold plate in *Scn9a*$^{R185X/wt}$ mice at 2- and 6-month-age..

Figure	Test		Analysis	Groups	Statistics
Figure 4.2E	Cold Plate 0 ℃ Latency		Three-way ANOVA	Genotype	p=0.6322 "F (1, 90) = 0.2307"
				Sex	p=0.4226 "F (1, 90) = 0.6489"
				Age	p=0.8381 "F (1, 90) = 0.04201"
Figure 4.2E	2-mo		Two-way ANOVA	Genotype	p=0.8601 "F (1, 45) = 0.03140"
				Sex	p=0.9746 "F (1, 45) = 0.001022"
Figure 4.2E	6-mo		Two-way ANOVA	Genotype	p=0.4022 "F (1, 45) = 0.7152"
				Sex	p=0.2527 "F (1, 45) = 1.343"
Figure 4.2E	2-mo	females	Mann-Whitney test two-tailed	*+/+ vs R185X/+*	p=0.7224
Figure 4.2E		males	Mann-Whitney test two-tailed	*+/+ vs R185X/+*	p=0.8918
Figure 4.2E	6-mo	females	Mann-Whitney test two-tailed	*+/+ vs R185X/+*	p=0.3337
Figure 4.2E		males	Mann-Whitney test two-tailed	*+/+ vs R185X/+*	p=0.4553
Figure 4.2F	Cold Plate 0 ℃ Duration of paw lift		Three-way ANOVA	Genotype	p=0.0647 "F (1, 90) = 3.497"
				Sex	p=0.9581 "F (1, 90) = 0.002779"
				Age	p=0.1911 "F (1, 90) = 1.735"
Figure 4.2F	2-mo		Two-way ANOVA	Genotype	p=0.2952 "F (1, 45) = 1.122"
				Sex	p=0.9033 "F (1, 45) = 0.01492"
Figure 4.2F	6-mo		Two-way ANOVA	Genotype	p=0.1048 "F (1, 45) = 2.740"
				Sex	p=0.9482 "F (1, 45) = 0.004269"
Figure 4.2F	2-mo	females	Mann-Whitney test two-tailed	*+/+ vs R185X/+*	p=0.5587
Figure 4.2F		males	Mann-Whitney test two-tailed	*+/+ vs R185X/+*	p=0.2170
Figure 4.2F	6-mo	females	Mann-Whitney test two-tailed	***+/+ vs R185X/+***	**p=0.0303**
Figure 4.2F		males	Mann-Whitney test two-tailed	*+/+ vs R185X/+*	p=0.8811

V General Discussion

1. Aims of the thesis

During my Ph.D. thesis project, I achieved the following objectives:

1. To establish two mouse models simultaneously by using the Crispr/Cas9 technology: (1) the mouse model for the R185H mutation in *Scn9a* gene encoding NAV1.7 sodium channel, by HDR repair, and (2) a mouse model for heterozygous Scn9a gene knockout, through the NHEJ pathway. The off-target effect was tested with no consequence found on the two mouse models.
2. To characterize these two mouse models using biochemical, genetic, behavioral neuro-physiology, and neuropathology assays.

2. Generation of CRISPR-Cas9 *Scn9a*^{R185H} and *Scn9a*$^{R185X/wt}$ Mice

We successfully established a pain-related sodium channel CRISPR-Cas9 mouse model for S*cn9a*^{R185H} as well as the *Scn9a*$^{R185X/wt}$ mutant mouse line. Since off-target effects concern the CRISPR-Cas9 system [130, 131], we selected seven interesting predicted off-target sites to test, including five genes encoded NAV sodium channels and two intergenic genes. Fortunately, we did not find any off-target in our project.

The bacterial CRISPR-Cas9 system allows sequence-specific gene editing in many organisms and holds promise as a tool to generate models of human diseases, for example, in human pluripotent stem cells. CRISPR/Cas9 introduces targeted double-stranded breaks (DSBs) with high efficiency, which are typically repaired by non-homologous end-joining (NHEJ), resulting in non-specific insertions, deletions, or other mutations (indels). Paquet [132] et al. found that homozygous introduction requires a guide RNA targeting close to the intended mutation, whereas heterozygous introduction can be accomplished by distance-dependent suboptimal mutation incorporation or by use of mixed repair templates. In our project, part of the guide RNA was located at the mutation site we wished to obtain, and PAM sequence just ahead of the mutation. We got a high rate of mutation editing and also three homozygous F0 founders. However, partial incorporation of the donor ssODN at the target site may also occur. Thus, we confirmed, by Sanger sequencing of PCR amplicons of the targeted locus when we screen potential F0 founders and F1 founders. that no other sequence changes occurred in the vicinity.

It is known that traditional pharmacological studies in sodium channels are difficult because currently available blockers do not distinguish between the different sodium channel subtypes. Although studies with small interfering RNAs (siRNAs) and antisense deoxynucleotides (ASODNs) can be used, they can have non-specific effects. CRISPR-Cas9 is a popular gene-editing tool; it can be used to generate point mutations (knock-in models) and can also produce gene deletion and therefore knockout models. There are two methods to generate a knockout model. Generating tailored deletions is achieved through the co-injection of sgRNAs targeting the sequences flanking the segment to delete. Using the introduction of indels to the targeted gene's coding frame leads to changes in the target gene expression, including genetic knockdown. However, for the NAV1.7 sodium channel, a global null mutant was found to die shortly after birth in a first study that used the C57BL/6 genetic background [129]. In our project, we used the second method

to create a novel *Scn9a* heterozygous knockout model. Therefore, the CRISPR-Cas9 system could be used to produce knockout and knockin models at the same time.

However, Fu et al. [130] and Mali et al. [133] reported that the specificity of the Cas9-gRNA complex had raised fears on cutting of "off-target" sites by the CRISPR-Cas9 system where Cas9-gRNA complexes are able to cut non-target sites that differ from the actual target site by 1-5 base pairs. Although the cutting of these off-target sites is orders of magnitude rarer than "on-target" sites, this phenomenon has raised concerns about the use of CRISPR-Cas9 technologies. However, recent studies have gone some way to addressing this issue. In mammals, The NAV channel family contains nine α membrane proteins distributed in different excitable tissues. Our predicted off-target sites were in 5 sodium channel encoding genes and two intergenic genes, *Scn1a*, *Scn3a*, *Scn4a*, *Scn5a* and *Scn11a*, and *Tshz3-Zfp536*, *Nipsnap3b-Abca1* with two mismatches. Nine genes (*Scn1a-Scn5a* and *Scn8a-Scn11a*) encode the diverse pore-forming sodium channel α-subunits that show distinct expression patterns and biophysical and pharmacological properties. SCN1A, like SCN9A, is expressed in adult peripheral sensory neurons and is blocked by nanomolar concentrations of the neurotoxin tetrodotoxin (TTX-S). SCN3A, another TTX-S channel, is predominantly expressed in embryonic sensory neurons but is up-regulated following traumatic or metabolic nerve injury in rodent DRG neurons. SCN11A is preferentially expressed in small-diameter (<30 μm diameter) DRG neurons, trigeminal ganglion neurons, including functionally identified nociceptors, and intrinsic myenteric neurons. Recently, several GOF mutations in SCN11A were reported in patients with pain disorders. When studied in cultured DRG neurons, these mutations led to massive hyperpolarizing shift inactivation, increased amplitude of ramp current, and slower deactivation [103]. SCN4A is the pore-forming subunit of the primary sodium channel present in skeletal muscles, related to channelopathies affecting skeletal muscle excitability. SCN5A is the pore-forming subunit of the cardiac sodium channel and is related channelopathies affecting cardiac excitability. Recently, gain or loss of function mutation of SCN4A and SCN5A have been found in muscular and cardiac channelopathies, respectively [134]. We therefore hypothesized that destructive influence would happen in *Scn9a*^{R185H} and Scn9a$^{R185X/wt}$ mouse lines if one or several off-targets mutations occur also in these sodium channel genes. Therefore, we selected these seven genes to analyze for mutations at these potential off-target sites. Fortunately, no mutation was found at these off-target sites in the F1 founder of each line. This result corroborated the results from Lyer, V. et al. [135] publication that off-target mutations are rare in Cas9-modified mice.

3. *Scn9a* mRNA expression in *Scn9a*^{R185H} and *Scn9a*$^{R185X/wt}$ mutant mice

On a molecular basis, the *Scn9a* mRNA is mainly expressed in DRG and less expressed spinal cord, brain, and cerebellum in *Scn9a*^{R185H} mutant mice. The SCN9A protein is expressed in DRG and sciatic nerves and mainly distributed in all size neurons. No alteration of *Scn9a* mRNA expression was detected in *Scn9a*^{R185H} mutant mice, suggesting that pain behavioral changes would not be caused by an altered SCN9A expression level.

In *Scn9a*^{R185X} mutants *Scn9a*^{wt} was expressed normally in DRG, and spinal cord, but *Scn9a*^{R185X} expression was reduced as compared to *Scn9a*^{wt} expression in heterozygote female and male carriers. Thus, this 2-nt deletions in *Scn9a* lead to mRNA degradation certainly through mRNA synthesis decay, which function is to reduce gene expression by discarding transcripts that contain premature stop codons.

4. Pain sensitivity in *Scn9a*^{R185H} and *Scn9a*$^{R185X/wt}$ mutant mice

We have already discussed my results in the paper manuscript. Here, I will briefly discuss our behavioral results. To investigate whether *Scn9a*^{R185H} and *Scn9a*$^{R185X/wt}$ mutant mice have pain-related phenotypes, the mutant mice were analyzed in a battery of pain-related behavioral tests of sensitivity to thermal and mechanical stimuli in young adult. The pain-related phenotype in *Scn9a*^{R185H} mutant mice, especially in homozygous female mice, mimicked the abnormal pain sensitivity in SFN patients carrying the same heterozygous mutation, indicating this mutation need more gene dose in mice. The loss-of-function of *SCN9A* by bi-allelic inactivating mutations results in the striking clinical phenotype of congenital insensitivity to pain (CIP) [88, 96]. The CIP individuals do not perceive pain in response to noxious stimuli. However, the carriers of one allelic inactivating mutation have normal pain sensitivity. Potential novel gene therapies may be developed for relieving pain in GOF SCN9A SFN patients by inactivating the gain-of-function mutant allele according to normal phenotype in the CIP carriers. In order to evaluate whether one *Scn9a* allele only can provide SCN9A function in mice at a correct physiological level, we developed a novel heterozygous *Scn9a* KO model (*Scn9a*$^{R185X/wt}$) and studied the pain behaviors of these mutants. We did not find any abnormal pain behaviors in the *R185X/+* males (Fig. 4D), and the female mutants showed only reduced response in some parameters of the hot plate test (Fig. 4C, Supplementary Fig. 6C, D). This result indicates that the inactivation of one *Scn9a* allele alters the hot plate assay's parameters in these mutant mice and not all other pain behavioral responses.

In the hot plate, when measuring jump latency at 56°C in *Scn9a*^{R185H} and *Scn9a*$^{R185X/wt}$ mutant mice, we observed that the female WT baselines in two mutant lines are different. The female *Scn9a*$^{R185X/wt}$ WT mice are more sensitive compare to *Scn9a*^{R185H} female WT. As this behavior is only found in female mice, we consider that it might be due to a batch effect with higher variability.

5. Sex effect on behavioral phenotypes

Clinical and epidemiological research indicates noticeable sex differences in pain perception, pain-related diseases, and analgesic effectiveness. Women exhibit a higher incidence of chronic pains and lower tolerance to pain than men, which may be attributed to gonadal hormones, endogenous analgesic matter, and sociopsychological factors [136]. This phenomenon is also reported in rodents, and more pain studies in rodents used both female and male animals [137]. In this study, sex differences were also found in the pain phenotypes of *Scn9a*-R185H mutant mice. The female homozygous mice are more sensitive than males. Although it is not known whether there is a gender difference in SFN patients carrying *SCN9A* mutations, we already discussed gender differences in different clinical studies of SFN disorder in the manuscript (see part X). The gender difference, if present or not, highly depends on the clinical cohorts or studies. In the preclinic study, nutrition-induced diabetic neuropathic mice showed differential sensitivity to pain between male and female mice. These findings suggest differential processing mechanisms in each sex, and it is essential to consider sex differences when exploring novel analgesics.

VI Perspectives

1. Spontaneous pain and emotional consequences of pain

Measures of reflexive behaviors such as withdrawal thresholds to noxious stimuli have been used for decades to examine pain mechanisms. However, pain is a multidimensional sensory-discriminative, cognitive, and affective experience, and it is useful to have measures that assess spontaneous pain behaviors.

The most common measure of spontaneous pain behavior is the quantification of paw elevation and paw licking following injection of an inflammatory compound, such as formalin, capsaicin, and mustard oil [138]. Preference for analgesics can also be investigated using the conditioned place preference (CPP) has been tested in models of neuropathic and inflammatory pain. In inflammation models, unilateral injection of formalin or carrageenan reduced the CPP effects of morphine. In neuropathic pain models, rats carrying a partial ligation of the sciatic nerve to induce chronic neuropathic pain also showed a reduced CPP response to morphine [139].

Moreover, chronic pain patients are highly prevalent with mood, anxiety, and somatic symptom disorders. Over time, different anxiety and depression tests have been used in rodents to study the emotional consequences of chronic pain. A series of anxiety-like and depression-like behaviors have been used in different chronic pain animal models. One of the most widely used tests to assess rodents' anxiety-like behaviors is the elevated plus maze (EPM). The successful presence of anxiety-like behaviors by EPM has been shown in both mouse and rat pain models. Furthermore, more other anxiety-like behavioral tests were also studied in pain animal models, such as elevated zero maze (EZM), open field (OF), Light/dark box test and Marble burying test, hole-board test as well. Novelty-suppressed feeding test can be assessed both anxiety- and depressive-like behaviors. More useful and exciting information focusing on studying anxiety and depression in chronic pain rodent models could found in the review by Kremer M. et al., 2020 [140].

It would be very interesting to record spontaneous pain, anxiety and depression in our mutant mice, but unfortunately, there was not enough time to do them during my PhD project. Project partner will continue to explore if there are spontaneous pain, anxiety and depression phenotypes in our mutant mice.

2. Small fiber neuropathy in mutant mice

2.1 IENFD

The skin is our largest sensory organ, transmitting pain, temperature, itch, and touch information to the central nervous system. Mammalian skin comprises both hairy and non-hairy, or glabrous, skin. Hairy skin covers more than 90% of the body surface and is strongly associated with the affective touch that evokes an emotional response, such as during nurturing. Glabrous skin is predominantly found on the hands and feet of most mammals. It is specialized for discriminative touch, determining texture and shape to recognize objects accurately, and providing feedback to the central nervous system to mediate proper grip control, reaching, and locomotion [141, 142].

Reduced IENFD has been reported to correlate with pain severity, health status, and function. Recently, the value of skin biopsy with IENFD in patients is generally considered the "gold standard" for the SFN diagnosis, although a real gold standard for SFN is lacking [143]. Intra-epidermal nerve fibers (IENF) are unmyelinated sensory endings with the exclusive somatic function that arises from nerve bundles of the subpapillary dermis. In the clinic, a skin biopsy is commonly taken with a 3-mm disposable punch from the lower leg, 10 cm proximal from the lateral malleolus, within the sural nerve's territory. Protein gene product (PGP9.5) as IENFs maker was used to evaluate the IENFD value by quantifying the number of fibers crossing the dermal-epidermal junctions per length of the section [144]. Age- and gender-adjusted normative values have been reported for the clinical use of IENFD in skin biopsy. The reduced length of dermal nerves has been reported in SFN patients [145]. The subpapillary dermis contains most of the bundles running parallel to the dermal-epidermal junction from which a single IENF arises. Dermal nerves were quantified in this area. Additionally, new techniques, such as automated PGP9.5 immunofluorescence staining[146] and 3D analysis [147], have been reported to determine the IENFD.

IENFD in the skin also has been used in animal studies. Peripheral neuropathy is one of the most common and severe complications of type-2 diabetes. In the type-2 diabetic mice model, the number of IENFD was significantly reduced [62] [148]. Generally, the skin of hind paws (footpad and glabrous skin) was evaluated for IENFD in rodent models; less forepaw or hair skin was used. It is coincident that many classical behavioral assessments of rodent sensation, such as the Hargreaves test or von Frey hairs, are actually carried out by stimulating the glabrous skin. Whereases rodent's forepaws use to explore their environment, for example, selecting food objects or engaging in grooming behavior. Furthermore, one study indicated that there are different mechanoreceptors between hind paw glabrous and hairy skin [149].

Two patients with *SCN9A*-R185H mutation have been reported reduced IENFD in the sural nerve of the leg. In CIP patients, compound heterozygous mutations in *SCN9A* were predicted to cause loss of protein function, which showed a reduction of IENFD in the lower leg [98, 117, 126]. Contrastingly, in the loss function of *Scn9a* mice [150] and rat [151] model, there was no difference between WT and heterozygous and knockouts. However, in this study, the IENFD in $Scn9a^{R185H}$ and $Scn9a^{R185X/wt}$ mutant mice skin is not clear. At present, more data of IENFD in these mutant mice of skin need to be collected. These data will be helpful to explain more/less pain sensitivity found in mutant mice if it is caused by small fiber neuropathy or not.

2.2 Microneurography

Repetitive firing in axons can lead to their sub-excitability and reduced conduction velocity as prolonged hyperpolarization. Microneurography was used to record activity-dependent changes in membrane potential and conduction velocity in unmyelinated fibers [152]. Stimulating repetitively could segregate C fibers into discrete groups, and these differences were used to determine the functional class of fiber in humans and rodents [153, 154]. Cutaneous C fibers were classified, based primarily on their activity-dependent slowing profile, as Type 1A (mechano-responsive nociceptors; CMR), Type 1B (mechano-insensitive nociceptors; CMI), Type 2 (cold units), Type 3 units (unknown function) or Type 4 (presumed sympathetic) units [6].

C-nociceptors do not generally fire action potentials unless challenged by adequate noxious stimuli. However, in pathological states, nociceptors may become hyperexcitable and may generate spontaneous ectopic discharges. Microneurographic recordings have identified spontaneous activity in C-nociceptors in neuropathic pain states in humans and rats [155]. Additionally, in diabetic patients with small fiber neuropathy, the ratio of mechano-responsive to mechano-insensitive nociceptors was 1:2 as compared to a 2:1 ratio in the healthy controls [156]. Furthermore, patients showed a fairly large percentage of C-fibers resembling mechano-responsive nociceptors that had lost their mechanical and heat responsiveness. This condition indicated a loss of polymodal nociceptors function and might help to explore typical mechanisms responsible for small fiber dysfunction [152]. In type-2 diabetic rat some authors also found significant alterations in several parameters of activity-dependent slowing of mechano-insensitive C-nociceptors and spontaneous activity in three different rat strains by microneurography [157]. In three CIP patients, a total of 38 C-fibers were recorded and analyzed by microneurography. Small fibers with the characteristics of C- and A-low-threshold thermoreceptors, as well sympathetic efferent, could be recorded and identified based on the profile of ADS of conduction velocity and natural activation using well-

established criteria previously. In healthy volunteers, the proportion of identified C-nociceptors using the same searching technique as those employed in this study amounts to roughly 60% of all C-fibers in the superficial peroneal nerve. Unfortunately, no microneurographic study in the loss function of *Scn9a* rodent models has been published yet.

During my Ph.D. study, *Scn9a*^{R185H} mutant mice have been analyzed by microneurography with the project partner Neuroscience Technology company. The results still need to be analyzed.

2.3 Peripheral nerve morphology

Nerve biopsy is the removal of a small piece of a nerve for examination. Though a small incision, a sample of the nerve is removed and examined under a microscope. Nerve biopsy may be performed to identify nerve degeneration, identify inflammatory nerve conditions (neuropathies), or confirm specific diagnoses. The study of peripheral nerve morphology on nerve biopsy is often the final step in the diagnostic work-up of unknown origin's neuropathies, and its diagnostic yield is still debated [158]. The neuropathy level was based on histopathological findings categorized as either nonspecific (axonal degeneration, segmental demyelination, and mixed axonal/demyelinating) or specific (vasculitis neuropathy, leprous neuropathy, and inflammatory neuropathy).

For our mutant mice, light and electron microscopy analysis with morphometry of transverse sections of the sciatic nerve will provide more information and reveal whether the pain sensitivity phenotype found in mutant mice is due to abnormality in peripheral nerve neuropathy or not. Furthermore, changes in the extracellular space within the peripheral nerve and/or change in the non-neuronal connective tissue surrounding the axons may also contribute to small nerve neuropathy. One study already addressed how cutaneous glia (Schwann cells) distribute and interact with nociceptive nerve terminals using different genetic labeling [159]. They found that Schwann cells, which are intimately associated with unmyelinated nociceptive nerves, are inherently mechanosensitive and transmit nociceptive information to the nerve [159]. Besides, chronic inflammatory demyelinating polyneuropathy has also been involved in diabetic neuropathy patients, not infrequent neuropathy. Chronic inflammatory demyelinating polyneuropathy is a heterogeneous progressive or relapsing-remitting, immune-mediated disorder of the peripheral nervous system with an estimated prevalence of 1-8.9 per 100,000 population [160]. Patients with chronic inflammatory demyelinating polyneuropathy typically present with progressive weakness in both proximal and distal muscles, areflexia, sensory symptoms with proximal weakness, and preferential loss of sensation for vibration or joint position [160]. However, in our mutant mice, no abnormal muscle strength was found. Thus, further research will explore whether small fiber neuropathy,

microenvironment and chronic inflammatory demyelinating polyneuropathy are found in *Scn9a*$^{R185H/+}$ and *Scn9a*$^{R185X/+}$mutant mice.

3. Autonomic dysfunction symptoms

Changes in peripheral autonomic nervous system function may be an early manifestation in SFN. Dysfunction of the sudomotor system may increase or decrease sweat production, resulting in thermoregulation [143]. Several tests for SFN patients are already described in the Introduction part. The autonomic symptoms also include dry eyes, dry mouth, palpitations, orthostatic hypotension, constipation, urinary retention, sexual dysfunction, sweating abnormalities, and skin discoloration. Only one SFN patient with *SCN9A* R185H mutation showed autonomic symptoms with dry mouth and orthostatic dizziness with minimal autonomic dysfunction. The functional profiles of *SCN9A* variants show that R185H mutation does not produce detectable changes in sympathetic ganglion neurons' properties, while I739V, from patients with severe autonomic dysfunction, has a profound effect on the excitability of sympathetic ganglion neurons [107].

In rodent animal studies, it is challenging to measure dry mouth and orthostatic dizziness. Additionally, the symptoms in patients are variable with the same mutations, and therefore it is difficult to predict whether there are autonomic dysfunction phenotypes in mice. We did not find visible autonomic dysfunction phenotype in our mutant mice, although we did not investigate the same autonomic functions as in the clinics. Other advanced techniques will help provide more information and explorations of autonomic dysfunction mechanisms in our mutant mice.

4. Glial cell activation in the spinal cord

Growing studies have identified glial cell activation in the spinal cord, including microglia and astrocytes, as integral mediators in chronic pain.

Microglia, which are known as tissue-resident macrophages in the central nervous system, represent 5-10% of the spinal cord cells. Recently, various studies have shown that microglia activation is involved in the development and maintenance of neuropathic pain. After nerve injury, differentiation and proliferation of the spinal macrophage/microglia take place. In a normal adult, microglia presented small cell bodies bearing branched and motile processes. After activation, the cell body changed to hypertrophy, and the processes thickened and retracted. Additionally, the cell number and staining markers (CD11b, Iba1, and OX-42) are also increased. Toll-like receptors, ATP combined purinergic receptors, and other numerous receptors expressed on the microglia, are crucial for microglia to activate and exchange information between glia and neurons.

Activated microglia release many nociceptive factors by responding to many intracellular cascades' reaction in the early pathological state of chronic pain.

In general, astrocytes activation is thought to occur latter and last longer than microglia activation in neuropathic pain. Plenty of evidence has indicated that communication among astrocytes, microglia, and neurons is critical in the spinal cord following peripheral nerve damage. Previous studies implied that astrocytes participated in various actions, for instance, synaptic transmission and plasticity, synaptogenesis, tissue or nerve injury, and cell proliferation. Morphological changes accompany astrocytes activation. They include cell body size changed to larger, and the cell processes become thicker and form glial scar. The astrocyte marker GFAP is expressed at higher level. Activated astrocytes stimulate neuropathic pain via releasing a lot of pro-inflammatory factors, activating some signal pathways, and communicating with microglia and neuron in the spinal cord. IL-1β is recognized as a significant pro-inflammatory cytokine and released from astrocytes following bone cancer, nerve injury, and inflammatory reaction.

However, the role of SCN9A in spinal glia activation in chronic pain animal models is not known. As *Scn9a*^{R185H} mutant mice show increased pain sensitivity and this mutation was shown to render DRG neurons hyperexcitable, these hyperactivated neurons may in turn activate glial cells, it would be interested to investigate whether glial activation occurs in our mutant mice.

VII Conclusions

In this study, we first successfully established the *Scn9a*^{R185H} mouse model, which is modeling the human *SCN9A*^{R185H} mutation found in SFN patients with chronic pain, by using the CRISPR-Cas9 technique. We used this model to explore the p.R185H genotype-phenotype association and the mechanism of Nav1.7 sodium channel mutation in idiopathic SFN. These two mouse lines showed no alteration of growth, survival and global health state. We found that there is no significant difference in *Scn9a* mRNA expression levels in DRG, spinal cord, and brain in *Scn9a*^{R185H} mice. Pain sensitivity of the in *Scn9a*^{R185H} mutant line was investigated on both sexes using behavioral tests of sensitivity to thermal and mechanical stimuli. Our results indicate that *Scn9a*^{R185H} mice show increased pain sensitivity, suggesting that the *Scn9a*^{R185H} mutation identified in the SFN patients contributes to their pain symptoms. This exploration will benefit to drug screen. We also successfully established the *Scn9a*^{R185H} mouse model. *Scn9a*$^{R185X/wt}$ mice showed normal pain sensitivity to mechanical stimuli, and normal pain sensitivity to heat except in one test. In these mice, one Scn9a allele is not functional, indicating that one Scn9a functional allele is sufficient for pain sensitivity in most of the behavioral tests investigated. Therefore, we provide more evidence that Nav1.7 encoded by *SCN9A* gene plays an important role in nociception and in painful SFN.

VIII References

1. Raja, S.N., et al., *The revised International Association for the Study of Pain definition of pain: concepts, challenges, and compromises.* Pain, 2020.
2. Yam, M.F., et al., *Overview of Neurological Mechanism of Pain Profile Used for Animal "Pain-Like" Behavioral Study with Proposed Analgesic Pathways.* Int J Mol Sci, 2020. **21**(12).
3. in *Pain and Disability: Clinical, Behavioral, and Public Policy Perspectives*, M. Osterweis, A. Kleinman, and D. Mechanic, Editors. 1987: Washington (DC).
4. Yam, M.F., et al., *General Pathways of Pain Sensation and the Major Neurotransmitters Involved in Pain Regulation.* Int J Mol Sci, 2018. **19**(8).
5. Prescott, S.A., Q. Ma, and Y. De Koninck, *Normal and abnormal coding of somatosensory stimuli causing pain.* Nat Neurosci, 2014. **17**(2): p. 183-91.
6. George, A., et al., *Velocity recovery cycles of single C fibres innervating rat skin.* J Physiol, 2007. **578**(Pt 1): p. 213-32.
7. Wood, J.N., A.J. Todd, and F. Wang, *Central Nervous System Pain Pathways*, in *The Oxford Handbook of the Neurobiology of Pain*. 2020. p. 414-444.
8. Sharif, B., et al., *Differential Coding of Itch and Pain by a Subpopulation of Primary Afferent Neurons.* Neuron, 2020.
9. Peirs, C., R. Dallel, and A.J. Todd, *Recent advances in our understanding of the organization of dorsal horn neuron populations and their contribution to cutaneous mechanical allodynia.* J Neural Transm (Vienna), 2020. **127**(4): p. 505-525.
10. Zheng, Y., et al., *Deep Sequencing of Somatosensory Neurons Reveals Molecular Determinants of Intrinsic Physiological Properties.* Neuron, 2019. **103**(4): p. 598-616 e7.
11. Haring, M., et al., *Neuronal atlas of the dorsal horn defines its architecture and links sensory input to transcriptional cell types.* Nat Neurosci, 2018. **21**(6): p. 869-880.
12. Li, C.L., et al., *Somatosensory neuron types identified by high-coverage single-cell RNA-sequencing and functional heterogeneity.* Cell Res, 2016. **26**(1): p. 83-102.
13. Usoskin, D., et al., *Unbiased classification of sensory neuron types by large-scale single-cell RNA sequencing.* Nat Neurosci, 2015. **18**(1): p. 145-53.
14. Grace, P.M., et al., *Pathological pain and the neuroimmune interface.* Nat Rev Immunol, 2014. **14**(4): p. 217-31.
15. Armstrong, S.A. and M.J. Herr, *Physiology, Nociception*, in *StatPearls*. 2020: Treasure Island (FL).
16. Deuis, J.R., L.S. Dvorakova, and I. Vetter, *Methods Used to Evaluate Pain Behaviors in Rodents.* Front Mol Neurosci, 2017. **10**: p. 284.
17. Barrot, M., *Tests and models of nociception and pain in rodents.* Neuroscience, 2012. **211**: p. 39-50.
18. Yalcin, I., et al., *Differentiating thermal allodynia and hyperalgesia using dynamic hot and cold plate in rodents.* J Pain, 2009. **10**(7): p. 767-73.
19. Huang, T., et al., *Identifying the pathways required for coping behaviours associated with sustained pain.* Nature, 2019. **565**(7737): p. 86-90.

20. Bokiniec, P., et al., *The neural circuits of thermal perception.* Curr Opin Neurobiol, 2018. **52**: p. 98-106.
21. Minett, M.S., K. Quick, and J.N. Wood, *Behavioral Measures of Pain Thresholds.* Curr Protoc Mouse Biol, 2011. **1**(3): p. 383-412.
22. Pogorzala, L.A., S.K. Mishra, and M.A. Hoon, *The cellular code for mammalian thermosensation.* J Neurosci, 2013. **33**(13): p. 5533-41.
23. Castillo, K., et al., *Thermally activated TRP channels: molecular sensors for temperature detection.* Phys Biol, 2018. **15**(2): p. 021001.
24. Vriens, J., B. Nilius, and T. Voets, *Peripheral thermosensation in mammals.* Nat Rev Neurosci, 2014. **15**(9): p. 573-89.
25. Huang, S.M., et al., *TRPV3 and TRPV4 ion channels are not major contributors to mouse heat sensation.* Mol Pain, 2011. **7**: p. 37.
26. Vriens, J., et al., *TRPM3 is a nociceptor channel involved in the detection of noxious heat.* Neuron, 2011. **70**(3): p. 482-94.
27. MacDonald, D.I., J.N. Wood, and E.C. Emery, *Molecular mechanisms of cold pain.* Neurobiol Pain, 2020. **7**: p. 100044.
28. Bautista, D.M., et al., *The menthol receptor TRPM8 is the principal detector of environmental cold.* Nature, 2007. **448**(7150): p. 204-8.
29. Ran, C., M.A. Hoon, and X. Chen, *The coding of cutaneous temperature in the spinal cord.* Nat Neurosci, 2016. **19**(9): p. 1201-9.
30. Story, G.M., et al., *ANKTM1, a TRP-like channel expressed in nociceptive neurons, is activated by cold temperatures.* Cell, 2003. **112**(6): p. 819-29.
31. Bautista, D.M., M. Pellegrino, and M. Tsunozaki, *TRPA1: A gatekeeper for inflammation.* Annu Rev Physiol, 2013. **75**: p. 181-200.
32. Jensen, T.S. and N.B. Finnerup, *Allodynia and hyperalgesia in neuropathic pain: clinical manifestations and mechanisms.* Lancet Neurol, 2014. **13**(9): p. 924-35.
33. Abrahamsen, B., et al., *The cell and molecular basis of mechanical, cold, and inflammatory pain.* Science, 2008. **321**(5889): p. 702-5.
34. Ghitani, N., et al., *Specialized Mechanosensory Nociceptors Mediating Rapid Responses to Hair Pull.* Neuron, 2017. **95**(4): p. 944-954 e4.
35. Hill, R.Z. and D.M. Bautista, *Getting in Touch with Mechanical Pain Mechanisms.* Trends Neurosci, 2020. **43**(5): p. 311-325.
36. Ranade, S.S., et al., *Piezo2 is the major transducer of mechanical forces for touch sensation in mice.* Nature, 2014. **516**(7529): p. 121-5.
37. Murthy, S.E., et al., *The mechanosensitive ion channel Piezo2 mediates sensitivity to mechanical pain in mice.* Sci Transl Med, 2018. **10**(462).
38. Beaulieu-Laroche, L., et al., *TACAN Is an Ion Channel Involved in Sensing Mechanical Pain.* Cell, 2020. **180**(5): p. 956-967 e17.
39. Arenas, O.M. and E.A. Lumpkin, *Touching Base with Mechanical Pain.* Cell, 2020. **180**(5): p. 824-826.
40. Huang, J., et al., *Circuit dissection of the role of somatostatin in itch and pain.* Nat Neurosci, 2018. **21**(5): p. 707-716.
41. Chan, A.C. and E.P. Wilder-Smith, *Small fiber neuropathy: Getting bigger!* Muscle Nerve, 2016. **53**(5): p. 671-82.

42. Devigili, G., D. Cazzato, and G. Lauria, *Clinical diagnosis and management of small fiber neuropathy: an update on best practice.* Expert Rev Neurother, 2020: p. 1-14.
43. Zhou, L., *Small Fiber Neuropathy.* Semin Neurol, 2019. **39**(5): p. 570-577.
44. Terkelsen, A.J., et al., *The diagnostic challenge of small fibre neuropathy: clinical presentations, evaluations, and causes.* Lancet Neurol, 2017. **16**(11): p. 934-944.
45. Ghasemi, M. and Y.A. Rajabally, *Small fiber neuropathy in unexpected clinical settings: a review.* Muscle Nerve, 2020. **62**(2): p. 167-175.
46. Devigili, G., et al., *Diagnostic criteria for small fibre neuropathy in clinical practice and research.* Brain, 2019. **142**(12): p. 3728-3736.
47. Sene, D., *Small fiber neuropathy: Diagnosis, causes, and treatment.* Joint Bone Spine, 2018. **85**(5): p. 553-559.
48. Cazzato, D. and G. Lauria, *Small fibre neuropathy.* Curr Opin Neurol, 2017. **30**(5): p. 490-499.
49. Themistocleous, A.C., et al., *The clinical approach to small fibre neuropathy and painful channelopathy.* Pract Neurol, 2014. **14**(6): p. 368-79.
50. Hoeijmakers, J.G., et al., *Small-fibre neuropathies--advances in diagnosis, pathophysiology and management.* Nat Rev Neurol, 2012. **8**(7): p. 369-79.
51. Devigili, G., et al., *The diagnostic criteria for small fibre neuropathy: from symptoms to neuropathology.* Brain, 2008. **131**(Pt 7): p. 1912-25.
52. Tavakoli, M., et al., *Corneal confocal microscopy: a novel means to detect nerve fibre damage in idiopathic small fibre neuropathy.* Exp Neurol, 2010. **223**(1): p. 245-50.
53. Bostock, H., et al., *Velocity recovery cycles of C fibres innervating human skin.* J Physiol, 2003. **553**(Pt 2): p. 649-63.
54. Fabry, V., et al., *Which Method for Diagnosing Small Fiber Neuropathy?* Front Neurol, 2020. **11**: p. 342.
55. Younger, D.S., *Diabetic neuropathy: a clinical and neuropathological study of 107 patients.* Neurol Res Int, 2010. **2010**: p. 140379.
56. Cox, J.J., et al., *An SCN9A channelopathy causes congenital inability to experience pain.* Nature, 2006. **444**(7121): p. 894-8.
57. Einarsdottir, E., et al., *A mutation in the nerve growth factor beta gene (NGFB) causes loss of pain perception.* Hum Mol Genet, 2004. **13**(8): p. 799-805.
58. Pham, V.M., et al., *Diabetic neuropathy research: from mouse models to targets for treatment.* Neural Regen Res, 2019. **14**(11): p. 1870-1879.
59. Sasaki, H., et al., *Spectrum of diabetic neuropathies.* Diabetol Int, 2020. **11**(2): p. 87-96.
60. Dauch, J.R., et al., *Neuron-astrocyte signaling network in spinal cord dorsal horn mediates painful neuropathy of type 2 diabetes.* Glia, 2012. **60**(9): p. 1301-15.
61. Sullivan, K.A., et al., *Mouse models of diabetic neuropathy.* Neurobiol Dis, 2007. **28**(3): p. 276-85.
62. Pham, V.M., et al., *Impaired peripheral nerve regeneration in type-2 diabetic mouse model.* Eur J Neurosci, 2018. **47**(2): p. 126-139.
63. Muller, K.A., et al., *Abnormal muscle spindle innervation and large-fiber neuropathy in diabetic mice.* Diabetes, 2008. **57**(6): p. 1693-701.

64. Shaikh, A.S. and R.S. Somani, *Animal models and biomarkers of neuropathy in diabetic rodents.* Indian J Pharmacol, 2010. **42**(3): p. 129-34.
65. Zhou, L., et al., *Metabolic syndrome in small fiber sensory neuropathy.* J Clin Neuromuscul Dis, 2011. **12**(4): p. 235-43.
66. Hoeijmakers, J.G., et al., *Painful peripheral neuropathy and sodium channel mutations.* Neurosci Lett, 2015. **596**: p. 51-9.
67. Faber, C.G., et al., *Gain of function Nanu1.7 mutations in idiopathic small fiber neuropathy.* Ann Neurol, 2012. **71**(1): p. 26-39.
68. Adams, D., et al., *First European consensus for diagnosis, management, and treatment of transthyretin familial amyloid polyneuropathy.* Curr Opin Neurol, 2016. **29 Suppl 1**: p. S14-26.
69. Bertelsen, A.K., et al., *Small fibre neuropathy in Fabry disease.* J Neurol, 2013. **260**(3): p. 917-9.
70. Dworkin, R.H., et al., *Pharmacologic management of neuropathic pain: evidence-based recommendations.* Pain, 2007. **132**(3): p. 237-51.
71. Finnerup, N.B., et al., *Pharmacotherapy for neuropathic pain in adults: a systematic review and meta-analysis.* Lancet Neurol, 2015. **14**(2): p. 162-73.
72. Cregg, R., et al., *Novel mutations mapping to the fourth sodium channel domain of Nav1.7 result in variable clinical manifestations of primary erythromelalgia.* Neuromolecular Med, 2013. **15**(2): p. 265-78.
73. Namadurai, S., et al., *A new look at sodium channel beta subunits.* Open Biol, 2015. **5**(1): p. 140192.
74. Calhoun, J.D. and L.L. Isom, *The role of non-pore-forming beta subunits in physiology and pathophysiology of voltage-gated sodium channels.* Handb Exp Pharmacol, 2014. **221**: p. 51-89.
75. Dib-Hajj, S.D. and S.G. Waxman, *Sodium Channels in Human Pain Disorders: Genetics and Pharmacogenomics.* Annu Rev Neurosci, 2019. **42**: p. 87-106.
76. Payandeh, J., et al., *The crystal structure of a voltage-gated sodium channel.* Nature, 2011. **475**(7356): p. 353-8.
77. Shen, H., et al., *Structures of human Nav1.7 channel in complex with auxiliary subunits and animal toxins.* Science, 2019. **363**(6433): p. 1303-1308.
78. Catterall, W.A., *Voltage-gated sodium channels at 60: structure, function and pathophysiology.* J Physiol, 2012. **590**(11): p. 2577-89.
79. Mantegazza, M. and W.A. Catterall, *Voltage-Gated Na(+) Channels: Structure, Function, and Pathophysiology*, in *Jasper's Basic Mechanisms of the Epilepsies*, th, et al., Editors. 2012: Bethesda (MD).
80. Yu, F.H. and W.A. Catterall, *Overview of the voltage-gated sodium channel family.* Genome Biol, 2003. **4**(3): p. 207.
81. Motoike, H.K., et al., *The Na+ channel inactivation gate is a molecular complex: a novel role of the COOH-terminal domain.* J Gen Physiol, 2004. **123**(2): p. 155-65.
82. Wang, J., S.W. Ou, and Y.J. Wang, *Distribution and function of voltage-gated sodium channels in the nervous system.* Channels (Austin), 2017. **11**(6): p. 534-554.
83. Lukowski, A.L. and A.R.H. Narayan, *Natural Voltage-Gated Sodium Channel Ligands: Biosynthesis and Biology.* Chembiochem, 2019. **20**(10): p. 1231-1241.

84. Yang, Y., et al., *Nav1.7-A1632G Mutation from a Family with Inherited Erythromelalgia: Enhanced Firing of Dorsal Root Ganglia Neurons Evoked by Thermal Stimuli.* J Neurosci, 2016. **36**(28): p. 7511-22.
85. Lai, H.C. and L.Y. Jan, *The distribution and targeting of neuronal voltage-gated ion channels.* Nat Rev Neurosci, 2006. **7**(7): p. 548-62.
86. Dokken, K. and P. Fairley, *Sodium Channel Blocker Toxicity*, in *StatPearls*. 2020: Treasure Island (FL).
87. Brunklaus, A. and D. Lal, *Sodium channel epilepsies and neurodevelopmental disorders: from disease mechanisms to clinical application.* Dev Med Child Neurol, 2020. **62**(7): p. 784-792.
88. Bennett, D.L., et al., *The Role of Voltage-Gated Sodium Channels in Pain Signaling.* Physiol Rev, 2019. **99**(2): p. 1079-1151.
89. Black, J.A., et al., *Expression of Nav1.7 in DRG neurons extends from peripheral terminals in the skin to central preterminal branches and terminals in the dorsal horn.* Mol Pain, 2012. **8**: p. 82.
90. Branco, T., et al., *Near-Perfect Synaptic Integration by Nav1.7 in Hypothalamic Neurons Regulates Body Weight.* Cell, 2016. **165**(7): p. 1749-1761.
91. Kanellopoulos, A.H., et al., *Mapping protein interactions of sodium channel NaV1.7 using epitope-tagged gene-targeted mice.* EMBO J, 2018. **37**(3): p. 427-445.
92. Fukuoka, T. and K. Noguchi, *Comparative study of voltage-gated sodium channel alpha-subunits in non-overlapping four neuronal populations in the rat dorsal root ganglion.* Neurosci Res, 2011. **70**(2): p. 164-71.
93. Fukuoka, T., K. Kobayashi, and K. Noguchi, *Laminae-specific distribution of alpha-subunits of voltage-gated sodium channels in the adult rat spinal cord.* Neuroscience, 2010. **169**(3): p. 994-1006.
94. Akin, E.J., et al., *Building sensory axons: Delivery and distribution of NaV1.7 channels and effects of inflammatory mediators.* Sci Adv, 2019. **5**(10): p. eaax4755.
95. Schon, K.R., A.P.J. Parker, and C.G. Woods, *Congenital Insensitivity to Pain Overview*, in *GeneReviews((R))*, M.P. Adam, et al., Editors. 1993: Seattle (WA).
96. Drissi, I., W.A. Woods, and C.G. Woods, *Understanding the genetic basis of congenital insensitivity to pain.* Br Med Bull, 2020. **133**(1): p. 65-78.
97. Drenth, J.P. and S.G. Waxman, *Mutations in sodium-channel gene SCN9A cause a spectrum of human genetic pain disorders.* J Clin Invest, 2007. **117**(12): p. 3603-9.
98. McDermott, L.A., et al., *Defining the Functional Role of NaV1.7 in Human Nociception.* Neuron, 2019. **101**(5): p. 905-919 e8.
99. Blesneac, I., et al., *Rare NaV1.7 variants associated with painful diabetic peripheral neuropathy.* Pain, 2018. **159**(3): p. 469-480.
100. Han, C., et al., *Nav1.7-related small fiber neuropathy: impaired slow-inactivation and DRG neuron hyperexcitability.* Neurology, 2012. **78**(21): p. 1635-43.
101. Waxman, S.G. and S.D. Dib-Hajj, *The Two Sides of NaV1.7: Painful and Painless Channelopathies.* Neuron, 2019. **101**(5): p. 765-767.
102. Baker, M.D. and M.A. Nassar, *Painful and painless mutations of SCN9A and SCN11A voltage-gated sodium channels.* Pflugers Arch, 2020. **472**(7): p. 865-880.

103. Dib-Hajj, S.D., P. Geha, and S.G. Waxman, *Sodium channels in pain disorders: pathophysiology and prospects for treatment.* Pain, 2017. **158 Suppl 1**: p. S97-S107.
104. Dib-Hajj, S.D., et al., *The Na(V)1.7 sodium channel: from molecule to man.* Nat Rev Neurosci, 2013. **14**(1): p. 49-62.
105. Estacion, M., et al., *Intra- and interfamily phenotypic diversity in pain syndromes associated with a gain-of-function variant of NaV1.7.* Mol Pain, 2011. **7**: p. 92.
106. Eijkenboom, I., et al., *Yield of peripheral sodium channels gene screening in pure small fibre neuropathy.* J Neurol Neurosurg Psychiatry, 2019. **90**(3): p. 342-352.
107. Han, C., et al., *Functional profiles of SCN9A variants in dorsal root ganglion neurons and superior cervical ganglion neurons correlate with autonomic symptoms in small fibre neuropathy.* Brain, 2012. **135**(Pt 9): p. 2613-28.
108. Ahn, H.S., et al., *Differential effect of D623N variant and wild-type Na(v)1.7 sodium channels on resting potential and interspike membrane potential of dorsal root ganglion neurons.* Brain Res, 2013. **1529**: p. 165-77.
109. Hoeijmakers, J.G., et al., *Small nerve fibres, small hands and small feet: a new syndrome of pain, dysautonomia and acromesomelia in a kindred with a novel NaV1.7 mutation.* Brain, 2012. **135**(Pt 2): p. 345-58.
110. Ahmad, S., et al., *A stop codon mutation in SCN9A causes lack of pain sensation.* Hum Mol Genet, 2007. **16**(17): p. 2114-21.
111. Goldberg, Y.P., et al., *Loss-of-function mutations in the Nav1.7 gene underlie congenital indifference to pain in multiple human populations.* Clin Genet, 2007. **71**(4): p. 311-9.
112. Cox, J.J., et al., *Congenital insensitivity to pain: novel SCN9A missense and in-frame deletion mutations.* Hum Mutat, 2010. **31**(9): p. E1670-86.
113. Kurban, M., et al., *A nonsense mutation in the SCN9A gene in congenital insensitivity to pain.* Dermatology, 2010. **221**(2): p. 179-83.
114. Yuan, R., et al., *Two novel SCN9A gene heterozygous mutations may cause partial deletion of pain perception.* Pain Med, 2011. **12**(10): p. 1510-4.
115. Bartholomew, F., et al., *Channelopathy: a novel mutation in the SCN9A gene causes insensitivity to pain and autonomic dysregulation.* Br J Dermatol, 2014. **171**(5): p. 1268-70.
116. Sawal, H.A., et al., *Biallelic truncating SCN9A mutation identified in four families with congenital insensitivity to pain from Pakistan.* Clin Genet, 2016. **90**(6): p. 563-565.
117. Nilsen, K.B., et al., *Two novel SCN9A mutations causing insensitivity to pain.* Pain, 2009. **143**(1-2): p. 155-8.
118. Staud, R., et al., *Two novel mutations of SCN9A (Nav1.7) are associated with partial congenital insensitivity to pain.* Eur J Pain, 2011. **15**(3): p. 223-30.
119. Ma, A. and A. Turner, *A life without pain: congenital insensitivity to pain due to compound heterozygous SCN9A mutation.* J Paediatr Child Health, 2012. **48**(3): p. 285-6.
120. Yuan, J., et al., *Hereditary sensory and autonomic neuropathy type IID caused by an SCN9A mutation.* Neurology, 2013. **80**(18): p. 1641-9.
121. Shorer, Z., et al., *A novel mutation in SCN9A in a child with congenital insensitivity to pain.* Pediatr Neurol, 2014. **50**(1): p. 73-6.

122. Wheeler, D.W., et al., *Case Report: Neuropathic pain in a patient with congenital insensitivity to pain.* F1000Res, 2014. **3**: p. 135.
123. Ramirez, J.D., et al., *Null mutation in SCN9A in which noxious stimuli can be congenital insensitivity to pain*

. Neurology, 2014. **83**(17): p. 1577-80.
124. Bogdanova-Mihaylova, P., et al., *SCN9A-associated congenital insensitivity to pain and anosmia in an Irish patient.* J Peripher Nerv Syst, 2015. **20**(2): p. 86-7.
125. Rajasekharan, S., et al., *SCN9A channelopathy associated autosomal recessive Congenital Indifference to Pain. A case report.* Eur J Paediatr Dent, 2017. **18**(1): p. 66-68.
126. Marchi, M., et al., *A novel SCN9A splicing mutation in a compound heterozygous girl with congenital insensitivity to pain, hyposmia and hypogeusia.* J Peripher Nerv Syst, 2018. **23**(3): p. 202-206.
127. Akopian, A.N., et al., *The tetrodotoxin-resistant sodium channel SNS has a specialized function in pain pathways.* Nat Neurosci, 1999. **2**(6): p. 541-8.
128. Waxman, S.G., et al., *Sodium channel genes in pain-related disorders: phenotype-genotype associations and recommendations for clinical use.* Lancet Neurol, 2014. **13**(11): p. 1152-1160.
129. Nassar, M.A., et al., *Nociceptor-specific gene deletion reveals a major role for Nav1.7 (PN1) in acute and inflammatory pain.* Proc Natl Acad Sci U S A, 2004. **101**(34): p. 12706-11.
130. Fu, Y., et al., *High-frequency off-target mutagenesis induced by CRISPR-Cas nucleases in human cells.* Nat Biotechnol, 2013. **31**(9): p. 822-6.
131. Pattanayak, V., et al., *High-throughput profiling of off-target DNA cleavage reveals RNA-programmed Cas9 nuclease specificity.* Nat Biotechnol, 2013. **31**(9): p. 839-43.
132. Paquet, D., et al., *Efficient introduction of specific homozygous and heterozygous mutations using CRISPR/Cas9.* Nature, 2016. **533**(7601): p. 125-9.
133. Mali, P., et al., *CAS9 transcriptional activators for target specificity screening and paired nickases for cooperative genome engineering.* Nat Biotechnol, 2013. **31**(9): p. 833-8.
134. Loussouarn, G., et al., *Physiological and Pathophysiological Insights of Nav1.4 and Nav1.5 Comparison.* Front Pharmacol, 2015. **6**: p. 314.
135. Iyer, V., et al., *Off-target mutations are rare in Cas9-modified mice.* Nat Methods, 2015. **12**(6): p. 479.
136. Mogil, J.S., *Sex differences in pain and pain inhibition: multiple explanations of a controversial phenomenon.* Nat Rev Neurosci, 2012. **13**(12): p. 859-66.
137. Mogil, J.S., *Qualitative sex differences in pain processing: emerging evidence of a biased literature.* Nat Rev Neurosci, 2020. **21**(7): p. 353-365.
138. Prus, A.J., J.R. James, and J.A. Rosecrans, *Conditioned Place Preference*, in *Methods of Behavior Analysis in Neuroscience*, nd and J.J. Buccafusco, Editors. 2009: Boca Raton (FL).
139. Tzschentke, T.M., *Measuring reward with the conditioned place preference (CPP) paradigm: update of the last decade.* Addict Biol, 2007. **12**(3-4): p. 227-462.
140. Kremer, M., et al., *How to study anxiety and depression in rodent models of chronic pain?* Eur J Neurosci, 2020.

141. Zimmerman, A., L. Bai, and D.D. Ginty, *The gentle touch receptors of mammalian skin.* Science, 2014. **346**(6212): p. 950-4.
142. Lechner, S.G. and G.R. Lewin, *Hairy sensation.* Physiology (Bethesda), 2013. **28**(3): p. 142-50.
143. Sopacua, M., et al., *Small-fiber neuropathy: Expanding the clinical pain universe.* J Peripher Nerv Syst, 2019. **24**(1): p. 19-33.
144. Lauria, G. and G. Devigili, *Skin biopsy as a diagnostic tool in peripheral neuropathy.* Nat Clin Pract Neurol, 2007. **3**(10): p. 546-57.
145. Lauria, G., et al., *Morphometry of dermal nerve fibers in human skin.* Neurology, 2011. **77**(3): p. 242-9.
146. Van Acker, N., et al., *Automated PGP9.5 immunofluorescence staining: a valuable tool in the assessment of small fiber neuropathy?* BMC Res Notes, 2016. **9**: p. 280.
147. Dauch, J.R., et al., *Three-dimensional imaging of nociceptive intraepidermal nerve fibers in human skin biopsies.* J Vis Exp, 2013(74): p. e50331.
148. De Gregorio, C., et al., *Characterization of diabetic neuropathy progression in a mouse model of type 2 diabetes mellitus.* Biol Open, 2018. **7**(9).
149. Walcher, J., et al., *Specialized mechanoreceptor systems in rodent glabrous skin.* J Physiol, 2018. **596**(20): p. 4995-5016.
150. Gingras, J., et al., *Global Nav1.7 knockout mice recapitulate the phenotype of human congenital indifference to pain.* PLoS One, 2014. **9**(9): p. e105895.
151. Grubinska, B., et al., *Rat NaV1.7 loss-of-function genetic model: Deficient nociceptive and neuropathic pain behavior with retained olfactory function and intra-epidermal nerve fibers.* Mol Pain, 2019. **15**: p. 1744806919881846.
152. Donadio, V. and R. Liguori, *Microneurographic recording from unmyelinated nerve fibers in neurological disorders: an update.* Clin Neurophysiol, 2015. **126**(3): p. 437-45.
153. Serra, J., et al., *Activity-dependent slowing of conduction differentiates functional subtypes of C fibres innervating human skin.* J Physiol, 1999. **515 (Pt 3)**: p. 799-811.
154. Serra, J., H. Bostock, and X. Navarro, *Microneurography in rats: a minimally invasive method to record single C-fiber action potentials from peripheral nerves in vivo.* Neurosci Lett, 2010. **470**(3): p. 168-74.
155. Serra, J., et al., *Microneurographic identification of spontaneous activity in C-nociceptors in neuropathic pain states in humans and rats.* Pain, 2012. **153**(1): p. 42-55.
156. Orstavik, K., et al., *Abnormal function of C-fibers in patients with diabetic neuropathy.* J Neurosci, 2006. **26**(44): p. 11287-94.
157. Garcia-Perez, E., et al., *Behavioural, morphological and electrophysiological assessment of the effects of type 2 diabetes mellitus on large and small nerve fibres in Zucker diabetic fatty, Zucker lean and Wistar rats.* Eur J Pain, 2018. **22**(8): p. 1457-1472.
158. Pant, I., et al., *Peripheral neuropathy and the role of nerve biopsy: A revisit.* Indian J Pathol Microbiol, 2018. **61**(3): p. 339-344.
159. Abdo, H., et al., *Specialized cutaneous Schwann cells initiate pain sensation.* Science, 2019. **365**(6454): p. 695-699.

160. Fatehi, F., et al., *Chronic inflammatory demyelinating polyneuropathy associated with diabetes mellitus.* J Res Med Sci, 2013. **18**(5): p. 438-41.

Résumé en français suivi des mots-clés en français

Au cours de ce projet de doctorat, nous avons créé un modèle de souris pour la mutation *Scn9a*^{R185H} identifiée chez les patients douloureux souffrant de neuropathie à petite fibre grâce à l'approche CRISPR/Cas9 et nous avons étudié les conséquences sur la sensibilité à la douleur. Le modèle murin *Scn9a*^{R185H} a permis d'explorer l'association génotype-phénotype et le méca-nisme de la mutation des canaux sodiques NAV1.7 et le modèle *Scn9a*$^{R185X/wt}$ d'explorer l'effet de l'inactivation d'un allèle du gène *Scn9a*. Ces deux lignées de souris n'ont montré aucune altéra-tion de la croissance, de la survie et de l'état de santé global. Nous avons montré qu'il n'y a pas de différence dans l'expression de l'ARNm de Scn9a dans les DRG (ganglions de la racine dor-sale), la moelle épinière, le cerveau et le cervelet chez les souris *Scn9a*^{R185H}, et une diminution de l'expression chez les souris *Scn9a*$^{R185X/wt}$. La sensibilité à la douleur de ces nouvelles lignées de souris mutantes a été étudiée chez les deux sexes à l'aide de tests comportementaux de sensibilité aux stimuli thermiques et mécaniques. Nos résultats indiquent que globalement les souris Scn9aR185H présentent un phénotype douloureux, suggérant que la mutation Scn9aR185H identifiée chez les patients SFN contribue à leurs symptômes douloureux. Ces résultats pourront servir à la recherche de nouveaux analgésiques. Les souris *Scn9a*$^{R185X/wt}$ sont moins sensibles à la douleur de type chaleur. Chez ces souris, un allèle Scn9a n'est pas fonctionnel. Par consé-quent, nous avons montré par nos approches génétiques que le canal *SCN9A* joue un rôle cru-cial dans la nociception et dans les pathologies SFN douloureuses.

Mots clés : *SCN9A*, La neuropathie à petites fibres, douleur neuropathique, modèles de souris, CRISPR-Cas9

Résumé en anglais suivi des mots-clés en anglais

The NAV1.7 channel, encoded by Scn9a gene, is a voltage-gated sodium channel that plays a critical role in the generation and conduction of action potentials. In peripheral sensory neurons, the expres-sion and dynamic regulation of *SCN9A* is involved in pain sensitivity and chronic pain development. Several *SCN9A* gain-of-function mutations have been found in chronic pain pa-tients with idiopathic small fiber neuropathy (SFN). Recently, loss-of-function of *SCN9A* due to bi-allelic inactivating muta-tions results in the striking clinical phenotype of congenital insensitivity to pain (CIP). These individuals do not perceive pain in response to noxious stimuli. However, the heterozygous carriers of one inac-tivating mutation have normal pain sensitivity. The generation of animal models with CRISPR/Cas9 gene editing is an important tool for investigating the role of a mutation in the pathogenesis of disease and provide an avenue for functional drug screening. We have successfully established two mouse models, one carrying the R185H patient-derived mutation and the second one, R185X carrying an early stop in the open reading frame in the Scn9a locus R185X/wt using the CRISPR/Cas9 technology. We have characterized the effect of these two mutations on pain sensitivity and molecular and cellular alteration. The two mouse lines showed no alteration of growth, survival and global health state. Pain sensitivity of the new mu-tant mouse line was investigated on both sexes using behavioral tests of sensitivity to thermal and mechanical stimuli. Our results indicate that the *Scn9a*^{R185H} mice show an increased pain phenotype, suggesting that the *Scn9a*^{R185H} mutation identified in the SFN patients is responsi-ble for their pain symptoms. This exploration will benefit to drug screen. However, *Scn9a*$^{R185X/wt}$ mice did not show normal pain phenotype rather they are less sensitive to heat. In these mice, one Scn9a allele is not functional. Therefore, we provide more evidence that SCN9A plays an important role in nociception and in painful idiopathic SFN.

Keywords : *SCN9A*, Small Fiber Neuropathy, Neuropathic Pain, Mouse Model, CRISPR-Cas9